NOV 15 1948

VOLUME 108 NUMBER 2

THE ASTROPHYSICAL JOURNAL

AN INTERNATIONAL REVIEW OF SPECTROSCOPY AND ASTRONOMICAL PHYSICS

Founded in 1895 by GEORGE E. HALE and JAMES E. KEELER

Edited by

W. W. MORGAN, Managing Editor
S. CHANDRASEKHAR
Yerkes Observatory of the University of Chicago

PAUL W. MERRILL
Mount Wilson Observatory of the Carnegie Institution of Washington

HARLOW SHAPLEY
Harvard College Observatory
Cambridge, Massachusetts

N. U. MAYALL
Lick Observatory
University of California

SEPTEMBER 1948

INFRARED *CN* BANDS . . . . . *G. Herzberg and J. G. Phillips* 163

FINE STRUCTURE OF THE RED SYSTEM OF ATMOSPHERIC OXYGEN BANDS *Harold D. Babcock and Luise Herzberg* 167

THE MAGNETIC FIELD OF GAMMA EQUULEI . . . . . *Horace W. Babcock* 191

THE NUCLEAR AND NEBULAR SPECTRA OF THE PLANETARY NEBULA NGC 2392 *O. C. Wilson* 201

ON THE PULSATION IN THE ATMOSPHERE OF ETA AQUILAE *M. Schwarzschild, B. Schwarzschild, and W. S. Adams* 207

SPECTROSCOPIC OBSERVATIONS OF 90 STARS . . *Alfred H. Joy and S. A. Mitchell* 234

NOTES ON THE SPECTRUM OF ZETA AURIGAE DURING ECLIPSES *Dean B. McLaughlin* 237

ON THE DENSITY DISTRIBUTION AND CHEMICAL COMPOSITION OF THE INTERSTELLAR GAS . . . . . *Bengt Strömgren* 242

THE DISTRIBUTION OF INTERSTELLAR SODIUM . . . . *Lyman Spitzer, Jr.* 276

ON THE CHEMICAL COMPOSITION OF THE SUN FROM ITS INTERNAL CONSTITUTION . . . . . *Marjorie Hall Harrison* 310

LINE STRENGTHS IN THE IRON SPECTRUM IN INTERMEDIATE COUPLING WITH APPLICATION TO THE SOLAR CURVE OF GROWTH *Winston M. Gutenkalt* 326

THE PRIMARY AND SECONDARY SCATTERING OF SUNLIGHT IN A PLANE-STRATIFIED ATMOSPHERE OF UNIFORM COMPOSITION . . . *A. Hummel* 336

THE UNIVERSITY OF CHICAGO PRESS
CHICAGO, ILLINOIS, U.S.A.

September 1948 Vol. 108, No. 2

THE ASTROPHYSICAL JOURNAL

AN INTERNATIONAL REVIEW OF SPECTROSCOPY AND ASTRONOMICAL PHYSICS

Edited by

W. W. MORGAN
Managing Editor
Yerkes Observatory of the University of Chicago

S. CHANDRASEKHAR

PAUL W. MERRILL
Mount Wilson Observatory of the Carnegie Institution of Washington

HARLOW SHAPLEY
Harvard College Observatory
Cambridge, Massachusetts

N. U. MAYALL
Lick Observatory
University of California

With the Collaboration of the American Astronomical Society

Collaborating Editors:

1946-48
C. S. BEALS
Dominion Astrophysical Observatory, Victoria

LUIS E. ERRO
Astrophysical Observatory, Tonanzintla

O. C. WILSON
Mount Wilson Observatory

1947-49
LYMAN SPITZER, JR.
Princeton University Observatory

A. N. VYSSOTSKY
Leander McCormick Observatory

ALBERT E. WHITFORD
Washburn Observatory

1948-50
CECILIA H. PAYNE-GAPOSCHKIN
Harvard College Observatory

H. N. RUSSELL
Princeton University

ANDREW McKELLAR
Dominion Astrophysical Observatory, Victoria

The Astrophysical Journal is published bimonthly by the University of Chicago at the University of Chicago Press, 5750 Ellis Avenue, Chicago, Illinois, during July, September, November, January, March, and May. ¶The subscription price is $12.00 a year; the price of single copies is $3.00. Orders for service of less than a full year will be charged at the single-copy rate. ¶Postage is prepaid by the publishers on all orders from the United States and its possessions, Argentina, Bolivia, Brazil, Chile, Colombia, Costa Rica, Cuba, Dominican Republic, Ecuador, Guatemala, Haiti, Republic of Honduras, Mexico, Morocco (Spanish Zone), Nicaragua, Panama, Paraguay, Peru, Rio de Oro, El Salvador, Spain (including Balearic Islands, Canary Islands, and the Spanish Offices in Northern Africa; Andorra), Spanish Guinea, Uruguay, and Venezuela. ¶Postage is charged extra as follows: for Canada and Newfoundland, 42 cents on annual subscriptions (total $12.42); on single copies, 7 cents (total $3.07); for all other countries in the Postal Union, 96 cents on annual subscriptions (total $12.96), on single copies 16 cents (total $3.16). ¶Patrons are requested to make all remittances payable to The University of Chicago Press, in United States currency or its equivalent by postal or express money orders or bank drafts.

The following is an authorized agent:

For the British Empire, except North America and Australasia: The Cambridge University Press, Bentley House, 200 Euston Road, London, N.W. 1, England. Prices of yearly subscriptions and of single copies may be had on application.

Claims for missing numbers should be made within the month following the regular month of publication. The publishers expect to supply missing numbers free only when losses have been sustained in transit, and when the reserve stock will permit.

Business correspondence should be addressed to The University of Chicago Press, Chicago 37, Illinois.

Communications for the editors and manuscripts should be addressed to: W. W. Morgan, Editor of THE ASTROPHYSICAL JOURNAL, Yerkes Observatory, Williams Bay, Wisconsin.

Line drawings and photographs should be made by the author, and all marginal notes such as co-ordinates, wave lengths, etc., should be included in the cuts. It will not be possible to set up such material in type.

One copy of the corrected galley proof should be returned as soon as possible to the editor, Yerkes Observatory, Williams Bay, Wisconsin. Authors should take notice that the manuscript will not be sent to them with the proof.

The cable address is "Observatory, Williamsbay, Wisconsin."

The articles in this journal are indexed in the *International Index to Periodicals*, New York, N.Y.

Applications for permission to quote from this journal should be addressed to The University of Chicago Press, and will be freely granted.

Entered as second-class matter, July 31, 1940, at the Post-Office at Chicago, Ill., under the Act of March 3, 1879.
Acceptance for mailing at special rate of postage provided for in United States Postal Act of October 3, 1917, Section 1103, amended February 28, 1925.

[PRINTED IN U.S.A.]

THE ASTROPHYSICAL JOURNAL

AN INTERNATIONAL REVIEW OF SPECTROSCOPY AND ASTRONOMICAL PHYSICS

VOLUME 108 SEPTEMBER 1948 NUMBER 2

INFRARED *CN* BANDS

G. HERZBERG AND J. G. PHILLIPS
Yerkes Observatory
Received May 22, 1948

ABSTRACT

New bands belonging to the red *CN* band system are found in the infrared above 1.0μ. It is shown that the v' numbering of the band system must be raised by one unit. The 0–0 band is at 10,933 A. The revised constants of the upper $^2\Pi$ state according to this new numbering are listed in Table 3.

Using the infrared spectrometer recently described by Kuiper, Wilson, and Cashman,[1] we have studied the infrared emission spectrum of a discharge through a mixture of argon, nitrogen, and benzene vapor. In the visible and near ultraviolet region this discharge shows the red and violet *CN* bands with great prominence. The spectrum from 8000 to 16,000 A as obtained with the infrared spectrometer is shown in Figure 1. The spectrum from 16,000 to 25,000 A was also investigated, but no distinct features occur in this region.

Apart from a number of sharp peaks due to argon lines, the most characteristic feature of the spectrum in Figure 1 is a very strong broad band at 10,950 A with several peaks. In addition, somewhat weaker bands occur at 14,100, 9150, and 7875 A. Table 1 gives the wave lengths and wave numbers of all those observed peaks that are believed to have a molecular origin and are not bands of the first positive group of N_2.

The bands below 10,000 A given in Table 1 are readily identified as belonging to the red *CN* bands. In fact they represent the 0–0 and 1–0 sequences in the numbering of Asundi and Ryde.[2] The question then arises concerning what transition the strongest band at 10,950 A represents. It is not the 0–1 band which would occur at 11,240 A, but it fits exactly the position obtained by extrapolating the v' progression with $v'' = 0$ to longer wave lengths. In other words the 10,950 A band rather than the 9140 A band is the 0–0 band of the red *CN* bands, and the v' values of all bands of this system must be raised by one unit.

Asundi and Ryde, who in 1929 extended the system into the red and shifted the 0–0 band from 6928 A to 9141 A, did indeed leave open the possibility that further work might reveal additional bands in the infrared, making necessary a revision of the numbering. One might ask whether further investigation might not shift the 0–0 band even

[1] *Ap. J.*, **106**, 243, 1947.

[2] *Nature*, **124**, 57, 1929.

beyond the value of 10,950 A given here. However, this is definitely excluded since no band is found at the extrapolated position of 13,632 A, while the group of bands at 14,100 A fits the 0–1 sequence in the numbering here suggested.

It may be noted that the new bands at 10,950 A and 14,100 A, just like the other red *CN* bands, have each four heads (R_{21}, R_2, R_1, and Q_1) as indicated in Figure 1. The subsequent bands in the respective sequences do not show all these heads because of strong overlapping by the first bands.

If, in the vibrational formula for the red *CN* bands, the numbering in the upper state is changed as indicated, one obtains (using the constants of Jenkins, Roots, and Mulliken[3] for the upper state but those of Jenkins and Wooldridge[4] for the lower state)

$$\nu_0 = 9241.66 + 1814.43\,(v'+\tfrac{1}{2}) - 12.883\,(v'+\tfrac{1}{2})^2 - [2068.705\,(v''+\tfrac{1}{2}) - 13.144\,(v''+\tfrac{1}{2})^2].$$

TABLE 1

OBSERVED INFRARED *CN* BANDS

λ(A)	Intensity	ν(Cm^{-1})	Assignment	ν_{calc}
7852.9	3	12734	2–0 R_{21}	
7876.4		12696	R_2	12697.34
7898.6		12660	R_1	
7915.3		12634	Q_1	
9148.3	7	10931	1–0 R_2	10935.15
9174.7		10899	R_1	
9198.1		10872	Q_1	
9392.5	4	10647	2–1 R_2	10655.48
10879	10	9192	0–0 R_{21}	
10933		9147	R_2	9147.40
10970		9116	R_1	
11009		9083	Q_1	
11247	1	8891	1–1 R_2	8893.46
13981	4	7153	0–1 R_{21}	
14074		7105	R_2	7105.98
14135		7075	R_1	
14201		7042	Q_1	
14545	2	6875	1–2 R_2	6878.28
14610		6845	R_1	
15050	0.1	6645	2–3 R_2	6651.13

This formula applies to band origins. Adding half the doublet-splitting (26.10 cm^{-1}) and correcting for the separation between band head and subband origin, one obtains the values for R_2 heads given in the last column of Table 1. These agree in a very satisfactory way with the observed wave numbers, whose accuracy is about ± 3 cm^{-1}. This accuracy is not sufficient to derive an improved band formula. Table 2 gives a Deslandres table of the most intense bands of the red *CN* band system (up to $v' = 5$). Further bands with higher v' may be found in the paper by Jenkins, Roots, and Mulliken.[3]

It should be emphasized that the intensity of the bands usually observed in the red part of the spectrum is quite small compared to the infrared bands 0–0, 1–1, . . . , 0–1, 1–2, . . . and 1–0, 2–1, . . . (see Fig. 1). The small intensity ratio of the 2–0 red band to the 0–0 *violet* band found by King and Swings[5] does not therefore mean that the ab-

[3] *Phys. Rev.*, **39**, 16, 1932.

[4] *Phys. Rev.*, **53**, 137, 1938.

[5] *Ap. J.*, **101**, 6, 1945.

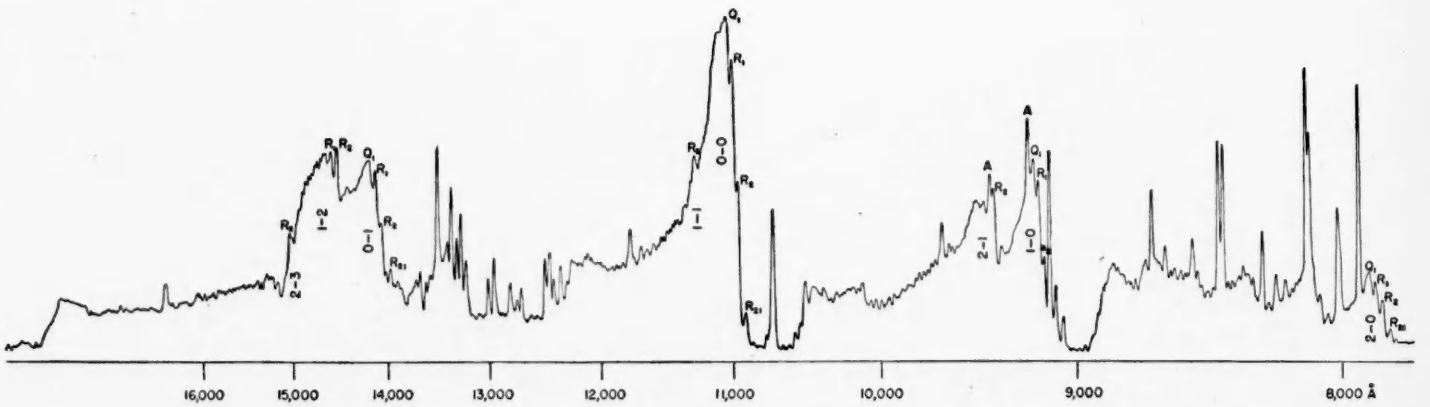

FIG. 1.—Infrared emission spectrum of the *CN* molecule. The sharp peaks that are not marked are due to argon lines

solute intensity (f value) of the red *CN* band system as a whole is very small compared to that of the violet *CN* bands. They are both apparently of the same order.

Table 3 summarizes the revised constants of the $^2\Pi$ state of *CN*, obtained from the original data of Jenkins, Roots, and Mulliken but converting to the new numbering.

TABLE 2

DESLANDRES TABLE OF THE STRONGEST *CN* BANDS
(Observed Wave Numbers of the R_2 Heads)

v' \ v''	0	1	2	3
0	9147	7105	(5090)*	.....
1	10931	8891	6875	(4889)
2	12696	10647	.....	6645
3	14432	12393	.....	.....
4	16145	14099	12086	.....
5	17830	15787	13769	11782

* The values in parentheses are calculated from the band formula.

TABLE 3

MOLECULAR CONSTANTS OF *CN* IN THE $^2\Pi$ STATE

$\nu_e = 9241.66\ \text{cm}^{-1}$	$B_e = 1.7165\ \text{cm}^{-1}$
$\nu_{00} = 9114.59\ \text{cm}^{-1}$	$\alpha_e = 0.01746\ \text{cm}^{-1}$
$\omega_e = 1814.43\ \text{cm}^{-1}$	$(D_e = 6.145 \times 10^{-6}\ \text{cm}^{-1})$*
$\omega_e x_e = 12.883\ \text{cm}^{-1}$	$(\beta_e = 2.59 \times 10^{-8}\ \text{cm}^{-1})$*
$A = -52.2\ \text{cm}^{-1}$	$r_e = 1.2327 \times 10^{-8}\ \text{cm}$

* These values are not observed but are calculated from the usual theoretical formulae.

As is well known, the red *CN* bands form the dominant feature of the spectrum of carbon stars (type R as well as N) in the spectral range 6000–9000 A. From the intensity ratios in Figure 1 it is clear that, at 9200, 10,900 and 14,000 A, still much stronger absorptions belonging to this band system will be found. It must also be expected that these bands in emission form strong features of cometary spectra. The absorption bands found by Kuiper[1] in this region in the spectra of late M-type stars (particularly R Leonis) are not *CN* bands.

We are very much indebted to Dr. G. P. Kuiper for letting us use his infrared spectrometer for this investigation.

FINE STRUCTURE OF THE RED SYSTEM OF ATMOSPHERIC OXYGEN BANDS*

HAROLD D. BABCOCK AND LUISE HERZBERG
Mount Wilson and Yerkes Observatories
Received May 12, 1948

ABSTRACT

Improved high-dispersion spectrograms of the red bands of atmospheric oxygen have been obtained, with air paths ranging from 30 meters to about 100 km. For unblended lines of medium intensity the wave lengths have been determined with an accuracy of about one part in seven million, and as a result the molecular constants of the molecules, O_2^{16}, $O^{16}O^{18}$, and $O^{16}O^{17}$ in the $^3\Sigma_g^-$ ground state and the $^1\Sigma_g^+$ excited state, have been evaluated much more precisely than previously.

Careful analysis shows a variation in the triplet splitting of the $^3\Sigma_g^-$ state which is dependent both on the vibrational quantum number and on the mass of the molecule, in addition to the variation due to the change of rotational energy.

A. INTRODUCTION

The most extensive and accurate measurements of the atmospheric oxygen bands previously published are those by Dieke and Babcock,[1] which were based on wave lengths obtained with interferometers by H. D. Babcock.[2] Dieke and Babcock discussed the 0–0, 1–0, 2–0, and 3–0 bands of O_2^{16} and also a new weak band, which was shown to belong to O_2 but which seemed independent of the main system. They called this weak band "A′" because it is intermingled with the 0–0 band, long designated "A" in the solar spectrum. Their paper served as a basis for R. S. Mulliken's[3] interpretation of the band system as a $^1\Sigma - {}^3\Sigma$ transition of the oxygen molecule and also for the theoretical discussion of the triplet-splitting in the $^3\Sigma$ ground state by H. A. Kramers[4] and by R. Schlapp.[5]

The new weak band, A′, which Dieke and Babcock[1] described, was shown by Giauque and Johnston[6] to arise from an isotopic molecule, $O^{16}O^{18}$—a result which stimulated the search for other isotopes through spectroscopic observation. From additional data specially obtained by H. D. Babcock,[7] Giauque and Johnston[8] also established the existence of the molecule $O^{16}O^{17}$; and, following the later determination of the mass ratios of $O^{16} : O^{18} : O^{17}$ and the relative abundance of these isotopes, a new system of physical atomic weights, based on $O^{16} = 16$, was distinguished from the familiar system of chemical atomic weights in which O (natural mixture of isotopes) $= 16$.

The work of Dieke and Babcock was also used by Giauque and Johnston[9] in their determination of the entropy of oxygen, from which we quote:

> It is suggested that entropy values deduced from reliable spectroscopic data are preferable as a basis for thermodynamic calculations to the less accurate values obtained from heat capacity measurements and the third law [of thermodynamics]. . . . The general agreement of the various physical facts concerning the oxygen molecule in relation to entropy and particularly the close agreement of the entropy as obtained by the two methods support our confidence that the third law of thermodynamics is an exact law.

* *Contributions from the Mount Wilson Observatory, Carnegie Institution of Washington*, No. 750.

[1] *Proc. Nat. Acad. Sci.*, **13**, 670, 1927.

[2] *Mt. W. Contr.*, No. 328; *Ap. J.*, **65**, 140, 1927.

[3] *Phys. Rev.*, **32**, 880, 1928.

[4] *Zs. f. Phys.*, **53**, 422, 1929.

[5] *Phys. Rev.*, **51**, 342, 1937.

[6] *J. Amer. Chem. Soc.*, **51**, 1436, 1929.

[7] *Proc. Nat. Acad. Sci.*, **15**, 471, 1929.

[8] *J. Amer. Chem. Soc.*, **51**, 3528, 1929.

[9] *Ibid.*, pp. 2319–2321.

The exact calculation of free energy and other properties of gases has been discussed by Giauque,[10] who took into account molecular rotation, vibration, nuclear spin, and electronic excitation.

In the present paper further measurements of the red bands of oxygen, made with air paths up to a maximum of the order of 100 km, are combined with the earlier Mount Wilson data. The results are more precise and more complete than are those in preceding papers. Besides the bands described by Dieke and Babcock and the 1–1 band of O_2^{16}, which was first observed by Babcock[11] and later studied by Mecke and Baumann,[12] the weaker 2–1 and 3–1 bands are now observed and also the 1–0 bands of both $O^{16}O^{18}$ and $O^{16}O^{17}$.

Refinement of the observations and also of the theoretical treatment now permits a more critical analysis (by L. H.), from which improved values of the molecular constants are derived. The accuracy of the new constants for O_2^{16} in the ground state, $^3\Sigma_g^-$, and in the electronically excited state, $^1\Sigma_g^+$, surpasses that for the constants of any other molecule.

B. OBSERVATIONAL DATA

Most of the later measurements have been obtained on Mount Wilson with the Snow telescope and a plane-grating spectrograph of 30-foot focus. A few plates were made with the 75-foot spectrograph of the 150-foot tower telescope and others in the laboratory at Pasadena, where interferometers were used to observe the absorption in 30 meters of air. This short air path permitted precise measurements of the principal lines of the 0–0 band of O_2^{16}, which are much too wide in the solar spectrum for satisfactory measurement, even with the midday summer sun on Mount Wilson.

All wave lengths in the present compilation of data were referred ultimately to the secondary standards in the spectrum of neon.[13]

Three excellent gratings were available, two ruled by Michelson at the University of Chicago and one by Anderson at the Johns Hopkins University. Second-, third-, and fourth-order spectra were used, with dispersions ranging from 0.88 to 0.12 A per millimeter.

Because of the range of intensity among the lines of O_2 and the overlapping of the bands from different isotopic molecules, spectrograms were made with various air paths. The weakest lines, i.e., most of those due to $O^{16}O^{17}$, part of those belonging to $O^{16}O^{18}$, and those with greatest K'' in the other bands, are seen only when the sun is close to the horizon. Under this condition, however, the strongest lines become so wide that they obscure many weak lines. The best that can be done is to observe the sun at various altitudes and to hunt for the close faint companions of the stronger lines.

At the lowest solar altitudes the weakening of the light, even in the deep red, is rapid and variable; at the same time the rate of change of the intensities of telluric lines with respect to length of air path varies rapidly. Since spectrographs having high dispersion usually do not provide high brightness, each exposure made with very low sun corresponds to an integration through the range of the variables. It will be apparent, therefore, that the labor of producing a consistent set of estimated line intensities throughout such a system of bands is very great. Photometric measures for numerous lines in the bands of O_2 have been published by various observers, and H. C. van de Hulst[14] has given a theoretical discussion of the intensities of atmospheric lines.

Readers interested in the obscuration of lines in spectra of celestial objects by telluric absorption will find a convenient arrangement of the wave lengths of oxygen band lines ($\lambda > 6600$ A) in *The Solar Spectrum*, $\lambda 6600$–$\lambda 13495$.[15] The work cited contains also

[10] *J. Amer. Chem. Soc.*, **52**, 4808, 1930.

[11] *Phys. Rev.*, **35**, 125, 1930.

[12] *Zs. f. Phys.*, **72**, 139, 1931.

[13] *Trans. I.A.U.*, **1**, 40, 1922.

[14] *Ann. d'ap.*, **8**, 1–25, 1945.

[15] Babcock and Moore, *Pub. Carnegie Inst. Washington*, No. 579 (Washington, 1947).

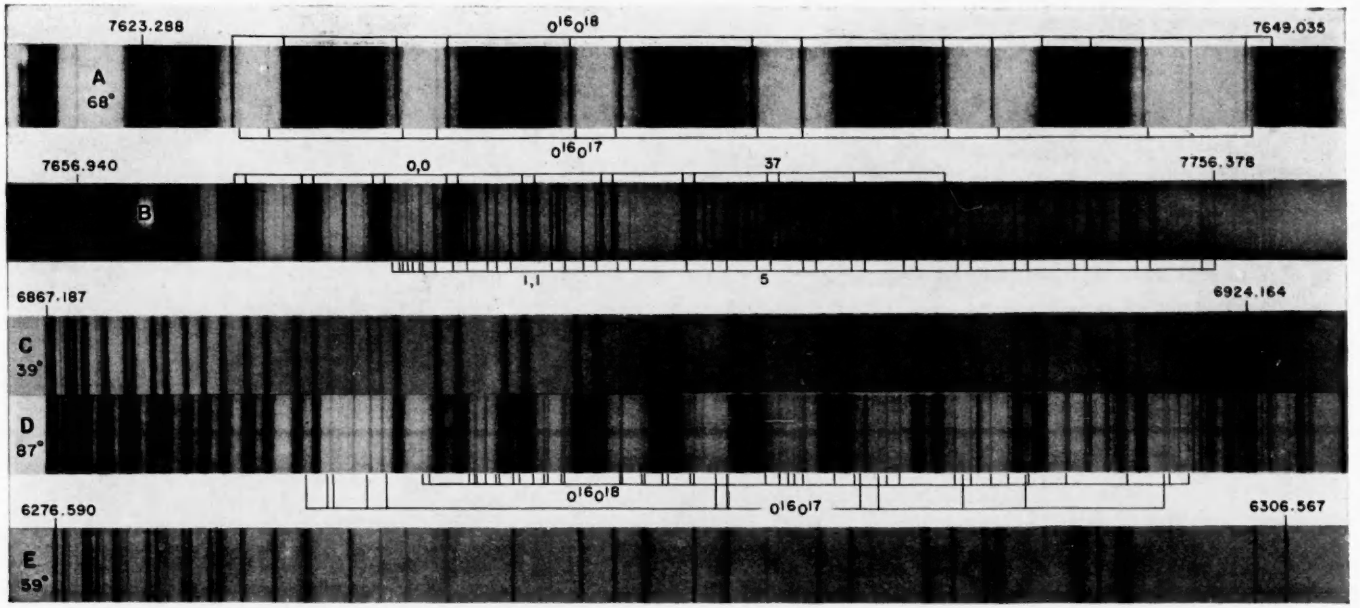

FIG. 1.—Parts of the $^1\Sigma \leftarrow {}^3\Sigma$ system of oxygen bands, observed at Mount Wilson. Zenith distances of sun at mid-exposure at the left. *A*, 0, 0 *P*-branches, O_2^{16}, $O^{16}O^{18}$, $O^{16}O^{17}$; *B*, 0, 0 and 1, 1 lines of O_2^{16} (note nearly complete absorption toward the origin and near-equality of intensity for pairs marked 37 and 5); *C* and *D*, 1, 0 of O_2^{16}, $O^{16}O^{18}$, and $O^{16}O^{17}$; *E*, 2, 0 of O_2^{16}.

the wave lengths of the O_2 lines in the $^1\Delta - {}^3\Sigma$ system: 1, 0 λλ 10584–10720, and 0,0 λλ 12493–12782.

In Tables 1, 2, and 3 are given wave lengths, wave numbers, and rotational assignments, K'', of lines observed in the bands 0–0, 1–0, 2–0, 3–0, 1–1, 2–1, and 3–1 of O_2^{16}, and in the 0–0 and 1–0 bands of $O^{16}O^{18}$ and of $O^{16}O^{17}$. Visual estimates of intensity are included for the first two bands mentioned; but even within a single band these estimates are chiefly useful as an indication of the range and for showing some small but real differences between ^PP and ^PQ lines or ^RQ and ^RP lines that have the same values of K″. For each of the other bands a note shows the range of intensity, but the numbers stated usually have different meanings from band to band. Intensities indicated in Tables 1, 2, and 3 relate to high sun on Mount Wilson. Weak lines were measured at low sun.

No data appear in Table 1 for two bands of O_2^{16} reported by others: the 4–0 band (head = λ 5378), described by O. C. Lester,[16] and the 0–1 band (near λ 8624), suggested by Mecke and Baumann,[17] and observed in emission in the laboratory by J. Kaplan.[18]

From accurate predictions of the wave lengths of the lines in the 4–0 band, we conclude that our spectrograms do not show this band and that it is absent from the extensive observations of L. Becker.[19] Lester believed that his relative wave lengths were reliable to ±0.05 A, and it is possible that, among some twenty lines which he assigned to this band, a few were due to O_2^{16}. But the evidence is too weak to permit further statements.

Positions of lines in the 0–1 band of O_2^{16} are accurately predictable, but our spectrograms do not show this band. On the other hand, some of the lines which Mecke and Baumann assigned to the 0–1 band are now found[15] to originate in the sun. Further observation is required to establish the occurrence of this band in absorption.

The wave numbers in the tables were computed to 0.0001 cm^{-1}, with the refractivity of air as given by Barrell and Sears,[20] and were rounded off to 0.001 cm^{-1} for tabulation. In order to avoid the accumulation of arithmetical errors, the computation of the band constants (secs. D and E) was based on the wave numbers as computed to 0.0001 cm^{-1}. These numbers are systematically smaller than those calculated from the refractivity of air as determined by Meggers and Peters[21] and used in Kayser's *Schwingungszahlen*, by 0.0135 cm^{-1} at λ 5500 and by 0.0045 cm^{-1} at λ 8000.

In Figure 1 are shown spectrograms illustrating the appearance of portions of various oxygen bands.

Within the tabular range of K'' in Tables 1, 2, and 3 every blank space is accounted for either as a forbidden line (e.g., $K'' = 1$ in ^PQ) or by masking attributable to another oxygen line, a solar line, or a telluric line presumably due to water vapor.

C. BAND STRUCTURE

The characteristic structure of the red atmospheric oxygen bands—two *R*-form branches forming a head and two *P*-form branches, separated from the former by a zero gap—has been interpreted by R. S. Mulliken[22] as a transition from the $^3\Sigma_g^-$ ground state of the O_2 molecule to a $^1\Sigma_g^+$ excited state. As was pointed out by J. H. Van Vleck,[23] a $\Sigma_g - \Sigma_g$ transition, though strictly forbidden as electric dipole radiation, is possible as

[16] *Ap. J.*, **20**, 81, 1904.

[17] *Das ultrarote Sonnenspektrum* (Leipzig, 1934).

[18] *Phys. Rev.*, **71**, 274, 1947.

[19] *Trans. R. Soc. Edinburgh*, Vol. **36**, Part I, 1900.

[20] *Phil. Trans. R. Soc. London, A*, **238**, 1, 1939.

[21] *Bull. Nat. Bureau Standards*, **14**, 697, 1917.

[22] *Phys. Rev.*, **32**, 880, 1928; and *Rev. Mod. Phys.*, **4**, 1, 1932.

[23] *Ap. J.*, **80**, 161, 1934.

TABLE 1

LINES IN THE $^1\Sigma_g^+ \leftarrow {}^3\Sigma_g^-$ SYSTEM OF O_2^{16}

0–0 BAND

λλ 7593.695–7733.738

K''	λ_{air}	ν_{vac}	INT.	λ_{air}	ν_{vac}	INT.
	^PP Branch			^PQ Branch		
1	7620.996	13118.034	25 a*	.....	.....	.....
3	24.500	12.005	32 a	7623.288	13114.089	30 a
5	28.225	05.602	35 a	27.054	07.614	32 a
7	32.168	13098.831	38 a	31.016	00.809	35 a
9	36.328	91.695	38 a	35.192	13093.643	35 a
11	40.707	84.193	35 a	39.585	86.114	32 a
13	45.312	76.312	30 a	44.200	78.214	30 a
15	50.135	68.068	20 a	49.035	69.947	20 a
17	55.182	59.452	18 a	54.094	61.308	18 a
19	60.454	50.465	12 a	59.370	52.311	15 a
21	65.944	41.118	10	64.872	42.942	12
23	71.670	31.385	10	70.600	33.203	10
25	77.618	21.289	9	76.563	23.079	9
27	83.800	10.813	8	82.756	12.581	8
29	90.217	12999.956	6	89.177	01.715	6
31	96.868	88.723	4	95.836	12990.465	4
33	7703.759	77.105	3	7702.739	78.823	3
35	10.874	65.131	− 1	09.871	66.817	− 1
37	18.257	52.729	− 2	17.251	54.417	− 2
39	25.862	39.978	− 4	24.880	41.623	− 4
41	7733.738	12926.801	− 2†	7732.746	12928.459	− 4
	^RR Branch			^RQ Branch		
1	7616.146	13126.387	17 a	7615.061	13128.257	20 a
3	13.194	31.477	20 a	12.060	33.433	25 a
5	10.455	36.203	25 a	09.302	38.193	50 a
7	07.933	40.557	30 a	06.767	42.572	30 a
9	05.635	44.528	30 a	04.453	46.571	40 a
11	03.556	48.122	30 a	02.363	50.185	30 a
13	01.697	51.337	25 a	00.493	53.420	25 a
15	00.066	54.159	25 a	7598.847	56.269	25 a
17	7598.650	56.611	25 a	97.438	58.709	30 a†
19	97.438	58.709	30 a†	96.228	60.806	20 a
21	96.503	60.329	12	95.235	62.526	14 †
23	95.768	61.603	12	94.507	63.788	12 a
25	95.235	62.526	13 †	93.997	64.672	10 a
27	94.974	62.979	6 †	93.695	65.195	10 †
29	7594.974	13162.979	6 †	93.695	65.195	10 †
31	.....	.....	.....	7593.850	13164.927	2

* Lines marked "a" were observed with artificial light and an air path of 30 meters. All lines not having this mark were observed in the solar spectrum.

† Either unresolved blend with another oxygen line, with a solar line, or with a telluric line (probably due to water vapor) or so close to such a line that the wave length is probably affected by it.

TABLE 1—*Continued*

1–0 BAND

λλ 6867.187–6967.650

K''	λ_{air}	ν_{vac}	Int.	λ_{air}	ν_{vac}	Int.
	^{P}P Branch			^{P}Q Branch		
1	6883.833	14522.783	11	.....	.....	.....
3	86.743	16.646	15	6885.754	14518.733	13†
5	89.903	09.989	17	88.948	12.001	15
7	93.309	02.821	19	92.369	04.798	17
9	96.965	14495.133	20	96.037	14497.083	18
11	6900.868	86.935	19	99.954	88.853	17
13	05.023	78.218	17	6904.117	80.117	15
15	09.431	68.979	13	08.534	70.860	12
17	14.090	59.230	10	13.200	61.091	10
19	19.002	48.966	8	18.122	50.803	8
21	24.164	38.193	9†	23.286	40.026	6†
23	29.599	26.870	5	28.727	28.685	5
25	35.280	15.051	3	34.422	16.837	3
27	41.218	02.721	5†	40.375	04.470	0
29	.....	.....	.....	46.590	14391.582	− 2
31	53.912	14376.429	− 4	53.072	78.167	− 4
33	60.647	62.520	− 3?	59.812	64.243	− 3?
35	6967.650	14348.085	− 4†	6966.837	14349.758	− 4
	^{R}R Branch			^{R}Q Branch		
1	6879.928	14531.027	10	6879.041	14532.900	12
3	77.637	35.867	12	76.715	37.816	14
5	75.590	40.195	14	74.653	42.177	16
7	73.798	43.985	14	72.843	46.006	16
9	72.247	47.268	14	71.285	49.304	15
11	70.946	50.022	13	70.007	52.011	12
13	69.887	52.265	12	68.915	54.324	12†
15	69.096	53.947	11	68.105	56.040	11
17	68.525	55.152	8†	67.547	57.226	8
19	68.245	55.750	5	67.252	57.856	6
21	68.208	55.828	4	67.187	57.993	4
23	68.421	55.372	2	67.394	57.548	3
25	68.915	54.324	12†	67.856	56.575	2
27	69.627	52.816	2	68.577	55.042	2†
29	70.620	50.712	− 1	69.567	52.945	− 3†
31	71.872	48.062	− 3	6870.819	14550.291	− 3†
33	6873.392	14544.844	− 4	.....	.....	.....

TABLE 1—*Continued*

2–0 BAND

λλ 6276.590–6353.099; Intensity −4 to 3

K''	λ_{air}	ν_{vac}	λ_{air}	ν_{vac}
	^{P}P Branch		^{P}Q Branch	
1	6287.749	15899.546	.....	.....
3	90.222	93.294	6289.397	15895.379
5	92.959	86.381	92.162	88.394
7	95.962	78.806	95.179	80.780
9	99.230	70.567	98.457	72.515
11	6302.764	61.668	6302.000	63.591
13	06.567	52.104	05.810	54.006
15	10.636	41.883	09.886	43.766
17	14.977	30.993	14.235	32.854
19	19.591	19.434	18.853	21.282
21	24.479	07.208	23.750	09.030
23	29.636	15794.329	28.913	15796.134
25	35.072	80.777	34.358	82.555
27	40.791	66.544	40.078	68.316
29	46.796	51.626	46.086	53.388
31	6353.099	15735.997	6352.379	15737.781
	^{R}R Branch		^{R}Q Branch	
1	6284.536	15907.674	6283.795	15909.550
3	82.726	12.257	81.956	14.207
5	81.178	16.178	80.393	18.168
7	79.896	19.427	79.101	21.443
9	78.878	22.008	78.073	24.049
11	78.126	23.916	77.312	25.982
13	77.638	25.153	76.818	27.234
15	77.419	25.709	76.590	27.813
17	77.470	25.580	76.633	27.704
19	77.785	24.781	76.938	26.930
21	78.374	23.286†	77.525	25.440
23	79.233	21.108	78.374	23.286†
25	.....	.....	79.506	20.416
27	81.781	14.650	80.910	16.856
29	6283.468	15910.378	6282.588	15912.606

TABLE 1—*Continued*

3–0 BAND

λλ 5788.102–5829.917; Intensity −4 to 0

K''	λ_{air}	ν_{vac}	λ_{air}	ν_{vac}
	^{P}P Branch		^{P}Q Branch	
1	5796.092	17248.221†	.....	.....
3	98.195	41.965†	5797.530	17243.943
5	5800.640	34.698	99.963	36.710
7	03.327	26.718	5802.663	28.689
9	06.289	17.930	05.631	19.882
11	09.523	08.345	08.878	10.256
13	13.041	17197.931	12.400	17199.828
15	16.833	86.720†	16.263	88.404†
17	20.912	74.677	20.278	76.547
19	25.272	61.822	24.636	63.696
21	5829.917	17148.148	5829.288	17149.999
	^{R}R Branch		^{R}Q Branch	
1	5793.411	17256.203†	5792.769	17258.115
3	91.946	60.568	91.293	62.514†
5	90.769	64.076	90.101	66.068
7	89.865	66.771	89.189	68.788
9	89.234	68.653	88.549	70.697
11	88.877	69.718	88.187	71.777
13	88.801	69.945	88.102	72.031
15	88.995	69.366	88.289	71.473
17	89.489	67.893†	88.763	70.059
19	90.227	65.692	89.489	67.893†
21	5791.293	17262.514†	5790.534	17264.777

TABLE 1—*Continued*

1-1 BAND

λλ 7684.331–7768.513; Intensity −4 to −3

K''	λ_{air}	ν_{vac}	λ_{air}	ν_{vac}
	${}^{P}P$ Branch		${}^{P}Q$ Branch	
1	7710.099	12966.434	.....	.....
3	13.658	60.451	7712.416	12962.538
5	17.450	54.083	16.251	36.096
7	21.482	47.319	20.304	49.294
9	25.746	40.173	24.586	42.116
11	30.254	32.627	29.101	24.556
13	34.995	24.700	33.854	26.607
15	39.978	16.379	38.848	18.265
17	45.202	07.667	44.080	09.537
19	50.670	12898.561	49.554	00.418
21	56.378	89.069	55.275	12890.902
23	62.334	79.179	61.232	81.008
25	7768.513	12868.935	7767.458	12870.683
	${}^{R}R$ Branch		${}^{R}Q$ Branch	
1	7705.207	12974.666	7704.076	12976.571
3	02.240	79.664	01.078	81.622
5	7699.506	84.273	7698.322	86.270
7	96.996	88.507	.....	.....
9	94.748	92.301	93.530	94.358
11	92.722	95.723	91.487	97.810
13	90.939	98.736	89.703	13000.825
15	89.387	13001.360	88.127	03.491
17	88.127	03.491	86.830	05.684
19	87.034	05.339	85.764	07.488
21	86.203	06.745	84.964	08.842
23	85.629	07.717	7684.331	13009.914
25	7685.281	13008.306	.....	.....

TABLE 1—*Continued*

2–1 BAND

λλ 6954.014–6996.310; Intensity −4 to −3

K''	λ_{air}	ν_{vac}	λ_{air}	ν_{vac}
	^{P}P Branch		^{P}Q Branch	
1	6970.055	14343.133	.....	.....
3	73.207	37.020†	.....	.....
5	.....	.....	6975.239	14332.473
7	79.705	23.303	78.740	25.283
9	83.452	15.617	82.501	17.667
11	87.482	07.361	.....	.....
13	.....	.....	90.839	00.491
15	6996.310	14289.312	6995.378	14291.212
	^{R}R Branch		^{R}Q Branch	
3	6963.773	14356.072	6962.804	14358.070
5	61.707	60.332	60.746	62.315
7	59.946	63.966	.....	.....
9	58.462	67.029	.....	.....
11	57.204	69.627	56.214	71.672†
13	56.214	71.672†	.....	.....
15	6955.621	14373.104	54.494	75.226
17	.....	.....	6954.014	14376.219

3–1 BAND

λλ 6360.045–6390.320; Intensity −4

K''	λ_{air}	ν_{vac}	λ_{air}	ν_{vac}
	^{P}P Branch		^{P}Q Branch	
7	6379.270	15671.44	6378.520	15673.29
9	82.728	62.95	81.876	65.05
11	86.268	54.27	85.597	55.92
13	6390.320	15644.34	6389.599	15646.11
	^{R}R Branch		^{R}Q Branch	
7	6363.135	15711.18	.....	.....
9	62.122	13.68	.....	.....
11	61.453	15.33	6360.593	15717.46
13	6360.981	15716.50	.....	.....
15	.....	.....	6360.045	15718.81

TABLE 2

LINES IN THE $^1\Sigma_g^+ \leftarrow {}^3\Sigma_g^-$ SYSTEM OF $O^{16}O^{18}$

0–0 BAND

λλ 7594.287–7684.964; Intensity −4 to 3

K''	λ_{air}	ν_{vac}	λ_{air}	ν_{vac}	K''	λ_{air}	ν_{vac}	λ_{air}	ν_{vac}
	^PP Branch		^PQ Branch			^RR Branch		^RQ Branch	
1	7619.698	13120.268	.....	.....	1	.....	.....	7614.026	13130.042
2	21.323	17.471	7620.077	13119.615	2	7613.705	13130.595	12.578	32.539
3	23.012	14.564	21.801	16.648	3	12.314	32.995	11.194	34.927
4	.....	.....	23.552	13.635	4	11.007	35.250	09.868	37.216
5	26.524	08.525	25.353	10.538	5	09.746	37.427	08.586	39.430
6	.....	.....	.....	.....	6	08.530	39.526	07.366	41.537
7	30.245	02.133	29.092	04.113	7	07.366	41.537	06.198	43.555
8	.....	.....	.....	.....	8	06.238	43.486	05.076	45.494
9	34.170	13095.396	33.036	13097.342	9	05.186	45.304	04.013	47.331
10	.....	.....	.....	.....	10	.....	.....	02.996	49.090
11	38.308	88.302	37.183	90.230	11	03.216	48.710	02.036	50.751
12	40.457	84.621	39.339	86.536	12	.....	.....	01.127	52.323
13	42.651	80.865	41.535	82.775	13	01.470	51.730	.....	.....
14	44.900	77.016	43.793	78.910	14	.....	.....	7599.463	55.203
15	47.204	73.076	46.098	74.967	15	.....	.....	.....	.....
16	49.552	69.064	48.454	70.940	16	7599.228	55.610	98.006	57.726
17	51.963	64.946	50.894	66.771	17	.....	.....	.....	.....
18	54.428	60.739	53.343	62.590	18	98.006	57.726	96.768	59.870
19	56.940	56.454	55.847	58.318	19	.....	.....	.....	.....
20	.....	.....	58.420	53.931	20	96.975	59.511	.....	.....
21	62.122	47.623	61.05	49.449	21	.....	.....	.....	.....
22	.....	.....	63.726	44.893	22	.....	.....	.....	.....
23	67.518	38.441	66.447	40.263	23	.....	.....	.....	.....
24	70.31	33.696	69.233	35.526	24	.....	.....	.....	.....
25	73.127	28.910	72.09	30.671	25	95.590	61.911	94.287	64.169
26	76.026	23.990	74.962	25.795	26	95.590	61.911	94.287	64.169
27	78.953	19.025	.....	.....	27	7595.590	13161.911	7594.287	13164.169
28	81.953	13.941	7680.912	13015.705					
29	7684.964	13008.842	.....	.....					

TABLE 2—*Continued*

1–0 BAND

λλ 6885.279–6938.548; Intensity −4 to −3

K''	λ_{air}	ν_{vac}	λ_{air}	ν_{vac}
	^{P}P Branch		^{P}Q Branch	
1	6901.271	14486.088*	.....	.....
2	02.620	83.257	6901.607	14485.383
3	.....	.....	03.040	82.376*
4	05.494	77.229	04.531	79.246
5	07.023	74.025	06.059	76.045*
6	.....	.....	07.655	72.700*
7	10.250	67.265	09.32	69.218*
8	11.952	63.703	11.015	65.664
9	13.713	60.019	12.786	61.958*
10	15.533	56.213	.....	.....
11	17.409	52.293	16.475	54.245*
12	19.327	48.287*	18.429	50.162
13	21.338	44.089	20.426	45.993
14	23.369	39.852*	22.478	41.710
15	25.497	35.415*	24.597	37.290
16	27.675	30.876	.....	.....
17	.....	.....	.....	.....
18	32.150	21.560*	.....	.....
19	34.531	16.610	.....	.....
20	6936.962	14411.557	36.066	13.418
21	.....	.....	6938.548	14408.451
	^{R}R Branch		^{R}Q Branch	
1	6897.562	14493.879	6896.664	14495.765
2	96.445	96.225	95.521	98.168
3	95.382	98.460	94.451	14500.418
4	94.397	14500.569*	93.40	02.628*
5	93.40	02.628*	92.57	04.375*
6	92.57	04.375*	91.593	06.431
7	91.719	06.166	90.760	08.185
8	90.948	07.789	90.10	09.574*
9	90.240	09.279	89.271	11.320
10	89.585	10.659	88.612	12.709
11	.....	.....	88.000	13.998*
12	88.457	13.035	87.476	15.102
13	88.000	13.998*	87.000	16.105*
14	87.564	14.917	86.579	16.993*
15	87.196	15.692	86.209	17.774*
16	87.000	16.105*	.....	.....
17	86.579	16.993*	.....	.....
18	86.476	17.211	85.477	19.317
19	86.372	17.430*	85.349	19.587*
20	86.209	17.774*	85.279	19.734*
21	86.303	17.575	85.279	19.734*
22	6886.372	14517.430*	6885.349	14519.587*

* Either unresolved blend with another oxygen line, with a solar line, or with a telluric line (probably due to water vapor) or so close to such a line that the wave length is probably affected by it.

TABLE 3

LINES IN THE $^1\Sigma_g^+ \leftarrow {}^3\Sigma_g^-$ SYSTEM OF $O^{16}O^{17}$

0–0 BAND

λλ 7599.550–7675.240; Intensity −4 to −3

K''	λ_{air}	ν_{vac}	λ_{air}	ν_{vac}
	^PP Branch		^PQ Branch	
1	7620.322	13119.194		
2	21.988	16.326		
3	23.715	13.355	7622.503	13115.440
4	25.475	10.328		
5			26.157	09.156
6	29.196	03.934		
7			29.988	02.574
8	33.131	13097.179		
9			34.052	13095.599
10	37.276	90.071		
11				
12	41.644	82.588		
13			42.786	80.633
14	46.209	74.777		
15	48.580	70.725	47.460	72.639
16				
17	53.47	62.373	52.383	64.229
18	56.00	58.057		
19	58.50	53.624		
20				
21	63.90	44.597	62.84	46.401
22	66.669	39.885		
23	69.47	35.123	68.399	36.944
24	72.32	30.281		
25	7675.240	13025.324	7674.183	13027.117
	^RR Branch		^RQ Branch	
1	7615.552	13127.412		
2	14.15	29.828		
3	12.745	32.251	7611.584	13134.254
4	11.364	34.634		
5	10.06	36.885	08.91	38.870
6	7608.82	13139.025		
14			01.240	52.128
17			7599.550	13155.053

TABLE 3—*Continued*

1–0 BAND

λλ 6876.972–6920.149; Intensity—4

K''	λ_{air}	ν_{vac}	λ_{air}	ν_{vac}
	^{P}P Branch		^{P}Q Branch	
4	6897.352	14494.319	.....	.....
5	98.918	91.029	6897.946	14493.071*
6	6900.543	87.616	99.596	89.605
7	02.230	84.075	6901.271	86.088*
8	.....	.....	03.040	82.376*
9	05.786	76.617	.....	.....
10	07.655	72.700*	06.728	74.643
11	.....	.....	.....	.....
12	.....	.....	10.648	66.432
13	13.615	60.224	6912.73	14462.075*
14	.....	.....	.....	.....
15	.....	.....	.....	.....
16	6920.149	14444.484*	.....	.....
	^{R}R Branch		^{R}Q Branch	
1	.....	.....	6888.323	14513.317
2	6888.000	14513.998*	87.154	15.781
3	87.000	16.105*	86.048	18.112
4	.....	.....	85.004	20.314*
5	85.004	20.314*	84.041	22.345*
6	84.041	22.345*	83.108	24.313*
7	83.230	24.056	82.277	26.067
8	82.447	25.708*	81.463	27.785*
9	.....	.....	80.757	29.276
10	81.054	28.649*	80.08	30.705
11	80.446	29.933	79.481	31.971*
12	.....	.....	.....	.....
13	79.393	32.157*	78.436	34.179
14	.....	.....	77.991	35.119*
15	78.630	33.769	.....	.....
16	78.315	34.434	.....	.....
17	6877.991	14535.119*	6876.972	14537.273

* Either unresolved blend with another oxygen line, with a solar line, or with a telluric line (probably due to water vapor) or so close to such a line that the wave length is probably affected by it.

magnetic dipole or electric quadrupole radiation. The observed four branches of the red atmospheric oxygen bands can be accounted for only by the selection rules for magnetic dipole radiation,

$$\Delta J = 0, \pm 1 \qquad (J = 0 \leftarrow\!\!+\!\!\rightarrow J = 0) \; + \longleftrightarrow +\,, \quad - \longleftrightarrow -\,, \quad - \leftarrow\!\!+\!\!\rightarrow + \;. \tag{1}$$

The corresponding transitions are indicated in Figure 2 by full lines. There is an ${}^{R}R$ branch ($\Delta J = +1$, $\Delta K = +1$), a ${}^{P}P$ branch ($\Delta J = -1$, $\Delta K = -1$), an ${}^{R}Q$ branch ($\Delta J = 0$, $\Delta K = +1$), and a ${}^{P}Q$ branch ($\Delta J = 0$, $\Delta K = -1$). In the $O^{16}O^{18}$ and $O^{16}O^{17}$ molecules the alternate rotational levels, with even values of K'', are present on account of the unequal masses of the atomic nuclei, but these even levels are absent in the symmetrical O_2^{16} molecule.

The over-all intensity of the bands is even less than that expected for ordinary magnetic dipole radiation. As Van Vleck[12] pointed out, this is due to the fact that, in addition, they represent a singlet-triplet intercombination.

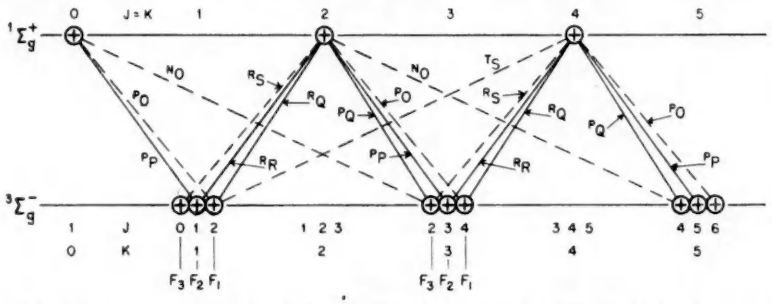

FIG. 2.—Combinations associated with branches of the red system of atmospheric oxygen bands of O_2^{16}. Branches corresponding to the dashed lines have not been observed. Spectra of $O^{16}O^{18}$ and $O^{16}O^{17}$ contain additional combinations, homologous to the full lines in the figure, among the alternate levels.

The selection rules for electric quadrupole radiation are:

$$\Delta J = 0, \pm 1, \pm 2\,; \qquad J = 0 \leftarrow\!\!+\!\!\rightarrow J = 0\,, \qquad J = 1 \leftarrow\!\!+\!\!\rightarrow J = 0\,;$$
$$+ \longleftrightarrow +\,, \quad - \longleftrightarrow -\,, \quad + \leftarrow\!\!+\!\!\rightarrow -\,. \tag{2}$$

Accordingly, all the branches which are observed as magnetic dipole transitions are also possible as quadrupole radiation. In addition, branches with $\Delta J = \pm 2$ should occur. The latter are indicated in Figure 2 by broken lines. Of these, the transitions with $\Delta J = \pm 2$, $\Delta K = \pm 1$, almost coincide with the magnetic dipole ${}^{R}Q$ and ${}^{P}Q$ lines, since the F_1 and F_3 levels of the ${}^3\Sigma_g^-$ state lie very close together (see sec. F). These lines could hardly be observed even under the most favorable circumstances, since the intensity of the electric quadrupole lines is only one-thousandth to one ten-thousandth[23] the intensity of the magnetic dipole lines. On the other hand, the electric quadrupole lines with $\Delta J = +2$, $\Delta K = \pm 3$, are about three times as widely spaced as are the magnetic dipole lines and are well separated from them. In fact, lines of the ${}^{T}S$ branch ($\Delta J = +2$, $\Delta K = +3$) should occur in the region beyond the band head, where no masking is possible by the much stronger magnetic dipole lines. However, they have not as yet been observed.

D. DETERMINATION OF THE ROTATIONAL AND VIBRATIONAL CONSTANTS OF O_2^{16}

As indicated in Figure 2, the three components of the ${}^3\Sigma_g^-$ ground state of oxygen are designated by F_1, F_2, and F_3, according as $J = K + 1$, $J = K$, and $J = K - 1$. The

^{P}P and ^{R}R branches of the red atmospheric bands correspond to transitions from the F_2 component, the ^{R}Q and ^{P}Q branches to transitions from the F_1 and F_3 components, respectively. According to the theory developed by Kramers[4] and by Schlapp[5] (see sec. F), the F_2 component follows the formula for the ordinary nonrigid rotator

$$F_2(K) = BK(K+1) - DK^2(K+1)^2 + \ldots , \tag{3}$$

while F_1 and F_3 follow more complicated formulae containing F_2 and additional terms. The rotational constants B and D can therefore be determined by an analysis of the ^{P}P and ^{R}R branches only. The ^{P}Q and ^{R}Q branches have to be taken into consideration only for the discussion of the triplet-splitting in the ground state.

TABLE 4

SPACING OF ROTATIONAL LEVELS FOR O_2^{16}, $^3\Sigma_g^-$ STATE, $v''=0$
(Unit = 1 Cm^{-1})

K	Δ_2F_2'' (OBSERVED)*				Δ_2F_2'' (COMPUTED)	O−C
	0–0	1–0	2–0	Mean		
2	14.382	14.380	14.380	14.381	14.372	+0.009
4	25.875	25.878	25.875	25.876	25.876	0
6	37.371	37.374	37.372	37.372	37.371	+ .001
8	48.862	48.853	48.861	48.859	48.860	− .001
10	60.335	60.333	60.340	60.336	60.340	− .004
12	71.810	71.805	71.812	71.809	71.811	− .002
14	83.269	83.286†	83.270	83.270	83.270	0
16	94.707	94.710	94.717	94.711	94.716	− .005
18	106.146	106.186†	106.146	106.146	106.146	0
20	117.591†	117.557†	117.573	117.565	117.558	+ .007
22	128.944	128.958	128.957	128.953	128.951	+ .002
24	140.313	140.321	140.332	140.322	140.323	− .001
26	151.713†	151.603†	.....	.....	151.671	.....
28	163.022†	.....	163.025	163.025	162.995	+ .030
30	174.256†	174.284	174.381†	174.284	174.292	− .008
32	.....	185.542	.....	185.542	185.560	− .018
34	.....	196.760	.....	196.760	196.797	−0.037

* $\Delta_2F_2''(K) = {}^{R}R(K-1) - {}^{P}P(K+1)$.

† Omitted from the means or given low weight because one or both lines involved are blends.

For the determination of the rotational constants of O_2^{16}, only the most accurately measured bands, namely, 0–0, 1–0, 2–0, 3–0, and 1–1 were used. Of these, the rather weak 3–0 band was disregarded in the determination of the constants of the lower state, since these could be determined more accurately from the 0–0, 1–0, and 2–0 bands alone.

As is well known, the combination differences,

$$\Delta_2F_2''(K) = {}^{R}R(K-1) - {}^{P}P(K+1), \tag{4}$$

should agree for bands with the same lower state. Table 4, which contains these differences formed from the observed wave numbers of the 0–0, 1–0, and 2–0 bands, shows that this condition is very accurately fulfilled. With very few exceptions, the agreement is within 0.005 cm^{-1}, an accuracy only rarely obtained in measurements of band spectra.

From equation (3) it follows that

$$\begin{aligned}\Delta_2F_2''(K) &= F_2''(K+1) - F_2''(K-1) \\ &= (4B'' - 6D'')(K+\tfrac{1}{2}) - 8D''(K+\tfrac{1}{2})^3\end{aligned} \tag{5}$$

and

$$\frac{\Delta_2 F_2''(K)}{K+\frac{1}{2}} = (4B'' - 6D'') - 8D''(K+\tfrac{1}{2})^2 . \tag{5a}$$

By plotting $\Delta_2 F_2''(K)/(K+\frac{1}{2})$ against $(K+\frac{1}{2})^2$, using the mean values of $\Delta_2 F_2''(K)$ obtained from the 0–0, 1–0, and 2–0 bands, the rotational constants,

$$B_0'' = 1.43777_0 \pm 0.000015 \text{ cm}^{-1}$$

and

$$D_0'' = (4.91_3 \pm 0.020) \times 10^{-6} \text{ cm}^{-1} ,$$

were obtained.[24]

In the two last columns of Table 4 the $\Delta_2 F_2''(K)$ values, computed with these constants according to equation (5), and their deviations from the mean observed values are given. For all K values up to $K = 24$ these deviations are well below 0.01 cm^{-1}.

The same method was less satisfactory when applied to the determination of the rotational constants B and D of the vibrational level $v'' = 1$ of the lower electronic state and of the levels $v' = 0$, 1, 2, and 3 of the upper electronic state, because many fewer accurately measured lines were available to form the combination differences.

On the other hand, the *differences* between the rotational constants of the upper and lower states of a band, that is $B' - B''$ and $D' - D''$, can be determined from the sums of the lines of the R and P branches according to the equation

$$\tfrac{1}{2}[{}^R R(K) + {}^P P(K)] = (\nu_0 + B' - 2D') + (B' - B'' - 6D')K(K+1) - (D' - D'')K^2(K+1)^2 . \tag{6}$$

By plotting the observed values of the left-hand side of this equation against $K(K+1)$, we obtain a curve whose intercept with the ordinate axis gives $(\nu_0 + B' - 2D')$, whose initial slope gives $(B' - B'' - 6D')$ and whose curvature gives $(D' - D'')$.

The values obtained in this way are only approximate. If, with their aid, again using the observed values $[{}^R R(K) + {}^P P(K)]$, the quantities

$$\frac{\tfrac{1}{2}[{}^R R(K) + {}^P P(K)] - (\nu_0 + B' - 2D')}{K(K+1)}$$

are calculated and plotted against $K(K+1)$, it is readily seen from equation (6) that a straight line is obtained whose slope is $(D' - D'')$ and whose intercept with the ordinate axis is $(B' - B'' - 6D')$.

If the improved values for B' and D' thus derived are substituted in the right-hand side of equation (6) and the differences between these calculated and the observed values of $\frac{1}{2}[{}^R R(K) + {}^P P(K)]$ are plotted against $K(K+1)$, final corrections to the values $(\nu_0 + B' - 2D')$, $(B' - B'' - 6D')$, and $(D' - D'')$ are obtained.

The accuracy of the $(B' - B'')$ and $(D' - D'')$ values determined in this way is greater than the accuracy of the individual rotational constants obtained from the combination differences. It is therefore best to determine only one pair of rotational constants, B and D, from combination differences and all the others from the $(B' - B'')$ and $(D' - D'')$ values, especially if there is one state, as in the present case the one with $v'' = 0$, for which the combination differences are known with particular accuracy.

The final values of B', B'', D', and D'' obtained by this method are given in Table 5, those of ν_0 in Table 6. The band origins of Table 6 refer to the nonexisting rotational F_2

[24] For a more detailed discussion of the method see G. Herzberg, *Molecular Spectra and Molecular Structure*, Vol. I (New York: Prentice-Hall Inc., 1939).

level, $K = 0$, $J = 0$. As indicated by the number of significant figures given, the accuracy of the values of B_3', D_3', $\nu_0(2, 1)$, and $\nu_0(3, 1)$ is appreciably smaller than that of the other constants.[25]

In order to check the accuracy of the calculations, the ${}^PP$ and ${}^RR$ branches of all the bands measured were computed with the constants given in Tables 5 and 6. The deviations from the observed values of well-measured lines (that is, all lines except blends and a few lines with high J values) are well within 0.01 cm^{-1} for the 0–0 band and within 0.02 cm^{-1} for the 1–0, 2–0, and 1–1 bands. For the weak 3–0, 2–1, and 3–1 bands

TABLE 5

INDIVIDUAL ROTATIONAL CONSTANTS OF THE ${}^3\Sigma_g^-$ AND ${}^1\Sigma_g^+$ STATES OF O_2^{16}

(Unit = 1 Cm^{-1})

	${}^3\Sigma_g^-$ State	${}^1\Sigma_g^+$ State
B_0	1.43777_0	1.39132_8
B_1	1.42197_9	1.37305_4
B_2	.....	1.35473_1
B_3	.....	1.33620
D_0	$4.91_3\times10^{-6}$	$5.40_9\times10^{-6}$
D_1	$4.82_5\times10^{-6}$	$5.45_8\times10^{-6}$
D_2	.....	$5.56_7\times10^{-6}$
D_3	.....	$5.6_1\times10^{-6}$

TABLE 6

ZERO LINES ν_0 OF THE ${}^1\Sigma_g^+$–${}^3\Sigma_g^-$ BAND SYSTEM OF O_2^{16}

(Unit = 1 Cm^{-1})

v'	v''	
	0	1
0	13120.9080	.....
1	14525.6602	12969.274_4
2	15902.4156	14346.030
3	17251.109_6	15694.7_6

the agreement is not so good but is still satisfactory. No systematic trend is noticeable in the deviations. It is therefore unnecessary to introduce a term $HK^3(K+1)^3$ in formula (3).

If, in the usual way, the values B_v and D_v of Table 5 are represented by the formulae,

$$B_v = B_e - \alpha_e(v+\tfrac{1}{2}) + \gamma_e(v+\tfrac{1}{2})^2 + \dots, \tag{7}$$

$$D_v = D_e + \beta(v+\tfrac{1}{2}) + \dots, \tag{8}$$

the rotational constants given in Table 7 are obtained.

The constants B_0, B_1, and B_2 of the ${}^1\Sigma_g^+$ state are represented by formula (7) with the values for B_e, α_e, and γ_e as given in Table 7 within an accuracy of 0.00001 cm^{-1}, the less accurately determined constant B_3 within 0.0001 cm^{-1}.

[25] The last decimal is printed in full size when the accuracy is well within one unit of the next to the last decimal. If the accuracy is less, the last decimal is a subscript.

The vibrational constants given in Table 7 correspond to the usual representation of the zero lines by a formula,

$$\nu_0(v'v'') = \nu_e + \omega_e'(v'+\tfrac{1}{2}) - \omega_e'x_e'(v'+\tfrac{1}{2})^2 + \omega_e'y_e'(v'+\tfrac{1}{2})^3 \ldots - \omega_e''(v''+\tfrac{1}{2}) + \omega_e''x_e''(v''+\tfrac{1}{2})^2 - \omega_e''y_e''(v''+\tfrac{1}{2})^3 \ldots . \quad (9)$$

Since in the red atmospheric band system no bands occur with $v'' > 1$, ω_e'' was determined from $\Delta G_{1/2}''$ with the aid of the constants $\omega_e''x_e''$, $\omega_e''y_e''$, and $\omega_e''z_e''$, derived by Curry and Herzberg from an analysis of the Schumann-Runge bands.[26] The value $\Delta G_{1/2}''$ itself

TABLE 7

CONSTANTS OF THE O_2^{16} MOLECULE*†

	$^3\Sigma_g^-$ State	$^1\Sigma_g^+$ State
$A_0=\nu_{00}$		13120.9080 cm^{-1}
ν_e		13195.2221 cm^{-1}
$\Delta G_{\frac{1}{2}}$	1556.3856 cm^{-1}	1404.7521 cm^{-1}
ω_e	1580.3613 cm^{-1}	1432.6874 cm^{-1}
$\omega_e x_e$	12.0730 cm^{-1}‡	13.95008 cm^{-1}
$\omega_e y_e$	0.0546 cm^{-1}‡	−0.01075 cm^{-1}
$\omega_e z_e$	−0.00143 cm^{-1}‡	
k_e	$11.7664_1\times10^5$ dynes/cm	$9.6701_7\times10^5$ dynes/cm
D_0 (diss. energy)	5.081 e.v.§	3.455 e.v.
B_0	1.43777_0 cm^{-1}	1.39132_0 cm^{-1}
B_e	1.44566_6 cm^{-1}	1.40041_6 cm^{-1}
a_e	0.01579_1 cm^{-1}	0.01817_0 cm^{-1}
γ_e		-0.00004_3 cm^{-1}
D_0 (rot. const.)	$4.91_3\times10^{-6}$ cm^{-1}	$5.39_5\times10^{-6}$ cm^{-1}
D_e (rot. const.)	$4.95_7\times10^{-6}$ cm^{-1}	$5.35_6\times10^{-6}$ cm^{-1}
β	$0.08_8\times10^{-6}$ cm^{-1}	$0.07_7\times10^{-6}$ cm^{-1}
I_0	$19.4652_1\times10^{-40}$ gm cm^2	$20.1136_3\times10^{-40}$ gm cm^2
I_e	$19.3589_6\times10^{-40}$ gm cm^2	$19.9844_2\times10^{-40}$ gm cm^2
r_0	$1.21071_5\times10^{-8}$ cm	$1.23075_9\times10^{-8}$ cm
r_e	$1.20740_4\times10^{-8}$ cm	$1.22675_6\times10^{-8}$ cm

* The last decimal is printed in full size when the accuracy is well within one unit of the next to the last decimal. If the accuracy is less, the last decimal is a subscript.

† R. T. Birge, *Phys. Soc. London, Reports on Progress in Physics*, **8**, 90, 1941.

‡ Curry and Herzberg, *Ann. d. Phys.*, **19**, 800, 1934.

§ G. Herzberg, *Molecular Spectra and Molecular Structure*, Vol. I.

could be obtained from the zero lines with considerable accuracy. The value obtained as difference between $\nu_0(1, 1)$ and $\nu_0(1, 0)$ and the value obtained as difference between $\nu_0(2, 1)$ and $\nu_0(2, 0)$ agree within 0.0002 cm^{-1}. Even though this perfect agreement may be accidental, it is believed that the $\Delta G_{1/2}''$ value is accurate within 0.001 cm^{-1}. Similar remarks hold for the vibrational quanta of the upper state.

The definition of the quantities given in Table 7 and the notation used are in agreement with general usage (see, e.g., G. Herzberg[24]). For example, quantities with subscript 0 refer to the lowest vibrational level; quantities with subscript e to the nonexisting vibrationless level. The first two entries in Table 7 refer to the energy of electronic excitation; the next six concern the vibrational energy. The dissociation energy, D_0'', for the $^3\Sigma_g^-$ state is the value given by G. Herzberg,[24] recalculated with the more recent values for the basic physical constants (see below). The dissociation energy, D_0', for the $^1\Sigma_g^+$ state was obtained by subtracting the electronic excitation energy ν_{00} from the dissociation energy of the $^3\Sigma_g^-$ state.

[26] *Ann. d. Phys.*, **19**, 800, 1934.

B, α, γ, D (rotational constant), and β concern the energy of rotation, including the effect of centrifugal stretching of the molecule with increase of angular momentum. The moments of inertia, I, and the internuclear distances, r, were determined from the rotational constants in the usual way. (Attention is called to the use of D in two different senses, a peculiarity of the notation which has become fixed in the literature.)

Values of the basic physical constants used in deriving Table 7 are those adopted by R. T. Birge,[27] such as wave length associated with one absolute volt = 12395.4×10^{-8} cm; and $h/8\pi^2c = 27.9865 \times 10^{-40}$ gm. cm.

TABLE 8

CONSTANTS OF THE $^3\Sigma_g^-$ AND THE $^1\Sigma_g^+$ STATES OF $O^{16}O^{18}$

(Unit = 1 Cm^{-1})

	$^3\Sigma_g^-$ STATE		$^1\Sigma_g^+$ STATE	
	Observed	Computed	Observed	Computed
$A_0 = \nu_0(0, 0)$	.....	.....	13122.98_6	13123.0194
$\nu_0(1, 0)$	.....	.....	14488.8_4	14488.8741
$\Delta G_{\frac{1}{2}}$	.....	.....	1365.8_5	1365.8547
B_0	1.3579_3	1.357932	1.3141_2	1.314100
B_1	.....	.....	1.2974_0	1.297350
D_0	$4.4_2 \times 10^{-6}$	4.381×10^{-6}	$5.0_5 \times 10^{-6}$	4.811×10^{-6}

TABLE 9

CONSTANTS OF THE $^3\Sigma_g^-$ AND THE $^1\Sigma_g^+$ STATES OF $O^{16}O^{17}$

(Unit = 1 Cm^{-1})

	$^3\Sigma_g^-$ STATE		$^1\Sigma_g^+$ STATE	
	Observed	Computed	Observed	Computed
$A_0 = \nu_0(0, 0)$	.....	.....	13121.97_8	13122.0207
$\nu_0(1, 0)$	.....	.....	14506.2_6	14506.2820
$\Delta G_{\frac{1}{2}}$	.....	.....	1384.2_8	1384.2613
B_0	1.395_8	1.395417	1.352_0	1.350357
B_1	.....	.....	1.333_1	1.332906

E. DETERMINATION OF THE ROTATIONAL AND VIBRATIONAL CONSTANTS OF THE ISOTOPIC MOLECULES $O^{16}O^{18}$ AND $O^{16}O^{17}$

In the spectra of the isotopic molecules $O^{16}O^{18}$ and $O^{16}O^{17}$, only the 0–0 and 1–0 bands were measured (Tables 2 and 3). The rotational constants and zero lines given in Tables 8 and 9 were determined by the methods used in the analysis of the O_2^{16} bands. Because of the low intensity of the isotopic bands and the very frequent occurrence of blends, the accuracy as a whole is much lower than that of the constants of O_2^{16}.

In addition to the observed values of the molecular constants of $O^{16}O^{18}$ and $O^{16}O^{17}$,

[27] *Phys. Soc. London, Reports on Progress in Physics*, **8**, 90, 1941.

Tables 8 and 9 contain the values computed from the theoretical formulae for the isotope effect by means of the constants of O_2^{16}. The following relations were used:

$$B_e^i = \rho^2 B_e\,; \qquad a_e^i = \rho^3 a_e\,; \qquad D^i = \rho^4 D\,; \qquad \gamma_e^i = \rho^4 \gamma_e \tag{10}$$

$$\begin{aligned} {}^i = \nu_e &+ \rho\omega_e'\,(v'+\tfrac{1}{2}) - \rho^2\omega_e' x_e'\,(v'+\tfrac{1}{2})^2 + \dots \\ &- \rho\omega_e''\,(v''+\tfrac{1}{2}) + \rho^2\omega_e'' x_e''\,(v''+\tfrac{1}{2})^2 - \dots\,, \end{aligned} \tag{11}$$

where the superscript i refers to the heavier isotopic molecule and where

$$\rho = \sqrt{\frac{\mu}{\mu^i}} \qquad (\mu = \text{reduced mass})\,.$$

Using the mass values $O^{16} = 16.00000$, $O^{18} = 18.00485$,[28] and $O^{17} = 17.00450$,[28] we obtained and used the following values for ρ:

$$\rho\,(O^{16}O^{18}) = 0.9717637\,; \qquad \rho\,(O^{16}O^{17}) = 0.9851212\,.$$

The agreement between the observed and the computed values of the molecular constants of the isotopic molecules (Tables 8 and 9) is very satisfactory. The very slight systematic deviations from the calculated values in the case of $\nu_0(0, 0)$ and $\nu_0(1, 0)$ are probably due to the fact that the value of $\omega_e'' x_e''$ (Table 7), which had to be used in the determination of ν_e, is not exact. A more accurate value for $\omega_e'' x_e''$ is not available, since no bands with v'' between 2 and 12 have yet been measured.

It should perhaps be emphasized that, with the exception of the values for $\nu_0(0, 0)$ and $\nu_0(1, 0)$, the computed values of the molecular constants of the isotopic molecules are of higher accuracy than are the observed ones.

If the values of the constants in Table 8 are recomputed, using $O^{18} = 18.00369$,[29] the agreement with observation is not quite so close as that shown in the table.

F. TRIPLET-SPLITTING OF THE ${}^3\Sigma_g^-$ GROUND STATE OF THE O_2 MOLECULE

Schlapp[5] has given theoretical expressions for the energy of the three component levels of a ${}^3\Sigma$ state:[30]

$$\begin{aligned} F_3 &= W_0 - (2K-1)B - \lambda + [(2K-1)^2B^2 + \lambda^2 - 2\lambda B]^{1/2} - \gamma K && (J = K-1)\,, \\ F_2 &= W_0\,, && (J = K)\,, \\ F_1 &= W_0 + (2K+3)B - \lambda - [(2K+3)^2B^2 + \lambda^2 - 2\lambda B]^{1/2} + \gamma(K+1) && (J = K+1)\,. \end{aligned} \tag{12}$$

Here $W_0 = F_2$ is given by formula (3); λ and γ are two numerical parameters: λ, in a first approximation, is a measure of the spin-spin interaction of the uncompensated electrons and γ of the interaction of the uncompensated electron spin with the magnetic field due to the rotation of the molecule. The symbol γ here is to be distinguished from γ as used in Table 7.

According to H. A. Kramers,[31] the spin-spin interaction of the uncompensated elec-

[28] Flügge and Mattauch, *Phys. Zs.*, **43**, 1, 1942.

[29] Livingston and Bethe, *Rev. Mod. Phys.*, **9**, 245, 1937.

[30] In Schlapp's paper the energy levels F_1, F_2, and F_3 are called "W_{K+1}," "W_K," and "W_{K-1}," respectively.

[31] *Zs. f. Phys.*, **53**, 422, 1929.

trons is mathematically equivalent to an interaction of the total spin with the axis of figure of the molecule. The presence of the parameter λ is therefore an indication of the fact that the molecule does not belong completely to Hund's case *b*.

In the case of the ground state of the O_2 molecule, Schlapp obtained the values

$$\lambda = 1.985 \text{ cm}^{-1} \quad \text{and} \quad \gamma = -0.008 \text{ cm}^{-1}$$

from Dieke and Babcock's[1] measurements of the red atmospheric band system. The new measurements presented here (Tables 1–3) make it possible to redetermine these constants with higher accuracy. This was done for the vibrational levels with $v'' = 0$

TABLE 10*

TRIPLET-SPLITTING OF THE $^3\Sigma_g^-$ GROUND STATE OF O_2^{16}: $v'' = 0$

K''	$F_2-F_3={}^PP(K)-{}^PQ(K)$			$F_2-F_1={}^RR(K)-{}^RQ(K)$		
	Observed Mean	Computed $\gamma=-0.008$ $\lambda=1.985$	Computed $\gamma=-0.00837$ $\lambda=1.984$	Observed Mean	Computed $\gamma=-0.008$ $\lambda=1.985$	Computed $\gamma=-0.00837$ $\lambda=1.984$
1	.....	3.9620	3.9596	1.873_2	1.8770	1.8766
3	2.084_8	2.0850	2.0830	1.952_0	1.9485	1.9490
5	2.012_3	2.0135	2.0107	1.987_2	1.9856	1.9868
7	1.976_4	1.9764	1.9728	2.014_8	2.0128	2.0148
9	1.947_8	1.9492	1.9449	2.041_9	2.0357	2.0384
11	1.921_0	1.9263	1.9212	2.064_5	2.0564	2.0598
13	1.901_3	1.9056	1.8998	2.081_8	2.0758	2.0799
15	1.880_7	1.8862	1.8797	2.104_2	2.0944	2.0993
17	1.859_5	1.8676	1.8604	2.124_4	2.1124	2.1180
19	1.844_2	1.8496	1.8416	2.128_0	2.1300	2.1364
21	1.823_0	1.8320	1.8232	2.165_6	2.1473	2.1545
23	1.816_5	1.8147	1.8052	2.180_3	2.1645	2.1723
25	1.784_7	1.7975	1.7873	.....	2.1814	2.1900
27	1.770_4	1.7806	1.7696	2.205_5	2.1982	2.2076
29	1.760_2	1.7638	1.7521	2.228_2	2.2149	2.2250
31	1.740_0	1.7471	1.7346	.....	.....	.....
33	1.720_5	1.7305	1.7173	.....	.....	.....
35	1.686_5	1.7140	1.7000	.....	.....	.....
37	1.688_4	1.6974	1.6827	.....	.....	.....
39	1.645_0	1.6810	1.6656	.....	.....	.....

* Unit = 1 cm^{-1}.

and 1 of the electronic ground state of O_2^{16}, as well as for the levels with $v'' = 0$ of the ground states of $O^{16}O^{18}$ and $O^{16}O^{17}$.

The separations of the triplet components are given by the term differences,

$$\begin{aligned} {}^PP(K) - {}^PQ(K) &= F_2 - F_3 , \\ {}^RR(K) - {}^RQ(K) &= F_2 - F_1 . \end{aligned} \tag{13}$$

These term differences are given for the $v'' = 0$ and $v'' = 1$ levels of O_2^{16} in Tables 10 and 11. The values given for $v'' = 0$ are mean values obtained from the 0–0, 1–0, and 2–0 bands; the values given for $v'' = 1$ are those obtained from the 1–1 band. Only unblended lines were used to form the term differences.

The third and sixth columns of Table 10 contain the triplet-splittings computed with the aid of equation (12) with the values of the parameters λ and γ given by Schlapp and the new B_0'' value from Table 7. It can be seen that there is a slight, but systematic,

difference between observed and computed values. This systematic difference can be made to disappear by choosing for the parameters the values

$$\lambda = 1.984 \text{ cm}^{-1}, \qquad \gamma = -0.00837 \text{ cm}^{-1}.$$

The splittings calculated according to equation (12) with these parameters are given in the fourth and seventh columns of Table 10.

The agreement between the observed and the computed values is very satisfactory indeed and gives confidence that the extrapolation of Schlapp's formula (12) to the F_3 state with $K = 1, J = 0$, is reliable. The position of this state cannot be obtained from the atmospheric oxygen bands but could be found from the ultraviolet bands, if lines with $K = 1$ were completely resolved.

TABLE 11*

TRIPLET-SPLITTING OF THE $^3\Sigma_g^-$ GROUND STATE OF O_2^{16}: $v'' = 1$

K''	$F_2-F_3={}^PP(K)-{}^PQ(K)$		$F_2-F_1={}^RR(K)-{}^RQ(K)$	
	Observed	Computed $\gamma=-0.00837$ $\lambda=1.993$	Observed	Computed $\gamma=-0.00837$ $\lambda=1.993$
1	.....	3.9776	1.904_7	1.8895
3	.....	2.1882	1.958_4	1.9601
5	2.012_8	2.0176	1.997_1	1.9973
7	1.975_5	1.9803	.....	2.0249
9	1.943_2	1.9528	2.057_0	2.0483
11	1.929_3	1.9293	.....	2.0696
13	1.906_5	1.9075	2.089_3	2.0897
15	1.886_0	1.8880	.....	2.1089
17	1.870_1	1.8687	.....	2.1276
19	1.857_5	1.8500	2.149_2	2.1459
21	1.833_0	1.8317	.....	2.1639
23	1.828_6	1.8137	2.196_9	2.1818
25	1.74_8	1.7959	.....	.....

* Unit = 1 cm^{-1}.

The separations of the F_1 and F_3 levels from the F_2 levels have recently taken on new interest, since they give directly the wave lengths of the magnetic dipole spectrum of oxygen in the micro-wave region. This spectrum has been investigated experimentally by R. Beringer[32] and theoretically by J. H. Van Vleck.[33] Beringer found an absorption maximum of O_2 in the region $\lambda = 0.5$ cm ($\nu = 2$ cm^{-1}), and Van Vleck, using the data of Table 10, interpreted this absorption as an unresolved band consisting of the transitions $F_2(K) - F_1(K)$ for $K = 1, 3, 5, \ldots$, and $F_2(K) - F_3(K)$ for $K = 3, 5, 7, \ldots$. A secondary maximum, so far not investigated experimentally, ought to occur in the region $\lambda = 0.25$ cm ($\nu = 3.960$ cm^{-1}), corresponding to the transition $F_2(K) - F_3(K)$ for $K = 1$.

If the triplet-splittings in the $v'' = 1$ level are calculated with the same parameters λ and γ as for $v'' = 0$, but, of course, with B_1'' instead of B_0'', a slight systematic difference from the observed values of Table 11 is found. This can be corrected by changing the parameter λ to

$$\lambda = 1.993 \text{ cm}^{-1}.$$

[32] *Phys. Rev.*, **70**, 53, 1946.

[33] *Phys. Rev.*, **71**, 413, 1947.

The splittings computed with this changed value of λ and the same value of γ as before are given in the third and fifth columns of Table 11. The slight increase of λ in going from $v'' = 0$ to $v'' = 1$ corresponds to a strengthening of the coupling of the spin to the internuclear axis, that is, a greater deviation from Hund's case *b*.

In Table 12 the observed and computed triplet-splittings in the $v'' = 0$ level of the isotopic molecule $O^{16}O^{18}$ are given. The computed values were obtained by substituting $\lambda = 1.984\ \text{cm}^{-1}$, $\gamma = -0.00740\ \text{cm}^{-1}$, and $B = B_0'' = 1.35793\ \text{cm}^{-1}$ in equation (12).

TABLE 12*

TRIPLET-SPLITTING OF THE $^3\Sigma_g^-$ GROUND STATE OF $O^{16}O^{18}$: $v'' = 0$

K	$F_2-F_3=\,^PP(K)-\,^PQ(K)$		$F_2-F_1=\,^RR(K)-\,^RQ(K)$	
	Observed	Computed $\gamma=-0.00740$ $\lambda=1.984$	Observed	Computed $\gamma=-0.00740$ $\lambda=1.984$
1	.....	3.9606	1.886_3	1.8910
2	2.135_3	2.1515	1.943_3	1.9295
3	2.083_7	2.0696	1.945_2	1.9541
4	2.017_0	2.0311	1.966_0	1.9723
5	2.013_0	2.0066	2.002_9	1.9872
6	.....	1.9883	.....	2.0001
7	1.980_1	1.9734	2.018_9	2.0117
8	1.961_1	1.9605	2.008_2	2.0225
9	1.942_2	1.9489	2.034_3	2.0325
10	.....	1.9382	2.049_5	2.0422
11	1.928_0	1.9281	2.040_9	2.0514
12	1.915_9	1.9185	2.067_0	2.0604
13	1.907_0	1.9092	.....	.....
14	1.893_9	1.9002	.....	.....
15	1.891_0	1.8914	.....	.....
16	1.876_2	1.8829	.....	.....
17	1.825_5	1.8744	.....	.....
18	1.851_6	1.8661	.....	.....
19	1.864_4	1.8579	.....	.....
20	1.861_1	1.8497	.....	.....
21	.....	1.8416	.....	.....
22	.....	1.8336	.....	.....
23	1.821_4	1.8257	.....	.....
24	1.830_0	1.8178	.....	.....
25	1.761_0	1.8099	.....	.....
26	1.805_2	1.8021	.....	.....
27	.....	1.7943	.....	.....
28	1.763_9	1.7865	.....	.....

* Unit = $1\ \text{cm}^{-1}$.

The agreement between the observed and the computed values is within the accuracy of the measurements (which is lower than for O_2^{16}). If, instead of the above value for γ, the one used for O_2^{16} ($\gamma = -0.00837\ \text{cm}^{-1}$) is substituted, a systematic deviation is found.

It is significant that the value of λ is unchanged, while γ changes in going from O_2^{16} to $O^{16}O^{18}$. This is in agreement with theoretical expectation. Since, in a first approximation, the electronic structure of a molecule and the nuclear separation are not affected by a small change in the masses of the nuclei, the interaction of the electron spin with the internuclear axis in the nonrotating and nonvibrating molecule and, consequently, the parameter λ should be the same for different isotopic molecules.[34] The influence of the

[34] The effect expected because of the change in the zero-point vibration is too small to be detected with the present accuracy.

nuclear masses on the rotational decoupling of the spin from the axis is accounted for by the changed value of B, substituted in formula (12).

On the other hand, the constant γ, representing the magnetic coupling between the electron spin and the axis of rotation, will be different for different isotopic molecules, since the magnetic moment produced by the rotation varies with the nuclear masses because of the change in angular velocity. N. F. Ramsey[35] found experimentally that the magnetic moments of the hydrogen isotopes, H_2, HD, and D_2, vary in proportion to the inverse reduced mass, that is, simply in proportion to the angular velocity of the molecule as a whole.

In the case of a molecule like O_2 with more than two electrons, one cannot expect such a simple relation to hold. As G. C. Wick[36] has shown, the electrons do not rotate rigidly with the molecule but "slip back." Therefore, the influence of the inner shells on the magnetic moments of isotopic molecules may be rather complicated.

TABLE 13*

TRIPLET-SPLITTING OF THE $^3\Sigma_g^-$ GROUND STATE OF $O^{16}O^{17}$

K	$F_2-F_3={}^PP(K)-{}^PQ(K)$ Observed	$F_2-F_1={}^RR(K)-{}^RQ(K)$ Observed
3	2.085_2	2.003_0
5	.....	1.985_7
6	1.988_6	.....
7	.....	2.011_0
15	1.897_1	.....
17	1.855_4	.....
21	1.770_4	.....
23	1.820_4	.....

* $v'' = 0$; unit = 1 cm^{-1}.

If one assumes that γ depends solely on the inverse reduced mass of the molecule, the constant γ for $O^{16}O^{18}$, calculated from the above value of γ for O_2^{16}, would be

$$\gamma_{\text{comp.}}(O^{16}O^{18}) = 0.00790 ,$$

while the observed value is

$$\gamma_{\text{obs.}}(O^{16}O^{18}) = 0.0074 .$$

The accuracy of the determination of the observed value for $O^{16}O^{18}$ is insufficient to decide whether the deviation from the computed value is significant.

In Table 13 the observed triplet-splitting of $O^{16}O^{17}$ is given. These data are not sufficiently accurate to warrant a separate determination of γ and λ.

We wish to thank Mr. G. Herzberg for his many helpful suggestions as to the methods of evaluation of the measurements and the interpretation of the results.

NOTE ADDED IN PROOF.—The measurements in this paper strongly support the conclusion of St. John and Babcock (*Mt. W. Contr.*, No. 223; *Ap. J.*, **55**, 36, 1922) that the measured wave lengths of atmospheric oxygen lines are remarkably constant.

[35] *Phys. Rev.*, **58**, 226, 1940.

[36] *Zs. f. Phys.*, **85**, 25, 1933.

THE MAGNETIC FIELD OF GAMMA EQUULEI*

HORACE W. BABCOCK
Mount Wilson Observatory
Received May 25, 1948

ABSTRACT

The present status of the observational work on stellar magnetic fields determined through analysis of the Zeeman effect is briefly summarized. The strongest fields have been found in the peculiar stars of types A and early F, particularly in the spectrum variables. Some of the magnetic fields are variable. In γ Equulei, however, there is no conclusive evidence that the field varies; measures of forty-seven lines on each of four or five plates of dispersion 2.9 A/mm give $H_p = 1900 \pm 250$ (p.e.) gauss. The magnetic polarity observed is positive in γ Equ, negative in 78 Virginis. Magnetic moment and rotation in γ Equ are probably antiparallel, as in the earth.

Lines of medium and strong intensity yield a somewhat smaller H_p than do weak lines. This result is interpreted as the effect of the curve of growth on the Zeeman components of the stronger lines.

The proportionality between magnetic moment and angular momentum is briefly discussed, with consideration of variable fields.

INTRODUCTION

The initial measurement of the magnetic field of a star was reported in an earlier paper[1] (referred to later as "Paper I"), in which were presented observations of 78 Virginis, showing that its polar field intensity was about 1500 gauss. The occurrence in axially rotating stars of general magnetic fields of such strength, which seems generally to have been unexpected, has implications not only for astrophysics and cosmogony, but for the study of cosmic rays[1a] and for the theory of magnetism as well. For this reason, the scope of the observing program has been expanded, with the aim of establishing the essential facts of stellar magnetism as far as they are accessible to available instruments.

The possibility of detecting stellar magnetic fields was anticipated at least as early as 1915 by Hale,[2] who held it not improbable, as Schuster had suggested,[3] that every star (and perhaps every rotating body of whatever nature) becomes a magnet through the fact of its rotation. Indeed, it is evident that one of Hale's hopes in planning the 100-inch reflector with its coudé spectrograph was that tests for stellar magnetism could be applied. In 1937, Minnaert foresaw the possibility of detecting the Zeeman effect in the spectrum of the integrated light of a rotating star,[4] but his suggestion was unknown to me until A. D. Thackeray[5] referred to it after my paper on 78 Vir had been published.

To advance the observational work, a preliminary series of spectrograms is being made of sharp-line stars, mostly of early type and brighter than about the sixth magnitude. These plates are made with a double analyzer in front of the slit of the coudé spectrograph of the 100-inch telescope, in such a way that two parallel spectra of the star, analyzed, respectively, for right-handed and left-handed circular polarization, are photographed simultaneously. Detection and measurement of stellar magnetic fields, if stronger than a few hundred gauss, are then possible, as the Zeeman effect in the spectral lines causes differential shifts proportional to the magnetic field strength of the star.

* *Contributions from the Mount Wilson Observatory, Carnegie Institution of Washington*, No. 748.

[1] H. W. Babcock, *Mt. W. Contr.*, No. 727; *Ap. J.*, **105**, 105, 1947.

[1a] H. W. Babcock, *Phys. Rev.*, **74**, 489, 1948.

[2] *Ten Years' Work of a Mountain Observatory* (Carnegie Institution of Washington, 1915), p. 45.

[3] *Proc. R. Inst.*, **13**, 273, 1891; *Report B.A.A.S. for 1892*, p. 634; *Proc. Phys. Soc. London*, **24**, 121, 1912.

[4] *Observatory*, **60**, 292, 1937.

[5] *Observatory*, **67**, 105, 1947.

When, in the course of this survey, stars showing good evidence of a strong magnetic field are found, they are observed repeatedly with the highest feasible dispersion, in order to provide for each such object a series of spectrograms from which a reliable average value of the magnetic field intensity may be determined or which may serve as a basis for the study of variations in field strength or in line intensity.

Up to the present, fields stronger than 1000 gauss have been found in 78 Vir, HD 125248 (BD−18°3789), γ Equ, β Coronae Borealis, HD 188041, and HD 15144 (HR 710).[6] In addition, strong fields are suspected in about twenty other stars, but their spectra are not all equally suitable for measurement, usually because of rotational broadening of the lines. In contrast to the foregoing, many sharp-line stars have been observed in which evidence of a magnetic field is lacking or very small; this group includes some normal A-type main-sequence stars, supergiants, and stars of spectral type later than G. These objects showing no Zeeman effect may be regarded as "controls," adding assurance that the positive results obtained for certain stars are real.

A great many more observations are required before it will be possible to attempt a comprehensive discussion of stellar magnetism in relation to spectral type, rotational velocity, anomalous line intensities, spectrum variability, and related topics. This is particularly evident from the fact that the magnetic field of the spectrum variable HD 125248 has been found to vary periodically over a wide range and even to reverse its polarity;[7] similar variations are suspected for some of the other stars possessing strong fields. There seems to be a marked tendency for strong magnetic fields to occur in the spectrum variables of type A; in fact, HD 125248, 78 Vir, and γ Equ are included in A. J. Deutsch's list of spectrum variables.[8] The fact that some of the fields vary indicates that the observational work connected with recording and describing the phenomena will be extensive.

Of the stars already mentioned as showing evidence of a strong field, γ Equ has been selected for discussion for the following three reasons:

1. Since an examination of the spectrograms with a hand magnifier showed no gross differences in field intensity, the star seemed to present a simpler problem than would a magnetic variable.

2. The lines in the spectrum (Draper type F0p) are numerous, and most metallic lines of moderate or weak intensity are exceedingly sharp; measurement of the differential shift between right-handed and left-handed spectra is therefore comparatively easy. The sharpness further indicates that the axis of stellar rotation is very nearly parallel to the line of sight.

3. γ Equ has an eleventh-magnitude companion for which the direction of orbital revolution is known from the work of double-star observers. Upon the reasonable assumption that the axial rotation of the star is in the same direction, it is possible to determine the sign of the relationship between magnetic moment and rotation or angular momentum.

OBSERVATIONAL MATERIAL AND MEASUREMENTS

Seven plates of γ Equ (R.A. $21^h7^m55^s$, Dec. $+9°56'$, 1950; m_v 4.76; Sp. F0p), listed in Table 1, have been obtained with the analyzer and coudé grating spectrograph. Only the five plates of highest dispersion, taken with the 114-inch camera, are discussed in this section, the spectral region covered with good density being roughly from λ 3900 to λ 4800.

[6] I am indebted to Dr. W. P. Bidelman for directing my attention to HR 710, which was discovered by Miss Nancy Roman at the Yerkes Observatory to be a "peculiar" star.

[7] H. W. Babcock, *Pub. A.S.P.*, **59**, 260, 1947.

[8] *Ap. J.*, **105**, 283, 1947.

The double analyzer for circularly polarized light used in taking these spectrograms was described in Paper I. It has been improved by the addition of a "window" in front of the mica quarter-wave plate and calcite crystal. The width of the window is such that its two images, seen from the back of the calcite, are contiguous; thus purity of polarization in the two spectra is assured even under conditions of poor seeing.

The plates were measured on a comparator having a vertical wire that could be accurately adjusted parallel to the long lines of the comparison spectrum. The difference in scale reading was noted in microns for each line. Emphasis was placed upon obtaining a reliable average value of the field intensity without making an exhaustive series of measurements of all the hundreds of lines on each plate. For this reason very weak or very strong lines were usually avoided, and attention was given largely to lines of moderate intensity which could be measured most accurately. Although most of the measurements were confined to the region λλ 4000–4385, on Ce 4438 they were continued to λ 4919.

TABLE 1

MAGNETIC OBSERVATIONS OF γ EQUULEI

Plate No.	Date	Dispersion (A/Mm)	H_p (Gauss)	Number of Lines Measured
Ce 4433	1946 Oct. 6	10.5	.....	.....
4438	Oct. 7	2.9	1400	124
4695	1947 May 11	4.5	2480	40
4724	June 27	2.9	1960	57
4776	Aug. 1	2.9	2240	61
4842	Sept. 2	2.9	2170	63
4887	Sept. 30	2.9	1810	30

Mean $H_p = 1900 \pm 250$ (p.e.)

In the first two columns of Table 2 are listed the laboratory wave lengths and identifications of the lines, followed in the third column by the theoretical Zeeman effect, averaged for anomalous patterns according to Russell's rule. For most of these lines the predicted effects were computed from the term designations given in Miss C. E. Moore's *Revised Multiplet Table*,[9] with the aid of "Tables of Theoretical Zeeman Effects" by Kiess and Meggers.[10] Where possible, the predicted effects for *Fe* I have been checked against the laboratory measurements of the Zeeman effect given by Miss Weeks;[11] in a few instances where there was disagreement, the laboratory values have been used, with the symbol "W" affixed. The next five columns list the differential measurements in microns for lines on the 114-inch camera plates. The last column gives mean values for the individual lines, which have been corrected to λ 4500; such a correction is necessary because the Zeeman effect varies as the square of the wave length.

For forty-seven of the lines listed, measurements were obtained on either four or five of the plates; and for these lines of greatest weight a correlation plot of measured shift against theoretical Zeeman effect is given in Figure 1. The correlation is obviously better than that for 78 Vir in Paper I; the reason for this is believed to lie largely in the sharpness and measurability of the lines in the spectrum of γ Equ, as well as in the larger

[9] *A Multiplet Table of Astrophysical Interest, Revised Edition* (Princeton University, 1945).

[10] *Bureau Standards J. Research*, **1**, 641, 1928.

[11] D. W. Weeks, "The Arc Spectrum of Iron (*Fe* I)," *Trans. Amer. Phil. Soc.*, Vol. **34**, Part III, 1944.

TABLE 2

DIFFERENTIAL MEASUREMENTS IN MICRONS IN THE SPECTRUM OF γ EQUULEI

IDENTIFICATION			PLATE NUMBER					MEAN REDUCED TO λ 4500
λ	El.	Z	Ce 4438	Ce 4724	Ce 4776	Ce 4842	Ce 4887	
3977.743	*Fe* I	1.83	.....	.....	.....	5	.....	6½
3991.123	*Cr* I	0.67	1½	.....	.....	.....	.....	2
3992.845	*Cr* I	1.67	5	.....	.....	.....	.....	6½ wk
3995.306	*Co* I	1.22	.....	.....	.....	6	.....	7½ str
3997.394	*Fe* I	1.11W	2	.....	.....	.....	.....	2½
4002.549	*Fe* II	1.07	3	.....	.....	.....	.....	4 wk
4005.246	*Fe* I	1.72W	4s	4	4	2	.....	4½ s med
4005.712	*V* II	1.20	.....	3	3	5	.....	4½
4009.714	*Fe* I	1.50	3½	1	3	5	.....	4
4014.534	*Fe* I	1.00	.....	4	5	6	.....	6½
4020.898	*Co* I	1.33	4½	5	9	6	.....	7½ n
4021.869	*Fe* I	1.22W	1	2:	3:	3	.....	3
4023.399	*Co* I	1.87	5½	7	5	6	.....	7½ s
4028.332	*Ti* II	1.06	2	.....	.....	.....	.....	2½
4029.640	*Fe* I	1.50, 1.75	.....	8	7	6	.....	8½ wk
4034.490	*Mn* I	1.80	4	5	7	6	.....	7 s, str
4039.100	*Cr* I	1.14	6	.....	4:	2	.....	5 wk
4041.361	*Mn* I	1.55	2½	5	7	5	.....	6 str
4045.815	*Fe* I	1.26	3½	4	.....	.....	.....	4½ str
4051.923	*Fe* I	0.67	.....	3	4	5	.....	5
4057.505	*Mg* I	1.00	1½	3:	3:	3	.....	3 n, str
4063.597	*Fe* I	1.09	0:	.....	6	4	.....	4½ str
4067.984	*Fe* I	1.62	5	.....	.....	.....	.....	6
4071.740	*Fe* I	0.69	½	1	2	3	.....	2 str
4073.760	*Fe* I	1.50	.....	3	5	7	.....	6
4077.714	*Sr* II	1.17	½	2:	5	7	.....	4½ str
4085.312	*Fe* I	1.71	4	.....	.....	.....	.....	5 wk
4118.549	*Fe* I	1.07W	1	8	6	7	.....	6½
4121.318	*Co* I	1.06	2½	3	5	4	4	4 s, str
4128.053	*Si* II	0.90	2	3	4	3	.....	3½ n
4132.060	*Fe* I	1.75W	2½	7	6	5	.....	6
4134.681	*Fe* I	1.10W	.....	3	1	3	.....	3
4137.002	*Fe* I	1.00	2	.....	.....	.....	.....	2½ n
4143.418	*Fe* I	1.00	2½	5	3	6	7	5½
4143.871	*Fe* I	1.67W	2	4	7	6	6	6 str
4145.77	*Cr* I	1.20	2	.....	.....	.....	.....	2½ wk
4153.067	*Cr* I	1.50	.....	.....	.....	6	.....	7
4154.502	*Fe* I	1.50	3	.....	.....	.....	.....	3½
4154.812	*Fe* I	1.48W	1½	7	6	4	7	6
4163.644	*Ti* II	1.07	4	5	5	4	1	4½
4171.904	*Fe* I	0.83	2	.....	.....	.....	.....	2½
4175.640	*Fe* I	1.16W	.....	3	4	3	4	4
4178.855	*Fe* II	0.80	1	3	5	4	3	3½
4181.758	*Fe* I	1.27W	4½	.....	.....	.....	.....	5½ wk
4184.895	*Fe* I *Cr* I	1.55W 1.50	2½	8	5	7	5	6½
4187.044	*Fe* I	1.41W	4	6	7	7	5	7
4187.802	*Fe* I	1.42	2½	4	6	5	5	5 n
4191.436	*Fe* I	1.28W	3	5	6	5	3	5
4195.337	*Fe* I	1.40W	.....	5	3	5	.....	5
4198.268	*Fe* I	1.25	.....	.....	8	4	.....	7 n
4199.098	*Fe* I	1.08W	.....	5	5	5	.....	5½
4200.930	*Fe* I	1.87	6	8	10	11	.....	10½ n wk
4202.031	*Fe* I	1.25W	2	3	7	3	2	4
4203.987	*Fe* I	1.45W	1	5	6	7	.....	5½
4210.352	*Fe* I	3.05W	.....	5	10	14	10	11½
4215.524	*Sr* II	1.33	.....	4	4:	4:	.....	4½ n str

TABLE 2—*Continued*

Identification			Plate Number					Mean Reduced to λ 4500
λ	El.	Z	Ce 4438	Ce 4724	Ce 4776	Ce 4842	Ce 4887	
4217.551	*Fe* I	0.50	4	.....	.....	.....	.....	4½
4219.364	*Fe* I	1.08	3	1	4	1	4	3
4222.219	*Fe* I	1.80W	6	.....	.....	.....	.....	7
4226.728	*Ca* I	1.00	1	.....	.....	.....	.....	1 n str
4233.167	*Fe* II	1.22	0	4	3	6	2	3½ str
4233.608	*Fe* I	1.52W	.....	9	8	8	5	8½
4238.027	*Fe* I	2.00 1.50	5	.....	.....	.....	.....	5½ wk
4242.38	*Cr* II	1.17	2	4	5	4	8	5 s
4245.258	*Fe* I	1.91W	4	7	8	6	2	6 n
4245.358	*Fe* I	1.20						
4247.432	*Fe* I	1.39W	3	.....	.....	.....	.....	3½
4250.125	*Fe* I	1.39W	3	5	6	7	3	5½
4250.790	*Fe* I	1.10	.....	6	2	2	4	4
4254.346	*Cr* I	1.38	.....	7	.....	7	.....	8 bl?
4260.479	*Fe* I	1.62W	4	5	7	4	7	6 str
4267.830	*Fe* I	1.57W	7½	.....	.....	.....	.....	8½ wk
4271.159	*Fe* I	1.43W	3	8	6	5	3	5½
4271.764	*Fe* I	1.26W	3½	3	5	4	3	4
4273.317	*Fe* II	2.17	5½	9	12	12	12:	11 wk
4274.803	*Cr* I	1.96	3	7	6	8	5	6½ str
4282.406	*Fe* I	1.22W	2	.....	.....	.....	.....	2
4283.010	*Ca* I	1.50	5	5	7	8	6	6½
4287.893	*Ti* II	1.50	6½	.....	.....	.....	.....	7 wk
4294.128	*Fe* I	1.20	2½	5	4	5	1	4 str
4298.986	*Ca* I	1.50	2	4	6	7	4	5
4299.25	*Fe* I	1.03	2	.....	.....	.....	.....	2
4300.052	*Ti* II	1.50	1½	2	8	1	3:	3½
4302.527	*Ca* I	1.50	5	5	7	4	5	5½ str
4318.652	*Ca* I	1.50	1½	6	4	5	.....	4½
4325.765	*Fe* I	0.99W	1½	4:	4:	4:	.....	3½ n
4371.279	*Cr* I	1.37	4½	.....	.....	.....	.....	5 wk
4375.932	*Fe* I	1.52W	1½	.....	8	5	.....	5
4383.547	*Fe* I	1.16W	3	.....	4	4	.....	3½ str

Ce 4438

Identification			Mean Reduced to λ 4500	Identification			Mean Reduced to λ 4500
λ	El.	Z		λ	El.	Z	
4394.057	*Ti* II	1.34	6½ wk	4494.568	*Fe* I	1.05W	4
4395.031	*Ti* II	1.07	2½	4508.283	*Fe* II	0.50	1½ str
4404.752	*Fe* I	1.17	3	4515.337	*Fe* II	1.03	4
4451.586	*Mn* I	1.43	3	4520.225	*Fe* II	1.50	3½
4455.887	*Ca* I	1.50	3½ n	4541.523	*Fe* II	0.80	1½
4458.538	*Cr* I	1.20	4½ wk	4547.850	*Ti* I	1.00	5½ wk
4459.121	*Fe* I	1.60W	3½ wk	4547.851	*Fe* I	1.00	
4462.022	*Mn* I	1.28	½	4554.033	*Ba* II	1.17	1 str
4466.554	*Fe* I	1.17W	3	4555.890	*Fe* II	1.24	2½ wk
4468.493	*Ti* II	1.05	4½	4563.761	*Ti* II	0.83	2
4470.864	*Ti* II	1.27	7 wk	4571.971	*Ti* II	0.93	1½
4489.185	*Fe* II	1.50	5½	4576.331	*Fe* II	1.20	2
4491.401	*Fe* II	0.40	0	4582.835	*Fe* II	1.50	5½ wk

TABLE 2—*Continued*

Identification			Mean Reduced to λ 4500	Identification			Mean Reduced to λ 4500
λ	El.	Z		λ	El.	Z	
4585.871	*Ca* I	1.12	2 n	4718.429	*Cr* I	1.25	3½
4585.923	*Ca* I	1.20		4728.468	*Gd* II	1.70	7 wk
4588.217	*Cr* II	1.07	4 str	4728.555	*Fe* I	2.00	
4592.09	*Cr* II	1.20	4	4748.12	*Sc* II	1.75	5½ n
4600.752	*Cr* I	1.58	8½ wk	4754.042	*Mn* I	1.65	6½
4602.944	*Fe* I	1.93W	6½ wk	4756.113	*Cr* I	1.10	3½ wk
4616.64	*Cr* II	0.80	2	4762.376	*Mn* I	1.17	4½
4618.83	*Cr* II	0.90	1½	4783.420	*Mn* I	1.97	7½
4626.188	*Cr* I	2.00	9 wk	4812.35	*Cr* I	1.50	5½
4634.11	*Cr* II	0.50	2½	4824.13	*Cr* II	1.33	6 str
4646.174	*Cr* I	1.25	5	4836.22	*Cr* II	1.50	7
4652.158	*Cr* I	1.17	1	4848.24	*Cr* II	1.24	5
4666.750	*Fe* II	1.50	3½	4883.69	*Y* II	1.12	4:
4707.281	*Fe* I	0.91	2 wk	4918.999	*Fe* I	1.62	6½ str

number of plates measured. The value of $\Sigma\Delta s/\Sigma Z$ for the forty-seven lines of high weight is 3.85. From Paper I, equation (12), it is known that the shift in wave length for the integrated Zeeman effect is related to H_p, the polar field strength, by the relationship

$$\Delta\lambda = 1.45 \times 10^{-5} \epsilon \lambda^2 H_p ,$$

where $\Delta\lambda$ is the shift for a normal triplet ($Z = 1.00$). By means of the ratio $\Delta s/Z = 3.85$, which represents the double shift (since the measures are differential), and the dispersion 2.89 A/mm, it is found that

$$\epsilon H_p = 1900 \pm 250 \text{ gauss} .$$

The probable error of 250 gauss has been estimated from the mean of the errors for the individual lines. The parameter ϵ, a polarization factor for the oblique reflection from the coudé flat mirror, is a little less than 1.00; as it is a function of the angle of incidence and of the optical constants of the aluminum surface of the mirror, it is constant for a given star (provided that aging of the mirror surface can be neglected). It has not yet been feasible to make an accurate determination of ϵ as a function of declination, but this is relatively unimportant; when it is finally determined, the figure obtained for the polar field intensity may be expected to be increased by several per cent. Other unknown parameters, such as the degree of distortion of the assumed dipole field of the star by space charge and oblateness of the figure or systematic errors depending upon line intensity, may well be of greater importance.

Although the measures are largely on stellar absorption lines of "medium" intensity, a number of lines classified as "weak" and "strong" were also measured, particularly on Ce 4438. As Hale found in the sun evidence of systematic differences between weak and strong lines,[12] it is of interest to compare the observed Zeeman effects for these intensity groups. This effect has sometimes been interpreted as an indication that the magnetic field falls off more rapidly than the inverse-cube law with increasing altitude in the solar atmosphere and that the form of the field external to the photosphere must therefore differ radically from a dipole field.[13]

[12] G. E. Hale, *Mt. W. Contr.*, No. 71; *Ap. J.*, **38**, 27, 1913.

[13] S. Rosseland, *Theoretical Astrophysics* (Oxford, 1936), p. 218; *Ap. J.*, **62**, 387, 1925.

On one plate of γ Equ, measures of seventy-seven medium lines and twenty-two strong lines are in agreement as to indicated field strength, but twenty-six weak lines yield a value for H_p about 45 per cent greater. This effect is probably real, but I doubt that it should be attributed primarily to a rapid decrease of field strength with height in the stellar atmosphere. A more plausible explanation seems to lie in the effect of the curve of growth on the intensities of the components of the pattern of the inverse Zeeman effect, as seen through a circular analyzer. In Paper I, an integration over a hemisphere was carried out to determine the shift in the center of light of the blended components of a Zeeman triplet as seen through a circular analyzer, with due account of the variation

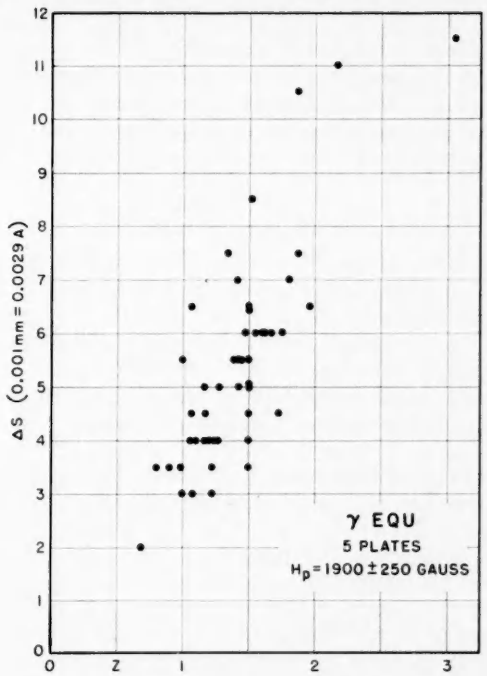

FIG. 1.—Plot of Δs (measured shift in microns between right-handed and left-handed analyzed spectra) against Z, the predicted Zeeman effect. Each point, representing a spectrum line, is a mean from measurements on 4 or 5 plates.

in the intensity and direction of the field with stellar latitude. It was pointed out that the result was valid only for emission lines or for very weak absorption lines. The reason is that the formulae for I_V, I_M, and I_R (eq. [3], Paper I) really specify the relative numbers of atoms acting to produce the three components of the line, so that, in the inverse Zeeman effect, the formulae give true intensities only for very weak absorption lines on the first part of the curve of growth, where the equivalent width is proportional to the number of atoms acting. For stronger absorption lines that fall on the nearly horizontal portion of the curve of growth, a rather large change in the number of effective atoms may produce only a very small change in the equivalent width. The components of the blended pattern of such an absorption line (Fig. 3, Paper I) may thus differ only a little among themselves in intensity, although the number of atoms effective in the various components may be quite disproportionate. In consequence, for a moderately strong line the center of gravity of the unresolved pattern may be considerably less displaced than for a weak line similarly affected by the field. This reasoning, together with the evidence that

the weak lines yield a larger value for H_p than do the medium and strong lines, suggests that the weak lines do indeed give the most realistic results in connection with the derived formula, provided that the practical difficulties of measuring the weak lines are not too serious. Indications are that a value of H_p for γ Equ based on weak lines would be in the neighborhood of 2500 gauss, in contrast to the 1900 gauss obtained from all lines measured. This numerical value should, however, be taken with some reserve, as it is based on only twenty-six lines measured on one plate.

It now appears possible to extend the foregoing considerations, in which the Zeeman pattern of a magnetically affected absorption line in the integrated light of a star is interpreted with the aid of the curve of growth, to the problem of the anomalous line intensities and their variations in the peculiar stars of type A. A paper is in preparation dealing with this subject more fully.

As an incidental result, the radial velocity of γ Equ has been computed from the measurements on two plates, Ce 4438 and Ce 4842, which give -17.7 ± 0.5 and -15.9 ± 0.5 km/sec, respectively. The precision might have been somewhat increased had settings been recorded on more comparison lines. The value published by J. H. Moore is -17.1 ± 0.4 km/sec (variable?).[14]

EVIDENCE FOR VARIABILITY

It was reported by W. W. Morgan[15] that in γ Equ the line "*Cr* II λ 4558 varies from an intensity equal to that of the well-marked line λ 4549 until it is among the weakest in the spectrum." Three plates by Deutsch[8] revealed no changes; but, as he remarks, "the number of plates is far too small to establish non-variability." He lists the star as a probable spectrum variable, requiring further verification.

An examination of my coudé plates fails to reveal any certain variations in line intensity, but it is of interest to examine the data at hand for indications of variation in field strength.

For the five plates of highest dispersion I have reduced the measurements separately, using all the lines measured on each plate. The resulting values for H_p range from 1400 to 2240 gauss, as indicated in Table 1, with estimated probable errors of 350–400 gauss. As these plates give some suggestion of variability, I have also measured the one plate of intermediate dispersion (Ce 4695), although its photographic density is a little less than the optimum. The polar field obtained from the average of forty lines on this plate is 2480 gauss, with an estimated probable error of 780. In view of the size of the probable errors, the evidence from the six plates is certainly not sufficient to establish γ Equ as a magnetic variable, but there is at least a suggestion of variation that remains to be confirmed or refuted by further observations.

MAGNETIC POLARITY

If a star rotates about an axis nearly parallel to the line of sight and if it possesses a dipole magnetic field having an axis coincident with the axis of rotation, as has been assumed, then the pole that we observe may be of either positive (north-seeking) or negative (south-seeking) magnetic polarity; and if a number of such stars are selected at random, we should expect to observe about equal numbers of each polarity. This is, in fact, found to be true among those stars in which the integrated Zeeman effect has been detected.

For the determination of magnetic polarity, plates taken with the analyzer in the normal position are used as standards. (It has occasionally been used in the inverted position as a check against systematic errors; this reverses the sign of the shifts.) To standardize the analyzer for polarity, test plates were taken of a spark source in the field of an electromagnet set up in front of the spectrograph. The magnet was capable of producing a field

[14] *Pub. Lick Obs.*, Vol. **18**, 1932.

[15] *Ap. J.*, **76**, 315, 1932.

of a few thousand gauss and had a bored-out pole-piece, permitting observation of the longitudinal Zeeman effect.[16] Its polarity was checked by means of a compass. Account was taken of the fact that starlight entering the 100-inch telescope undergoes three reflections before reaching the analyzer; an odd number of reflections changes the sign of circular polarization because of the phase reversal at each reflection. The fact that the spark source produced emission lines, while absorption lines are generally studied in stars, does not alter the sign of the line shifts, since displacements observed in the normal and inverse Zeeman effects with a given analyzer are of the same sign.[17]

A comparison of stellar spectrograms with the results of this standardization experiment showed that the magnetic polarity observed is positive in γ Equ and negative in 78 Vir.

Knott's eleventh-magnitude companion of γ Equ is, to judge from its color, of considerably later spectral type than is the primary. The available observations by double-star observers of the position angle and separation of the companion are listed in the accompanying tabulation. The first two observations are from Aitken's *New General*

Date	P.A.	Separation
1867.50	276°.8	2".13
1918.70	273.4	2.43
1933.60	269.7	2.07
1934.83	270.3	2.24

Catalogue of Double Stars;[18] the others were very kindly communicated to me by Dr. H. M. Jeffers from the card catalogue of recent observations maintained at the Lick Observatory. The data indicate that the position angle is decreasing, the relative orbital motion as seen in the sky being clockwise; in all probability the axial rotation of the primary is in the same direction. Since positive magnetic polarity is observed, it follows that the rotation and magnetization in γ Equ are antiparallel as in the earth and as reported for the sun in 1913 by Hale; in other words, the magnetic polarity is such as would be produced by a negative electric charge on the rotating star.

DISCUSSION

A guiding proposition in the initial work on stellar magnetic fields was that among stars roughly similar in mass and radius great differences in the rate of axial rotation are known and that the most intense fields are likely to be found in the stars that are rotating most rapidly. This association of magnetization with rotation is, I believe, physically plausible, regardless of the exact nature of the source of the magnetization. In a later paper,[19] taking into account the first results for the magnetic field of 78 Vir, I pointed out the somewhat more precise relationship that, when the earth, the sun, and 78 Vir are compared, the magnetic moment of each body is at least roughly proportional to its angular momentum and that the constant of proportionality (in cgs units) is about 1×10^{-15}. It was remarked that this result, embracing a wide range in radius, mass, and angular velocity, appears to support those theories (springing from the suggestion of Schuster)[3] that endeavor to interpret geomagnetism and solar magnetism as a funda-

[16] I am indebted to Dr. R. B. Leighton, of the California Institute of Technology, for placing this magnet at my disposal.

[17] A statement on this point in Paper I (p. 426) appears to be in error.

[18] *Pub. Carnegie Inst. Washington*, No. 417, 1932.

[19] *Pub. A.S.P.*, **59**, 112, 1947.

mental manifestation of matter in rotation. Dr. P. M. S. Blackett, using essentially the same data, has independently emphasized this proportionality relationship.[20]

The polar field $H_p = 1900$ gauss observed in γ Equ differs only a little in magnitude from the value of 1500 gauss found in 78 Vir in 1946, although it is opposite in sign. If one uses for γ Equ the values of radius, mass, and equatorial velocity appropriate to the average star of type F0 (namely, 9.7×10^{10} cm, 3.0×10^{33} gm, and 75: km/sec), one obtains for the magnetic dipole moment $D = \frac{1}{2}H_pR^3 = 8.7 \times 10^{35}$ gauss cm^3, and for the spin (angular momentum) the value $S = \frac{2}{5}MR^2\omega = 8.7 \times 10^{50}$ gm cm^2 sec^{-1}. As before, the spin is computed on the simplifying assumptions of uniform density and solid-body rotation.[21] For γ Equ the ratio $D/S = -1.0 \times 10^{-15}$, in agreement with the ratio previously derived for the earth, the sun, and 78 Vir. (The negative sign indicates antiparallelism.)

The discovery that the magnetic field of the sharp-line peculiar star HD 125248 not only varies but reverses its polarity in a regular cycle with a period of about 9 days, in synchronism with variations in the spectrum, has raised serious doubts regarding the suggested fundamental nature of the empirical proportionality between magnetic moment and angular momentum.[7] Additional negative evidence is the fact that a single plate of 78 Vir obtained in 1947 yielded a value of H_p about twice as great as did the plates of 1946. It appears not impossible that future observations will show that all spectrum variables of type A have variable fields and, indeed, that the spectrum variability results from the magnetic variations.

While a moderate variation in the measured H_p of a star can reasonably be accounted for on the assumption of changes in the *form* of the external field (as, for example, by space-charge effects), the magnetic moment remaining constant, the reversal of the field of HD 125248 is apparently a more deep-seated phenomenon. Data at present available suggest that this reversing field arises in a single star and that some alternating electromagnetic process is therefore active on an immense scale. The possibility of the existence of a constant component of magnetic moment is not ruled out, however.

The spectra of some normal main-sequence stars of early type, such as Sirius (A0) and γ Geminorum (A3), show little or no evidence of the Zeeman effect on plates taken with the analyzer. As there is a great range in equatorial velocity among the A-type stars, from practically zero up to about 250 km/sec, it is possible that Sirius and γ Gem have a low rate of axial rotation; and as a working hypothesis we may retain the modified proposition that the most intense magnetic activity occurs in the stars that are rotating most rapidly.

[20] *Nature*, **159**, 658, 1947.

[21] The spin of the typical F0 star corrected approximately for nonuniform density but not for nonsolid rotation is about 1.5×10^{50} gm cm^2 sec^{-1}; and it is noteworthy that this is of the same order as the total angular momentum, J, of the solar system. For the planets the orbital angular momentum $L = 3.1 \times 10^{50}$. The contribution of the sun with its low rate of rotation (and weak field) is only about $S_\odot = 0.02\,L$, so that $J = L + S_\odot = 3.2 \times 10^{50}$.

THE NUCLEAR AND NEBULAR SPECTRA OF THE PLANETARY NEBULA NGC 2392*

O. C. WILSON
Mount Wilson Observatory
Received June 2, 1948

ABSTRACT

Eighteen stellar absorption lines and three wide emission lines were measured on an excellent spectrogram of the nucleus of NGC 2392. Seven nebular lines also were measured. The two nebular lines of [*Ne* v], λ 3346 and λ 3426, are single and nearly monochromatic. Other nebular lines are double, with a separation of about 100 km/sec between the components. Radial velocities of the system given by the single [*Ne* v] lines, by means of the components of the double nebular lines, and by the stellar emission lines are, respectively, +70.8, +71.1, and +70.9 km/sec.

When the stellar absorption lines are grouped according to total excitation requirements, it is found that those of highest excitation (*N* IV) give approximately the velocity of the system. Lines of lower excitation show progressively larger displacements toward the violet. The lines of lowest excitation (*H*) yield a velocity of +45 km/sec. These results indicate a variation of outward velocity with depth in the atmosphere of the nuclear star such that the *N* IV lines are formed at the greatest depth, those of *H* at the least depth.

The single nebular lines of [*Ne* v] are unexplained. A slitless spectrogram indicates that these lines, as well as the double lines of [*Ne* III], [*O* II], etc., are all formed in the inner nebular ring. Some of the obvious problems raised by these observations are mentioned.

The planetary nebula NGC 2392 was described by H. D. Curtis[1] as follows: "Central star of magnitude 9, surrounded by an irregular elliptical ring 19″ × 15″; 7″ to 8″ outside of this ring are found broken patches of an outer ring. Fainter matter forms an oval disk 47″ × 43″ in p.a. about 18°." The object is of moderate brightness, having been assigned a "relative exposure" of 5 by Curtis.

Chiefly because of the brightness of the nucleus, this nebula was included in a spectroscopic survey of the brighter planetary nebulae being made with the coudé spectrograph of the 100-inch telescope. Some unusual features of the spectrum are described in the present *Contribution*.

In February, 1948, a 6-hour exposure, made under good observing conditions with the 32-inch Schmidt camera of the coudé spectrograph, produced an excellent spectrogram, dispersion 10.4 A/mm, extending from about 3300 A to somewhat beyond 5000 A. The nuclear spectrum is well exposed over this entire range, a number of well-defined absorption lines being present. Several of the stronger nebular lines also were visible and, with two exceptions, consisted of two components with separation corresponding to a velocity of about 100 km/sec, somewhat as shown in the illustration of the N_1 line given by Campbell and Moore.[2] The exceptions were the [*Ne* v] lines λ 3346 and λ 3426, which were essentially *monochromatic* except for a slight broadening of their outer extremities. The anomalous appearance of the [*Ne* v] lines was strikingly apparent with even the most casual inspection.

Measured wave lengths and corresponding radial velocities are given in Tables 1 and 2. The adopted wave lengths and the multiplet numbers have been taken from Miss Moore's *Revised Multiplet Tables*.[3] Wave lengths of nebular lines in these tables were derived from measures of nebular spectra and, in some instances, are probably not

* *Contributions from the Mount Wilson Observatory, Carnegie Institution of Washington*, No. 749.

[1] *Pub. Lick Obs.*, Vol. **13**, Pl. XI, 1918.

[2] *Pub. Lick Obs.*, Vol. **13**, Pl. XXXI, 1918.

[3] *Contr. Princeton U. Obs.*, No. 20, 1945.

of high accuracy. This is apparently true of the two [*Ne* v] lines whose wave lengths are given only to the nearest tenth of an angstrom, and it probably accounts for the fact that, although these two lines are accurately measurable on my spectrogram, the resulting velocities differ by 16 km/sec. Among the wave lengths of the absorption lines, only one adjustment has been made: for the lines of *He* I the adopted wave length is the weighted mean of the components given in Miss Moore's *Table*. The adopted wave length of the stellar emission band at λ 4640 is that of the *N* III line 4640.64. Another somewhat weaker line of the same multiplet falls at 4641.90; the measures indicate that this line contributes inappreciably to the band.

In Table 3 are collected the mean radial velocities from the single and double nebular lines and from the nuclear emission bands. The excellent agreement among the three values can leave small doubt that their mean, +71.0 km/sec, must closely represent the velocity of the system.

TABLE 1

NEBULAR LINES IN NGC 2392

Meas. Neb. λ	Adopted λ	Ident.	Mult. No.	Rad. Vel. (Km/Sec)	Remarks
3346.60	45.9	[*Ne* v]	1F	+ 62.7	Monochromatic
3426.67	25.8	[*Ne* v]	1F	+ 78.8	Monochromatic
3726.24	26.16	[*O* II]	1F	+ 6.4	Violet component
3727.75	26.16	[*O* II]	1F	+128.0	Red component
3729.28	28.91	[*O* II]	1F	+ 29.8	Violet component
3730.40	28.91	[*O* II]	1F	+120.1	Red component
3868.96	68.74	[*Ne* III]	1F	+ 16.7	Violet component
3870.43	68.74	.....	.....	+130.6	Red component
4959.26	58.91	[*O* III]	1F	+ 21.1	Violet component
4960.88	58.91	.....	.....	+119.1	Red component
5007.06	06.84	[*O* III]	1F	+ 13.4	Violet component
5008.94	06.84	.....	.....	+126.0	Red component

Table 2 shows a very considerable scatter among the radial velocities derived from the nuclear absorption lines. While none of these lines is of the best quality for accurate measurement and some, notably the two lines of *He* II, are very poor, the scatter is nevertheless much too great to be attributed to errors of measurement. This situation is clarified when the lines are grouped according to their total excitation requirements, as in Table 4, where the numbers of lines in the groups and the mean deviations have been included to give a rough idea of the order of accuracy.

From Tables 1 and 2 the mean separation of the components of the double nebular lines is 107.3 km/sec and the mean width of the three nuclear emission bands is 122.2 km/sec. Except for [*Ne* v], the nebular lines cannot be measured with the highest accuracy; the red components are fairly strong, but they are not sharp and show some indication of structure. Even worse, the violet components are much weaker and almost impossible to see where they cross the spectrum of the central star. These facts doubtless account for most of the scatter in the velocities from the double nebular lines.

Finally, although neither λ 4686 of *He* II nor any of the hydrogen lines were strong enough for measurement in the nebula, enough can be seen by examination with low magnifying power to show that they have essentially the same double character as do all the other nebular lines except those of [*Ne* v].

TABLE 2

LINES IN THE NUCLEUS OF NGC 2392

MEAS. λ	ADOPTED λ	IDENT.	MULT. NO.	RAD. VEL. (KM/SEC)	REMARKS
	Absorption Lines				
3383.93	83.76	*Ti* II	1	+ 15.1	Interstellar
3479.58	78.69	*N* IV	1	+ 76.7	
3483.82	82.98	*N* IV	1	+ 72.4	
3485.74	84.90	*N* IV	1	+ 72.4	
3705.66	05.04	*He* I	25	+ 50.2	
3771.12	70.63	*H*	2	+ 39.7	
3798.46	97.90	*H*	2	+ 44.3	
3820.31	19.64	*He* I	22	+ 52.5	
3836.18	35.39	*H*	2	+ 61.8	
3889.53	89.05	*H*	2	+ 37.1	
3933.39	33.66	*Ca* II	1	− 20.6	Interstellar; weak comp.
3933.82	33.66	*Ca* II	1	+ 12.2	Interstellar; strong comp.
3970.61	70.07	*H*	1	+ 40.8	
4026.91	26.22	*He* I	18	+ 51.5	
4098.22	97.31	*N* III	1	+ 66.6	
4102.30	01.74	*H*	1	+ 41.0	
4104.29	03.37	*N* III	1	+ 67.2	
4200.92	99.83	*He* II	3	+ 78.0	Very poor line
4341.19	40.47	*H*	1	+ 49.9	
4472.60	71.51	*He* I	14	+ 73.1	
4542.32	41.59	*He* II	2	+ 48.6	Very poor line
	Emission Lines				
4634.44	34.16	*N* III	2	+ 18.1	Violet edge
4635.27	34.16			+ 72.0	Center
4636.06	34.16			+123.0	Red edge
4640.80	40.64	*N* III	2	+ 10.3	Violet edge
4641.74	40.64			+ 71.2	Center
4642.51	40.64			+121.0	Red edge
4685.64	85.68	*He* II	1	− 2.6	Violet edge
4686.88	85.68			+ 76.9	Center
4688.00	85.68			+148.6	Red edge

TABLE 3

MEAN RADIAL VELOCITIES FROM VARIOUS LINES IN NGC 2392

Lines	Vel. (Km/Sec)
[*Ne* v]	+70.8
Other nebular lines*	+71.1
Stellar em. bands†	+70.9
Mean	+71.0

* Means of both components.
† Means of center and edge measures.

DISCUSSION

I. SPECTRUM OF THE NUCLEUS

All measured radial velocities are shown graphically in Figure 1, which clearly illustrates the considerable dependence of displacement of the absorption lines upon their excitation requirements. In view of the existence of the nebula, it can scarcely be doubted that the several groups of absorption lines are being formed at various depths in a highly stratified atmosphere, through which the outward expansion velocity is a function of depth. The first question to be considered is that of assigning correct relative depths to the various groups of lines, and here two possibilities present themselves:

TABLE 4

RADIAL VELOCITIES FROM NUCLEAR ABSORPTION LINES ARRANGED ACCORDING TO TOTAL EXCITATION

El.	No. Lines	Total Exc. (Volts)	Vel. (Km/Sec)	El.	No. Lines	Total Exc. (Volts)	Vel. (Km/Sec)
H	7	10.2	+44.9± 6.2 (m.d.)	*He* II	2	75.3	+63.3±14.7 (m.d.)
He I	4	20.9	+57.3± 8.8	*N* IV	3	137.8	+73.8± 1.9
N III	2	71.3	+66.9± 0.3				

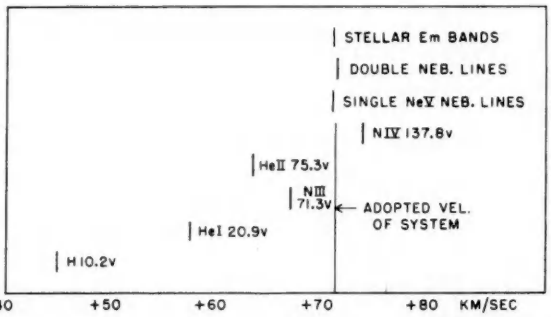

FIG. 1.—Excitation potentials and radial velocities of various lines in the nucleus and nebula of NGC 2392.

a) The *N* IV lines are formed at the least depth, the hydrogen lines at the greatest. Since the radial velocities from *N* IV agree within limits of error with the velocity of the system, the region of their formation is one of little or no outward velocity. This hypothesis, then, would be equivalent to the supposition that at some depth the atmospheric material is given a rather violent outward motion and subsequently decelerated to approximately zero velocity. Taken by itself, such a situation is perhaps not impossible. It is necessary, however, to consider the nuclear emission bands, which must definitely be formed well outside the body of the star in an external shell, for no trace of occultation effect[4] occurs, inasmuch as the radial velocities from the bands agree accurately with those of the nebular lines. Moreover, the band widths agree within limits of error with the separations of the nebular line components. Hence in the region of band formation the outgoing matter has attained its final constant velocity. Thus possibility *a* would require, first, an acceleration, then a deceleration, and, finally, a second accelera-

[4] S. Chandrasekhar, *M.N.*, **94**, 522, 1934.

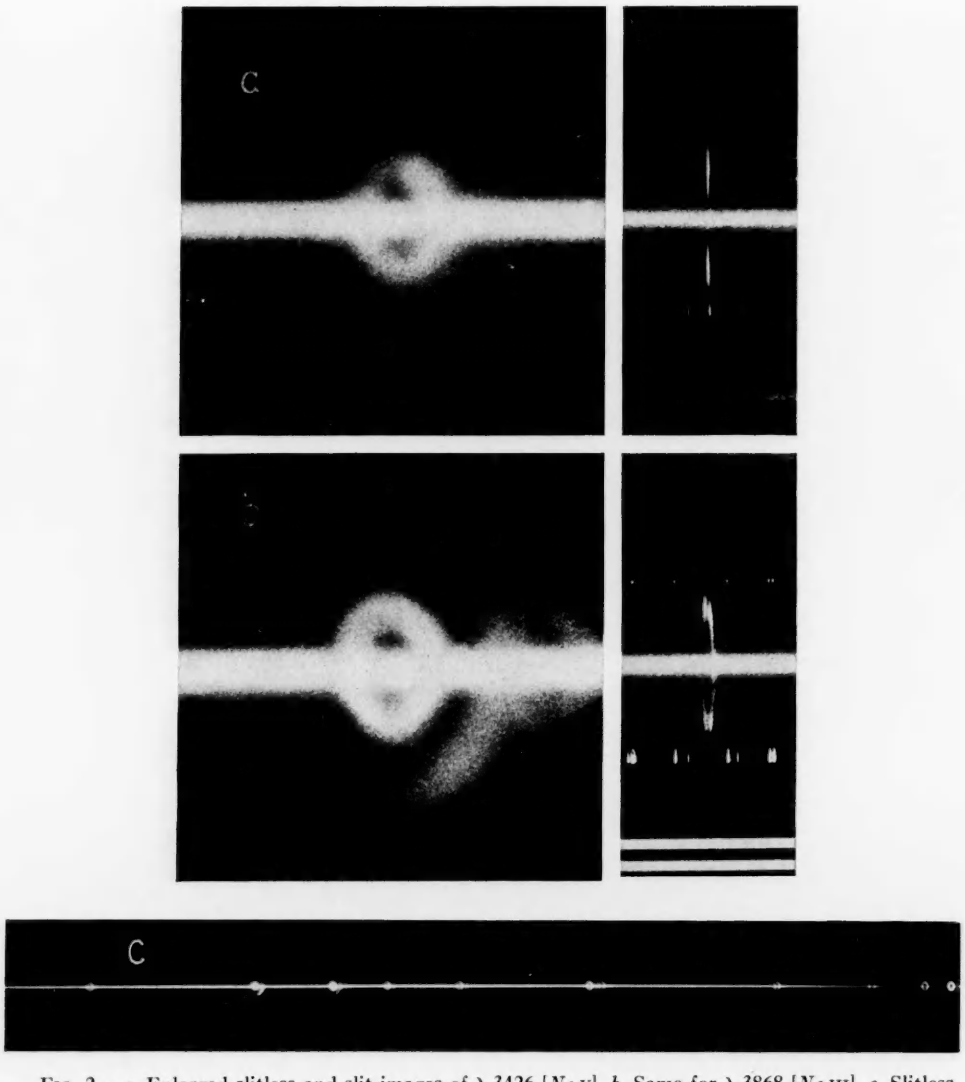

FIG. 2.—*a*, Enlarged slitless and slit images of λ 3426 [*Ne* V]. *b*, Same for λ 3868 [*Ne* III]. *c*, Slitless spectrogram approximately $\frac{3}{4}$ original size. λ 4959, λ 5007 [*O* III] at right end; λ 3346, λ 3426 [*Ne* V] at left end.

tion to the nebular velocity. Such a sequence of events appears somewhat artificial. The other possibility in the assignment of relative depths is as follows:

b) The *N* IV lines are formed at the greatest depth, the hydrogen lines at the least. The matter would start with very small outward velocities in the region of *N* IV line formation, would undergo continuous outward acceleration through the region of hydrogen-line formation, by which time something like half the final velocity would be attained, and would then accelerate still further into the region of emission-band formation. From the latter position it would move out into the nebula with constant velocity. Of the two possibilities, *b* appears the more reasonable and attractive.

If *b* is indeed correct, certain qualitative conclusions are possible. Consider a spherical surface in the atmosphere, concentric with the star. Let ρ be the total density at radius r, and let v be the outward velocity (assumed the same for all atoms and ions). Then, if we are dealing with steady flow,

$$\rho v r^2 = \text{const.} ,$$

or

$$\rho \propto \frac{1}{v r^2} .$$

Hence even if the change in r throughout the region of acceleration is small, the variation in v from negligibly small to considerable values can result in a very rapid density gradient. In fact, the density in the region of *N* IV line formation could be very much greater than the density where the hydrogen lines are formed. The region of *N* IV line formation must, however, be of much greater excitation, and a very rapid temperature gradient would thus be expected also. Such a temperature gradient, much steeper than that to be expected on the supposition of constancy of radiative flux, would probably be physically reasonable. Presumably, the energy required for the outward material acceleration is supplied by the radiation, which is thus gradually depleted in passing through the atmosphere. The usual condition of constancy of radiative flux should be replaced here by the condition that the total energy flux, radiative plus kinetic, is constant. In this fashion a very steep temperature gradient might well result.

II. NEBULAR SPECTRUM

The single lines of [*Ne* V] are very puzzling. Their radial velocities demonstrate clearly that the atoms responsible for them must have originated in the nuclear star, i.e., the lines cannot possibly be due to matter which merely happened to be in the vicinity. Neither can they be produced by an incomplete nebular shell, since their velocities agree with neither the red nor the violet components of the other nebular lines.

In an effort to solve the problem of the sources of the [*Ne* V] and other lines, a slitless spectrogram of the nebula was taken with the same spectrograph previously employed. The slit was replaced by a hinged mirror which could be lowered and raised at will. When the mirror was down, the central star could be centered with respect to a reticle in front of the guiding eyepiece. Raising the mirror allowed the light to enter the spectrograph. The exposure was therefore intermittent, with perhaps 20 per cent of the total exposure time consumed by guiding. There was no image rotator, and, since fine detail would be lost in any case, this crude procedure proved reasonably effective.

The result is illustrated by Figure 2, in which the slitless and slit images of λ 3426 [*Ne* V] are compared with those of λ 3868 [*Ne* III]. The latter line was chosen for the comparison both because it is due to a different stage of ionization of the same element and because it yields the strongest nebular image in the spectrum and should give the best reproduction. In all slitless images, except for [*Ne* V], the outer ring is clearly visible and has approximately the same broken structure as is shown for [*Ne* III]. For λ 3726 and λ 3728 [*O* II], the maximum intensity in the outer ring is about equal to that in the inner ring. For [*Ne* III] and [*O* III] the maximum intensity in the outer ring is per-

haps half that of the inner ring or less. The hydrogen images give somewhat similar results. In λ 4686 the outer ring is even fainter with respect to the inner, though still clearly visible.

The preceding statements, together with Figure 2, leave practically no doubt that the single [*Ne* v] lines are formed in the inner ring. Likewise, the relative intensities of the two rings and the appearance of [*Ne* III] in Figure 2 very strongly suggest that the double nebular lines of [*Ne* III] are also formed in the inner ring. If the latter statement is true, there is little reason to doubt that all the other observed double lines also originate in the inner ring.

The only alternative would be to ascribe the double lines to the outer ring. That this is almost certainly incorrect can be demonstrated by comparison of the images of λ 3868 [*Ne* III] and λ 3726 [*O* II]. On the slitless spectrogram the inner ring of λ 3868 is considerably stronger than the inner ring of λ 3726, while the opposite is true of the outer rings. The intensity ratio of the two lines on the slit spectrogram agrees at least roughly with the ratio of the two inner rings.

We are thus led to the conclusion that all the observed nebular lines, both single and double, originate in the inner ring. In order to see whether any differences in size are

TABLE 5

NEBULAR IMAGE DIMENSIONS IN DIRECTION OF DISPERSION IN SECONDS OF ARC

Line	Width		Diameter	
	Violet Side	Red Side	Inner	Outer
3426 [*Ne* v]	2.9	2.9	5.0	10.8
3868 [*Ne* III]	3.0	2.9	6.2	12.1
Hδ	2.5	3.0	5.6	11.2

detectable between the inner-ring images of [*Ne* v] and those of other lines on the slitless spectrogram, the images of λ 3426 [*Ne* v], λ 3868 [*Ne* III], and *Hδ* were measured in the direction of dispersion,[5] which happens to coincide approximately with the minor axis of the nebula. The line *Hδ* was included because its nebular image is of roughly the same intensity as that of λ 3426, while λ 3868 is considerably stronger. The results of these measures in seconds of arc are given in Table 5.

In view of the nature of the nebular images, I do not believe that the small differences between the three lines in Table 5 are anything but errors of measurement. This opinion is supported by a measure of the width of the star spectrum on the slitless spectrogram, which turns out to be 3″.3. Apparently, therefore, the ring widths in Table 5 represent nothing but seeing and guiding errors; any fine structure or substratification has been completely lost.

The dilemma created by these observations is obvious. First, if most of the nebular material arrived at its present position in the inner ring by moving out from the star with a velocity of 50 km/sec, how did the atoms responsible for the [*Ne* v] lines attain the same distribution in space with zero outward velocity? Conversely, if these atoms previously had an outward velocity of 50 km/sec in order to arrive at their present distance from the star, how was the velocity subsequently reduced to zero? Finally, how can a group of particles with zero velocity be apparently coextensive in space with another (probably vastly more numerous) group whose velocities are 50 km/sec.? While there must be reasonable answers to these questions, none has so far occurred to me.

[5] Guiding errors should be least in this orientation.

ON THE PULSATION IN THE ATMOSPHERE OF ETA AQUILAE*

M. SCHWARZSCHILD, B. SCHWARZSCHILD, AND W. S. ADAMS
Princeton University Observatory and Mount Wilson Observatory
Received June 17, 1948

ABSTRACT

On twenty spectra of η Aquilae, taken with the coudé spectrograph of the 100-inch telescope with a dispersion of 2.9 A/mm and covering the entire pulsation cycle, forty-three lines of iron were selected for measurement. The radial-velocity variations of these lines were found to indicate that the selected lines of *Fe* I and *Fe* II arise essentially from the same atmospheric layers. From the depth measurements of these lines the variations of the excitation temperature and of the electron pressure were determined.

The equivalent widths, determined for a few iron lines at mid-descending branch, showed that the hydrogen-metal ratio in η Aquilae can differ from that in the sun by only a small factor. The curve of growth at the same phase gave turbulent velocities much smaller than the velocities determined from line profiles, which may possibly indicate the existence of a fast turbulence with very large elements.

From the above data the density variation was computed. The comparison of this variation with that of the velocity suggests that possibly in the atmosphere of η Aquilae the kinetic temperature increases greatly with height and that in the highest layers the pulsation has the character of a simple progressive wave.

I. INTRODUCTION

The character of a wave in a compressible gas is not determined completely if only the variation of the displacement is given. In addition to the displacement, the measurement of a second variable, such as the density, is needed. In the case of the pulsation in the atmosphere of a cepheid, the radial velocity-curve gives the displacement variation, while the density variation may be deduced from the light-curve.[1] The latter deduction, however, appears at present none too reliable, since the dependence of the light-flux on the density in a pulsating giant atmosphere is not yet known with certainty. It would seem preferable to determine the density variation from temperatures and electron pressures derived from line-intensity measurements made on high-dispersion spectra.

In 1939–1942 twenty spectra of η Aquilae were taken with the coudé spectrograph of the 100-inch telescope at Mount Wilson. In the present paper are described, first, the measurements for a selected number of iron lines made on these spectra; second, the derivation of the density variation based on the line measurements; and, third, the discussion of the character of the atmospheric pulsation as indicated by the density variation.

The details of the investigations are given in the following sequence: In Sections II and III the basic data for η Aquilae are assembled, as far as they are needed for the subsequent discussions. The measurements of line depths made on the coudé spectrograms are given in Section IV. The assumption that all the lines used arise essentially from the same atmospheric level is tested with the help of radial-velocity measurements for the same lines on the same spectra, as described in Section V. Section VI gives the temperatures and electron pressures derived from the measurements of line depths. Before these temperatures and electron pressures can be used to determine the density variation, an estimate of the hydrogen abundance is needed. How this estimate was obtained is shown in Section VII, and the final density variation is given in Section VIII. Before the density variation can be used for a discussion of the dynamics of atmospheric pulsations, the degree of turbulence in the atmosphere has to be determined. This was done both with the help of the curve of growth and from measurements of line profiles, as

* This investigation was made possible by a co-operative arrangement between the Princeton University Observatory and the Mount Wilson Observatory.

[1] M. Schwarzschild, *Harvard Circ.*, Nos. 429 and 431, 1938.

described in Section IX. The equilibrium state which corresponds to this turbulence and which underlies the pulsations is discussed in Section X. Finally, in Sections XI and XII the character of the atmospheric pulsation, as indicated by the density variation, is discussed.

II. THE RADIAL VELOCITY-CURVE

The displacement variation for the atmospheric pulsation of η Aquilae can be derived directly from the radial velocity-curve. The radial-velocity measurements used are those of Jacobsen[2] (1923–1925) and those obtained from the Mount Wilson spectra (1939–1942). The latter are given in the last line of Table 4. For all observations the phases were computed with Gliese's ephemeris:[3]

$$\text{Phase} = \frac{\text{JD} - 2414827.30}{7.176678}. \tag{1}$$

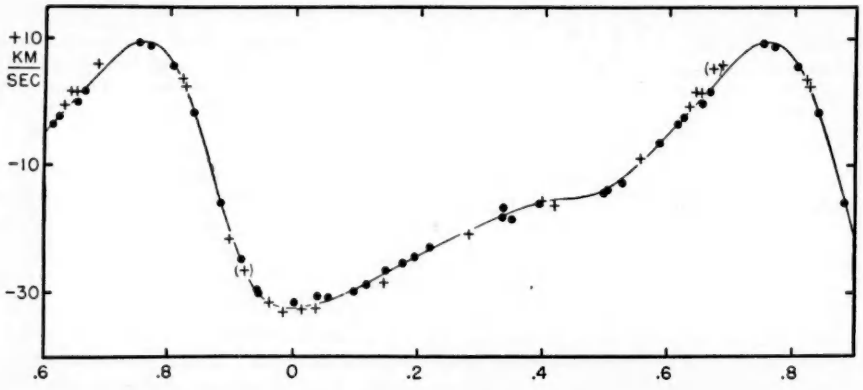

FIG. 1.—Radial velocity-curve of η Aquilae

Perfect agreement in phase was found for the two sets of measurements, which insures the adequacy of Gliese's period. The systematic difference in velocity between the two sets of observations (Lick − Mt. Wilson = +0.2 km/sec) was negligible. All these radial-velocity measurements were plotted in one graph, as shown in Figure 1. A smooth curve was drawn through the points, and this curve was read at 31 phases. These velocities had to be reduced, first, to account for the radial velocity of the star as a whole and, second, to account for the fact that the observations correspond to an integration over a hemisphere of the star's surface.[4] If an intermediate value is used for the limb-darkening coefficient, the two reductions can be performed by the following equation:

$$\frac{dr}{dt} = \tfrac{24}{17}\,(\overline{V_R} - V_R). \tag{2}$$

From the surface velocities thus obtained, the displacements were found by numerical integration. The integration constant was chosen such that the time average of the displacements, $r - R$, is zero, corresponding to a definition of R as the mean radius. The velocity-curve was further used to derive the accelerations by numerical differentiation. The displacement, the surface velocity, and the acceleration—all as functions of the phase—are listed in Table 1 and shown on the left-hand side of Figure 2.

[2] *Lick Obs. Bull.*, **12**, 138, 1926.

[3] *A.N.*, **273**, 94, 1942.

[4] I. A. Getting, *M.N.*, **95**, 141, 1934.

For the sake of comparison, Wylie's photoelectric light-curve[5] of η Aquilae (1920) is also shown in Figure 2. The phases for this light-curve were again computed with Gliese's ephemeris. The accuracy of this ephemeris could once more be checked with the help of a set of six-color photoelectric observations of η Aquilae made by Stebbins and Whitford in 1946 at Mount Wilson and kindly made available to the authors. Again, perfect agreement in phase was found between the old and the new observations when reduced with Gliese's period. It appears, therefore, that the reduction to one epoch of all observational data used is accurately determined.

TABLE 1

Phase	Δm_{pg} ηAql−βAql	dr/dt (Km/Sec)	$r-R$ 10^{10} Cm	d^2r/dt^2 (Cm/Sec^2)
0.00	−0.42	+24.9	−16.2	− 1
.04	− .35	+23.7	−10.1	− 7
.08	− .26	+21.6	− 4.5	−10
.12	− .16	+18.9	+ 0.5	−11
.16	− .08	+16.0	+ 4.9	−12
.20	− .01	+13.0	+ 8.4	−11
.24	+ .01	+10.2	+11.3	−11
.28	+ .02	+ 7.5	+13.5	−10
.32	+ .04	+ 5.1	+15.1	− 9
.36	+ .13	+ 3.0	+16.0	− 7
.40	+ .28	+ 1.4	+16.6	− 5
.44	+ .37	+ 0.6	+16.8	− 2
.48	+ .43	− 0.3	+16.9	− 7
.52	+ .48	− 3.1	+16.5	−16
.56	+ .54	− 7.9	+15.2	−22
.60	+ .60	−13.7	+12.5	−24
.64	+ .67	−19.8	+ 8.4	−25
.68	+ .70	−26.1	+ 2.7	−26
.72	+ .67	−31.8	− 4.5	−17
.76	+ .58	−34.0	−12.8	+ 2
.78	+ .50	−33.2	−17.0	+14
.80	+ .42	−30.3	−20.9	+32
.82	+ .32	−25.2	−24.4	+49
.84	+ .22	−18.2	−27.1	+65
.86	+ .11	− 9.4	−28.8	+74
.88	.00	0.0	−29.4	+76
.90	− .10	+ 8.9	−28.8	+64
.92	− .22	+15.7	−27.3	+47
.94	− .32	+20.5	−25.0	+31
.96	− .41	+23.4	−22.3	+17
0.98	−0.44	+24.7	−19.3	+ 5

III. MEAN RADIUS AND MASS

For the subsequent discussion of the dynamics of the motions in the atmosphere of η Aquilae, the mean radius and the mass are needed. The derivation of the mean radius with the help of the effective temperature and of the mass with the help of the mass-luminosity law is given in this section.

Since the spectrum at minimum phase seems somewhat more normal as regards type

[5] *Ap. J.*, **56**, 217, 1922.

than at other phases, it seems best to use color measurements at minimum as a measure for the effective temperature. Two good color measurements are available for η Aquilae. First, Pettit and Nicholson[6] have measured the water-cell absorption and found at minimum a water-cell absorption temperature of 4400° K. With the correction determined by Kuiper,[7] this leads to an effective temperature of 4820° K. Second, the recent six-color photoelectric measurements of Stebbins and Whitford give at minimum

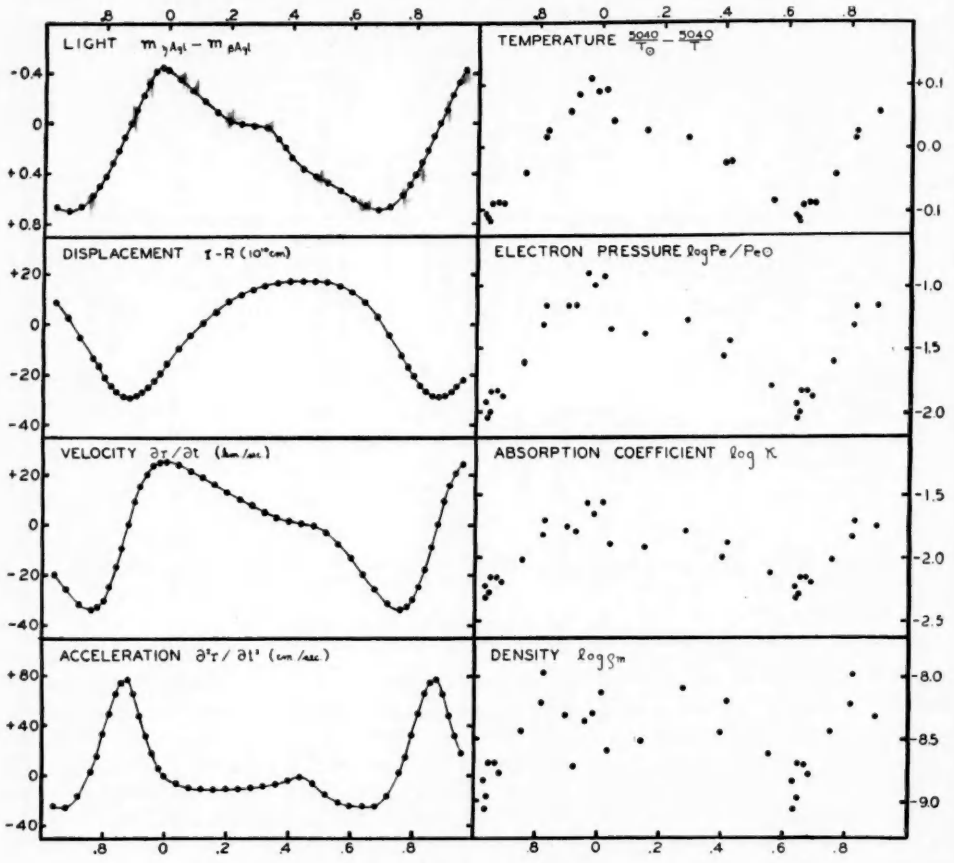

FIG. 2.—Variations in the atmosphere of η Aquilae

a color $(v - i)$ corresponding to that of spectral type cG4. According to Kuiper,[7] this spectral type has an effective temperature of 4750° K. The average of these two determinations gives

$$T_e = 4800° \text{ K at minimum} .$$

Shapley's period-luminosity relation[8] gives for the period of η Aquilae a median visual absolute magnitude of -2.4. Using a visual amplitude of 0.8, we find

$$M_{vis} = -2.0 \text{ at minimum} .$$

[6] *Ap. J.*, **78**, 347, 1933.

[7] *Ap. J.*, **88**, 464, 1938.

[8] *Star Clusters* (New York: McGraw-Hill Book Co., 1930), p. 130.

From the above data the radius may be computed with the help of Hertzsprung's formula[9]

$$M_{vis} = 2.3\left(\frac{14300}{T_e}\right)^{0.93} - 5\log r + 53.71\,. \qquad (3)$$

If the constant of equation (3) is used, the bolometric correction implicitly contained in this formula is found to agree sufficiently well with the values for the bolometric correction derived by Kuiper[7] for the range of spectral types here considered. Using this equation, we find

$$r = 2.58 \times 10^{12} \text{ at minimum}\,.$$

Since at minimum (phase = 0.68), $r - R = 0.03 \times 10^{12}$, we obtain for the mean radius

$$R = 2.55 \times 10^{12}\,.$$

For later comparison with the excitation temperature it is useful to compute the effective temperature at maximum in the following way: at maximum (phase = 0.00), $r - R = -0.16 \times 10^{12}$, and hence $r = 2.39 \times 10^{12}$. Further, the visual absolute magnitude at maximum is -2.8. These data give, with Hertzsprung's formula,

$$T_e = 5760^\circ \text{ K at maximum}\,.$$

Finally, the mass of η Aquilae is to be estimated. With a median bolometric correction of -0.3, the median bolometric absolute magnitude is -2.7. From this absolute magnitude one finds for the mass, under the assumption that Kuiper's mass-luminosity relation[10] is applicable,

$$M = 1.35 \times 10^{34}\,.$$

IV. MEASUREMENTS OF LINE DEPTHS

The twenty spectra of η Aquilae taken with the coudé spectrograph of the 100-inch telescope at Mount Wilson are listed in Table 2. The dispersion of these spectra is 2.9 A/mm. The slit width used was approximately 0.03 mm except for plates Nos. 2592, 2594, and 2607, for which a slit width of approximately 0.05 mm was employed. (The focal lengths of the collimator and the spectrograph camera used are nearly equal.) Cramer High Speed Special plates were used for all spectrograms except the last one, which was taken on an Eastman 103*a*-O plate.

To the red of λ 4650 these spectra show a steady decrease of density. Since it was feared that this strong variation of photographic density might introduce differential errors into the line measurements, no measurements were made in this range of wave length. To the violet of λ 4370 the lines were so crowded that hardly any reasonably unblended lines could be found. In the remaining wave-length range, 280 A wide, forty-three lines of neutral and ionized iron were selected for measurement. They are listed in Table 3. Though many of these lines have blended wings, the centers of all seemed reasonably free of blending.

For the wave-length range in question, the spectra were registered with the Mount Wilson recording microphotometer. Forty-fold enlargement was used for the recording. The calibration spectra were registered at each end of the wave-length range used, at one end before the registration of the stellar spectrum and at the other end afterward. Particular attention was paid to the consistency of focus and sensitivity of the photometer during all registrations on one plate. The spectra taken near maximum of η Aquilae were so strongly exposed that it was necessary to use a scale giving large deflections

[9] A. S. Eddington, *Internal Constitution of the Stars* (Cambridge: At the University Press, 1930), p. 139.

[10] *Op. cit.*, p. 472.

in such cases, in order to obtain a reasonable difference of the deflection for the continuum and the line centers. With this scale the recording on the clear plate beside the spectrum would normally not fall on the recording paper. To bring the clear reading back to the paper, the photometric wedge (in the scanning beam of the photometer) was used at a denser setting for the clear readings than for the registration of the stellar spectrum and the comparison spectra.

The calibration-curves obtained from the registrations at the two ends of the wave-length range in question proved to be so nearly equal that only one mean calibration-curve was used for each spectrum. Since most measurements corresponded to fairly high photographic densities, it was found that rather straight calibration-curves were ob-

TABLE 2

Plate No.	Date	Exposure (Min.)	JD	Phase
2333	June 16, 1940	125	2429797.946	0.013
2394	Aug. 20, 1940	220	2429862.708	.037
2335	June 17, 1940	125	2429798.890	.145
2425	Oct. 11, 1940	340	2429914.684	.280
2070	Aug. 1, 1939	212	2429477.756	.398
2428	Oct. 12, 1940	335	2429915.680	.418
2431	Oct. 13, 1940	315	2429916.669	.556
2373	July 12, 1940	222	2429823.915	.632
2422	Sept. 22, 1940	390	2429895.729	.638
2802	June 1, 1942	122	2430512.958	.643
2587	July 6, 1941	260	2430182.889	.651
2054	June 28, 1939	300	2429443.833	.671
2592	Aug. 4, 1941	204	2430211.846	.686
2375	July 13, 1940	250	2429824.799	.755
2594	Aug. 5, 1941	230	2430212.809	.820
2397	Sept. 9, 1940	260	2429882.705	.824
2391	Aug. 19, 1940	230	2429861.711	.898
2035	June 1, 1939	186	2429416.935	.923
2401	Sept. 10, 1940	215	2429883.689	.961
2607	Sept. 4, 1941	240	2430242.700	0.985

tained when the logarithm of the relative deflection was plotted against the logarithm of the intensity. As a measure of the intensity at the center of a line, not the lowest deflection in the line was used but rather that deflection below which the registration-curve (unsmoothed) runs for 0.03 A. This way of measuring line centers may have introduced slight systematic errors but appears to have resulted in good consistency from line to line, which was the main requirement for the purposes of this investigation. The continuum was measured in the following way. The entire wave-length range covered was divided into seventeen intervals, each approximately 16 A long. At each interval one measurement of the continuum was obtained by using the mean of all the line-free parts of the continuum in the interval. The seventeen measurements thus obtained were then plotted against wave length, and a smooth curve was drawn through them. From this curve were taken the final readings for the continuum.

Table 3 gives the resulting measurements of line depth in terms of D, which is defined as

$$D = \log \frac{\text{intensity of continuum}}{\text{intensity of line center}}.$$

TABLE 3

λ	*Fe*	χ_e	LOG x_0	LOG x_0'	LINE DEPTH, *D*, FOR EACH COUDÉ PLATE							
					2333	2394	2335	2425	2070	2428	2431	2373
4375.93	I	0.00	+2.19	+2.12	0.33	0.38	0.39	0.32	0.45	0.37	0.49	0.51
4383.55	I	1.48	+4.00	.....	.58	.67	.66	.57	.71	.56	.69	.76
4387.90	I	3.06	+1.04	+1.39	.20	.24	.24	.26	.30	.24	.34	.37
4388.41	I	3.59	+1.44	+1.44	.24	.27	.27	.26	.30	.24	.34	.35
4389.24	I	0.05	+1.04	+1.00	.09	.18	.17	.20	.26	.21	.32	.34
4404.75	I	1.55	+3.68	.....	.53	.62	.59	.54	.69	.53	.65	.72
4413.60	II	2.66	−0.12	−0.11	.22	.28	.24	.24	.29	.22	.28	.32
4415.12	I	1.60	+3.14	.....	.52	.60	.57	.50	.63	.51	.62	.68
4416.82	II	2.77	+0.90	+0.95	.45	.50	.46	.40	.46	.37	.43	.47
4427.31	I	0.05	+2.50	+2.69	.38	.45	.46	.43	.54	.45	.57	.67
4430.62	I	2.21	+1.87	+2.00	.30	.35	.36	.35	.43	.35	.44	.48
4433.22	I	3.64	+1.44	+1.38	.22	.25	.26	.24	.30	.25	.33	.38
4439.88	I	2.27	+0.29	.....	.05	.09	.12	.12	.17	.12	.22	.23
4442.34	I	2.19	+2.27	+2.24	.34	.40	.39	.38	.45	.39	.49	.53
4447.72	I	2.21	+2.21	+2.04	.32	.37	.38	.36	.42	.35	.44	.50
4466.55	I	2.82	+2.27	+2.28	.34	.39	.37	.36	.45	.39	.49	.54
4485.68	I	3.67	+1.04	+1.06	.18	.20	.19	.21	.27	.20	.28	.31
4489.18	II	2.82	+0.57	+0.77	.38	.45	.42	.36	.43	.35	.41	.44
4489.74	I	0.12	+1.78	+1.74	.20	.25	.25	.27	.38	.31	.41	.51
4491.40	II	2.84	+0.72	+0.75	.39	.45	.40	.34	.43	.36	.40	.44
4494.57	I	2.19	+2.37	+2.39	.37	.42	.43	.39	.50	.42	.48	.57
4508.28	II	2.84	+1.19	+0.99	.44	.52	.48	.39	.48	.39	.42	.46
4515.34	II	2.83	+0.99	+1.03	.44	.49	.48	.41	.47	.39	.45	.48
4517.53	I	3.06	+0.64	+0.73	.11	.16	.13	.17	.24	.18	.25	.27
4520.22	II	2.79	+0.99	+0.91	.41	.48	.46	.38	.47	.39	.42	.47
4547.85	I	3.53	+1.09	+1.08	.19	.17	.24	.20	.27	.21	.28	.30
4576.33	II	2.83	+0.41	+0.42	.34	.34	.35	.31	.38	.31	.35	.38
4582.84	II	2.83	+0.25	+0.35	.32	.34	.34	.30	.36	.29	.34	.36
4583.83	II	2.79	+1.55	.....	.....	.62	.56	.51	.58	.46	.55	.58
4587.13	I	3.56	+0.31	.....	.10	.11	.10	.14	.16	.16	.19	.20
4602.00	I	1.60	+0.81	+0.76	.12	.14	.15	.17	.24	.21	.26	.31
4602.94	I	1.48	+1.78	+1.78	.26	.30	.31	.29	.38	.34	.40	.46
4611.28	I	3.64	+1.50	+1.46	.21	.25	.24	.26	.33	.29	.36	.39
4619.29	I	3.59	+1.04	+1.04	.17	.19	.21	.18	.26	.21	.27	.30
4620.51	II	2.82	+0.23	+0.06	.29	.31	.29	.26	.31	.26	.29	.32
4625.05	I	3.23	+1.23	+1.30	.19	.23	.23	.24	.31	.26	.33	.37
4630.12	I	2.27	+0.76	+0.77	.11	.16	.16	.18	.23	.18	.25	.27
4632.92	I	1.60	+1.19	+1.34	.18	.18	.23	.26	.30	.27	.35	.40
4635.33	II	5.93	−0.42	.....	.13	.16	.14	.11	.13	.10	.11	.15
4637.51	I	3.27	+1.14	+1.05	.13	.17	.18	.18	.24	.22	.28	.32
4638.02	I	3.59	+1.04	+0.97	.14	.18	.17	.19	.24	.20	.26	.30
4643.47	I	3.64	+0.76	+0.74	.11	.12	.14	.16	.19	.18	.24	.27
4647.44	I	2.94	+1.40	+1.46	0.20	0.23	0.26	0.25	0.32	0.28	0.35	0.40

TABLE 3—*Continued*

λ	Line Depth, *D*, for Each Coudé Plate											
	2422	2802	2587	2054	2592	2375	2594	2397	2391	2035	2401	2607
4375.93	0.43	0.54	0.47	0.42	0.41	0.31	0.34	0.33	0.35	0.28	0.26	0.34
4383.55	.62	.79	.74	.62	.63	.56	.57	.54	.61	.53	.53	.57
4387.90	.31	.41	.35	.33	.30	.30	.24	.23	.22	.16	.15	.18
4388.41	.30	.38	.34	.29	.28	.26	.26	.25	.27	.19	.19	.23
4389.24	.29	.38	.34	.28	.27	.24	.18	.18	.18	.10	.09	.12
4404.75	.60	.76	.71	.63	.65	.53	.57	.53	.59	.49	.51	.52
4413.60	.26	.34	.30	.26	.27	.23	.26	.22	.25	.17	.20	.22
4415.12	.57	.69	.63	.60	.61	.54	.58	.54	.58	.48	.50	.51
4416.82	.37	.48	.41	.36	.38	.36	.41	.40	.48	.39	.40	.45
4427.31	.54	.67	.55	.55	.53	.44	.45	.43	.42	.34	.30	.39
4430.62	.38	.50	.43	.41	.37	.32	.36	.34	.32	.25	.24	.32
4433.22	.28	.36	.34	.31	.30	.24	.26	.25	.22	.18	.16	.22
4439.88	.16	.21	.20	.17	.17	.11	.12	.13	.07	.06	.06	.11
4442.34	.41	.53	.46	.43	.43	.36	.40	.39	.35	.30	.28	.36
4447.72	.37	.47	.43	.37	.38	.32	.36	.35	.34	.30	.27	.33
4466.55	.42	.53	.48	.45	.42	.37	.38	.40	.38	.31	.32	.35
4485.68	.25	.29	.29	.24	.25	.19	.21	.20	.18	.14	.15	.17
4489.18	.35	.41	.41	.37	.34	.32	.41	.39	.41	.38	.40	.42
4489.74	.38	.45	.42	.39	.40	.33	.35	.33	.24	.21	.19	.23
4491.40	.33	.42	.39	.35	.35	.31	.40	.39	.42	.41	.40	.42
4494.57	.43	.52	.47	.44	.42	.36	.42	.40	.42	.38	.36	.38
4508.28	.37	.43	.40	.40	.36	.34	.42	.43	.47	.47	.44	.46
4515.34	.38	.47	.43	.40	.40	.35	.41	.40	.47	.47	.43	.46
4517.53	.20	.26	.25	.22	.21	.16	.17	.15	.13	.12	.10	.12
4520.22	.37	.45	.41	.38	.37	.34	.39	.39	.45	.44	.41	.44
4547.85	.22	.30	.28	.22	.24	.19	.21	.20	.21	.16	.18	.19
4576.33	.29	.38	.34	.31	.31	.30	.35	.33	.35	.34	.36	.36
4582.84	.28	.36	.34	.30	.30	.30	.33	.30	.34	.34	.35	.36
4583.83	.44	.58	.50	.50	.49	.45	.52	.49	.53	.....	.58	.55
4587.13	.14	.22	.20	.16	.16	.14	.13	.13	.10	.09	.09	.10
4602.00	.19	.31	.27	.22	.22	.18	.17	.16	.14	.11	.06	.12
4602.94	.33	.46	.42	.35	.35	.32	.33	.31	.28	.29	.21	.27
4611.28	.29	.41	.35	.32	.30	.27	.27	.24	.22	.21	.15	.22
4619.29	.22	.32	.29	.23	.24	.21	.20	.19	.20	.17	.12	.17
4620.51	.23	.33	.29	.25	.24	.25	.27	.25	.31	.31	.26	.30
4625.05	.26	.36	.32	.28	.27	.24	.23	.21	.23	.20	.16	.21
4630.12	.22	.30	.27	.22	.21	.19	.17	.15	.12	.12	.11	.12
4632.92	.27	.37	.35	.33	.32	.26	.24	.22	.21	.18	.15	.18
4635.33	.09	.13	.13	.11	.10	.10	.12	.11	.13	.13	.10	.16
4637.51	.24	.31	.28	.25	.27	.24	.23	.21	.19	.16	.12	.19
4638.02	.21	.29	.26	.24	.22	.19	.21	.18	.19	.18	.12	.19
4643.47	.20	.26	.24	.20	.22	.18	.19	.17	.15	.12	.12	.14
4647.44	0.29	0.36	0.33	0.30	0.32	0.27	0.28	0.25	0.25	0.22	0.20	0.22

V. MEASUREMENTS OF RADIAL VELOCITIES

In the subsequent discussion of the measurements of line depths the assumption is made that all lines used arise essentially from the same atmospheric level. To check this assumption, the radial velocities were measured for the same set of lines on the same spectra in which the measurements of line depth were obtained.

On two of the twenty available spectrograms, Nos. 2375 and 2422, the definition of the comparison lines proved to be somewhat unsatisfactory for measurements of radial velocity, and these plates were omitted. Two other spectrograms have comparison lines too faint for measurement to the red of λ 4525, and the results which are given include only the violet portion of these spectra.

A preliminary examination of the original list of forty-three iron lines showed that a few of them could not yield values of the precision required. The lines λλ 4383.6, 4404.8, and 4415.1 were too strong and broad; λ 4439.9 and λ 4587.1 were too faint; λ 4427.3 was blended with a prominent *Ti* I line; and λ 4583.8 was affected seriously by a close *Fe* II line. After omission of these seven lines, thirty-six were available for measurement. The individual results for these lines on the eighteen spectrograms which were measured are given in Table 4. The letter "p" indicates a poor line and a somewhat uncertain result.

Some individual lines, such as those at λ 4413.6 and λ 4632.9, consistently show deviations from the mean from plate to plate. In general, these deviations appear to be larger at minimum than at maximum. It appears possible that some of these deviations are caused by blends. Such blends might affect the measurements strongly at minimum, since at this phase the spectra are less strongly exposed, so that the appearance of the line wings may more easily affect the setting on the line center.

The spectrum of η Aquilae shows some marked differences at maximum and at minimum of light on these high-dispersion photographs. In the region under consideration the most striking change is the great weakening of λ 4481 of *Mg* II at minimum. In general, most lines become wider and shallower at minimum, with occasional lack of symmetry and apparent wings. Lines of *Fe* II are usually somewhat weakened and widened and are less deep than at maximum. Lines of *Fe* I, for the most part, show little change of intensity but are more diffuse at minimum. These changes resemble those observed between the spectrum of the disk of the sun and that of sun spots. The character of the spectrum of η Aquilae at minimum makes accurate measurement of radial velocity much more difficult than at maximum and occasionally introduces uncertainties due to apparent structure and lack of symmetry in several of the lines.

Since the principal change in the spectrum of η Aquilae at minimum of light consists in a widening of many of the lines on the violet side, thus producing a lack of symmetry, a systematic difference in radial velocity is found between lines in which the whole width is measured and those in which the maximum of intensity is measured. The maximum is normally the correct portion to measure, as is shown by the agreement of the values when it is measured with those from lines which are little affected at minimum of light. It is occasionally possible, as in the case of some of the strong *Fe* II lines, to measure both the entire width and the maximum; but usually only one or the other can be observed satisfactorily.

The short supplementary Table 5 gives the radial velocities derived from measurements of the whole widths of certain lines on four spectrograms taken near minimum of light. These values have not been included in Table 4 or used in the derivation of the mean radial velocity for each spectrogram. A comparison of the results with the mean values shows an average systematic difference of about −3.5 km/sec, the centers of these wide and often unsymmetrical lines being displaced toward the violet with reference to the maximum of intensity in the lines.

If the lines of neutral iron and of ionized iron should arise at different atmospheric levels, the two sets of lines would give two separate radial velocity-curves which would

TABLE 4

λ	*Fe*	Radial Velocity for Each Coudé Plate								
		2333	2394	2335	2425	2070	2428	2431	2373	2802
4375.946....	I	−34.03	−33.71	−28.32	−21.44	−15.09	−16.25	−10.76	−2.05	+1.24
4387.901....	I	−31.64	−32.43	−26.50	−19.96	−13.49	−14.91	− 6.64	+1.31	+2.86
4388.416....	I	−32.73	−32.08	−29.02	−20.64	−14.51	−17.10	− 7.94	+0.84	+2.18
4389.256....	I	−32.45	−33.38	−29.70	−20.57	−15.81	−17.24	− 9.58	−0.26	+2.11
4413.601....	II	−31.37	−33.33	−28.09	−18.03	−12.35	−13.36	− 6.22	+5.34	+4.46
4416.829....	II	−32.90	−31.82	−27.24	−21.36	−14.18	−16.42	− 8.27	−0.09	+1.14
4430.624....	I	−31.40	−32.98	−28.80	−21.25	−15.30	−17.07	− 9.48	−1.85	+2.15
4433.232....	I	−33.67	−33.20	−29.39	−20.64	−14.41	−16.80	− 8.48	−0.01	+1.35
4442.351....	I	−31.81	−31.75	−26.46	−20.19	−14.87	−15.41	− 8.72	−0.75	+1.39
4447.730....	I	−32.50	−32.98	−27.15	−19.66	−15.06	−16.03	− 8.95	−0.94	+1.95
4466.564....	I	−32.78	−34.37	−28.66	−21.70	−15.75	−17.35	−10.70	−2.40	+0.01
4485.685....	I	−34.23	−33.41	−28.87	−22.86	−17.97	−19.13	−10.31	−2.37	+0.17
4489.189....	II	−32.86	−34.13	−28.70	−21.73	−15.43	−17.27	−11.66	−1.23	.....
4489.750....	I	−33.92	−32.72	−29.23	−19.93	−14.96	−16.00	− 8.92	+1.17	+1.92
4491.410....	II	−33.10	−32.51	−27.01	−20.00	−14.82	−15.88	− 9.26	−0.23	+0.53
4494.575....	I	−34.14	−33.17	−29.39	−20.84	−16.75	−17.35	−10.94	−3.63	.....
4508.293....	II	−32.29	−32.81	−27.78	−21.29	−15.11	−15.79	−10.73	−2.37	+0.57
4515.345....	II	−33.31	−32.68	−27.72	−22.56	−17.09	−16.87	−10.69	−4.18	.....
4517.537....	I	−33.55	−31.27	−27.70	−19.91	−15.62	−14.95	− 8.11	+0.46	+1.78
4520.231....	II	−33.06	−31.73	−28.60	−21.84	−15.88	−16.21	−11.77	−5.43	.....
4547.856....	I	−32.11	−33.46	−29.26	−20.22	−15.81	−16.35	− 8.90	−0.44	+0.91
4576.342....	II	−32.28	−30.85	−27.16	−19.29	−15.09	−14.45	− 8.36	+0.24	+1.29
4582.835....	II	−32.79	−31.87	−27.09	−20.28	−14.42	−14.87	− 7.60	+1.05	+2.30
4602.011....	I	−32.01	−30.30	−28.09	−20.77	−15.10	−15.31	− 8.99	−0.66	+1.80
4602.951....	I	−31.63	−31.41	−28.15	−20.90	−15.68	−15.12	− 8.93	−1.18	+0.50
4611.295....	I	−34.13	−33.38	−29.83	−22.54	−18.65	−18.65	−11.24	−1.82	.....
4619.299....	I	−32.19	−30.65	−27.74	−21.44	−15.19	−15.81	− 7.37	+0.05	+1.58
4620.522....	II	−32.15	−30.88	−28.24	−20.73	−15.77	−16.14	− 9.06	+0.08	+0.50
4625.054....	I	−34.37	−33.42	−30.73	−23.65	−17.18	−18.61	−10.63	−2.51	.....
4630.130....	I	−33.28	−34.47	−29.65	−20.74	−16.46	−16.03	− 7.87	−0.14	+2.07
4632.927....	I	−32.99	−35.75	−30.72	−23.53	−18.13	−18.37	−10.41	−3.76	.....
4635.316....	II	−31.15	−32.95	−27.85	−21.85	−14.95	−18.05	− 8.48	−1.07	.....
4637.512....	I	−31.71	−31.97	−30.15	−20.24	−15.21	−15.92	− 7.32	−0.03	+2.64
4638.019....	I	−32.35	−30.94	−29.11	−20.95	−17.21	−17.28	−10.56	+0.06	+0.57
4643.472....	I	−32.17	−32.59	−27.13	−21.54	−15.39	−15.55	− 8.32	−0.75	+1.69
4647.445....	I	−33.67	−32.25	−29.80	−22.77	−17.38	−17.43	− 9.69	−2.74	.....
Av. neutral...		−32.86	−32.72	−28.78	−21.16	−15.88	−16.64	− 9.19	−0.98	+1.54
Av. ionized...		−32.48	−32.13	−27.77	−20.81	−15.01	−15.94	− 9.28	−0.72	+1.54
Neut.−ion....		− 0.38	− 0.59	− 1.01	− 0.35	− 0.87	− 0.70	+ 0.09	−0.26	0.00
Average....		−32.74	−32.60	−28.47	−21.05	−15.61	−16.43	− 9.22	−0.90	+1.54

TABLE 4—*Continued*

λ	*Fe*	Radial Velocity for Each Coudé Plate								
		2587	2054	2592	2594	2397	2391	2035	2401	2607
4375.946	I	+0.53	+3.76	+5.94	+3.38	+0.55	−22.89	−27.75	−32.81	−34.45
4387.901	I	+3.82	+6.10	+8.91	+4.17p	+5.35p	−22.38p	−24.34p	−31.14	−31.81
4388.416	I	+1.23	+5.49	+7.68	+4.64p	+3.70p	−21.22p	−26.24p	−32.57	−33.24
4389.256	I	+0.55	+5.90	+6.38	+3.75p	+1.99p	−21.56p	−27.33p	−32.23	−33.51
4413.601	II	+3.09	+8.58p	+6.85	+4.85p	+5.47	−19.88p	−24.75p	−30.67	−32.01
4416.829	II	+2.22	+5.05	+5.82	+4.43	+3.27	−21.30	−27.30	−31.75	−32.74
4430.624	I	0.00	+5.27p	+5.99	+2.30	+2.39	−21.82	−25.12	−31.48	−33.24
4433.232	I	+1.49	+4.53	+7.47	+2.57p	+0.96p	−21.61p	−26.75p	−31.34	−32.69
4442.351	I	+0.42	+4.14	+5.35	+4.57	+2.73	−21.19	−25.94	−31.92	−32.06
4447.730	I	+0.23	+4.08	+4.12	+3.01	+2.10	−20.77	−25.68	−33.16	−33.05
4466.564	I	.....	+4.17	+3.61	+2.63	+1.47	−22.82	−26.49	−31.90	−34.27
4485.685	I	.....	+2.80p	+3.63	+3.39p	+1.44p	−21.51p	−25.56p	−32.52	−33.80
4489.189	II	.....	.....	.....	+2.45p	−0.72	−22.03	−28.60	−32.31	−34.66
4489.750	I	+2.49	+5.41	+7.09	+7.06p	+5.49p	−20.63p	−28.26p	−33.04	−34.05
4491.410	II	+1.49	+4.54	+5.08	+4.91	+3.48	−21.16	−27.03	−31.04	−33.11
4494.575	I	.....	+3.48	+4.34	+1.91p	+1.59	−22.62	−28.20	−31.90	−34.64
4508.293	II	.....	.....	.....	+3.08	+2.99	−21.66	−27.05	−31.63	−33.36
4515.345	II	.....	.....	.....	+3.13	+0.69	−22.58	−27.11	−31.11	−32.90
4517.537	I	+2.32	+6.11	+5.55	+4.25p	+1.15p	−22.37p	−26.96	−28.78	−32.10
4520.231	II	.....	.....	.....	+1.72	+1.60	−22.17	−26.53	−31.70	−33.42
4547.856	I	+0.17	.....	+4.02	+2.92	+2.78	−22.31	.....	−32.10	−32.34
4576.342	II	+0.80	.....	+6.31	+3.65	+2.44	−20.88	.....	−31.12	−33.71
4582.835	II	+2.32	.....	+8.25	+2.59p	+2.14p	−21.78	.....	−31.23	−33.88
4602.011	I	+0.77	.....	+5.07	+5.09	+0.62	−21.35p	.....	−31.97	−33.11
4602.951	I	+0.63	.....	+5.59	+3.78	+1.14	−21.68	.....	−31.19	−32.58
4611.295	I	.....	.....	+3.55	−0.46	−0.34p	−21.79	.....	−31.75	−33.21
4619.299	I	+0.40	.....	+6.35	+5.30p	+3.52p	−21.58p	.....	−30.34	−34.19
4620.522	II	.....	.....	+5.02	+2.84p	+2.67	−21.90	.....	−30.63	−32.53
4625.054	I	.....	.....	.....	+1.53	+0.97	−23.38	.....	−30.75	−34.72
4630.130	I	.....	.....	+7.64	+3.92	+1.91p	−23.18p	.....	−30.80	−34.18
4632.927	I	.....	.....	+3.88	+0.29p	+0.02	−24.72p	.....	−31.89	−34.17
4635.316	II	.....	.....	+4.59	+3.84p	+4.79p	−19.22p	.....	−32.73	−32.93
4637.512	I	+1.92	.....	+3.74	+3.58p	+2.26p	−21.61p	.....	−32.33	−33.96
4638.019	I	+0.37	.....	+6.39	+3.25p	+1.94	−22.06p	.....	−30.39	−33.12
4643.472	I	+0.69	.....	+5.47	+3.37p	+2.69	−20.89p	.....	−30.13	−31.11
4647.445	I	.....	.....	.....	+2.13	+1.83	−22.62	.....	−31.61	−32.00
Av. neutral		+1.06	.....	+5.55	+3.29	+2.01	−22.02	.....	−31.60	−33.26
Av. ionized		+1.98	.....	+5.99	+3.41	+2.62	−21.32	.....	−31.45	−33.39
Neut.−ion.		−0.92	.....	−0.44	−0.12	−0.61	− 0.70	.....	− 0.15	+ 0.13
Average		+1.27	+4.96	+5.66	+3.33	+2.20	−21.81	−26.65	−31.55	−33.30

show a slight shift in phase with reference to each other. In this case the two sets of lines would show a marked difference on the steep descending branch of the radial velocity-curve, while a small opposite difference might be expected during the long ascending branch. The observed differences given in the next to the last line of Table 4 do not show this effect. The average observed difference (neutr. − ion.) is −0.43 km/sec, and the maximum deviation from this mean for an individual plate is only ±0.6 km/sec.

It may be concluded that the radial-velocity measurements do not show any definite indication of a difference in effective atmospheric level for the lines of neutral and ionized iron used in this investigation.

TABLE 5

λ	*Fe*	Radial Velocity for Each Coudé Plate			
		2802	2587	2054	2592
4375.946	I	−0.68	.....	.....	.....
4466.564	I	.....	−0.08	.....	.....
4485.685	I	.....	−1.99	.....	.....
4489.189	II	−1.15	−1.18	.....	−0.78
4494.575	I	−0.92	−1.84	.....	.....
4508.293	II	−1.75	−1.05	+1.91	+2.95
4515.345	II	−2.21	−3.52	+0.20	+1.78
4520.231	II	−4.05	−3.64	+1.00	+1.70
4611.295	I	−1.93	−1.75	.....	.....
4620.522	II	.....	−0.37	.....	.....
4625.054	I	−1.49	−1.44	.....	+0.61
4630.130	I	.....	−0.75	.....	+3.18
4632.927	I	−1.45	−3.07	.....	+0.20
4635.316	II	−2.47	−0.61	.....	.....
4638.019	I	.....	.....	.....	+2.90
4647.445	I	−0.55	−1.11	.....	+2.43

VI. VARIATION OF TEMPERATURE AND ELECTRON PRESSURE

From the measurements of line depth discussed in Section IV temperatures and electron pressures were derived under the following two assumptions: First, it was assumed that there exists at each phase a unique relation (pseudo-curve of growth) between the measured line depth D and the quantity x, which is proportional to the number of absorbing atoms and to the oscillator strength (any effect of the wave length on this relation could here be neglected, since only a very small range of wave lengths was used). Second, it was assumed that the number of absorbing atoms follows the Boltzmann-Saha equations. If the sun is used as a standard, these equations take the form

for *Fe* I: $$\log \frac{x}{x_0} = a + (\chi_e - 2.43)\Delta\theta; \tag{4}$$

for *Fe* II: $$\log \frac{x}{x_0} = a + \delta + (\chi_e - 2.80)\Delta\theta, \tag{5}$$

with

$$\Delta\theta = \frac{5040}{T_0} - \frac{5040}{T} \tag{6}$$

and

$$\delta = (\chi_i + 0.37)\Delta\theta + \tfrac{5}{2}\log\frac{T}{T_0} - \log\frac{P_e}{P_{e0}}. \tag{7}$$

Here the subscript zero refers to the sun, χ_e denotes the excitation potential, and χ_i the ionization potential. The parameter a, which is a constant for each spectrum, depends on the zero point of the log x values, which was chosen arbitrarily for each spectrum, as described below. The numerical values subtracted from χ_e in equations (4) and (5) represent the mean excitation potentials of the neutral and ionized lines used. These values are introduced only for convenience in the subsequent least-squares solutions. Their difference occurs in equation (7) as a correction to χ_i.

In Table 3 are listed χ_e and x_0 for all the lines used. The values for x_0 were derived from Allen's solar equivalent widths[11] with the help of K. O. Wright's empirical curve of growth[12] for the sun.

The pseudo-curve of growth relating the observed D values with the theoretical x values was derived for each spectrum in the following way: Log x was computed for each of the thirty-one lines of neutral iron, with the help of equation (4), from log x_0 as given in Table 3, by setting $a = 0$ and using a preliminary estimate for the temperature. The observed D values were plotted against these preliminary log x values, and a smooth curve was drawn through the points. Next, the deviations of the individual points from the smooth curve were inspected for their dependence on the excitation potential, and thus an improved temperature value was found for each spectrum. At the same time an improved value of x_0 was found for each line as follows: From the preliminary pseudo-curves of growth a log x value corresponding to the observed D was read for each line of neutral iron for each spectrum. The twenty log x values for any one line were averaged, and the differences, $\overline{\log x} - \log x_0$, were plotted against the excitation potential. This plot showed a small dependence of the difference upon the excitation potential. A correction corresponding to this correlation was subtracted from each $\overline{\log x}$ value, and the $\overline{\log x}$ values thus corrected were used in place of the original log x_0 values. Now final pseudo-curves of growth could be obtained by plotting the observed D values against log x values computed with the new temperature estimates and with the new log x_0 values. For these plots only twenty-six of the *Fe* I lines were used, leaving out the four lines of lowest excitation potential. Thus the range in excitation potential for the lines plotted was reduced to 2.2 volts, so that any error in the temperature estimate had little influence upon the relative positions of the points. Again a smooth curve was drawn through the points for each spectrum.

From these final pseudo-curves of growth, final log x values corresponding to the observed D values were read for all spectra and all observed lines, with the following exceptions: the three strongest lines (λλ 4383.5, 4404.7, and 4415.1) and the two faintest lines (λ 4439.9 and λ 4587.1) of neutral iron, which had been essential for determining the ends of the pseudo-curves of growth, could not, in turn, be used for an accurate derivation of log x values; the line of ionized iron at λ 4583.8 was found too bright, and the line at λ 4635.3 too weak on many spectra to permit accurate log x readings. The last line gave x values, on those spectra on which reasonably accurate x values could be derived, which were approximately fifteen times larger than the values corresponding to the solar x_0. This observation may be taken to indicate that the state of ionized iron from which this line arises and which has an excitation potential of 5.93 volts is either superexcited in the sun or subnormally excited in η Aquilae. Though this line shows systematically abnormal weakness in η Aquilae, its variation with phase, so far as observed, is in agreement with what would be expected from the variation of temperature and electron pressure as derived from the other lines. Hence the abnormality shown by this line does not appear to cast any doubt upon the results derived from the other lines.

From the final log x values, final log x_0 values were derived by again averaging the log x values for each line on the twenty spectra, by finding the correlation of $\overline{\log x} -$

[11] *Mt. Stromlo Commonwealth Solar Obs., Memoir* No. 5, Part II, 1934.

[12] *Ap. J.*, 99, 249, 1944.

log x_0 with the excitation potential for the lines of *Fe* I, by applying a correction corresponding to this correlation to the $\overline{\log x}$ values of all lines, and, finally, by subtracting from the $\overline{\log x}$ value of each line of *Fe* II the average value of $\overline{\log x} - \log x_0$ for the ten lines of *Fe* II. The final values for x_0, denoted by x_0', are given in Table 3. A comparison of the x_0' values with the original x_0 values shows that the two sets are systematically identical in the sense that the difference $\log x_0' - \log x_0$ does not show any correlation with line intensity, excitation potential, or degree of ionization. Individually, however, the x_0' values represent much more accurately the line-depth measurements in η Aquilae than do the original x_0 values and hence form a better basis for the following derivation of temperatures and electron pressures.

For each spectrum the final relative temperature was derived from a least-squares solution for the log x values of the remaining twenty-six lines of *Fe* I, according to equation (4). Here a and $\Delta\theta$ were considered as unknowns and the x_0' values just derived were used in place of x_0. The resulting values of $\Delta\theta$ are listed in Table 6 and plotted in Figure 2.[13]

The relative temperatures thus derived correspond to the excitation temperatures, whereas in the following discussions the ionization temperatures are needed. From the data given in Section III we find for the effective temperature

$$\frac{5040}{T_{\min}} - \frac{5040}{T_{\max}} = 0.17 ,$$

whereas the temperature plot in Figure 1 gives for the excitation temperature

$$\frac{5040}{T_{\min}} - \frac{5040}{T_{\max}} = 0.19 .$$

Because of the fair agreement between these two temperature amplitudes, it may be reasonably safe to assume that the ionization temperature also has the same amplitude and that the variation of the excitation temperature with phase is represented with sufficient accuracy by the variation of $\Delta\theta$ for the excitation temperature. To obtain not only the variation of the ionization temperature but also its absolute value, the appropriate value of T_0 has to be found. The iron lines used here may be expected to arise in the sun at a level with an optical depth of approximately 0.3. At this level the local temperature[14] is about 5300°. This value for T_0 gives for η Aquilae at mid-descending branch ($\Delta\theta = 0$) an ionization temperature of 5300°. At this phase the effective temperature of η Aquilae is also approximately 5300°. Since an ionization temperature essentially larger than the effective temperature could hardly be expected, the above value for T_0 appears to be an upper limit. On the other hand, a smaller value for T_0 leads to dynamical difficulties, as indicated in Section X. Hence the value used in all subsequent computations is

$$T_0 = 5300° .$$

Finally, the electron pressure may be derived for each spectrum in the following way. According to equation (5), δ can be obtained from the log x value of any one line of *Fe* II if the values for a and $\Delta\theta$ as determined from the *Fe* I lines are used. For each spectrum the values of δ obtained from the ten *Fe* II lines were averaged. These averages are given in Table 6. With δ, $\Delta\theta$, and hence T known, the relative electron pressure can be computed from equation (7). The results are listed in Table 6 and plotted in Figure 2.[13]

[13] Very similar results have been published recently for δ Cephei by Th. Walraven, *Pub. Astr. Inst. U. Amsterdam* No. 8, 1948.

[14] B. Strömgren, *Festschrift für Elis Strömgren* (Copenhagen: E. Munksgaard, 1940), p. 218.

The accuracy of the resulting temperatures and electron pressures may best be judged by an inspection of the plots in Figure 2. A measure for the accuracy of the original observations of line depths was obtained in the following way. From equations (4) and (5) values of log x may be computed with the help of the final data for x_0, a, δ, and $\Delta\theta$. From the differences between these computed values and those found directly from the observations, the probable error of one value of log x is found to be ± 0.08. With an average slope of the pseudo-curves of growth of $dD/d \log x = 0.15$, the above value corresponds to a probable error in D of ± 0.012, or, expressed in magnitudes, ± 0.03. This small probable error characterizes only the internal accuracy of the line-depth measurements in one spectrum. In the present investigation this high internal accuracy

TABLE 6

Plate No.	Phase	$\Delta\theta$	δ	$\log \frac{P_e}{P_{e0}}$	$h \cdot 10^8$	$\log \rho$	$\log \kappa$	$\log \rho_m$
2333	0.013	+0.090	+1.773	−0.92	1782	−8.51	−1.58	−8.14
2394	.037	+ .041	+1.724	−1.34	875	−8.64	−1.90	−8.60
2335	.145	+ .026	+1.627	−1.38	582	−8.55	−1.92	−8.52
2425	.280	+ .016	+1.418	−1.27	318	−8.26	−1.79	−8.10
2070	.398	− .024	+1.332	−1.56	160	−8.39	−2.00	−8.45
2428	.418	− .021	+1.247	−1.44	136	−8.26	−1.90	−8.20
2431	.556	− .084	+1.004	−1.79	36	−8.44	−2.13	−8.62
2373	.632	− .109	+0.919	−1.93	22	−8.56	−2.23	−8.84
2422	.638	− .111	+1.011	−2.04	26	−8.67	−2.34	−9.06
2802	.643	− .117	+0.924	−2.01	20	−8.63	−2.29	−8.97
2587	.651	− .091	+0.989	−1.84	32	−8.48	−2.16	−8.70
2054	.671	− .089	+1.005	−1.84	34	−8.48	−2.17	−8.70
2592	.686	− .090	+1.037	−1.88	36	−8.53	−2.20	−8.78
2375	.755	− .041	+1.220	−1.60	100	−8.36	−2.02	−8.44
2594	.820	+ .017	+1.467	−1.31	361	−8.34	−1.83	−8.22
2397	.824	+ .028	+1.431	−1.17	380	−8.22	−1.71	−7.98
2391	.898	+ .057	+1.694	−1.16	993	−8.51	−1.75	−8.32
2035	.923	+ .084	+1.947	−1.16	2472	−8.86	−1.80	−8.72
2401	.961	+ .109	+1.926	−0.90	3199	−8.72	−1.58	−8.36
2607	0.985	+0.087	+1.820	−1.00	1914	−8.61	−1.65	−8.31

was necessary, whereas systematic errors, affecting equally lines of equal depths in one spectrum, would only distort the pseudo-curves of growth and not affect the relative log x values.

VII. HYDROGEN ABUNDANCE

Before the density variation could be determined from the data presented in the preceding section, it was found necessary to obtain an estimate of the hydrogen to metal ratio, A (by atom numbers), for η Aquilae. If the sun is again used as standard and if it is assumed that the relative abundances of the different metals are essentially equal in η Aquilae and the sun, then A can be determined for η Aquilae by the measurement of the equivalent width of one *Fe* I line, on the basis of the following considerations.

The equivalent width of a weak line falling on the linear portion of the curve of growth is proportional to the number of absorbing atoms multiplied by the oscillator strength and divided by the continuous-absorption coefficient. Hence

$$\frac{W}{W_0} = \frac{N}{N_0} \frac{\kappa_0}{\kappa}, \tag{8}$$

where W denotes equivalent width, N the number of absorbing atoms, and κ the continuous-absorption coefficient. The subscript zero again refers to the sun. The quantities N and κ may both be measured per gram of hydrogen. The total number of iron atoms per gram of hydrogen is proportional to the reciprocal of A. Of this total the fraction of atoms which are neutral and exicted to a certain level may be found from the Boltzmann-Saha equations. Hence one finds, for the ratio of absorbing atoms in η Aquilae and the sun,

$$\log \frac{N}{N_0} = \log \frac{A_0}{A} + \log \frac{P_e}{P_{e0}} - (\chi_i - \chi_e)\,\Delta\theta - \tfrac{5}{2} \log \frac{T}{T_0}. \tag{9}$$

In the derivation of this equation it has been assumed that the majority of the iron atoms are in the ground state of the ionized atom, which appears to be a good approximation both for the sun and for η Aquilae.

Next the ratio of the continuous-absorption coefficients in the sun and η Aquilae has to be found. In the sun H^- provides nearly the entire continuous absorption. The same is found to be true for η Aquilae if the metal absorption[15] is compared with H^- absorption,[16] assuming the temperatures and electron pressures derived in the preceding section. For wave lengths near λ 4500 and for temperatures in the range here in question, the numerical values for the H^- absorption coefficient may be represented with fair accuracy by

$$\log \kappa = -3.153 + \log P_e + 1.80\,\frac{5040}{T}. \tag{10}$$

This gives for the ratio of κ in η Aquilae and the sun

$$\log \frac{\kappa}{\kappa_0} = \log \frac{P_e}{P_{e0}} - 1.80\Delta\theta. \tag{11}$$

Introducing the expressions for the ratios in N and κ given by equations (9) and (11) into the basic equation (8), we obtain

$$\log \frac{W}{W_0} = \log \frac{A_0}{A} - (\chi_i - \chi_e - 0.6)\,\Delta\theta. \tag{12}$$

Here the last term of equation (9) was replaced with sufficient accuracy by $1.2\Delta\theta$.

To determine A for η Aquilae with the help of equation (12) it is sufficient in principle to apply this equation only at one phase to one *Fe* I line. The phase chosen was that of the mean of the four spectra available near mid-descending branch (plates Nos. 2070, 2335, 2425, and 2428). The value chosen for the line was the mean of the two weak lines at λ 4439.9 and λ 4587.1. The equivalent widths of these two lines were measured on the four spectra. The mean values are given in Table 7.

Before these equivalent widths could be used in equation (12), it was necessary to ascertain how closely the two selected lines lay to the linear portion of the curve of growth. For this purpose six more lines were measured on the four spectra. The mean results for these lines are also listed in Table 7. In Figure 3 the measured values of W are shown plotted against the corresponding values of $\log x_0$ directly obtained from the sun, as discussed in Section VI. No temperature corrections had to be applied to the values of $\log x_0$ because at mid-descending branch the excitation temperature of η Aquilae is equal to that of the sun, as shown by the temperature plot in Figure 2. A theoretical curve of growth[17] was drawn through the eight observed points and reproduced in

[15] A. Pannekoek, *Pub. Astr. Inst. U. Amsterdam*, **4**, 40, 1935.

[16] S. Chandrasekhar and Frances H. Breen, *Ap. J.*, **104**, 444, 1946.

[17] A. Unsöld, *Physik der Sternatmosphären* (Berlin: Julius Springer, 1938), p. 268.

Figure 3. From this graph it is apparent that the two lines selected (corresponding to the two left-most points in Fig. 3) do not fall on the linear portion of the curve of growth but that their equivalent widths are already appreciably affected by saturation of their cores. However, from their vertical distance from the linear asymptote of 0.3 in log W, one may conclude that their equivalent width would not be 0.08 A, as observed, but rather 0.16 A, if the saturation effect had been absent. A similar situation is found from the curve of growth of the sun.[12] The observed mean equivalent width of the two lines

TABLE 7

λ	log x_0	W
4383.55	+4.00	0.41A
4404.75	+3.68	.41
4439.88	+0.29	.08
4466.55	+2.27	.26
4547.85	+1.09	.14
4587.13	+0.31	.08
4602.00	+0.81	.11
4602.94	+1.78	0.22

TABLE 8

Distance from Line Center (A)	Normalized Depth
0.031	2.87
.094	2.36
.163	1.44
.234	0.71
.298	0.26
0.369	0.03

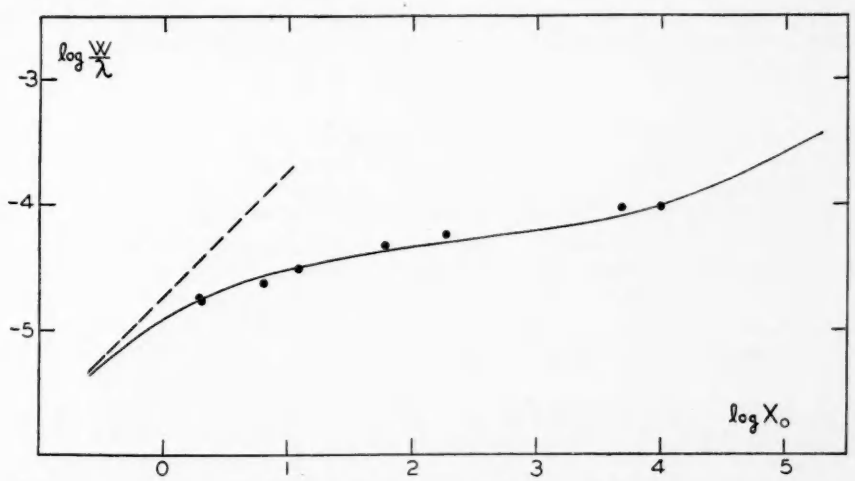

FIG. 3.—Curve of growth of η Aquilae at mid-descending branch

is 0.05 A in the sun. The saturation effect is approximately 0.2 in log W, and hence the equivalent width freed of the saturation effect would be 0.08 A. Accordingly, the value chosen for use in equation (12) was

$$\frac{W}{W_0} = \frac{0.16}{0.08} = 2 .$$

Figure 2 shows that, at the selected phase at mid-descending branch, $\Delta\theta$ is equal to 0. According to the discussion of Section VI, this should apply not only to the excitation temperature but also to the ionization temperature. Hence the last term of equation (12) was taken to be 0. Equation (12) then gave

$$\frac{A_0}{A} = 2 \qquad \text{or} \qquad A = 4000 ,$$

where $A_0 = 8000$ was taken for the sun.[14] The value of A obtained is somewhat sensitive to the temperature difference used. A decrease of 200° in the representative temperature of η Aquilae relative to that of the sun would increase A, according to equation (12), by 50 per cent. Nevertheless, it may be concluded that the hydrogen-metal ratio in the atmosphere of η Aquilae is not different from that in the sun by a large factor, and, in fact, it seems likely that this ratio is somewhat smaller in η Aquilae than in the sun.

VIII. VARIATION OF DENSITY

From the data given in the two preceding sections, the density variation in the atmosphere of η Aquilae may be derived. The density may be computed from the equation of state for a perfect gas if the temperature, the mean molecular weight m, and the gas pressure P_g are known. The line-depth measurements give only the electron pressure, not the gas pressure directly. Hence it is necessary to determine the ratio of P_g to P_e, which is equal to the ratio of the number of all particles to the number of free electrons. The number of all particles per gram is equal to $1/m$. The number per gram of free electrons produced by the ionization of hydrogen is equal to $(X/H)h$. Here X denotes the hydrogen abundance by mass, which is taken to be 0.35 in the following computations; H is the mass of the proton; and h is the fraction of the hydrogen atoms which are ionized. The number of free electrons produced by the ionization of the metals is equal to $(X/H)(1/A)$, if the majority of the metal atoms are singly ionized. Hence we find

$$\frac{P_g}{P_e} = \frac{\frac{1}{m}}{\frac{X}{H}\left(h + \frac{1}{A}\right)}. \tag{13}$$

The degree of ionization of hydrogen, h, is determined by the Saha equation,

$$\log h = 13.54\Delta\theta + \tfrac{5}{2}\log\frac{T}{T_0} - \log\frac{P_e}{P_{e0}} + \text{const.}, \tag{14}$$

with

$$\text{const.} = -13.54\,\frac{5040}{T_0} + \tfrac{5}{2}\log T_0 - \log P_{e0} - 0.48 = -5.00.$$

Here $\log P_{e0} = +0.95$[13] was used for the representative level in the solar atmosphere. With equation (13) we find, from the perfect gas law,

$$\rho = \frac{HP_{e0}}{XkT_0}\frac{T_0}{T}\frac{P_e}{P_{e0}}\left(h + \frac{1}{A}\right)^{-1}, \tag{15}$$

where the sun has again been used as a standard. From equations (14) and (15), h and ρ have been computed for each of the twenty spectra. The results are listed in Table 6.

The data derived thus far for the atmosphere of η Aquilae all refer to the representative level for the iron lines used. During the pulsation period this representative level may move up and down relatively to the matter of the atmosphere and hence cannot be assumed to coincide with a given mass element throughout the cycle. Indeed, the variation of the absorption coefficient at the representative level (computed per gram of hydrogen from eq. [10], listed in Table 6, and plotted in Fig. 1) shows that the opacity is high near maximum phase as compared with minimum phase and hence that the representative level will coincide with higher mass elements at maximum than at minimum. Therefore, the density variation computed above does not represent the density variation of a given mass element. The latter, however, is needed for the discussion of the pulsation dynamics and may be derived as follows:

Because of the limited height of the photosphere, the absorption coefficient may be assumed to differ at one phase compared with another by the same factor at all photospheric levels. With this approximation, the optical depth for a given mass element will vary during a cycle in proportion to the absorption coefficient at that element. In passing from one mass element to a deeper one, the optical depth will increase proportionately to the mass above the element. Because of the hydrostatic equilibrium underlying the pulsation, the average density will also be proportional to the mass above the element so long as the average gradient of the total kinetic temperature is not large. The optical depth at a given mass element and time will therefore be proportional to the instantaneous absorption coefficient at the element multiplied by the average density of the element.

Applying this general relation to the representative level of the iron lines used, which is characterized by an essentially fixed optical depth, we find that the absorption coefficient in the representative level varies in proportion to the reciprocal of the average density of the mass element with which the representative level happens to coincide at any moment. On the other hand, the actual density of the coinciding mass element is equal to the density in the representative layer at the time considered, as computed above. Hence the ratio of the actual density of the coinciding mass element at any time to its average density is proportional to the density multiplied by the absorption coefficient in the representative level at the time considered. Since for a fixed mass element the average density is a constant, the density, ρ_m, in a given mass element is found from the relationship

$$\rho_m \propto \rho\kappa \,. \tag{16}$$

From the data for ρ and κ given in Table 6, ρ_m was computed according to equation (16), where the proportionality factor was chosen so that the average of log ρ_m was equal to the average of log ρ. The results for ρ_m are listed in Table 6 and plotted in Figure 2.

The scatter in the density plot of Figure 1 indicates that the accuracy reached in the measurements of line depths was only just sufficient to permit the determination of the main features of the density variation. In addition to the observational scatter, a second source of error in the derivation of the density variation is to be noted. If one is concerned not with absolute values but with the variation of T or P_e or κ, the values used for T_0, P_{e0}, or A have little or no influence. The determination of the density variation, however, is affected appreciably by these values because of the occurrence of the last factor in equation (15). Table 6 shows that, near maximum, h is larger than $1/A$, while the reverse is true near minimum. This indicates that at maximum most free electrons come from hydrogen, and at minimum from the metals. Hence the total amplitude of the variation of the last factor in equation (15) depends on the value of A and on the value of h at maximum. The value of h, in turn, is sensitive to the value of T_0, according to equation (14). The consequences of possible errors from this source are discussed in Section XI.

IX. TURBULENCE IN THE PHOTOSPHERE

Before the density variation derived in the previous section can be used for the discussion of the dynamics of the atmospheric pulsations, the degree of turbulence in the photosphere has to be determined. This can be done either with the help of the curve of growth or from measurements of line profiles. Both these methods were applied to η Aquilae for the determination of the degree of turbulence at mid-descending branch (as represented by the mean of the four spectra used in Sec. VII).

The equivalent widths of the eight lines listed in Table 7 were plotted, and a theoretical curve of growth was adjusted to them, as shown in Figure 2. This fit gave $R_c\xi_0 = 3.4$ in Unsöld's terminology.[18] Since the entire flat portion of the curve of growth is covered

[18] *Ibid.*, pp. 158 and 268.

by the observed points, the value for $R_c\xi_0$ will depend but little on the model of the atmosphere upon which the theoretical curve of growth is based. The representative value of R_c, however, does depend upon the model and also upon the relative importance of true absorption and scattering.[19] Approximate extreme values for R_c are 0.6 and 1.0. With an intermediate value of $R_c = 0.85$, we find:

$$\xi_0 = 4 \text{ km/sec}$$

from the curve of growth. This value for ξ_0 may be compared with the representative value,

$$\xi_0 = \sqrt{2\frac{k}{m}T} = \frac{9.3}{\sqrt{\mu}}, \tag{17}$$

for the thermal motion, where $\mu = m/H$ is the molecular weight in proton units. This equation gives $\xi_0 = 1.2$ km/sec for the thermal motion of iron ($\mu = 56$). The comparison of this value with that obtained from the curve of growth clearly shows the existence of turbulence in the atmosphere of η Aquilae.

For the second determination of the degree of turbulence, from line profiles, the four weakest lines of Table 7 were used. An average profile was determined for each of these four lines from the four spectra representing the mid-descending branch. The wings on the short-wave-length side of the lines at λ 4439.88 and λ 4587.13 were not included in the measurements, since they appeared to be affected by possible blends. The portions of the four lines included in the measurements seemed to be entirely free of blending. The four profiles were normalized by dividing each measurement of depth (intensity of continuum − intensity of line/intensity of continuum) by the equivalent width of the line in question. Finally, all the normalized depths obtained from the measurements of the four lines were averaged into the six normal points listed in Table 8 and plotted in Figure 4.

As shown by the heavy curve in Figure 4, the measurements are well represented by an error-curve, with a dispersion corresponding to $\xi_0 = 12.7$ km/sec. Since the instrumental profile may be estimated to correspond approximately to $\xi_0 = 3.5$ km/sec,[20] we find

$$\xi_0 = 12.2 \text{ km/sec}$$

for the true line profile. This result shows that the line profiles indicate much faster motions than does the curve of growth. The difference between the two ξ_0 values appears too large to have been caused by observational errors. The discrepancy cannot be explained by the assumption of an increase of the turbulence, with height affecting lines of different strength differently,[21] since the same lines were used for the curve of growth and for the line profiles. Moreover, the reduction of the observed line profiles to the profile of the line-absorption coefficient with the help of the radiation-transfer equation does not explain the discrepancy. The four lines used all have central intensities of more than 60 per cent of the continuum, and hence this reduction decreases the value of ξ_0 by less than 2 km/sec.

The discrepancy between the results from the curve of growth, on the one hand, and the line profiles, on the other, may be explained by large-scale motions in the photosphere of η Aquilae, which will broaden the line profiles but not affect the equivalent widths. These large-scale motions may be of two types: either a rotation of the star as a whole or a convection with turbulent elements so large that their linear dimensions

[19] *Ibid.*, p. 248.

[20] L. Spitzer, Jr., *Ap. J.*, **90**, 498, 1939.

[21] For comparison see O. Struve, *Ap. J.*, **104**, 138, 1946.

exceed the depth of the effective photospheric layers and hence have but little effect upon the equivalent widths and the curve of growth.

That the measured line profiles may be represented by a rotation is shown by the lighter curve in Figure 4. This curve was computed from a rotation profile[22] with $w \sin i = 15$ km/sec, where w stands for the equatorial velocity and i for the inclination of the axis to the line of sight (an intermediate value was used for the limb-darkening coefficient). On this rotation profile was superimposed a Doppler broadening according to an error-curve with $\xi_0 = 5$ km/sec, which should represent approximately the combined effects of the instrumental broadening and those of the small turbulence found from the curve of growth. Figure 4 shows that the observed profile is practically as well represented by this modified rotation profile as by the error-curve corresponding to

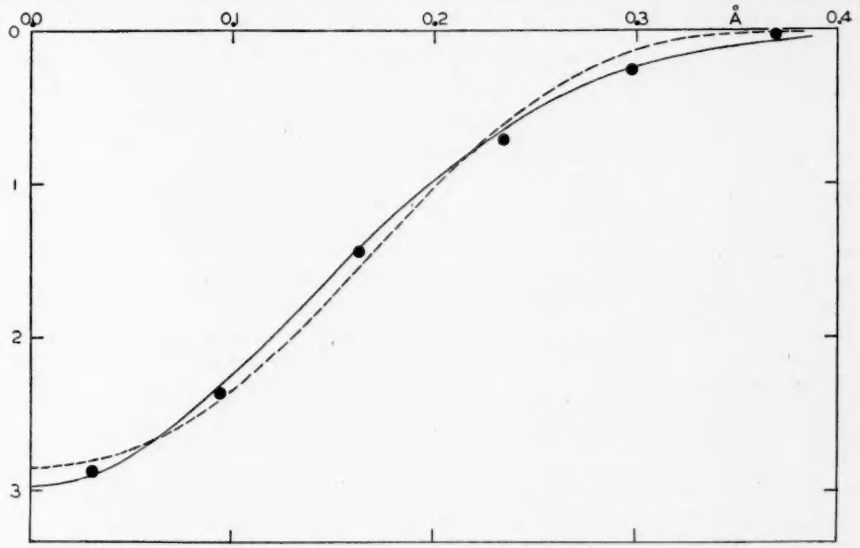

FIG. 4.—Normalized line profile for η Aquilae at mid-descending branch

$\xi_0 = 12.2$ km/sec (plus instrumental broadening), which may be taken to represent high-speed turbulence.

Therefore, it does not seem possible to decide, on the basis of the line-profile measurements alone, which of the two types of large-scale motion actually occurs in η Aquilae. A tentative decision on the basis of dynamical considerations is given in the following section.

X. QUASI-STATIONARY EQUILIBRIUM

The two types of large-scale convection (discussed in the preceding section as possible explanations for the observed wide line profiles) differ greatly in their dynamical consequences. The first type consists of a rotation with $w \sin i = 15$ km/sec and a small degree of turbulence with $\xi_0 = 4$ km/sec. Since it is geometrically improbable that $\sin i$ is smaller than 0.3, it is not likely that w is larger than 50 km/sec. With this probable upper limit, one finds the centrifugal acceleration at the equator to be, at most, 10 per cent of the gravitational acceleration. Hence the rotation will produce, at most, a moderate distortion of the star. The additional weak turbulence has velocities large compared with the thermal velocities of iron. Dynamically, however, it is not the ther-

[22] A. Unsöld, *op. cit.*, p. 318.

mal motions of the relatively few metal atoms that are of importance but rather the thermal velocities corresponding to the mean molecular weight, which is essentially determined by the relative abundance of hydrogen and helium. Since the mean molecular weight, μ, may be expected to lie between 1.4 and 2.0, the corresponding thermal motion would give $\xi_0 \approx 7$ km/sec, according to equation (17). Compared with this velocity (considering squares of velocities), the turbulent velocities shown by the curve of growth ($\xi_0 = 4$ km/sec) are small. Altogether, therefore, the first type of large-scale convection has only small dynamical consequences.

The second type of convection, consisting of large-scale turbulence, has velocities ($\xi_0 = 12.2$ km/sec) which are large compared with the essential thermal velocities. The total kinetic pressure, P_k, will in this case exceed appreciably the gas pressure, P_g. Since the pressures are proportional to the squares of their respective velocities, we find, with the help of equation (17),

$$\frac{P_k}{P_g} = \frac{(12.2)^2 + \left(\frac{9.3}{\sqrt{\mu}}\right)^2}{\left(\frac{9.3}{\sqrt{\mu}}\right)^2} = 1.7\mu + 1 . \tag{18}$$

The use of an intermediate value, $\mu = 1.7$, for the mean molecular weight gives a total kinetic pressure four times as large as the gas pressure. If the turbulent motions should not be isotropic but, instead, preferentially radial, even larger radial turbulent velocities would have to be assumed for the explanation of the line profiles; and, as a result, the total kinetic pressure would exceed the gas pressure by a somewhat larger factor. Hence the dynamical consequences of the second type of large-scale convection are great.

Because of the great difference in the dynamical effects of the two convection types, a decision between them may be attempted with the help of Pannekoek's gravity test. At the phase of mid-descending branch the pulsational velocities and accelerations are so small that the assumption of quasi-stationary equilibrium should give a reasonable approximation. At this phase the total kinetic pressure at a given layer is determined by the weight of the material above the layer:

$$P_k = g \int_b^\infty \rho \, db , \tag{19}$$

where g is the gravitational acceleration and b measures the height in the atmosphere. For the same layer the optical depth is given by

$$\tau = X \int_b^\infty \kappa \rho \, db . \tag{20}$$

The hydrogen abundance, X, appears in the equation because κ is reckoned per gram of hydrogen. Dividing these two equations, we find

$$\frac{\tau g}{P_k X} = \frac{\int_b^\infty \kappa \rho \, db}{\int_b^\infty \rho \, db} = \bar{\kappa} . \tag{21}$$

If κ decreases approximately in proportion to ρ and if ρ decreases approximately exponentially with height, we have $\bar{\kappa} = \kappa/2$. With this relation the above equation becomes

$$g = \frac{X}{\tau} \frac{P_k}{P_g} \frac{P_g}{P_e} P_e \frac{\kappa}{2} . \tag{22}$$

Using for the ratio of P_g to P_e the expression of equation (13) and for the ratio of P_k to P_g that of equation (18), which represents the convection type with high turbulence, we finally obtain

$$g = \frac{(1.7 + \mu^{-1})}{(h + A^{-1})} \frac{P_e \kappa}{2\tau}. \tag{23}$$

This relation may be applied to the representative layer of the observed iron lines at mid-descending branch. With $\tau = 0.3$, $\mu = 1.7$, $\log P_e = -0.46$, $\log \kappa = -1.90$, and $\log (h + A^{-1}) = -3.28$ (where the last three values were taken from Table 6 by averaging the values for the four spectra representing mid-descending branch, Nos. 2335, 2425, 2070, and 2428), we obtain 32 for the right-hand side of equation (23). For the left-hand side we find 123 if the gravitational acceleration is computed with the mass derived from the mass-luminosity law in Section III. This discrepancy of a factor 4 does not appear too serious in view of the uncertainties, particularly in the mass of the star, in the representative optical depth, in the relation between κ and κ, and in the possible deviation of the turbulence from isotropy. The discrepancy would have been appreciably increased if a smaller ionization temperature had been chosen in Section VII, since this change would have decreased both P_e and κ.

On the other hand, if the ratio of P_k to P_g is not taken from equation (18) but is set equal to 1, corresponding to the convection type with rotation, the result is 8 for the right-hand side of equation (22), which increases the discrepancy to a factor of 16. This discrepancy appears much too large.

The preceding discussion indicates that the first type of large-scale convection, consisting of a rotation with a small degree of turbulence, leads to an appreciable discrepancy with the quasi-stationary equilibrium condition at mid-descending branch, whereas the second type, consisting of large-scale turbulence, does not lead to serious difficulties. Therefore, one may tentatively conclude that the photosphere of η Aquilae is in a state of turbulence with superthermal velocities ($\xi_0 = 12.2$ km/sec) and with elements of linear dimensions exceeding the depth of the effective photospheric layers.

XI. SIMPLE PROGRESSIVE WAVE

In the preceding section the convective state underlying the pulsation in the atmosphere of η Aquilae was discussed. The character of the pulsation may be investigated on this basis, with the help of the velocity variation as given in Section II and the density variation as derived in Section VIII.

If the character of the pulsation in the photosphere corresponds to a standing wave, the variations of the displacement and of the reciprocal of the density should be similar in form and phase. That such a similarity does not occur in the photospheric pulsation is shown with reasonable certainty by a comparison of the two corresponding drawings in Figure 2, in spite of the appreciable inaccuracy in the density determinations. If, on the other hand, the pulsation has the character of a progressive wave, the similarity in form and phase should occur between the variations of the velocity and the density. Figure 2 shows that, as regards form, these two variations appear, in fact, to be reasonably similar. In phase the density variation seems to precede the velocity variation by about 0.1 period. This phase shift can be understood as a result of the sphericity of the pulsation and of the increase of the amplitude outward, as shown in the following section.

A more quantitative test of the progressive wave picture for the photospheric pulsation can be obtained by considering the relation between the velocity amplitude and the density amplitude. If r denotes the position of a given atmospheric layer at time t and if r_0 denotes the mean position of the same layer, then a simple progressive wave of small amplitude is represented by

$$r - r_0 = f\left(r_0 - \frac{\xi_0}{\sqrt{2}} t\right). \tag{24}$$

Here the sound velocity has been expressed in terms of ξ_0, since, in accordance with equation (17),

$$\xi_0 = \left(\frac{2P}{\rho}\right)^{1/2}. \tag{25}$$

Here P and ξ_0 should refer to the total random motion. According to the preceding section, the thermal motion is characterized by $\xi_0 = 7$ km/sec, while the turbulent motion is probably characterized by $\xi_0 = 12$ km/sec. By adding the squares of these values, one finds for the total random motion $\xi_0 = 14$ km/sec. This value, therefore, would be expected to be appropriate for ξ_0 in the above equation. Approximately isothermal conditions may be applied to the photospheric pulsation, since the ordinary temperature does not vary appreciably (compared with the large variation of the density) and since the line profiles over the entire cycle seem to indicate that the turbulent velocity does not vary by a large percentage.

From the above representation of a simple progressive wave a relation between the two first partial derivatives follows:

$$\frac{\partial r}{\partial t} = -\frac{\xi_0}{\sqrt{2}}\left(\frac{\partial r}{\partial r_0} - 1\right). \tag{26}$$

In the plane approximation the continuity law takes the form $\rho \partial r = \rho_0 \partial r_0$, where ρ_0 refers to the mean density of the layer in question. With the help of this law, the derivative with respect to r_0 on the right-hand side of equation (26) may be expressed in terms of the density. Thus a relation between the velocity and the density is obtained. In applying this relation to maximum and minimum phase, we find

$$\left(\frac{\partial r}{\partial t}\right)_2 - \left(\frac{\partial r}{\partial t}\right)_1 = \frac{\xi_0}{\sqrt{2}} \frac{\rho_2 - \rho_1}{\rho_0}. \tag{27}$$

This equation represents the relation between the velocity amplitude and the density amplitude. As it stands, it holds only for waves with small amplitudes, while, on the other hand, the observations give a large density variation. Going to the opposite extreme, we find, for a shock wave of any amplitude, from the Rankine-Hugoniot[23] equations for the isothermal case,

$$\left(\frac{\partial r}{\partial t}\right)_2 - \left(\frac{\partial r}{\partial t}\right)_1 = \frac{\xi_0}{\sqrt{2}} \frac{\rho_2 - \rho_1}{\sqrt{(\rho_1 \rho_2)}}. \tag{28}$$

Since equation (27) holds for a continuous wave of small amplitude and since equation (28), which is identical with equation (27) in the case of small amplitudes, holds for discontinuous waves of any amplitude, equation (28) may be assumed to hold also in fair approximation for continuous waves of appreciable amplitudes.

From Figure 2 one finds that the velocity amplitude is approximately 60 km/sec and that the density variation for the ratio between the extremes gives

$$\frac{\rho_2}{\rho_1} = 4.$$

After introducing these two observational data into equation (28), this equation is found to be fulfilled if $\xi_0 = 60$ km/sec. This value is four times as large as the value to be expected for the photosphere as discussed above. To remove this discrepancy, the ratio of ρ_2 to ρ_1 would have to be 40, a value so different from the observed value of 4 as not to be explicable by the uncertainties in the determination of the density variation.

[23] H. Lamb, *Hydrodynamics* (5th ed.; Cambridge: At the University Press, 1924), p. 460, eq. (9).

The discrepancy between the observed amplitudes in velocity and in density with the theoretical relation (28) indicates that the picture of a simple progressive wave is not a sufficiently good representation of the photospheric pulsation. To give a possible,though not proved, explanation of the observed data, a more complicated model for the atmosphere of η Aquilae and its pulsations is given in Section XII.

XII. WAVE IN COMPOSITE ATMOSPHERE

The following discussion is based on the assumption that the atmosphere of η Aquilae consists of two parts: a photosphere with a moderate total kinetic temperature, with $\xi_0 = 14$ km/sec, and above this a corona with a high total kinetic temperature (of the order of half a million degrees), with $\xi_0 = 85$ km/sec. In addition, it is assumed that the pulsation in the corona has the character of a wave progressing outward.

If the displacement of a given layer is characterized by y and if the mean position of the same layer is indicated by x, with the definitions

$$y = \frac{r - r_0}{r_0}, \qquad x = \frac{r_0 - R}{R}, \tag{29}$$

then the fundamental pulsation equation for a harmonic pulsation of small amplitude takes the form[24]

$$\frac{\partial^2 y}{\partial x^2} - (q-4)\frac{\partial y}{\partial x} + (u - \alpha q)\, y = 0, \tag{30}$$

where the auxiliary quantities are defined by

$$\alpha = 3 - \frac{4}{\gamma}, \qquad n = \frac{2\pi}{\text{Period}}, \qquad q = \frac{\rho_0}{P_0}\frac{GM}{R}, \qquad u = \frac{\rho_0}{P_0}\frac{n^2R^2}{\gamma}. \tag{31}$$

Here the change of r_0 and of the ratio P_0/ρ_0 with height have been ignored, so that the two coefficients in equation (30) can be considered as constants in each of the two parts of the atmosphere. After a solution for y is found from equation (30), the density variation can be determined from the continuity law, which in the spherical case takes the form

$$\frac{\rho - \rho_0}{\rho_0} = -3y - \frac{\partial y}{\partial x}. \tag{32}$$

With a convenient choice of the phase zero point and of the amplitude normalization, the solution of equation (30), which corresponds to a progressive wave in the corona, may be represented by

$$y = e^{\beta x}\cos(nt - \nu x). \tag{33}$$

The two constants occurring in this solution may be determined by introducing the solution into the fundamental equation (30), from which it follows that

$$\beta = \tfrac{1}{2}q - 2, \qquad \nu = +\,[u - (\tfrac{1}{2}q - 2)^2 - \alpha q]^{1/2}. \tag{34}$$

The choice of the positive sign in the equation for ν corresponds to a wave progressing outward. For the photosphere the general solution of equation (30) may be written

$$y = [c_1 e^{\delta_1 x} + c_2 e^{\delta_2 x}]\cos nt + [c_3 e^{\delta_1 x} + c_4 e^{\delta_2 x}]\sin nt. \tag{35}$$

[24] Eddington, *op. cit.*, p. 187.

By introducing this solution again into the fundamental equation (30), we find for the exponents

$$\delta_{1,2} = (\tfrac{1}{2}q - 2) \pm [(\tfrac{1}{2}q - 2)^2 - u + \alpha q]^{1/2} . \tag{36}$$

The four coefficients occurring in equation (35) may be determined by fitting the solution for the photosphere to the solution for the corona at the interface between these two layers. This may be taken to be at $x = 0$. From the continuity of y and ρ at the interface it follows that

$$c_1 = \frac{\beta - \delta_2}{\delta_1 - \delta_2}, \qquad c_2 = \frac{\delta_1 - \beta}{\delta_1 - \delta_2},$$
$$c_3 = +\frac{\nu}{\delta_1 - \delta_2}, \qquad c_4 = -\frac{\nu}{\delta_1 - \delta_2}. \tag{37}$$

The numerical values corresponding to η Aquilae may be introduced into these formal solutions. The values for M, R, and the period may be taken from Sections II and III. Furthermore, $\gamma = 1$ is to be chosen according to the isothermal approximation. The ratio P_0/ρ_0 can be found with the help of equation (25) from the values of ξ_0 listed under the assumptions at the beginning of this section for the two parts of the atmosphere. With these numerical data we find for the constants occurring in equations (30), (33), and (35)

$$\alpha = -1 , \quad q_{\text{corr}} = 9.8 , \quad u_{\text{corr}} = 18 , \quad q_{\text{phot}} = 360 , \quad u_{\text{phot}} = 660 ,$$
$$\beta = 2.9 , \quad \nu = 4.4 , \quad \delta_1 = 353 , \quad \delta_2 = 2.9 ,$$
$$c_1 = 0.00 , \quad c_2 = 1.00 , \quad c_3 = 0.013 , \quad c_4 = -0.013 .$$

When these numbers are used, the solution in the corona (positive x) becomes

for the displacement: $$y = +1.0\, e^{2.9x} \cos(nt - 4.4x) ,$$

for the velocity: $$\frac{1}{n}\frac{\partial y}{\partial t} = -1.0\, e^{2.9x} \sin(nt - 4.4x) ,$$

for the density: $$\frac{\rho - \rho_0}{\rho_0} = -4.4\, e^{2.9x} \sin(nt - 4.4x) - 5.9\, e^{2.9x} \cos(nt - 4.4x) , \tag{38}$$

whereas the solution in the photosphere (negative x) becomes

for the displacement: $$y = +1.0\, e^{2.9x} \cos nt ,$$

for the velocity: $$\frac{1}{n}\frac{\partial y}{\partial t} = -1.0\, e^{2.9x} \sin nt ,$$

for the density: $$\frac{\rho - \rho_0}{\rho_0} = -4.4\, e^{353x} \sin nt - 5.9\, e^{2.9x} \cos nt . \tag{39}$$

According to equations (39), the solution for the photosphere, which should be compared with the observations, has at great depths ($-x > 0.01$) the character of a standing wave, with synchronism in the variation of displacement and reciprocal density. Just below the base of the corona ($0 < -x < 0.001$), however, throughout a depth of approximately 25,000 km, the solution in the photosphere resembles closely that of the

corona. If the level represented by the observed lines falls in this photospheric layer not far below the base of the corona, the observed line profiles will correspond to the turbulence in the photosphere, whereas the observed pulsation will be determined closely by the pulsation in the corona. The latter has two consequences, both in approximate agreement with the observations. First, the observed relation between the amplitudes in velocity and in density corresponds, under the present assumptions, to the large velocities in the corona. Second, the observed phase shift of the density variation relative to the velocity variation corresponds to the shift apparent in equations (38), which arises from the sphericity of the wave and the increase of displacement amplitude with height in the corona.

Because of the uncertainty in the observed density variation and because of the lack of knowledge as to how to extrapolate the above formulae, derived for small amplitudes, to large amplitudes, it does not seem useful at present to try to fit the theoretical equations too closely to the observations. We may conclude from the above, however, that possibly, though not at all certainly, the assumed composite model atmosphere may represent approximately the atmosphere of η Aquilae; and that the observed features of the photospheric pulsation are determined to a large extent by the progressive wave which represents the pulsation in the corona.

XIII. SUMMARY OF RESULTS

Two results have come out of the present investigation of the motions in the atmosphere of η Aquilae. The first result is based on the determination of the curve of growth and on the measurement of line profiles. These data indicate that large-scale convection exists in the photosphere. It appears probable that this convection consists of a fast turbulence with elements of great linear dimensions. Under such conditions neither the thermal motions nor the fraction of the turbulence detectable in the curve of growth but rather the large-scale turbulence indicated by line profiles is found to be the essential factor determining the average structure of the atmosphere.

The second result is based on the comparison of the velocity variation with the density variation throughout the pulsation cycle, where the latter variation is derived from measurements of a selected number of iron lines. This comparison indicates that the pulsation in the photosphere has the character neither of a standing wave nor of a simple progressive wave in a homogeneous atmosphere. The observed relations, however, can perhaps be explained by the assumptions that the total random velocities increase greatly in the layers above the photosphere and that, in these coronal layers rather than in the photosphere, the pulsation consists of a simple progressive wave. Under these assumptions the observed photospheric pulsation, though falling in the transition region between the corona and the interior with its standing wave, might closely simulate the coronal progressive wave.

SPECTROSCOPIC OBSERVATIONS OF 90 STARS*

ALFRED H. JOY AND S. A. MITCHELL
Mount Wilson and Leander McCormick Observatories
Received May 13, 1948

ABSTRACT

Spectral types and radial velocities were derived for 90 stars whose parallaxes are being determined at the McCormick Observatory. The stars are mostly late-type dwarfs with right ascensions between 16 and 8 hours. Dispersion of 120 A/mm at $H\gamma$ was used.

In the summers of 1943 and 1944 during visits to California, Mr. Mitchell inaugurated a program of spectrographic observation of faint dwarf stars, for most of which parallaxes and proper motions had been obtained at the Leander McCormick Observatory. In the succeeding years the observations were continued, and measures of radial velocity as well as estimates of spectral type were made by Mr. Joy.

In order to increase the number of stars which could be observed in the time available, low dispersion of 120 A/mm at $H\gamma$ was employed, and with few exceptions only two spectrograms of each star were obtained. The 60-inch reflector and one-prism spectrograph were generally used, but for a few of the faintest stars photographs giving nearly the same dispersion were made with the two-prism spectrograph at the 100-inch telescope.

Although radial velocities derived in this way are not of the highest accuracy, the agreement of the two plates of the same star and our experience with this type of observation lead us to believe that for many statistical purposes the results may be used with considerable confidence. If 9 stars are omitted which show discordances greater than 18 km/sec and are probably spectroscopic binaries, the mean arithmetical difference in the velocities given by pairs of plates of the same star is 6.5 km/sec.

The program consists largely of dwarf stars of late spectral type which could be observed in summer and autumn. The data concerning the stars and the results obtained are in Table 1. Emission lines of *Ca* II (H and K) were found in 37 stars; in addition, bright hydrogen was observed in AC+2°2283–259. The spectrograms of many other stars, however, were not sufficiently exposed to determine whether or not H and K are present in emission.

The visual absolute magnitudes in the seventh column of Table 1 are computed with the aid of the trigonometric absolute parallaxes given in the next column. Most of these are determinations made at the McCormick Observatory; however, the weighted mean was used whenever other parallaxes were available. For stars having no trigonometric parallaxes the absolute magnitudes were read from the Russell diagram, by the use of the estimated spectral types.

We are indebted to Dr. A. N. Vyssotsky for furnishing, in advance of publication, data concerning 27 stars from his second list of M dwarfs.

* *Contributions from the Mount Wilson Observatory, Carnegie Institution of Washington*, No. 747.

TABLE 1

SPECTROSCOPIC OBSERVATIONS OF 90 STARS

Star	α(1900)	δ(1900)	m_v	μ	Spectrum	M_v	π Trig.	Vel. (Km/Sec)
BD−13°116	0h36m4	−13° 44′	10.3	0″.08	dM0	8.1	.....	+ 3
BD−19°111	0 39.5	−19 29	10.6	0.26	dM1.5	9.4	0″.057	+ 27
18C 112	0 46.1	+18 12	9.7	0.27	dK6	9.4	.088	+ 10
20C 65	0 55.1	+60 50	10.8	0.85	dM2.5	10.4	.081	+ 13
20C 68	0 56.3	+61 48	9.5	0.76	dM2	9.3	.092	0*†
BD−11°192	0 57.4	−10 57	10.1	0.13	dM0	8.1	.....	− 20
20C 82	1 3.4	+16 43	10.5	0.61	dK6	8.8	.046	− 36
20C 90	1 11.2	+24 48	10.3	0.41	dK5	7.6	.....	− 30
20C 96	1 14.5	+56 48	10.3	0.60	dK6	7.6	.028	+ 22
20C 99	1 17.3	+12 14	9.2	0.40	dK3	.....	.....	+ 10
20C 106	1 25.5	+15 3	9.5	0.42	dK6	5.8	.018	− 32
AC+77°742	1 25.7	+77 34	10.5	0.11	dM0	8.1	.....	− 6*
20C 131	1 46.7	+17 27	10.5	0.48	dM0	8.1	.....	+ 30
20C 140	1 56.9	+ 3 28	9.5	0.49	dK6	7.9	.....	− 48
20C 142	1 59.3	+22 20	9.1	0.48	dK1	5.6	.020	− 8
20C 146	2 0.7	+44 43	9.9	0.49	dM0	8.1	.043	+ 62
20C 163	2 11.5	+21 6	9.1	0.47	dG2	.....	.001	− 30
BD+47°612	2 15.7	+47 24	9.4	0.23	dM1.5	9.3	.095	− 35*
AC+49°2493–285	2 18.6	+49 21	11.2	0.18	dM0	8.1	.....	+ 36
18C 319	2 22.5	+ 3 59	8.6	0.26	dM1.5	7.8	.068	+ 2
20C 173	2 29.4	+ 5 1	9.3	0.69	dK3	6.5	.027	− 72
20C 179	2 37.7	+19 0	8.6	0.43	dK4	7.3	.056	+ 27
20C 180	2 38.4	+25 6	10.7	0.90	dM3.5	11.5	.143	+ 38†
20C 196	2 52.0	+10 24	12.	1.91	dM3.5	11.	.056	+ 49
BD+39°710	3 0.4	+39 58	9.5	0.38	dK6	7.0	.032	− 48
20C 213	3 7.4	+51 59	9.7	0.48	dM0	7.8	.042	− 55
20C 221	3 11.6	+37 53	10.0	0.78	dM1.5	9.2	.070	+ 9
BD+ 6°525	3 19.2	+ 6 39	10.0	0.04	dK5	7.3	.029	+ 27
AC+34°344–129	3 28.6	+34 17	10.5	0.25	dM0	8.1	.....	+ 39
BD+34°724	3 38.0	+34 37	10.7	0.25	dM0	7.7	.025	+ 8
20C 271	3 49.1	+53 17	10.5	0.51	dM1.5	9.2	.054	− 5
20C 270	3 49.7	− 7 8	8.3	0.54	dM0.5	8.3	.102	+ 53
20C 275	3 53.8	+25 49	12.2	0.80	dM4	11.5	.....	+ 94
BD+21°652	4 23.1	+21 41	9.0	0.22	dM1	8.5	.078	− 36
BD−11°916	4 33.0	−11 14	10.9	0.29	dM1	8.9	.....	− 13
BD+25°733	4 41.5	+26 0	10.2	0.14	dM0	8.1	.....	+ 45*
AC+ 2°2283–259	4 54.4	+ 1 36	10.0	0.16	dM1e†	8.9	.....	+ 39
BD−21°1051	4 58.2	−21 24	8.3	0.31	dM1	8.9	.132	− 19
BD+19°845	4 58.4	+19 54	10.0	.....	gM2	.....	.....	− 37
CD−23°2362	4 59.3	−23 24	10.2	0.32	dM0	8.1	.....	+124*

* Velocity range greater than 18 km/sec, probably a spectroscopic binary.

† Notes for stars marked with a dagger (†) follow:

20C 68	0h56m3	Radial velocity, −6 km/sec, and bright H and K lines found by D. M. Popper (*Ap. J.*, **95**, 307, 1942).
20C 180	2 38.4	The radial velocity measured by W. J. Luyten on one plate is +65 km/sec (*Ap. J.*, **102**, 38, 1945).
AC+2°2283–259	4 54.4	Hydrogen and calcium (H and K) appear in emission.
BD−1°3474	18 14.6	The motion of this star is in the line of sight. See note by A. N. Vyssotsky (*Pub. A.S.P.*, **58**, 166, 1946).
20C 1165A	19 42.4	A close visual double. The magnitude is that of the brighter component.
20C 1331	21 57.1	Radial velocity, +21 km/sec, and bright H and K lines found by D. M. Popper (*Ap. J.*, **95**, 307, 1942).

TABLE 1—*Continued*

Star	α(1900)	δ(1900)	m_v	μ	Spectrum	M_v	π Trig.	Vel. (Km/Sec)
BD−21°1131	5^h14^m6	−21° 29′	9.5	0″.14	dM0	8.1	.....	+ 24*
AC+56°35386	6 41.8	+55 58	10.5	0.21	dK6	7.8	0″.028	+ 45
BD+12°1343	6 49.4	+12 18	10.4	0.34	dM1.5	9.6	.068	+ 30
BD+27°1311	6 59.5	+27 37	10.7	0.11	dM0	9.6	.060	− 42
BD+59°1056	7 3.6	+59 26	10.2	0.29	dK5	7.7	.032	− 58
McC 491.14	7 31.9	+34 41	11.4	0.12	dM0.5	7.0	.013	+ 15
BD+44°1710	7 57.4	+44 14	9.9	0.15	dM0	7.3	.030	+ 27
BD−13°2439	8 8.6	−13 36	9.3	0.50	dM0	7.8	.049	+ 20
BD+14°1876	8 15.4	+14 23	10.5	0.28	dM0.5	8.3	.037	+ 15
18C 986	8 17.6	+22 11	9.5	0.39	dM0	8.1	.052	− 17
BD+43°1827	8 27.3	+42 54	10.0	0.20	dK5	7.3	.028	− 9
20C 504	8 55.5	+ 5 39	12.1	0.47	dM4	11.5	.....	+ 7
20C 505	8 55.6	+ 5 38	12.5	0.47	dM4	11.5	.....	− 11
ADS 8862A	13 15.4	+48 18	8.7	0.14	dM2	9.6	.....	+ 13
20C 975	16 10.3	+44 42	9.3	0.41	dK6	7.9	.....	− 18*
Ross 644	16 49.9	+12 4	10.5	0.65	dM1.5	9.3	.058	− 61
BD+46°2361	17 43.0	+46 53	10.3	0.03	dM1.5	8.4	.042	+ 18
BD− 6°4663	17 45.2	− 6 1	10.1	0.13	dM1.5	9.6	.078	− 21*
BD+18°3606	18 10.9	+18 27	10.0	0.11	dM1	9.0	.062	+ 8
BD+13°3578	18 11.5	+13 54	10.2	0.50	dM0	8.1	.....	+ 11
BD+26°3215	18 13.8	+26 37	9.2	0.35	dK5	7.6	.....	− 44
BD− 1°3474†	18 14.6	− 1 58	10.4	0.00	dM1	10.0	.083	− 23
20C 1111	18 45.0	+ 2 59	10.5	0.46	dM2	9.6	.067	+ 4
Ross 160	18 47.5	+16 29	10.5	0.61	dM1.5	10.1	.084	− 11
BD+33°3339	19 5.2	+33 54	9.2	0.10	dK6	7.9	.....	+ 22
20C 1151	19 18.6	+33 41	9.5	0.73	dK6	6.9	.031	− 63
BD+ 0°4241	19 27.5	+ 0 22	10.5	0.22	dM1	8.9	.....	− 39
20C 1165A	19 42.4	+31 47	9.8†	0.63	dM2	9.4	.084	+ 3
BD+26°3915	20 25.9	+26 31	10.5	0.20	dM1.5	8.7	.044	+ 30
20C 1213	20 29.2	+65 5	10.6	0.53	dM3	11.1	.125	+ 24
BD+56°2471	20 39.0	+57 4	10.3	0.22	dM0	7.9	.033	− 15
20C 1226	20 39.8	+19 24	10.5	0.58	dM1.5	9.6	.066	+ 9
20C 1237	20 50.3	+12 47	8.7	0.66	dK5	7.6	.....	− 32*
AC+ 3°2561–36	21 21.6	+ 3 17	10.2	0.10	dM1	8.9	.....	+ 2
BD+40°4631	21 40.5	+41 8	10.1	0.08	dK6	7.9	.....	− 21
20C 1320	21 49.9	+41 19	10.1	0.53	dM1.5	9.8	.086	− 35
20C 1329	21 56.0	+ 9 28	10.5	0.53	dK4	7.1	.....	+ 16
20C 1331	21 57.1	+ 0 56	9.2	0.55	dK6	9.6	.122	+ 21†
20C 1340	22 4.4	− 5 8	10.5	0.80	dM3	10.7	.111	− 12
20C 1344	22 7.6	+31 5	10.0	0.46	dM0	8.1	.....	+ 16
BD+21°4747	22 20.0	+22 3	9.1	0.20	dM0	8.1	.....	− 1
20C 1373	22 31.0	− 1 21	10.0	0.60	dM1.5	9.2	.068	+ 29
20C 1380	22 41.3	+44 51	10.5	0.40	dK6	8.1	.033	− 23
AC+24°44–11	22 43.7	+24 13	10.9	0.18	dM0	8.1	.....	+ 12
BD− 7°5871	22 45.1	− 7 38	10.2	0.18	dM1	8.9	.....	− 8
BD+65°1846	23 0.5	+66 14	9.9	0.31	dM1	7.5	.034	+ 21
BD+57°2735	23 20.0	+57 19	10.2	0.22	dM2	9.6	.....	− 5
BD− 2°5958	23 21.9	− 1 50	10.5	0.47	dM0	8.1	.....	+ 27
BD+15°4829	23 23.4	+15 31	9.5	0.10	dK5	7.6	.....	− 42
BD+ 0°5017	23 29.8	+ 1 3	9.5	0.34	dM1	8.2	.....	+ 1

NOTES ON THE SPECTRUM OF ZETA AURIGAE DURING ECLIPSES

DEAN B. MCLAUGHLIN
University of Michigan Observatory
Received April 23, 1948

ABSTRACT

Qualitative comparison of spectrograms of the eclipses in 1934, 1937, 1939–1940, 1942, and 1947–1948 shows approximate uniformity of extent of atmosphere, except during ingress in 1937, when it was more extensive than normal. A permanent asymmetry exists; absorption is stronger during ingress than during egress. The date of mid-eclipse in 1947–1948 is estimated as JD 2432553.5 to 2553.6, from the appearance of the spectrum during partial phases.

During the eclipse of ζ Aurigae in December, 1947, to January, 1948, a fairly well-distributed set of spectrograms was obtained with the one-prism spectrograph at the University of Michigan Observatory. In particular, observations were obtained during the partial phases of both ingress and egress. All plates have a dispersion of 40 A/mm at $H\gamma$ and 26 A/mm at K.

This preliminary description is presented in the hope that it may contribute to the dating of changes that may have taken place during interruptions of other series of observations. A qualitative comparison of the recent observations with less complete sets taken with the same instrument during previous eclipses shows a few significant systematic effects.

Table 1 lists all Michigan plates taken during or near the eclipses of 1937, 1939, 1942, and 1947–1948. Phases in the second column were computed from the formula: Min = JD 2427692.8 + 972.15E, which is based on photometric dates of earlier eclipses and a spectroscopically estimated date of the recent one. The "Atmospheric Eclipse Intensities" given in the third column are explained below.

SPECTRAL CHANGES DURING THE ECLIPSE OF 1947–1948

The last spectrogram taken before the atmospheric eclipse effects began was obtained JD 2432501. It shows simply the normal composite spectrum. Bad weather prevented the observation of the first faint eclipse absorption lines.

JD 2529.70.—The following atmospheric eclipse lines are very strong: cores of all hydrogen lines to *H*16 and probably beyond; *Ti* II 3759 and 3761; *Ca* II H and K. The *Mg* I lines 3832 and 3838 are moderately strong. *Ti* II 3900 and 3913 are weak, and *Sr* II 4078 is probably just traced.

JD 2531.72.—Lines newly appeared or greatly strengthened are: *Sr* II 4078; *Ti* II 3900 and 3913; *Mg* I 3829 (still weak); *Fe* I 3820, 3826, and 3860. Uncertain traces of *Fe* I 4045, 4064, and 4072 are superimposed on the lines of the normal K spectrum.

JD 2533.85.—The lines of *Ca* II are now decidedly winged, about 3 A wide. Numerous lines of *Fe* I have become very strong, e.g., 3813, 3820, 3840, 3860, 3878, 3920, 4045, etc. Other lines greatly strengthened include *Al* I 3961, *Mn* I 4031–4034. Lines of *Ti* I at 3956, 3958, 3982, 3990, and 3999 are of moderate strength.

JD 2534.59.—There is now a complete K-type spectrum in very strong absorption, but with a considerable extent of continuum in the ultraviolet. Most lines of the lowest atmospheric strata are very strong, e.g., *Ti* I 3958, 3982, etc. The H and K lines of *Ca* II are broadly winged, about 15 A wide. *This is surely the partial and not the total phase*, for the lines *Fe* I 4045, 4064, and 4072 are very sharp, without the hazy wings of the total phase, and *Sr* II 4078 is still narrow and much stronger than its low-level companion, *Fe* I 4077. The *Ti* I lines are not so strong as in totality.

JD 2534.66.—The line spectrum is not appreciably different from the previous one but is less strongly exposed and more suitable for comparison with the first plate taken during egress. That the eclipse was still partial is indicated by the lack of wings at *Fe* I 4045, etc., and the relative strength of *Sr* II 4078. The ultraviolet continuum is still appreciable.

JD 2541.61, 2557.67, and 2561.60.—These plates, taken during the total phase, show hazy wings on the lines *Fe* I 4045, 4064, and 4072. *Sr* II 4078 only slightly exceeds *Fe* I 4077. *Ti* I 3982, 3990, and 3999 are decidedly stronger than during the partial phase.

JD 2571.53.—This plate shows the eclipse still total, both by lack of ultraviolet continuum and by the appearance of *Fe* I, *Sr* II, and *Ti* I.

TABLE 1

SPECTROGRAPHIC OBSERVATIONS OF ζ AURIGAE

JD 2420000+	Phase (Days)	Atmospheric Eclipse Intensity (A.E.I.)	JD 2430000+	Phase (Days)	Atmospheric Eclipse Intensity (A.E.I.)
8593.66	−71.3	0.1	2534.59	−19.0	10.0
8611.57	−53.4	0.3	2534.66	−18.9	10.0
8635.57	−29.4	3.5	2541.61	−11.9	Total
8636.55	−28.4	3.5:	2557.67	+ 4.1	Total
8637.58	−27.4	3.8	2561.60	+ 8.0	Total
8639.62	−25.3	6:	2571.53	+18.0	Total
8642.59	−22.4	6.0	2572.80	+19.2	9.5
8643.57	−21.4	6.5	2573.59	+20.0	7.0
8647.58	−17.4	Total	2573.79	+20.2	7.0
9578.79	−58.3	0.1	2574.62	+21.1	6.0
9584.86	−52.2	0.2	2574.70	+21.2	6.0
9609.68	−27.4	1.0	2576.61	+23.1	3.5
9612.68	−24.4	3.2	2576.70	+23.2	3.5
9613.74	−23.4	3.8	2578.59	+25.0	2.0
9659.60	+22.5	3.8	2578.63	+25.1	2.0
2430000+			2579.63	+26.1	1.0
0596.90	−12.4	Total	2579.70	+26.2	1.0
0631.89	+22.6	4.0	2580.63	+27.1	0.5
0638.90	+29.6	0.5	2581.61	+28.1	0.5
2529.70	−23.8	4.0	2582.60	+29.1	0.2
2531.72	−21.8	6.0	2586.59	+33.0	0.0
2533.85	−19.7	8.0	2591.55	+38.0	0.0

JD 2572.80.—The spectrum is very similar to that obtained during ingress, JD 2534.66, in most details. However, the low-level lines, notably *Ti* I 3982, etc., are appreciably weaker than on the ingress plate. *Ca* II is very broadly winged. In spite of the large hour angle at which this plate was taken, there is an appreciable increase of the ultraviolet continuum.

JD 2573.59.—The spectrum appears truly intermediate between JD 2531 and JD 2533. All low-level lines have disappeared, and many of the *Fe* I lines are weak. Those that are still strong include 3764, 3820, 3840, 3860, 3878, and 4045. The H and K lines are a little wide but not appreciably winged. *Ti* II 3759 and 3761 and *Mg* I 3832 and 3838 remain very strong.

JD 2574.62.—The spectrum appears almost identical with that of JD 2531. All the *Fe* I lines have weakened considerably, as have *Ti* II 3900 and 3913 and *Mg* I 3829; but *Ti* II 3759 and 3761 and *Mg* I 3832 and 3838 remain strong. K is narrower but very strong. *Fe* I 3820 and 3860 are of moderate strength. *Sr* II 4078 is weakened.

JD 2576.61.—The spectrum closely resembles that of JD 2529. The hydrogen cores and *Ca* II lines remain strong. *Ti* II 3759 and 3761 have not yet weakened much, but 3900 and 3913 are almost gone. *Mg* I 3838 is weaker. *Fe* I 3820 and 3860 are very faint. *Sr* II 4078 has almost, if not quite, disappeared.

JD 2578.59.—Strong narrow cores are still seen in $H\delta$, $H\epsilon$, and $H\zeta$, but not in higher members of the Balmer series. *Mg* I 3838 is weak and *Ti* II 3759 and 3761 have now declined markedly but are still conspicuous. *Ca* II K remains fairly strong.

JD 2579.70.—The K line has faded considerably in only one day. *Ti* II 3759 and 3761 and *Mg* I 3838 are quite weak. A sharp core is still visible in $H\zeta$.

JD 2580.63 and 2581.61.—The K line and $H\zeta$ core continue to weaken, and the latter plate shows the last feeble record of *Ti* II 3759 and 3761.

JD 2582.60.—K is sharp and very weak, in the same position as on preceding days. Another line of equal strength and sharpness has appeared about 1.5 A toward longer wave length. It was not seen on any previous plate. The $H\zeta$ core is not seen.

JD 2586.59.—There is no trace of the sharp K line or its companion. A wide rather faint and hazy line has its center in the position of the K line. This is undoubtedly the feature observed at Cambridge just a few hours earlier.[1] Comparison with several plates taken far from eclipse in different years shows a similar feature to be normally present. It is believed to be the central portion of the wide K line of the normal K-type spectrum, whose outer wings are filled in by the strong continuum of the B-type star.

NOTES ON EARLIER ECLIPSES

In general, the plates of earlier eclipses could be accurately matched with, or interpolated between, those of 1947–1948. The "Atmospheric Eclipse Intensities" (A.E.I.) in Table 1 thus indirectly describe the plates. For a few dates, as noted below, there were appreciable differences for specific lines, or the atmospheric eclipse effects appeared abnormally far from totality.

THE 1937 ECLIPSE

JD 8593.66, phase −71.3 days.—A weak sharp K line is suspected.

JD 8611.57, phase −53.4 days.—Faint sharp K and *Ti* II 3759 and 3761 are present.

JD 8642.59, phase −22.4 days.—"A.E.I." = 6, but K is stronger and *Ti* II slightly weaker than in 1947–1948.

JD 8643.57, phase −21.4 days.—"A.E.I." = 6.5, but K and *Ti* II are abnormal as on the preceding day.

THE 1939–1940 ECLIPSE

JD 9578.79, phase −58.3 days.—A very faint sharp K line is seen.

JD 9584.86, phase −52.2 days.—The K line is not visible, but weak *Mg* I 3838 and *Ti* II 3759 and 3761 are present.

JD 9659.60, phase +22.5 days.—"A.E.I." = 3.8, but the K line is a little strong.

COMPARISON OF ECLIPSES

A detailed examination and intercomparison of all the plates taken during the eclipse of 1947–1948 was first made on the Hartmann spectrocomparator. This showed pretty definitely that the changes of line absorption progressed smoothly. There were certainly no marked reversals of the direction of change and probably no significant halts. The series was therefore taken as establishing a numerical scale of A.E.I.'s, ranging from 0 for no trace of absorption to 10 for the deepest observed phase of partial eclipse. The A.E.I.'s were assigned so as to progress smoothly with time during the egress. Absorption on the ingress plates was then estimated on the same scale by direct comparison with egress plates that showed equal, greater, and less absorption.

[1] *Harvard Announcement Card*, No. 888.

Values of A.E.I. were estimated in the same manner for the earlier series, 1937, 1939–1940, and 1942, by comparison with the plates of the series of 1947–1948. The resulting values are given in the third column of Table 1. In addition, a critical comparison was made, as far as possible, with the reproductions of Mount Wilson spectrograms[2] of the eclipse in 1934. The A.E.I. values for these dates are certainly less reliable than those for the directly compared spectrograms but are still believed to be of useful accuracy. Data on the Mount Wilson plates are given in Table 2.

Values of A.E.I. are plotted against phase in Figure 1, where ingress and egress are kept separate and each eclipse is identified by a different symbol. In Figure 2 all observations are plotted against phase without regard to sign, but ingress and egress are distinguished by dots and circles, respectively. From these plots three main conclusions can be drawn.

1. Except for the early phases of ingress in 1937, there is no evidence of variations of extent of the atmosphere of the K star at different eclipses. Regardless of the year, all observations, with the exception mentioned, fall very close to the curve that the eclipse of 1947–1948 defines.

TABLE 2

DATA FROM MOUNT WILSON REPRODUCTIONS (1934)

JD 2420000+	Phase (Days)	A.E.I.	JD 2420000+	Phase (Days)	A.E.I.
7672.01	−20.8	7.0	7714.0:	+21.2	5.3
7673.01	−19.8	9.5	7714.9:	+22.1	4.5
7711.91	+19.1	9.0	7716.03	+23.2	3.0
7712.91	+20.1	6.0			

2. It appears certain that in 1937 the atmosphere on the advancing side of the K star was abnormally extensive. From 29 to 25 days before mid-eclipse the line strengths were those normally observed from 25 to 22 days before. Weak lines were suspected 71 days before mid-eclipse and were certainly present at phase −53 days, as already noted. The abnormality did not continue down to the limb of the star; at phase −22 days the absorption was of normal strength.

3. There is a marked asymmetry of the atmosphere of the K star. At all eclipses the advancing side at a given negative phase has shown stronger absorption than has the following side at an equal positive phase. The asymmetry is obvious on inspection of the reproductions of Mount Wilson spectra. The difference is approximately equal to that which occurs in one day's motion of the B star, but a correction of the phases by 0.5 day is incompatible with the photometric data.

SPECTROGRAPHIC EVIDENCE ON THE TIMES OF CONTACTS

No photometric observations were attempted at Ann Arbor. Kopal[3] has indicated that the eclipse was apparently total before JD 2534.54. However, the Michigan spectrograms taken 1–3 hours later both show the characteristics of partial and not total eclipse. The evidence for this conclusion is discussed in the notes on spectral changes. If a difference of 0.10 mag. above minimum could have escaped detection on extra-focal plates taken under poor conditions, then, according to the light-curve by Christie,[4] the second contact could have been as late as JD 2534.84.

[2] *Ap. J.*, **81**, 431, Pl. IX, 1935.

[3] *Pop. Astr.*, **56**, 227, 1948.

[4] *Ap. J.*, **92**, 392, 1940.

The two immersion observations on JD 2534 and the emersion spectrogram on JD2572 would have phases of −19.31, −19.24, and +18.90 days, according to Christie's elements. But for two reasons it appears very probable that the immersion plates were closer to totality than was the emersion one: (1) The second immersion plate and the emersion plate are comparably exposed and have almost identical violet extent. The latter, however, was taken at a very large hour angle and, under equal conditions, would have had the greater violet extent. (2) The emersion plate shows some of the low-level

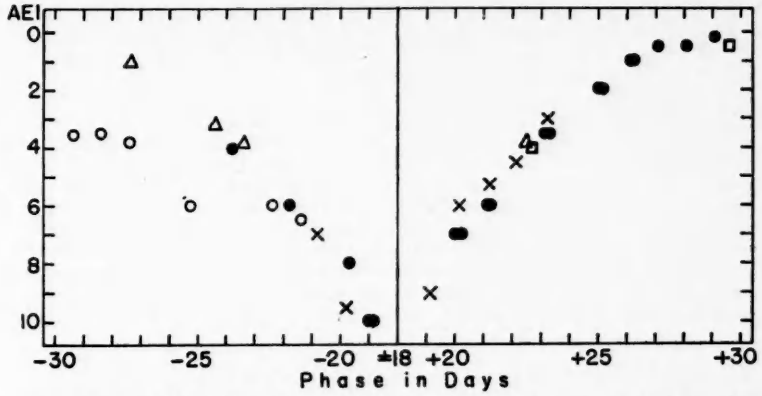

FIG. 1.—Atmospheric Eclipse Intensities (A.E.I.) related to phase in ζ Aurigae. *Crosses*, 1934; *circles*, 1937; *triangles*, 1939–1940; *squares*, 1942, *dots*, 1947–1948.

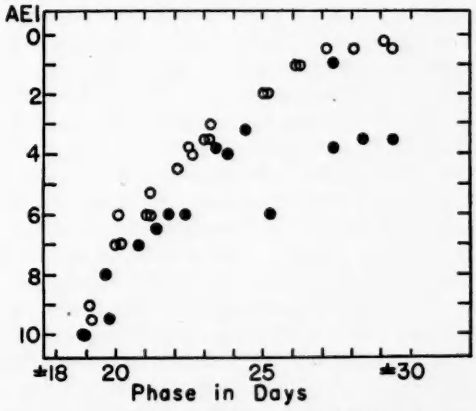

FIG. 2.—Comparison of A.E.I. during ingress (*dots*) and egress (*circles*)

lines (notably *Ti* I) definitely weaker than on the immersion plates. The significance of this difference, however, is a little uncertain on account of the asymmetry already noted.

From the strength of the violet continuum it is estimated that totality began at least as late as JD 2535.0 and possibly 0.1 day later. It is estimated that totality ended about 0.7–0.8 day before the emersion plate was taken, or about JD 2572.0–2572.1. Accordingly, mid-totality is believed to have occurred between JD 2553.5 and JD 2553.6. This date and those of earlier eclipses observed photometrically are satisfactorily represented by the approximate formula: Min. = JD 2427692.8 + 972.15*E*. The period of 972.24 days, given by Christie, is almost certainly too long. Miss Swope[5] found a period of 972.15 days. The epoch in the above formula is 0.2 day later than hers.

[5] *Harvard Circ.*, No. 399, 1935.

ON THE DENSITY DISTRIBUTION AND CHEMICAL COMPOSITION OF THE INTERSTELLAR GAS

BENGT STRÖMGREN
Yerkes Observatory and Copenhagen University Observatory
Received April 21, 1948

ABSTRACT

Observational data on interstellar absorption lines and emission lines are analyzed with a view to obtaining information on the density distribution and chemical composition of the interstellar gas. Section III deals with problems of the theoretical curves of growth of interstellar absorption lines. The theory of ionization in interstellar space is treated in Section IV. Correction factors to the Saha-Eddington equation of ionization are obtained. The numerical values of the correction factors for *Na* I, *K* I, *Ca* I, and *Ca* II range from 2.6 to 1600. In Section V the problem of the extent of the regions of ionization of hydrogen in interstellar space is considered. The results obtained in Sections III–V are utilized in the following sections, in an attempt to derive the gas density between interstellar clouds (Sec. VI), in the average cloud (Sec. VII), and in abnormal clouds, such as that producing the interstellar lines in χ^2 Orionis (Sec. VIII). In the last-mentioned case the problem of the chemical composition is also discussed.

I

The work of W. S. Adams[1] on the multiplicity of interstellar absorption lines has shown that the interstellar gas is largely concentrated in separate clouds, at least as far as calcium is concerned.

From the observational material on the multiplicity of interstellar absorption lines, J. H. Oort and H. C. van de Hulst[2] have concluded that the average number of clouds crossed by a line in or near the galactic plane in the vicinity of the sun is at least five per 1000 parsecs. F. Whipple[3] has similarly derived the number of six to eight per 1000 parsecs. Oort and van de Hulst have further noted that about 14 per cent of the stars of spectral classes O5–B2 (north of declination $-15°$ brighter than 7.5) are apparently connected with diffuse emission nebulosity. From the assumption that the space distribution of the stars and the diffuse nebulae are uncorrelated and the further assumption that the stars in question are actually involved in nebulosity, they conclude that a fraction 0.14 of space around the galactic plane is occupied by interstellar gas clouds. From the average number of clouds per 1000 parsecs and the fraction of space occupied by the clouds, the number of clouds per cubic parsec and the average radius of a cloud can be estimated. In this way Oort and van de Hulst find that there are about 4×10^{-6} clouds per cubic parsec and that the average radius is 20 parsecs. They emphasize the very rough nature of these estimates.

These authors, in the investigation quoted, have also discussed the question of the relation between clouds of interstellar solid particles (smoke) and clouds of interstellar gas. They have given strong reasons to support the assumption that the distribution of gas and smoke is generally identical, emphasizing, in particular, the result found by L. Spitzer[4] that the small interstellar particles must follow the motions of the gas. Once the

[1] *Ap. J.*, **97**, 105, 1943. Doubling of the interstellar H and K lines of ionized calcium in the spectra of several stars was discovered by C. S. Beals, *M.N.*, **96**, 661, 1936; cf. also R. F. Sanford, *Pub. A.S.P.*, **51**, 238, 1939.

[2] *B.A.N.*, No. 376, 1946.

[3] "Harvard Symposium on Interstellar Matter" (unpublished). An analysis of the problem of the determination of the number of clouds per kiloparsec from the observations of interstellar lines has also been carried out by A. Blaauw (unpublished).

[4] *Ap. J.*, **93**, 369, 1941; **94**, 232, 1941; **95**, 329, 1942.

assumption just mentioned is made, it becomes possible to draw conclusions regarding the smoke clouds from the observations on the gas clouds, and vice versa.

Ambarzumian and Gordeladse[5] have derived an estimate of the number of clouds of solid particles per cubic parsec from the observed number of reflection nebulae. First, they conclude that there is no correlation between the space distribution of particle clouds and that of the types of stars which, by illumination of such clouds, produce reflection nebulae. They then proceed to calculate what fraction of the particles is sufficiently illuminated to become observable as reflection nebulae. The fraction is quite low, of the order of 10^{-3}–10^{-4}. Combining this result with the observed number of reflection nebulae per cubic parsec in the neighborhood of the galactic plane and in the vicinity of the sun, we find that the number of particle clouds is about 10^{-4} per cubic parsec.

Ambarzumian, from an investigation of the effects of statistical fluctuations of galactic absorption on the number of extragalactic nebulae, finds that the average optical thickness of an absorbing particle cloud is about 0.27 mag. There are, of course, statistical variations around this value. The observed dark nebulae according to this picture are particle clouds near the sun and of higher optical thickness than the average.

The derived number of particle clouds per cubic parsec is somewhat higher than the number of gas clouds per cubic parsec, according to Oort and van de Hulst. Both figures are so uncertain, however, that this does not mean any contradiction of the hypothesis of generally identical distribution of smoke and gas. The figures can be reconciled, for example, if it is assumed that only 5 per cent (instead of 14 per cent) of the O–B2 stars are actually located in clouds. This leads to a picture characterized by clouds of an average radius of about 5 parsecs, occupying 5 per cent of space near the galactic plane with, on the average, 7 clouds per 1000 parsecs, and 10^{-4} clouds per cubic parsec.

In what follows we shall make use of this picture only as a rough guide regarding the gas clouds.

II

Our knowledge of the properties of the interstellar gas is derived from the observations of interstellar absorption and emission lines.[6] The first step in the analysis of observations of interstellar absorption lines consists in the derivation of the relation between line strength and the number of absorbing atoms (or ions) in a column of unit cross-section along the line of sight from the observer to the star in question. This relation can be derived when the distribution of the radial velocities of the absorbing atoms (or ions) is known.[7]

O. C. Wilson and P. W. Merrill[8] have developed methods of analysis of the strength of interstellar lines based on the use of observed intensities of doublets (the D lines of *Na* I and the H and K lines of *Ca* II). Making certain simplifying assumptions regarding the form of the distribution of the radial velocities of the absorbing atomic particles, they derive from the observations the parameter (or parameters) of this distribution and the relation between line strength and the number of absorbers.

Theodore Dunham,[9] in an analysis of the observed line strengths of interstellar lines in χ^2 Orionis, derived an empirical relation between line strength and the number of absorbers from the observed strength of the *Na* I doublets 5890–5896 A and 3302–3303 A.

[5] *Bull. Abastuman Obs.*, No. 2, p. 37, 1938. Cf. also V. Ambarzumian, *Bull. Abastuman Obs.*, No. 4, p. 17, 1940; *C.R. Acad. Sci. URSS*, **44**, 223, 1944. A discussion of the problem of clouds based on the observations of dark nebulae was carried out by J. L. Greenstein, *Harvard Circ.*, No. 422, 1937.

[6] For a general review see P. Ledoux, *Pop. Astr.*, **49**, 513, 1941 (summary of Yerkes symposium on interstellar lines, 1941); also O. Struve, *Jour. Washington Acad. Sci.*, **31**, 217, 1941.

[7] Cf. A. Unsöld, O. Struve, and C. T. Elvey, *Zs. f. Ap.*, **1**, 314, 1930.

[8] *Ap. J.*, **86**, 44, 1937.

[9] *Proc. Amer. Phil. Soc.*, **81**, 277, 1939.

Merrill and Wilson concluded from their investigation that the assumption of a Gaussian distribution of the radial velocities of the absorbing atoms in the line of sight, corresponding to thermal motion at a definite temperature, was insufficient to explain the observations. They were led to the assumption of separate interstellar gas clouds with differing radial velocities. In their picture the extent of a cloud was about 700 parsecs.

In Section III we shall consider briefly the problem of the relation between the strength of an interstellar absorption line and the number of absorbing atoms in the case of absorption in one, two, or more (relatively small) clouds of differing radial velocities. We shall not attempt to treat the problem of the derivation of the relation in question in its most general form, since a simplified treatment seems sufficient for our present purpose.

When the number of absorbing atoms in the column of unit cross-section between the observer and the star has been determined, the next step is the derivation of the space density of the atoms in question. Since the space density cannot be assumed to be uniform, the problem can be solved only in a statistical way, combining the information obtained from a number of stars. At present, some general picture of the geometry of the gas clouds, such as that outlined in Section I, seems necessary as a guide in the discussion of this problem.

After the densities have been obtained for those atoms and ions for which interstellar absorption lines are observed, the next step is to calculate the state of ionization, in order to find the total densities of the elements in question. This problem, which was first discussed by Eddington,[10] has been the subject of a number of investigations.[11] In the earlier investigations the Saha equation of ionization, modified by the introduction of the dilution factor of the ionizing radiation (and a factor correcting for the difference between the temperature of the ionizing radiation and the electrons) has been used. It was pointed out by Dunham[9] and by the author[12] that a detailed consideration of the ionization and recombination processes leads to a modified equation containing a correction factor corresponding to the influence of captures on excited states. In the investigations just mentioned,[9,12] these correction factors were not calculated. Such calculations are described in Section IV. It turns out that the correction factors may be quite large, ranging from 2.6 to 1500 for *Ca* I, *Ca* II, *K* I, and *Na* I.

In order to calculate the state of ionization in any given region in interstellar space, it is necessary to know the number of free electrons per cubic centimeter. From the observed strengths of interstellar emission lines, we know that hydrogen is by far the most abundant element in interstellar space.[13] Hence, in regions where hydrogen is ionized (*H* II regions), the density of free electrons is practically equal to the density of hydrogen. In interstellar regions where hydrogen is un-ionized (*H* I regions), the electrons are furnished by much less abundant elements, probably mainly by carbon.[12]

A discussion of the extent of the *H* I and *H* II regions in interstellar space is thus necessary to the solution of the problem of the ionization of the elements in general. In the discussion it is now essential to take into account the nonuniformity of the distribution of hydrogen in interstellar space. Thus the conditions under which interstellar hydrogen clouds are completely ionized, partially ionized, or completely un-ionized have to be examined. Also the state of ionization of hydrogen in interstellar space between the clouds has to be considered. In Section V we deal with certain aspects of these problems, making use of a method previously developed.[12]

[10] "Bakerian Lecture," *Proc. R. Soc., London, A*, **111**, 424, 1926.

[11] Cf. B. P. Gerasimovič and O. Struve, *Ap. J.*, **69**, 7, 1929; S. Rosseland, *Theoretical Astrophysics* (Oxford: Clarendon Press, 1936), chap. xxii; O. Struve, *Proc. Nat. Acad. Sci.*, **25**, 36, 1939; Dunham, *op. cit.*; B. Strömgren, *Ap. J.*, **89**, 526, 1939; D. R. Bates and H. S. W. Massey, *Proc. R. Soc., London, A*, **177**, 329, 1941.

[12] *Op. cit.*

[13] O. Struve and C. T. Elvey, *Ap. J.*, **88**, 364, 1938.

The application of the results derived in Sections III–V to the analysis of observed strengths of interstellar lines is considered in Sections VI–VIII. Section VI deals with the regions of interstellar space between the clouds, Section VII with the average cloud in the vicinity of the sun, and Section VIII with the cloud or clouds that give rise to the abnormally strong interstellar absorption lines in χ^2 Orionis.

III

The theoretical calculation of the contour and equivalent width of an interstellar absorption line can be carried out when the total number and the radial-velocity distribution of the absorbing atoms (or ions) is known.[14]

Let the total number of absorbing atoms (or ions) in a column of unit cross-section between the star and the observer be N. Further, let the line-absorption coefficient at wave length λ, referred to the whole column and reckoned per atom, be denoted by a_λ. Then the optical thickness of the column at wave length λ is

$$\tau_\lambda = N a_\lambda , \tag{1}$$

and the intensity observed, I_λ, at wave length λ within the interstellar absorption line is

$$I_\lambda = I_\lambda^{(0)} e^{-\tau_\lambda} , \tag{2}$$

where $I_\lambda^{(0)}$ is the intensity that would be measured in case of vanishing interstellar absorption.

By the usual definition, the equivalent width $w^{(\lambda)}$ of the interstellar absorption line, in wave-length units, is

$$w^{(\lambda)} = \int \frac{I_\lambda^{(0)} - I_\lambda}{I_\lambda^{(0)}} \, d\lambda \tag{3}$$

or

$$w^{(\lambda)} = \int (1 - e^{-\tau_\lambda}) \, d\lambda , \tag{4}$$

where the integral is to be extended over the entire line.

The absorbing atoms in interstellar space are practically undisturbed, so that the atomic absorption coefficient at wave length λ for an atom at rest (radial velocity $u = 0$) is given by the usual radiation damping expression,

$$a_\lambda^{(u=0)} = \frac{\lambda^4}{8\pi^2 c} \frac{q_k}{q_1} a_{k1} \frac{\delta_k^{(\lambda)}}{[\delta_k^{(\lambda)}]^2 + (\lambda - \lambda_0)^2} . \tag{5}$$

In equation (5) q_k and q_1 are the statistical weights of the upper and lower state corresponding to the line, a_{k1} is the transition probability,

$$\delta_k^{(\lambda)} = \frac{\lambda^2}{4\pi c} \sum_{E_r < E_k} a_{kr} \tag{6}$$

is the radiation damping constant in wave-length units, and c is the velocity of light.

[14] Cf. nn. 7 and 8; further, A. S. Eddington, *M.N.*, **95**, 2, 1934. The analogous problem of laboratory physics is treated by W. Schütz, *Zs. f. Ap.*, **1**, 300, 1930; and by Ladenburg and Levy, *Zs. f. Phys.*, **65**, 189, 1930. Cf. also A. C. G. Mitchell and M. W. Zemansky, *Resonance Radiation and Excited Atoms* (Cambridge: At the University Press, 1934); D. H. Menzel, *Pub. Lick Obs.*, **17**, 229, 1931; E. F. M. van der Held, *Zs. f. Phys.*, **70**, 508, 1931; F. Hjerting, *Ap. J.*, **88**, 508, 1938.

Let the number of atoms in the column that have radial velocities between u and $u + du$ be denoted by $N\psi(u)du$. Then the absorption coefficient, a_λ, is given by the expression

$$a_\lambda = \frac{\lambda^4}{8\pi^2 c}\frac{q_k}{q_1}a_{k1}\int_{-\infty}^{+\infty}\frac{\delta_k^{(\lambda)}}{(\delta_k^{(\lambda)})^2+\left[\lambda-\lambda_0\left(1+\frac{u}{c}\right)\right]^2}\psi(u)\,du. \tag{7}$$

If the atomic quantities are known, and the radial-velocity distribution function, $\psi(u)$, is given, then the absorption-line contour and equivalent width, $w^{(\lambda)}$, can be calculated as a function of N from equations (1), (4), and (7). (The contour and the equivalent width are, of course, independent of the spatial distribution of the atoms in the column.)

Suppose, now, that there is only one interstellar cloud between the observer and the star and, further, that the distribution of radial velocities can be sufficiently accurately described by a Gaussian distribution,

$$\psi(u) = \frac{1}{\sqrt{\pi}\,b}\,e^{-(u-u_0)^2/b^2}. \tag{8}$$

If there is no internal turbulent motion in the cloud but only thermal motion of the atoms corresponding to a kinetic temperature T, then

$$b = \left(\frac{2kT}{A\,m_0}\right)^{1/2}, \tag{9}$$

where A is the atomic weight of the atoms in question, expressed in units of m_0, and k is the Boltzmann constant. In the general case, b describes the velocity distribution within the cloud produced by both thermal and internal turbulent motion; an equivalent temperature can then be defined by equation (9).

When equation (8) is valid, equation (7) reduces to the well-known Doppler effect—damping expression for the absorption coefficient,

$$a_\lambda = \frac{\lambda^4}{8\pi^2 c}\frac{q_k}{q_1}a_{k1}\int_{-\infty}^{+\infty}\frac{1}{\sqrt{\pi}}\frac{\delta_k^{(\lambda)}}{b}\frac{e^{-(u-u_0)^2/b^2}du}{[\delta_k^{(\lambda)}]^2+\left[\lambda-\lambda_0\left(1+\frac{u_0}{c}\right)-\lambda_0\left(\frac{u-u_0}{c}\right)\right]^2}. \tag{10}$$

Introducing the integration variable,

$$y = \frac{u-u_0}{b}; \tag{11}$$

the Doppler constant,

$$b^{(\lambda)} = b\,\frac{\lambda_0}{c} \tag{12}$$

or

$$b^{(\lambda)} = \left(\frac{2kT}{A\,m_0}\right)^{1/2}\frac{\lambda_0}{c}; \tag{13}$$

and the ratio a of the damping constant $\delta_k^{(\lambda)}$ and the Doppler constant $b^{(\lambda)}$, both measured in wave-length units,

$$a = \frac{\delta_k^{(\lambda)}}{b^{(\lambda)}}, \tag{14}$$

we can write equation (10) in the form

$$a_\lambda = \frac{\lambda^4}{8\pi\sqrt{\pi}\,c}\frac{1}{b^{(\lambda)}}\frac{q_k}{q_1}a_{k1}\frac{a}{\pi}\int_{-\infty}^{+\infty}\frac{e^{-v^2}dy}{a^2+(v-y)^2}, \tag{15}$$

where

$$v = \frac{1}{b^{(\lambda)}}\left[\lambda - \lambda_0\left(1 + \frac{u_0}{c}\right)\right] = \frac{\Delta\lambda}{b^{(\lambda)}}$$

is the deviation $\Delta\lambda$ of the wave length λ, considered from the central wave length $\lambda_0 (1 + u_0/c)$ of the interstellar line corresponding to the cloud, measured in units of the Doppler constant, $b^{(\lambda)}$.

Defining a_0 by

$$a_0 = \frac{\lambda^4}{8\pi\sqrt{\pi}\,c}\,\frac{1}{b^{(\lambda)}}\,\frac{q_k}{q_1}\,a_{k1}\,, \tag{16}$$

we have

$$a_\lambda = a_0\,\frac{a}{\pi}\int_{-\infty}^{+\infty}\frac{e^{-y^2}\,dy}{a^2 + (v - y)^2}\,. \tag{17}$$

The second factor on the right-hand side, which gives the ratio a_λ/a_0, is a function of $a = \delta_k^{(\lambda)}/b^{(\lambda)}$ and $v = \Delta\lambda/b^{(\lambda)}$. This function has been tabulated by Hjerting.[14]

Equation (4), giving the equivalent width $w^{(\lambda)}$, can be written in the form

$$\frac{w^{(\lambda)}}{b^{(\lambda)}} = \int (1 - e^{-(a_\lambda/a_0)\tau_0})\,dv\,, \tag{18}$$

where we have introduced the optical thickness, τ_0, corresponding to a_0 defined by equation (16),

$$\tau_0 = N a_0\,. \tag{19}$$

Equation (18) shows that $w^{(\lambda)}/b^{(\lambda)}$ can be computed as a function of τ_0 and $a = \delta_k^{(\lambda)}/b^{(\lambda)}$, since a_λ/a_0 is a known function of the variable of integration v and the constant a. The calculations involve numerical quadratures according to equation (18), use being made of the tables of a_λ/a_0.

Now, for the interstellar lines in question, the ratio (a) of the damping constant $\delta_k^{(\lambda)}$ and the Doppler constant $b^{(\lambda)}$ is small, around 0.001 or smaller. Moreover, the interstellar lines that we are going to consider are not strong enough to show appreciable damping wings. We therefore expect that calculations of $w^{(\lambda)}/b^{(\lambda)}$, according to equations (17) and (18), with $a = 0$ will be sufficiently accurate for our purpose. That this is, in fact, the case is shown by Table 1 of $w^{(\lambda)}/b^{(\lambda)}$ as a function of τ_0, computed by numerical quadratures for $a = 0$ and $a = 0.001$.

We notice that it is only for τ_0 greater than about 1000 that the difference between the two sets of values becomes at all appreciable. Now, as we shall see, this part of the table will not be needed for our purposes.

In the following calculation we shall therefore put $a = 0$. Then

$$\frac{\tau_\lambda}{\tau_0} = \frac{a_\lambda}{a_0} = e^{-v^2}; \tag{20}$$

and the numerical calculations according to equation (18) are somewhat simplified. Table 2 gives $\log [w^{(\lambda)}/b^{(\lambda)}]$ in greater detail as a function of $\log \tau_0$ for $a = 0$.
The table was calculated by numerical quadratures and checked by the tables of Ladenburg and Levy.[14] (The explanation of the other columns of Table 2 will be given later.)

Representing the relation between $\tau_0 = Na_0$ and $w^{(\lambda)}/b^{(\lambda)}$ graphically, we obtain a theoretical curve of growth for interstellar lines, corresponding to the case of absorption by one cloud with a Gaussian radial-velocity distribution. We note that $w^{(\lambda)}/b^{(\lambda)}$ is proportional to τ_0 for small values of τ_0. As the optical thickness τ_0 at the center of the line increases, the line becomes more and more saturated, and hence the increase of $w^{(\lambda)}$ with τ_0, and therefore with N, becomes very slow.

With the aid of Table 2, theoretical values of the doublet ratio of such lines as the D1 and D2 lines of *Na* I and the H and K lines of *Ca* II can be calculated as a function of τ_0 for, say, the fainter line of the doublet; for, to any given value of $\tau_0^{(f)}$ for the fainter line there corresponds a value $\tau_0^{(s)} = 2\tau_0^{(f)}$ for the stronger line. The corresponding values of the equivalent widths and the Doppler constant (which, of course, is practically the same for the two lines) can be read from Table 2, and the ratio $w_s^{(\lambda)}/w_f^{(\lambda)}$ found. Table 2 also gives the theoretical doublet ratio as a function of log τ_0 for the fainter line, again for the case of absorption by atoms with a Gaussian radial-velocity distribution.

TABLE 1

τ_0	$\log \frac{w^{(\lambda)}}{b^{(\lambda)}}$ for $a=0$	$\log \frac{w^{(\lambda)}}{b^{(\lambda)}}$ for $a=0.001$	τ_0	$\log \frac{w^{(\lambda)}}{b^{(\lambda)}}$ for $a=0$	$\log \frac{w^{(\lambda)}}{b^{(\lambda)}}$ for $a=0.001$
0.1	9.24−10	9.24−10	100	0.66	0.66
1.0	0.11	0.11	1000	0.74	0.76
10.0	0.52	0.52			

TABLE 2

log τ_0 for D1 or H	log $w^{(\lambda)}/b^{(\lambda)}$ for D1 or H	Doublet Ratio D2/D1 or K/H	log $N/w^{(\lambda)}$ for D1	log $N/w^{(\lambda)}$ for H	Ratio D1/3303
9.0−10	9.24−10	1.91	12.98	13.30	.....
9.2	9.43	1.88	12.99	13.31	.....
9.4	9.61	1.84	13.01	13.33	.....
9.6	9.79	1.77	13.03	13.35	.....
9.8	9.96	1.66	13.06	13.38	.....
0.0	0.11	1.53	13.11	13.43	.....
0.2	0.24	1.39	13.18	13.50	.....
0.4	0.34	1.29	13.28	13.60	.....
0.6	0.42	1.21	13.40	13.72	81
0.8	0.48	1.16	13.54	13.86	59
1.0	0.52	1.13	13.70	14.02	42
1.2	0.56	1.11	13.86	14.18	29
1.4	0.59	1.10	14.03	14.35	20
1.6	0.62	1.08	14.20	14.52	14
1.8	0.64	1.07	14.38	14.70	10.2
2.0	0.66	1.07	14.56	14.88	7.4

When the equivalent widths of both the stronger and the fainter line of an interstellar doublet have been observed for a given star, and if the hypothesis is made that the absorbing atoms (or ions) have a Gaussian velocity distribution, then both the Doppler constant $b^{(\lambda)}$ and τ_0, and hence N, corresponding to the column of atoms between the observer and the star, can be determined. The measured doublet ratio gives $\tau_0 = Na_0$ and $w^{(\lambda)}/b^{(\lambda)}$ for the fainter line with the aid of Table 2. Since $w^{(\lambda)}$ is known, $b^{(\lambda)}$ follows, and hence a_0 (cf. eq. [16]) and N. This is, in principle, the method used by Merrill and Wilson.[8]

It appears from Table 2 that the method is limited to a certain range of τ_0, corresponding to doublet ratios roughly between 1.8 and 1.3. Outside these limits small errors in the observed doublet ratio lead to large errors in $b^{(\lambda)}$. However, the number of absorbing atoms, N, is well determined for all values of τ_0 up to about 2.5, corresponding to doublet ratios greater than about 1.3. The uncertainty in the determination of $b^{(\lambda)}$

for weak lines does not affect the determination of N. This is clearly seen in the case of very weak lines. In the limit of very small τ_0, we have, according to equations (18) and (20),

$$\frac{w^{(\lambda)}}{b^{(\lambda)}} = \sqrt{\pi}\,\tau_0 \quad (\tau_0 \text{ small}) \tag{21}$$

or (cf. eqs. [16] and [19])

$$N = \frac{8\pi c}{\lambda^4}\,\frac{q_1}{q_k}\,\frac{1}{a_{k1}}\,w^{(\lambda)}. \tag{22}$$

This is, in fact, the standard equation connecting line strength and the number of absorbing atoms in the case of absorption by an optically thin column.[9]

Quite generally, according to equations (16) and (19),

$$\frac{N}{w^{(\lambda)}} = \frac{8\pi\sqrt{\pi}\,c}{\lambda^4}\,\frac{q_1}{q_k}\,\frac{1}{a_{k1}}\left[\frac{b^{(\lambda)}}{w^{(\lambda)}}\,\tau_0\right]. \tag{23}$$

The last factor on the right-hand side of this equation can be found with the aid of Table 2 as a function of τ_0 or of the doublet ratio. The other factors on the right-hand side are known for the particular interstellar lines in question. Thus, for any of these lines, $N/w^{(\lambda)}$ can be tabulated as a function of the doublet ratio. This means essentially that the Doppler constant $b^{(\lambda)}$ is eliminated in the determination of N from the equivalent widths of the two lines of an interstellar doublet. Table 2 gives $\log N/w^{(\lambda)}$ for the fainter line of the *Na* I and *Ca* II doublets (i.e. for D1 and H) as a function of either τ_0 for the same line or the corresponding doublet ratio (D2/D1 or K/H). It is clear from this table that $N/w^{(\lambda)}$ is well determined by the doublet ratio up to the limit of τ_0 mentioned above, i.e., for all values of $\log N/w^{(\lambda)}$ up to about 13.3 for D1 and 13.6 for H. For larger values the doublet method fails. The lines become saturated and their strengths insensitive to variations of N as well as $b^{(\lambda)}$.

The failure of the doublet method for strong lines means a serious limitation. Dunham[9] has determined the number of absorbing *Na* I atoms in a case where the doublet method fails (interstellar lines in the spectrum of χ^2 Ori), from measures of equivalent widths of the two components of the second sodium doublet at 3302–3303 A. The ratio of the transition probabilities, a_{k1}, for the two sodium doublets is known[15] and is equal to 21.8. Hence, the ratio D1/3303 of the equivalent widths of the two fainter lines of the doublets can be calculated as a function of $N/w^{(\lambda)}$ for D1 by the same procedure that was used in the case of the doublet ratio D2/D1. The calculated values of D1/3303 are given in Table 2 and are valid for the case of a Gaussian radial-velocity distribution of the absorbing atoms.

It appears from Table 2 that the method of determining N and $b^{(\lambda)}$ from the relative strengths of one line from each of the two sodium doublets can be used up to much higher values of $N/w^{(\lambda)}$. The application of this method, however, requires measures of equivalent widths of quite faint lines if the method is to be used from the point where the D1/D2-method begins to fail.

In order to illustrate the use of Table 2, we shall first apply the method to the data given by Dunham for the two interstellar sodium doublets in χ^2 Orionis. The equivalent width of D1 is $w^{(\lambda)} = 0.39$ A, that of 3303 A is $w^{(\lambda)} = 0.040$ A. The ratio D1/3303 = 9.8, when used in Table 2, gives $\log N/w^{(\lambda)}$ for D1 equal to 14.40; hence $\log N = 13.99$. The number of absorbing sodium atoms is thus found from the strengths of D1 and 3303 A to be $N = 9.8 \times 10^{13}$. Also, $b^{(\lambda)}$ is found to be 0.09 A. Next, consider a case in which measures have given equivalent widths of the interstellar D1 and D2 lines in a star equal to 0.16 A and 0.24 A, respectively. The doublet ratio is 1.50, and Table 2 gives

[15] A. Filippov and W. Prokofjew, *Zs. f. Phys.*, **56**, 458, 1929.

log $N/w^{(\lambda)}$ for D1 equal to 13.12 so that log $N = 12.32$. The Doppler constant $b^{(\lambda)}$ is found to be 0.11 A in this case.

We shall now consider cases where the radial-velocity distribution of the absorbing atoms (or ions) is not Gaussian.

First, let us assume that there are between the observer and the stars a number, n, of equal clouds. Each cloud is supposed to be characterized by a Gaussian radial-velocity distribution of its atoms, as before. Let us further assume that the radial velocities of the clouds are such that the interstellar lines do not interfere. This means that the difference of the radial velocity of any two clouds is more than about four times the Doppler constant b (in velocity units) of each cloud. In this case the total number of absorbing atoms, N, is divided over n clouds, with N/n in each. The optical thickness of each cloud is then τ_0/n (cf. eq. [19]). The total equivalent width of the interstellar lines produced by the clouds is therefore $n \cdot w^{(\lambda)}(\tau_0/n)$. Consider, now, the theoretical relation between $w^{(\lambda)}$ and N in the case of the n clouds. It is seen to be the same as the standard relation for one cloud, only the Doppler constant has to be taken equal to nb. In using the doublet method, the case of n clouds that do not interfere is therefore equivalent to that of one cloud with a Doppler constant n times that which is valid for each cloud. In particular, we see that the relation between the doublet ratio and $N/w^{(\lambda)}$ (cf. Table 2), in which the Doppler constant is eliminated, remains unchanged.

On the other hand, a number of clouds with equal, or practically equal, radial velocities, have, of course, the same effect as one cloud with the Doppler constant b.

If the number of clouds intercepted by the line of sight to the star is large and if the distribution of the radial velocities of the individual clouds is Gaussian with a Doppler constant b', then the resulting velocity of all the absorbing atoms between the observer and the star is Gaussian, with a Doppler constant equal to $(b^2 + b'^2)^{1/2}$ or, since it can be assumed that b' is at least a few times larger than b, approximately b'. Again, the relation between the doublet ratio and $N/w^{(\lambda)}$ remains unchanged.

The case of a relatively small number of clouds with interstellar lines that partly overlap is rather complicated. We shall treat here only the case of two equal clouds. Call the radial velocity of the two clouds u_0' and u_0'', and b the Doppler constant characterizing the Gaussian radial-velocity distribution in each of the clouds about the radial velocity of the cloud. Then the radial-velocity distribution of the absorbing atoms is given by

$$\psi(u) = \frac{1}{2\sqrt{\pi}b} e^{-(u-u_0')^2/b^2} + \frac{1}{2\sqrt{\pi}b} e^{-(u-u_0'')^2/b^2}. \tag{24}$$

With $a = 0$ as before, we now have (cf. eq. [20])

$$\frac{\tau_\lambda}{\tau_0} = \frac{a_\lambda}{a_0} = \tfrac{1}{2} e^{-(v-[1/2]a)^2} + \tfrac{1}{2} e^{-(v+[1/2]a)^2}, \tag{25}$$

where

$$a = \frac{u_0' - u_0''}{b} \tag{26}$$

is equal to the velocity difference between the clouds measured in units of the Doppler constant b.

With the help of equations (18) and (25), $w^{(\lambda)}/b^{(\lambda)}$ can be found as before by the method of numerical quadrature, now as a function of τ_0 and a. Table 3 gives $w^{(\lambda)}/b^{(\lambda)}$ as a function of τ_0 for radial-velocity differences of the two clouds equal to 0, 1, 2, and 3 times the Doppler constant b. The values for velocity differences so large that the interstellar lines do not overlap at all are also given.

From the numerical values given in Table 3 it is found that the relations between τ_0 and $w^{(\lambda)}/b$ $^{(\lambda)}$for the different values of $a = \Delta u/b$ can be reproduced rather accurately

from the relation valid for one cloud by assuming a different Doppler constant, larger than the one valid for each cloud. The value of this effective Doppler constant, b_e, is $1.2b$, $1.5b$, $1.8b$, and $2b$ for $\Delta u = b$, $\Delta u = 2b$, $\Delta u = 3b$, and $\Delta u \gg b$, respectively; this is more clearly seen when the ratio $N/w^{(\lambda)}$ is tabulated as a function of the doublet ratio, so that the Doppler constant is eliminated. Table 4 gives $\log [\tau_0/(w^{(\lambda)}/b^{(\lambda)})]$ for the fainter line of a doublet, a quantity which, according to equation (23), is proportional to $N/w^{(\lambda)}$, as a function of the doublet ratio. The values have been calculated from those given in Table 3.

TABLE 3*

log τ_0	$\Delta u = 0$	$\Delta u = b$	$\Delta u = 2b$	$\Delta u = 3b$	$\Delta u \gg b$
9.6−10	9.79−10	9.80−10	9.81−10	9.82−10	9.82−10
9.8−10	9.96−10	9.97−10	9.99−10	0.00	0.00
0.0	0.11	0.13	0.16	0.18	0.18
0.2	0.24	0.27	0.31	0.34	0.34
0.4	0.34	0.39	0.45	0.48	0.48
0.6	0.42	0.48	0.56	0.59	0.59
0.8	0.48	0.54	0.63	0.67	0.68
1.0	0.52	0.59	0.68	0.74	0.75
1.2	0.56	0.63	0.71	0.78	0.80
1.4	0.59	0.66	0.74	0.80	0.84
1.6	0.62	0.68	0.76	0.82	0.87
1.8	0.64	0.70	0.78	0.84	0.90
2.0	0.66	0.72	0.79	0.86	0.93

* The table gives $\log w^{(\lambda)}/b^{(\lambda)}$.

TABLE 4*

Doublet Ratio	$\Delta u = 0$	$\Delta u = b$	$\Delta u = 2b$	$\Delta u = 3b$	$\Delta u \gg b$
2.0	9.75−10	9.75−10	9.75−10	9.75−10	9.75−10
1.9	9.76	9.76	9.76	9.76	9.76
1.8	9.80	9.80	9.80	9.80	9.80
1.7	9.83	9.83	9.83	9.83	9.83
1.6	9.86	9.87	9.88	9.86	9.86
1.5	9.90	9.91	9.92	9.90	9.90
1.4	9.95	9.97	9.97	9.95	9.95
1.3	0.07	0.04	0.03	0.03	0.07
1.2	0.21	0.19	0.15	0.16	0.21

* The table gives $\log [\tau_0/(w^{(\lambda)}/b^{(\lambda)})]$ for the fainter line of the doublet (cf. eq. [23]).

It appears from Table 4 that the values for the case of two equal clouds are practically the same as those valid for one cloud ($\Delta u = 0$) in the whole range of applicability of the doublet ratio method, irrespective of the velocity difference between the clouds. Less extensive calculations for the case of two unequal clouds indicate that the situation is the same here also.

Altogether, it appears that the doublet ratio method, based on the theoretical relations valid for a Gaussian radial-velocity distribution of the absorbing atoms, has a rather wide range of application. Only it must be kept in mind that, while N always refers to the same quantity, namely, the number of absorbing atoms in the entire column of unit cross-section between the observer and the star, the effective Doppler constant varies between the limits b and $(b^2 + b'^2)^{1/2}$ and generally increases with the number of clouds.

IV

In thermodynamical equilibrium at temperature T, the ionization is given by the Saha equation, valid for any two consecutive stages of ionization,

$$\frac{\mathfrak{N}_1'' \mathfrak{N}_e}{\mathfrak{N}_1'} = \frac{(2\pi m_e)^{3/2}}{h^3} \frac{2q_1''}{q_1'} (kT)^{3/2} e^{-I/kT}. \tag{27}$$

Here $\mathfrak{N}_1'$ and $\mathfrak{N}_1''$ are the numbers per cubic centimeter of atoms or ions in the ground states of the two consecutive stages of ionization in question; q_1' and q_1'' the corresponding statistical weights; I the ionization potential involved; and $\mathfrak{N}_e$ the number of free electrons per cubic centimeter.

Eddington[10] first considered the ionization of an element in interstellar space. He assumed the intensity I_ν of ionizing radiation from the stars for frequency ν at a typical point in interstellar space to be given by

$$I_\nu = wB_\nu(T_i)$$

where w is the so-called "dilution factor" and $B_\nu(T_i)$ is the Planck intensity corresponding to a temperature T_i which is of the general order of the effective temperatures of stellar atmospheres. Eddington estimated that $w = 10^{-14}$ and $T_i = 10{,}000°$ would give a reasonably good representation of the stellar radiation at a typical point in interstellar space. He further showed[16] that the velocity distribution of interstellar atomic particles might be expected to correspond to the thermal velocities for a temperature about equal to T_i, or 10,000°. Eddington finally derived the following ionization equation for interstellar space:

$$\frac{\mathfrak{N}_1'' \mathfrak{N}_e}{\mathfrak{N}_1'} = \frac{(2\pi m_e)^{3/2}}{h^3} \frac{2q_1''}{q_1'} (kT_i)^{3/2} e^{-I/kT_i} w, \tag{28}$$

which differs from the Saha equation by the occurrence of the dilution factor w.

If the kinetic temperature describing the thermal motion of the interstellar atomic particles is T_e, an additional factor $(T_e/T_i)^{1/2}$ occurs on the right-hand side of the equation (cf., e.g, Rosseland[17]),

$$\frac{\mathfrak{N}_1'' \mathfrak{N}_e}{\mathfrak{N}_1'} = \frac{(2\pi m_e)^{3/2}}{h^3} \frac{2q_1''}{q_1'} (kT_i)^{3/2} e^{-I/kT_i} \left(\frac{T_e}{T_i}\right)^{1/2} w. \tag{29}$$

For a further refinement of equation (29), consider the equilibrium between ionization and recombination processes in interstellar space. The atoms and ions are here practically all in the respective ground states, the number of atomic particles in excited states being reduced by a factor of the order of the dilution factor in comparison with thermodynamical equilibrium. This means that the ionization processes occur from the ground states only. The recombination processes, however, will occur as in a gas in thermodynamical equilibrium at a temperature equal to T_e. As a consequence, the ratio $\mathfrak{N}_1''/\mathfrak{N}_1'$ will be increased and the ionization equation (29) must be corrected accordingly.[9,12]

The calculation of the ratio $\mathfrak{N}_1''/\mathfrak{N}_1'$ can be carried out by the standard method of calculating the number of ionization processes from, and the number of recombination processes to, any particular stage of ionization and equating the two quantities.

[16] Eddington, *Proc. R. Soc., London, A*, **111**, 424, 1926; cf. also H. C. van de Hulst, *Ned. Tijdschr. v Natuurk.*, **12**, 168, 1946; L. H. Aller and D. Bohm, *Ap. J.*, **105**, 131, 1947.

[17] *Op. cit.*

The number of photoionizations from the ground state is found as follows: We write the intensity I_ν (averaged over all directions) of the ionizing radiation at frequency ν, in the form

$$I_\nu = G_\nu \frac{2h\nu^3}{c^2} e^{-h\nu/kT_i}. \tag{30}$$

When the intensity I_ν is given as a function of ν, any choice of a value of T_i defines the corresponding function G_ν. In certain connections the most favorable choice of T_i is the one which makes G_ν as nearly constant as is possible in the region of the spectrum that contributes most to the ionization of the element in question. (The reason that the definition of the function G_ν by eq. (30) is somewhat more convenient than a corresponding definition involving the Planck intensity is that the number of induced recombination processes is negligible in interstellar space.)

Call the continuous absorption coefficient, at frequency ν in the continuum corresponding to the ground state of the atom the ionization of which is considered, $a_\nu^{(1)}$. Then the number of photoionizations per unit time and unit volume is

$$n_1^{(\mathrm{ph})} = \mathfrak{N}_1' \int_{\nu_1}^{\infty} \frac{4\pi}{h\nu} a_\nu^{(1)} I_\nu d\nu, \tag{31}$$

where ν_1 is the limiting frequency of the continuum in question, or

$$n_1^{(\mathrm{ph})} = \mathfrak{N}_1' \frac{8\pi}{c^2} \int_{\nu_1}^{\infty} a_\nu^{(1)} \nu^2 G_\nu e^{-h\nu/kT_i} d\nu. \tag{32}$$

The continuous absorption coefficient will, in most cases, be a rapidly decreasing function of $\nu (\nu > \nu_1)$. For hydrogen $a_\nu^{(1)}$ is approximately proportional to ν^{-3}. We define $A_\nu^{(1)}$ by

$$a_\nu^{(1)} = a_1 \frac{\nu_1^2}{\nu^2} A_\nu^{(1)}, \tag{33}$$

where a_1 is the absorption coefficient at the series limit. Hence $A_\nu^{(1)}$ is unity at the series limit and usually varies considerably less with wave length than does $a_\nu^{(1)}$. With this definition,

$$n_1^{(\mathrm{ph})} = \mathfrak{N}_1' \frac{8\pi}{c^2} a_1 \nu_1^2 \int_{\nu_1}^{\infty} A_\nu^{(1)} G_\nu e^{-h\nu/kT_i} d\nu. \tag{34}$$

The number of recombinations to the stationary state k resulting from captures of free electrons in the energy range E_e, $E_e + dE_e$ corresponding to the frequency range ν and $\nu + d\nu$ of the emitted radiation, is

$$n_\nu^{(rc,k)} d\nu = \mathfrak{N}_1'' \beta_\nu^{(k)} v \, d\mathfrak{N}_e, \tag{35}$$

where v is the electron velocity corresponding to the energy and $d\mathfrak{N}_e$ the number of free electrons per unit volume in the energy range in question, while $\beta_\nu^{(k)}$ is the capture cross-section. The latter quantity can be expressed in terms of the continuous absorption coefficient $a_\nu^{(k)}$ in the continuum corresponding to the stationary state k with the help of the Milne relation:

$$\beta_\nu^{(k)} = \frac{2h^2\nu^2}{m_e^2 c^2} \frac{q_k'}{2q_1''} \frac{1}{v^2} a_\nu^{(k)}. \tag{36}$$

The velocity distribution of the free electrons in interstellar space can be assumed to be a Maxwellian distribution corresponding to temperature T_e. Then

$$d\mathfrak{N}_e = \mathfrak{N}_e \left(\frac{2}{\pi}\right)^{1/2} \frac{m_e^{3/2}}{(kT_e)^{3/2}} \, e^{-E_e/kT_e} v \, dE_e \,. \tag{37}$$

Inserting equations (36) and (37) in equation (35) and using equation (33), we get, after some reductions,

$$n_\nu^{(rc,k)} d\nu = \mathfrak{N}_1'' \mathfrak{N}_e \frac{h^3}{(2\pi m_e kT_e)^{3/2}} \frac{q_k'}{2q_1''} \frac{8\pi}{hc^2} \, a_k \nu_k^2 A_\nu^{(k)} \, e^{-E_e/kT_e} dE_e \,. \tag{38}$$

Here a_k denotes the continuous absorption coefficient at the frequency ν_k of the series limit corresponding to the stationary state k, while $A_\nu^{(k)}$ is analogous to $A_\nu^{(1)}$ (cf. eq. [33]). Integrating this expression over the energy range of the free electrons, we find the total number of recombinations to the stationary state k to be

$$n_k^{(rc)} = \mathfrak{N}_1'' \mathfrak{N}_e \frac{h^3}{(2\pi m_e kT_e)^{3/2}} \frac{q_k'}{2q_1''} \frac{8\pi}{hc^2} \, a_k \nu_k^2 \int_0^\infty A_\nu^{(k)} \, e^{-E_e/kT_e} dE_e \,. \tag{39}$$

We now equate the number $n_1^{(\mathrm{ph})}$ of photoionizations from the ground state (cf. eq. [34]) to the total number of recombinations (cf. eq. [39]) for all states:

$$n_1^{(\mathrm{ph})} = \sum_{k=1}^{\infty} n_k^{(rc)} \,. \tag{40}$$

With the substitutions

$$h\nu = I + E_e \tag{41}$$

and $dE_e = h d\nu$ in equation (34), we get, after inserting from equations (34) and (39) in equation (40),

$$\begin{aligned} &\mathfrak{N}_1' \frac{8\pi}{c^2} \, a_1 \nu_1^2 \frac{kT_i}{h} \, e^{-I/kT_i} \int_0^\infty A_\nu^{(1)} G_\nu \, e^{-E_e/kT_i} d\left(\frac{E_e}{kT_i}\right) \\ &\quad = \mathfrak{N}_1'' \mathfrak{N}_e \frac{h^3}{(2\pi m_e kT_e)^{3/2}} \frac{1}{2q_1''} \frac{kT_e}{h} \frac{8\pi}{c^2} \sum_{k=1}^{\infty} q_k' a_k \nu_k^2 \int_0^\infty A_\nu^{(k)} \, e^{-E_e/kT_e} d\left(\frac{E_e}{kT_e}\right). \end{aligned} \tag{42}$$

Solving for $\mathfrak{N}_1''\mathfrak{N}_e/\mathfrak{N}_1'$ (cf. eqs. [27], [28], and [29]) we finally obtain the required ionization equation:

$$\frac{\mathfrak{N}_1'' \mathfrak{N}_e}{\mathfrak{N}_1'} = \frac{(2\pi m_e)^{3/2}}{h^3} \frac{2q_1''}{q_1'} (kT_i)^{3/2} e^{-I/kT_i} \left(\frac{T_e}{T_i}\right)^{1/2} W \,, \tag{43}$$

where

$$W = \frac{q_1' \nu_1^2 a_1 \int_0^\infty A_\nu^{(1)} G_\nu \, e^{-E_e/kT_i} d\left(\frac{E_e}{kT_i}\right)}{\sum_{k=1}^{\infty} q_k \nu_k^2 a_k \int_0^\infty A_\nu^{(k)} \, e^{-E_e/kT_e} d\left(\frac{E_e}{kT_e}\right)} \,. \tag{44}$$

Equation (44) may be regarded as an expression giving the proper modified dilution factor W to be used in equation (43), which is otherwise identical with equation (29).

In order to interpret equation (44), we consider the case that $A_\nu^{(k)}$ and G_ν are independent of ν, $A_\nu^{(k)} = 1$, $G_\nu = G$. Then

$$W = \frac{q_1' \nu_1^2 a_1}{\sum_{k=1}^{\infty} q_k' \nu_k^2 a_k} G. \tag{45}$$

If in the sum over all the stationary states, all the terms arising from the excited states ($k = 2, 3, \ldots$) are neglected, then W reduces to G, and we recover the usual definition of the dilution factor. When the terms in question are retained, W is correspondingly reduced by a certain correction factor.

When $A_\nu^{(k)}$ and G_ν vary with frequency, equation (44) shows how the proper mean values are to be calculated.

The determination of W according to equation (44), i.e., of the correction factor to the Saha-Eddington equation as used in previous investigations, can be carried out if the ionizing radiation and all the continuous absorption coefficients $a_\nu^{(k)}$ are known. For the purpose of such calculations it is somewhat more advantageous to re-write equation (44) in the following form obtained by using equations (30) and (33):

$$W = \frac{q_1' \nu_1^2 \int_0^\infty a_\nu^{(1)} \left(\frac{\nu_1}{\nu}\right) \left[\frac{I_\nu}{B_{\nu_1}(T_i)}\right] d\left(\frac{E_e}{kT_i}\right)}{\sum_{k=1}^{\infty} q_k' \nu_k^2 a_k \int_0^\infty A_\nu^{(k)} e^{-E_e/kT_e} d\left(\frac{E_e}{kT_e}\right)}, \tag{46}$$

where $B_{\nu_1}(T_i)$ denotes the Planck intensity at the series limit ν_1 for the temperature T_i. It is easily verified that $\mathfrak{N}_1'' \mathfrak{N}_e / \mathfrak{N}_1'$ is independent of the choice of T_i, which could well be eliminated from the equation. What matters is, of course, only the strength of the ionizing radiation, while $B_{\nu_1}(T_i)$ is just a convenient unit for expressing the intensities.

With a view to application, it is desirable to calculate the modified dilution factor W for a number of atoms and ions (cf. Secs. VI–VII), including *Na* I, *K* I, *K* II, *Ca* I, *Ca* II, *Fe* I, and *Fe* II. The necessary data are available, more or less completely and accurately, for *Na* I, *K* I, *Ca* I, and *Ca* II. Continuous absorption coefficients of the ground state and of a number of excited states of *Na* 1 have been calculated theoretically by M. Rudkjöbing.[18] The difficult case of the ground state of *K* 1 has been treated theoretically by D. R. Bates,[19] and experimental values by R. W. Ditchburn, J. Tunstead, and J. G. Yates[20] are also available. For *Ca* I and *Ca* II, quantum-mechanical calculations have been carried out by H. S. W. Massey and D. R. Bates[21] for the ground state, by L. C. Green[22] for both the ground state and some of the excited states.

The cases of *Fe* I and *Fe* II are difficult, while *K* II is relatively simple.[23] The necessary data for *K* II are expected to be available in the near future.

Determinations of W according to equation (46) have been carried out for *Na* I, *K* I, *Ca* I, and *Ca* II. In calculating the sum in the denominator, the hydrogenic values of a_ν have been used. General quantum-mechanical arguments indicate that the values thus

[18] *D. Kgl. Danske Vidensk. Selskab, Mat.-fys. Medd.*, Vol. **18**, No. 2, 1940.

[19] *Proc. R. Soc., London, A*, **188**, 350, 1947.

[20] *Proc. R. Soc., London, A*, **181**, 386, 1943.

[21] *Proc. R. Soc., London, A*, **177**, 329, 1941.

[22] Unpublished. The author is indebted to Dr. Green for putting the preliminary results of his calculations at his disposal in advance of publication.

[23] Cf. D. R. Bates, *M.N.*, **106**, 432, 1946.

obtained are approximately correct.[24] This conclusion is confirmed by the calculations for excited states of *Na* I (Rudkjöbing) and *Ca* II (Green). In carrying out the calculations in question, it is, of course, important to use the proper radial quantum number of the stationary states. In actual practice the quantity

$$\sum_{k=4}^{\infty} q_k \nu_k^2 a_k \int_0^{\infty} A_\nu^{(k)} e^{-E_e/kT_e} d\left(\frac{E_e}{kT_e}\right) \tag{47}$$

can be calculated with the values of q_k, ν_k, a_k, and $A_\nu^{(k)}$ corresponding to hydrogen, and (relatively small) corrections applied, to reduce for any deviation from this according to the available information regarding the lowest excited states.

The quantity (47) was determined for three different values of the kinetic temperature T_e, namely, 10,000°, 1000°, 100°. The two latter values were chosen in view of Spitzer's investigations regarding the temperature of *H* I regions containing interstellar solid particles.

In the numerical calculations of the quantity (47) the correction factors to Kramers' expression for the hydrogenic absorption coefficients were put equal to 1 (the corresponding errors are quite small). Thus $a_\nu \sim \nu^{-3}$, and $A_\nu = \nu_1/\nu$, so that[25]

$$\int_0^{\infty} A_\nu^{(k)} e^{-E_e/kT_e} d\left(\frac{E_e}{kT_e}\right) = \frac{h\nu_k}{kT_e} e^{h\nu_k/kT_e} K_1\left(\frac{h\nu_k}{kT_e}\right), \tag{48}$$

where K_1 denotes the exponential integral of the first order.

The contribution of the stationary states with high quantum number to the sum in equation (47) is quite appreciable, especially for the lower temperatures. Beyond $n = 40$ an integral was substituted for the sum and evaluated by numerical quadrature; beyond $n = 200$ the quadrature was carried out analytically, using a sufficiently accurate approximation of the integrand, obtained from the well-known expansion of the exponential integral involved, which is valid for small values of its argument. Table 5 gives the values of the quantity (47) obtained for the three temperatures mentioned.

In calculating the numerator of the expression (44) for W, the intensity I_ν of the ionizing radiation must be known as a function of the frequency. In the present calculations the values derived by Dunham[9] were adopted. Dunham's values were derived from determinations of the integrated light of stars of the various spectral classes and on the basis of assumed intensity-curves (Planck curves of specified temperatures) for these classes. We adopted the values found by Dunham when the correction for interstellar selective absorption was neglected. No direct information is available regarding the interstellar particle absorption in the wave-length regions of the ionizing radiation. From the work of Oort and van de Hulst[2] on the size-distribution function of interstellar particles and from the results derived from them regarding the dependence of interstellar particle absorption upon wave length,[26] it appears quite probable that the absorption in the far ultraviolet is about equal to that in the photographic region, so that the correction in question would, in fact, be small.

In the cases of *Na* I, *K* I, and *Ca* I, the contribution of the ionizing radiation beyond the Lyman limit at 911 A to the number of photoionizations is negligible. For *Ca* II, with $I = 11.9$ volts, this is not the case. Here the calculation was carried out both for the assumption of complete cutoff of the radiation in question (*H* I region) and for the assumption of negligible cutoff (*H* II region).

In the case of *Na* I the existing data for the continuous absorption coefficient of the

[24] Cf. Bates, Buckingham, Massey, and Unwin, *Proc. R. Soc., London*, *A*, **170**, 322, 1939.

[25] G. Cillié, *M.N.*, **92**, 820, 1932; **96**, 771, 1936.

[26] Oort and van de Hulst, *op. cit.*; also H. C. van de Hulst, unpublished.

ground state are insufficient for the wave-length region beyond $\lambda = 2100$, which may contribute appreciably to the number of photoionizations. It would be desirable to carry the quantum-mechanical calculation to smaller wave lengths. This should present no special difficulties. For the present, the calculation was carried out on two assumptions, which were believed to give a lower and an upper limit to W, respectively. First, it was assumed that the number of photoionizations produced by radiation beyond the minimum of the absorption coefficient at about 2100 A was negligible.[18] This certainly gives a lower limit. Next, an absorption coefficient independent of the frequency and equal to the value at the series limit ($a_1 = 1 \cdot 6 \cdot 10^{-19}$) was assumed. This presumably gives an upper limit. The geometric mean of the two limiting values, which differ by a factor about equal to 7, was adopted. [Since this was written Dr. Rudkjöbing has calculated the continuous absorption coefficient of the ground state of sodium in the wave-length region 900–2100 A. His results confirm the value adopted.]

With a view to the uncertainties of the data regarding the continuous absorption coefficients, no attempt was made to improve Dunham's values for the ionizing radiation. In this connection it should be noted that recent work on the continuous spectrum of stars of spectral class around B0 has indicated that the radiation from such stars may be considerably higher than that assumed in Dunham's calculations, particularly in the wave-length region from 911 A to about 1500 or 2000 A. A revision of the adopted values would presumably not affect the values of W for *Na* I, *K* I, and *Ca* I very much. The values of W for *Ca* II, however, might be reduced by a factor of 3, or even more, since the ionization potential is relatively high.

TABLE 5

$$\sum_{n=4}^{\infty} q_n \nu_n^2 a_n \int_0^{\infty} A_\nu^{(n)} e^{-E_e/kT_e} d\left(\frac{E_e}{kT_e}\right)$$

10,000°	$1.3\ \nu_1^2$
1000	$3.1\ \nu_1^2$
100	$5.3\ \nu_1^2$

The consequences of the uncertainties just mentioned will be discussed in the following sections. It should be emphasized that improvement of the accuracy through further investigations of the continuous absorption coefficients and of the ionizing radiation, although requiring a considerable effort, seems entirely feasible.

The results of the present investigation regarding the state of ionization of *Na* I, *K* I *Ca* I, and *Ca* II in interstellar space are summarized in Table 6.

It appears from Table 6 that the correction factors to the equations previously used are quite large, the total range being from 2.6 to 1600. The corrections increase with decreasing temperature. This is due to the fact that the relative contribution of the highly excited states to the number of recombinations increases with decreasing temperature.

A second effect of decreasing temperature is already taken into account in equation (29) through the factor $(T_e/T_i)^{1/2}$. The two effects act in the same direction. Thus, for instance, the value of $\mathfrak{N}_1''\mathfrak{N}_e/\mathfrak{N}_1'$ for *Na* I found from the previously used equation (29) and temperature $T_e = 10{,}000°$ differs by a factor of 16,000 from that found here for $T_e = 100°$.

The value for *Ca* I and $T_e = 10{,}000°$, i.e., a correction factor equal to 2.6, agrees well with the value found by Massey and Bates,[21] neglecting the variation of A_ν and G_ν with frequency (cf. p. 255, especially eq. [45]).

The consequences resulting from the application of the derived correction factors will be discussed in Sections VI–VIII. It may already be noted here that their general effect is to diminish very considerably the interstellar gas densities, found by calculation, corresponding to given observed interstellar absorption line strengths.

V

In an earlier investigation,[12] the author discussed the problem of the extent of the regions of ionization of hydrogen in interstellar space (*H* II regions). The case treated was that of a star surrounded by a hydrogen medium of uniform density. It was shown that the *H* II and *H* I regions are sharply divided, the *H* II region extending to a certain

TABLE 6

Atom or Ion	T_e	$\log (\mathfrak{N}_1''\mathfrak{N}_e/\mathfrak{N}_1')$	Correction Factor to Equation (29)
Na I	10,000°	1.73	500
	1000	0.92	1000
	100	0.22	1600
K I	10,000	2.38	200
	1000	1.50	500
	100	0.77	900
Ca I	10,000	4.29	2.6
	1000	3.41	6
	100	2.68	10
Ca II	10,000	0.44	200
Cutoff at 911 A	1000	9.79−10	300
(*H* I regions)	100	9.18−10	400
Ca II	10,000	0.72	100
No cutoff at 911 A	1000	0.07	160
(*H* II regions)	100	9.46−10	200

TABLE 7

Spectral Class	Adopted Temperature*	Adopted Visual Absolute Magnitude†	s_0(psc.) $\times \mathfrak{N}_H^{2/3}$	Spectral Class	Adopted Temperature*	Adopted Visual Absolute Magnitude†	s_0(psc.) $\times \mathfrak{N}_H^{2/3}$
O5	79,000°	−4^{m}2	140	B1	23,000°	−2.5	17
O6	63,000	−4.1	110	B2	20,000	−1.8	11
O7	50,000	−4.0	87	B3	18,600	−1.2	7.2
O8	40,000	−3.9	66	B4	17,000	−1.0	5.2
O9	32,000	−3.6	46	B5	15,500	−0.8	3.7
B0	25,000	−3.1	26	A0	10,700	+0.9	0.5

* G. P. Kuiper, *Ap. J.*, **88**, 429, 1938.

† R. Trumpler, *Lick Obs. Bull.*, No. 402, 1930.

distance, s_0, from the star, s_0 being a function of the effective temperature and radius of the star and of the density of the interstellar hydrogen gas. The results are summarized in Table 7 (cf. Strömgren, *op. cit.*, p. 533), giving the radius s_0 of the *H* II region around a star as a function of the spectral class of the star, and the number $\mathfrak{N}_H$ of interstellar hydrogen atoms or ions per cubic centimeter.

The various approximations made in the derivation of the above values have been indicated in the investigation just mentioned. It was not deemed necessary to improve the accuracy for the purposes of the present investigation or to change, at present, the adopted temperatures and absolute magnitudes.

When the spatial distribution of the interstellar hydrogen gas is nonuniform, the problem becomes more complicated. In principle, the extent of *H* I and *H* II regions corresponding to a given distribution of ionizing stars and a given density distribution of interstellar hydrogen can be worked out. Our knowledge of the hydrogen density distribution is, however, still so incomplete that it would not seem justified, at present, to attempt any very accurate calculations regarding the extent of these regions. In this section we shall treat a few simplified cases that seem to be of interest, with a view to the general picture of the spatial distribution of the interstellar gas discussed in Section I.

We shall consider, first, the ionization of a hydrogen cloud by a neighboring star situated at a distance large compared to the dimensions of the cloud, assuming the density of interstellar hydrogen between the cloud and the ionizing star to be so small that the absorption of the ionizing radiation along the path from the star to the cloud can be neglected. This case can be treated according to a method previously developed.[27]

Let a star of radius R and effective temperature T be situated at a distance r from an interstellar hydrogen cloud of density $\mathfrak{N}_H$ hydrogen atoms or ions per cubic centimeter. We assume r to be large compared to the dimensions of the cloud. The dilution factor of the radiation from the star as seen from the cloud is

$$w = \frac{R^2}{4r^2}. \tag{49}$$

The degree of ionization, x, of hydrogen at a point inside the cloud at which the reduction of the ionizing radiation by the absorption in the cloud is $e^{-\tau_u}$, is given by

$$\frac{x^2}{1-x}\mathfrak{N}_H = \frac{(2\pi m_e)^{3/2}}{h^3}(kT)^{3/2}e^{-I_H/kT}w\,e^{-\tau_u} = C\,e^{-\tau_u}. \tag{50}$$

Denoting the effective absorption coefficient of the ionizing radiation per neutral hydrogen atom by a_u, the expression for the optical depth, τ_u, is

$$\tau_u = \int a_u \mathfrak{N}_H\, ds\ , \tag{51}$$

where the integral is extended along the path of the line of sight from the star through the cloud for the point considered. From the discussion quoted above, it follows that the *H* II region extends to the point S_0 on the path for which (cf. eq. [50])

$$\int_0^{S_0} \mathfrak{N}_H^2\, ds = \frac{C}{a_u}. \tag{52}$$

Assuming $\mathfrak{N}_H$ to be constant along the path, we find

$$S_0 = \frac{C}{a_u \mathfrak{N}_H^2}. \tag{53}$$

Comparing this with the expression[12] for the radius s_0 of the *H* II regions in a uniform medium surrounding a star of the same temperature and radius, we find

$$S_0 = \frac{1}{3}\frac{s_0^3}{r^2}, \tag{54}$$

where again r is the distance from the cloud to the star, assumed large compared to S_0, the distance of penetration of the ionizing radiation into the cloud. Table 8 gives S_0 as calculated from equation (54), using the values of s_0 given in Table 7.

[27] G. P. Kuiper, O. Struve, and B. Strömgren. *Ap. J.*, **86**, 570, 1937, Sec. III.

Let us consider an O5 star at a distance of 100 parsecs from a cloud of density $\mathfrak{N}_H = 10$ hydrogen atoms and ions per cubic centimeter. From Table 8 we find that the ionizing radiation penetrates to a distance of $S_0 = 0.9$ parsecs into the cloud, producing an *H* II region of corresponding extent. A clustering of n O5 stars would give $S_0 = n \times 0.9$ parsecs. For a B2 star at 100 parsecs, the penetration for $\mathfrak{N}_H = 10$ is 4×10^{-4} parsecs, and even for the distance 10 parsecs, S_0 is only 0.04 parsecs.

Next, we shall consider the ionization by the general galactic radiation. Let us assume for a moment that the general galactic radiation in the wave-length region beyond the Lyman limit is not appreciably reduced by the hydrogen gas surrounding the cloud considered, or by other clouds. Adopting, as before, Dunham's values of the intensity of the galactic radiation (not reduced for interstellar particle absorption, we find that the galactic radiation in the wave-length region beyond 911 A corresponds to one star of temperature $T = 25{,}000°$ and dilution factor $w = 2 \times 10^{-17}$. We have to allow for the fact that the radiation ionizing the cloud considered comes from one hemisphere only and also for the fact that the incident radiation is not normal to the surface of the cloud. This is done, roughly, by reducing the dilution factor by a factor of 3. Using the method already described, we find that this ionizing radiation produces an *H* II rim of a thickness of about 6 parsecs $\times \mathfrak{N}_H^{-2}$, where again $\mathfrak{N}_H$ is the hydrogen density of the cloud.

TABLE 8*

Ionizing Star	$S_0 r^2 \mathfrak{N}_H^2$	Ionizing Star	$S_0 r^2 \mathfrak{N}_H^2$	Ionizing Star	$S_0 r^2 \mathfrak{N}_H^2$	Ionizing Star	$S_0 r^2 \mathfrak{N}_H^2$
O5	$9 \cdot 10^5$	O8	$1 \cdot 10^5$	B1	$2 \cdot 10^3$	B4	50
O6	$5 \cdot 10^5$	O9	$3 \cdot 10^4$	B2	$4 \cdot 10^2$	B5	20
O7	$2 \cdot 10^5$	B0	$6 \cdot 10^3$	B3	$1 \cdot 10^2$	A0	0.04

* r is measured in parsecs.

Now in interstellar space the general galactic radiation in the wave-length region beyond the Lyman limit is certainly appreciably reduced by the surrounding hydrogen clouds, and possibly also by the hydrogen between the clouds. We shall discuss this question in the later sections. A very rough estimate, based on the results obtained there, leads to a thickness of the ionized rim produced by the general galactic radiation equal to 1 parsec $\times \mathfrak{N}_H^{-2}$.

The extent of the *H* II region produced by a star inside the cloud considered can be found with the help of Table 7. The radius will be s_0. Thus it is seen, for example, that an O5 star located at the center of a cloud will just ionize the entire cloud if the radius of the cloud multiplied by $\mathfrak{N}_H^{2/3}$ is 140 parsecs. If the radius of the cloud is 5 parsecs (cf. Sec. I), then the limiting density from complete ionization is $\mathfrak{N}_H = 150$. For a B0 star we similarly find $\mathfrak{N}_H = 12$.[28]

In *H* II regions the free electrons and the protons will recombine and give rise to emission of a corresponding line spectrum. The strength of any emission line, say *Hα*, will be proportional to the product $\mathfrak{N}_H \mathfrak{N}_e$, or $\mathfrak{N}_H^2$, since $\mathfrak{N}_e$ is practically equal to $\mathfrak{N}_H$ in *H* II regions. The relation between $\mathfrak{N}_H$ and the intensity of the Balmer lines has been discussed in a number of investigations.[29] In an investigation[12] relating to the extended interstellar emission regions in Cygnus and Cepheus, discovered by Struve and Elvey,[13] it was found that the observed intensity of interstellar *Hα* emission corresponded to $\mathfrak{N}_H = 4$ for an assumed path of 300 parsecs through the emission region. Later observa-

[28] For an application of this kind of argument to the Orion nebula cf. J. L. Greenstein, *Ap. J.*, **104**, 414, 1946.

[29] Cf. Strömgren, *op. cit.*, and the work of Cillié, and of Menzel and Baker quoted there.

tions by Struve and Elvey[30] have indicated that the intensities of the faintest interstellar hydrogen emissions observed are about six times fainter than the intensities upon which the calculations mentioned were based. The corresponding value of $\mathfrak{N}_H$ is 1.7 hydrogen ions per cubic centimeter for the emission path of 300 parsecs.

The intensity of interstellar $H\alpha$ (or $H\beta$) emission in the direction of any H II region is proportional to the product of $\mathfrak{N}_H^2$ and the length of the path along the line of sight through the H II region. We shall call the product of $\mathfrak{N}_H^2$ and the length of the emission path in parsecs the *emission measure* of the interstellar emission lines in question. We see that the faint emission regions in Cygnus and Cepheus have an emission measure of about 1000.

From the foregoing calculations of the extent of the H II regions produced in interstellar hydrogen clouds by the general galactic radiation or by a neighboring star, we can immediately deduce the corresponding emission measure. Let us consider, first, the ionized rims produced by the general galactic radiation. The emission path is 2×1 parsec $\times \mathfrak{N}_H^2$ multiplied by a factor equal to about 1.5, to allow for the average lengthening of the path through the rim due to the angle between the line of sight and the

TABLE 9

Star, at Distance r Parsecs	Emission Measure $\times r^2$	Distance in Parsecs for an Emission Measure Equal to 1000	Star, at Distance r Parsecs	Emission Measure $\times r^2$	Distance in Parsecs for an Emission Measure Equal to 1000
O5	$9 \cdot 10^5$	30	B1	$2 \cdot 10^3$	.....
O6	$5 \cdot 10^5$	21	B2	$4 \cdot 10^2$	.....
O7	$2 \cdot 10^5$	15	B3	100	.....
O8	$1 \cdot 10^5$	10	B4	50	.....
O9	$3 \cdot 10^4$	6	B5	20	.....
B0	$6 \cdot 10^3$	2.4	A0	0.04	.....

normal to the rim surface. The emission measure is thus seen to be about 3. This is so much smaller than the emission measure for the faintest observed interstellar hydrogen emissions, i.e., 1000, that we can conclude that the emission in question is unobservable.

Next, we consider the emission measure of the H II region produced in a hydrogen cloud by a neighboring star. In Table 9 are given the values of the emission measure derived from the extent of the H II region found in Table 8. No correction for skewness of the ray to the ionized star, or to the observer, has been applied.

Table 9 also gives the particular distance of the neighboring star which produces an emission with an emission measure of 1000. It was assumed in the calculations that the dimensions and density of the cloud are large enough to give this emission measure when the cloud is completely ionized. No values are given for stars beyond B1, since in these cases the distances become so small that they can no longer be considered large compared to the dimensions of the H II region, even for dense clouds. In the case of a clustering of n stars, the distances are $\sqrt{n}$ times as large. We see that O stars, even at considerable distances, and clusterings of, say, ten O stars at distances up to 100 parsecs produce observable emission.

Finally, we consider the emission measures of H II regions produced by a star involved in the cloud. Table 10, computed from the data given in Table 7, illustrates this case. It gives the emission measure, as well as that particular hydrogen density of the cloud which corresponds to the emission measure 1000 (assuming that the emission measure

[30] *Ap. J.*, **89**, 517, 1939.

of the completely ionized cloud exceeds 1000). It appears from the table that O stars involved in a cloud will always produce an observable emission, if $\mathfrak{N}_H$ is about 10 or more (and if the condition mentioned above regarding the cloud is fulfilled). For B stars, higher hydrogen densities are required, and the extent of the emission regions will be quite small. It should be emphasized in this connection that by "observable" we mean observable with the help of the nebular spectrograph technique.[13] The emissions are much fainter than those observed as nebulosities in ordinary direct photographs.

Having considered the influence of a neighboring star on the hydrogen ionization and hydrogen emission of a cloud, and also the influence of a star involved in a cloud, we shall now discuss the effects of clusterings of O stars on the surrounding clouds. In other words, we shall discuss the case of more extended *H* II regions containing several ionized clouds.

Let us consider, first, two specific examples. Let a clustering of ten O7 stars be involved in a medium of uniform density $\mathfrak{N}_H$.[12] The radius of the *H* II region produced by the clustering is $87 \times (10)^{1/3}\mathfrak{N}_H^{-2/3} = 190\,\mathfrak{N}_H^{-2/3}$ parsecs. The emission measure for a line of sight passing through the center of the region is $380\,\mathfrak{N}_H^{4/3}$. Thus $\mathfrak{N}_H = 2$ gives the emission measure 1000. The corresponding diameter of the *H* II region is about 250 parsecs.

TABLE 10

Star	Emission Measure $\times\,\mathfrak{N}_H^{-4/3}$	Value of $\mathfrak{N}_H$ Corresponding to Emission Measure 1000	Star	Emission Measure $\times\,\mathfrak{N}_H^{-4/3}$	Value of $\mathfrak{N}_H$ Corresponding to Emission Measure 1000
O5	280	3	B1	30	13
O6	220	3	B2	20	18
O7	170	4	B3	14	24
O8	130	5	B4	10	32
O9	90	6	B5	7	39
B0	50	9	A0	1	180

Now consider the case that the same clustering is surrounded by hydrogen clouds of radius 5 parsecs that occupy a fraction α equal to 0.05, or 5 per cent of space, the average number of clouds intercepted by a line being 7 per 1000 parsecs (cf. Sec. I). Let us assume that $\mathfrak{N}_H$ in between the clouds is negligible (cf. Sec. VI) and that in the clouds it is 10 (cf. Sec. VII). The large-scale average density is then $\rho = \alpha\mathfrak{N}_H = 0.5$. With the help of Table 8 we find that the ionizing radiation from the clustering of ten O7 stars just completely penetrates and ionizes a cloud when the distance of the cloud from the clustering is less than about 50 parsecs. For greater distances the ionization is incomplete, and the ionizing radiation does not penetrate farther. Now the average distance at which a line from the clustering hits a cloud will be somewhat over 100 parsecs. Thus the clustering considered produces an *H* II region 200–300 parsecs in diameter. The emission measure of a completely ionized cloud within this region is 1000; for a cloud at the distance 100 parsecs it is 200. Since a line of sight passing approximately centrally through the region will, on the average, intercept somewhat less than two clouds (seven clouds per 1000 parsecs), we conclude that the *H* II region in question will appear in emission with an intensity that is just observable. The average emission measure for a line of sight passing approximately centrally will be a little over 1000. The emission regions will mostly overlap, giving a roughly coherent, though somewhat patchy, emission region of a diameter of 200–300 parsecs.

The theoretical picture thus derived is seen to correspond approximately to that for the case of a uniform medium of density $\mathfrak{N}_H = 2$. Both correspond roughly to the observed interstellar hydrogen emission regions in Cygnus and Cepheus.[12] We note that

a large-scale average density four times smaller is sufficient in the case of the clouds to produce approximately the same effect as a uniform medium.

If the density of the clouds is assumed to be considerably smaller than $\mathfrak{N}_H = 10$, the situation becomes somewhat simpler from the theoretical point of view. The clouds will then be completely ionized up to distances from the clustering of O stars that are so large that a line from the clustering of ionizing stars to the limit of the ionized regions will, on the average, intercept several clouds instead of one or two in the case just considered. Conditions then become more similar to those of a clustering of ionizing stars surrounded by a uniform medium. In fact, we can now imagine each cloud being spread out over a region approximately the size of the distance between neighboring stars without greatly modifying the dilution factors of the ionizing radiations involved. In this case the average effect of the clouds in reducing the ionizing radiation is given approximately by $\mathfrak{N}_H^2 a$, where a is the fraction of space occupied by the clouds.[12] Consequently, the radius s_0 of the ionized region will be equal to that calculated for a uniform medium of density $\mathfrak{N}_H^{(u)} = a^{1/2}\mathfrak{N}_H$. As the large-scale average space density of the matter in the clouds is $\rho = a\mathfrak{N}_H$, this can also be written as $\mathfrak{N}_H^{(u)} = a^{-1/2}\rho$. Since in the case of a uniform medium (cf. p. 258) s_0 is proportional to $(\mathfrak{N}_H^{(u)})^{-2/3}$, it follows that s_0 in the case considered is proportional to $a^{1/3}\rho^{-2/3}$. Comparing the case of clouds occupying the fraction a of space and having large-scale average density ρ, with the case of a uniform medium of the density $\rho^{(u)} = \mathfrak{N}_H^{(u)}$, we see that the radius of the ionized region will be the same in the two cases, when $(\rho^{(u)})^{-2/3} = a^{1/3}\rho^{-2/3}$, or

$$\rho^{(u)} = a^{-1/2}\rho \ . \tag{55}$$

Thus we see that matter concentrated in clouds is more efficient in stopping the ionizing radiation than is matter uniformly distributed. For example, with $a = 0.05$ it is found that the large-scale average density in the case of the clouds is about 4.5 times smaller than for a uniform medium giving the same ionization radius s_0.

In the case just considered of an H II region large enough for a line passing centrally through the region to intercept several clouds, the emission measure is $\mathfrak{N}_H^2 \times 2as_0$. Since s_0 is proportional to $a^{-1/3}\mathfrak{N}_H^{-2/3}$, it follows that the emission measure is proportional to $a^{2/3}\mathfrak{N}_H^{4/3}$. Introducing again the large-scale average density, $\rho = a\mathfrak{N}_H$, we see that the emission measure is proportional to $a^{-2/3}\rho^{4/3}$. We thus get the same emission from the clouds as from a uniform medium with density $\rho^{(u)} = a^{-1/2}\rho$—in fact, the same relation that holds regarding the ionization radius. Thus a system of clouds characterized by a and ρ is equivalent to a uniform medium with density $\rho^{(u)} = a^{-1/2}\rho$ in regard to both the extent and the average intensity of the emission region.

Now comparing with the results obtained in the specific example of $a = 0.05$ and $\mathfrak{N}_H = 10$, we see that the relations derived above for the case of an H II region containing several clouds along their diameter hold here also to a good approximation.

From our discussion we derive the following approximate rule, holding for H II regions sufficiently extended for a line passing about centrally to intercept at least two clouds or, in other words, sufficiently extended in depth to appear as a more or less coherent emission region: A number of clouds, each of density $\mathfrak{N}_H$, occupying together the fraction a of space (thus having large-scale average density $\rho = a\mathfrak{N}_H$), when ionized by a clustering of O stars yields a hydrogen emission region, which with regard to both extent and intensity is equivalent to the hydrogen emission region produced by the same stars in a homogeneous medium of density equal to the geometric mean $(\mathfrak{N}_H\rho)^{1/2} = a^{1/2}\mathfrak{N}_H$ of the cloud density $\mathfrak{N}_H$ and the large-scale average density $\rho = a\mathfrak{N}_H$.

VI

According to the general picture of the interstellar gas (cf. Sec. I), we expect the density between the interstellar gas clouds to be considerably smaller than the density in

the clouds. Consider a column of unit cross-section between the observer and a typical star showing multiple interstellar lines. We presume that more absorbing atoms or ions in the column are present in clouds than between clouds. Since the clouds occupy, roughly, 5 per cent of the volume of the column, we expect the density of absorbing atoms in the clouds to be at least about twenty times higher than between the clouds.

This estimate is, of course, quite rough, and it is important to obtain further information regarding the gas between the clouds. Such information can be derived from Dunham's observations[31] on the interstellar lines of *Na* I and *Ca* II in two neighboring B stars—α Virginis and η Ursae Majoris.[32] The interstellar lines of *Na* I and *Ca* II are so faint here that it can be assumed that the line of sight from the observer to either of the stars does not pass through any interstellar cloud. The observed faint lines are therefore presumably produced by the gas between the clouds.

The possibility that the column between observer and star contains a small part of a cloud cannot, of course, be excluded. Assuming that the observed interstellar lines are wholly produced by absorbing atoms and ions between the clouds, we find a density which, with this possibility in view, is to be considered as an upper limit.

We consider, first, Dunham's observation regarding the interstellar *Na* I line 5890 A in α Virginis. Dunham finds an upper limit for the equivalent width $w^{(\lambda)}$ of this line. The line is so faint that the limiting value of $N/w^{(\lambda)}$ corresponding to the doublet ratio 2 may be assumed to be valid (cf. Table 12). The corresponding upper limit to the number N of *Na* I atoms in the column of unit cross-section between the observer and the star[31] is found to be 6×10^{10}.

In order to find the number of sodium atoms and ions which together correspond to the number of sodium atoms, it is necessary to compute the degree of ionization of sodium and hence to know the number $\mathfrak{N}_e$ of free electrons per cubic centimeter (cf. eq. [43]). This raises the question of whether the column between α Virginis and the observer is an *H* I or an *H* II region.

Let us assume, first, that it is an *H* II region. In this case the number $\mathfrak{N}_e$ of free electrons per cubic centimeter is practically equal to $\mathfrak{N}_H$. Applying the equation of ionization (43) and using the values of the ionization function, $\mathfrak{N}_1''\mathfrak{N}_e/\mathfrak{N}_1'$ given in Table 6, we can find the product $\mathfrak{N}_e\mathfrak{N}_{Na} = \mathfrak{N}_H\mathfrak{N}_{Na}$, where $\mathfrak{N}_{Na}$ is the total number of sodium atoms and ions per cubic centimeter, when we know the number $\mathfrak{N}_1'$ of sodium atoms per cubic centimeter. The latter quantity is found from the number of absorbers in the column, $N = 6 \times 10^{10}$ (upper limit). Assuming the temperature of the *H* II region to be equal to 10,000°, we derive from this that $\mathfrak{N}_H\mathfrak{N}_{Na} = 2 \times 10^{-8}$ as an upper limit.

At this point it should be emphasized that the information which can be derived from the observed strength of an interstellar *Na* I line, or of any other atom or ion of similar ionization properties, is limited in the sense that the density of the element in question cannot be found unless the density of the element (or elements) that furnishes the free electrons is also known. In the present case this means that we cannot find $\mathfrak{N}_{Na}$ without knowing $\mathfrak{N}_H$, the quantity determined by the analysis based on the observations regarding line strength being $\mathfrak{N}_H\mathfrak{N}_{Na}$. This situation is quite general and the following remarks apply also to the cases discussed in Sections VII and VIII.

Ultimately, it will no doubt become possible to derive from observations of interstellar absorption and emission lines the abundances of a number of elements, including those that furnish the free electrons. We shall return to this problem in connection with the discussion of the observations of interstellar atomic and molecular lines in χ^2 Orionis (cf. also the investigations by Struve [33] and Dunham[9]).

[31] *Pub. A.A.S.*, **10**, 50, 1941.

[32] The author is much indebted to Dr. W. W. Morgan for putting at his disposal his unpublished results regarding the distances of a number of B stars of importance in the present discussion.

[33] *Proc. Nat. Acad. Sci.*, **25**, 36, 1939.

For the present it would seem appropriate to base further discussion on an assumed value of the abundance ratio of the element absorbing the interstellar line (*Na*) and the element furnishing the free electrons (*H*). As we shall see, only the square root (in one case even the cube root) of this assumed value enters into the discussion, so that the resulting range of uncertainty of the results derived is not too great.

Accordingly, we write

$$\mathfrak{N}_H = (\mathfrak{N}_H \mathfrak{N}_{Na})^{1/2} \left(\frac{\mathfrak{N}_H}{\mathfrak{N}_{Na}}\right)^{1/2} \tag{56}$$

and

$$\mathfrak{N}_{Na} = (\mathfrak{N}_H \mathfrak{N}_{Na})^{1/2} \left(\frac{\mathfrak{N}_H}{\mathfrak{N}_{Na}}\right)^{-1/2} \tag{57}$$

and derive the densities $\mathfrak{N}_H$ and $\mathfrak{N}_{Na}$ of hydrogen and sodium from the observed value of $\mathfrak{N}_H \mathfrak{N}_{Na}$ and (the square root of) an assumed value of the abundance ratio $\mathfrak{N}_H/\mathfrak{N}_{Na}$.

In the present case the observed value of $\mathfrak{N}_H \mathfrak{N}_{Na} = 2 \times 10^{-8}$ (upper limit) leads to Table 11, giving the relation between $\mathfrak{N}_H$, $\mathfrak{N}_{Na}$, and $\mathfrak{N}_H/\mathfrak{N}_{Na}$.

TABLE 11

$\mathfrak{N}_H$	$\mathfrak{N}_{Na}$ (Upper Limit)	$\mathfrak{N}_H/\mathfrak{N}_{Na}$ (Lower Limit)
1	2×10^{-8}	5×10^{7}
0.1	2×10^{-7}	5×10^{5}
0.01	2×10^{-6}	5×10^{3}

The assumed value of the abundance ratio $\mathfrak{N}_H/\mathfrak{N}_{Na}$ is chosen with a view to the results of the relative abundance of the elements obtained for stellar interiors, stellar atmospheres, and planetary nebulae.[34] We shall assume here and in the following sections that $\mathfrak{N}_H/\mathfrak{N}_{Na} = 3 \times 10^5$. The uncertainty connected with the application of this value to interstellar space must, of course, be kept in mind.

The values of the hydrogen density and sodium density corresponding to this assumed value of $\mathfrak{N}_H/\mathfrak{N}_{Na}$, according to Table 11, are $\mathfrak{N}_H = 0.08$ (upper limit) and $\mathfrak{N}_{Na} = 3 \times 10^{-7}$ (upper limit).

A value of $\mathfrak{N}_H$ as high as 0.5 appears improbable, since it would correspond to $\mathfrak{N}_H/\mathfrak{N}_{Na} = 10^7$ (lower limit), much higher than the expected value. It is, however, not entirely out of the question in view of the possibility that the concentration of sodium in clouds might be much more pronounced than that of hydrogen.

We now have to consider the alternative hypothesis that the hydrogen in the column between α Virginis and the observer is not ionized by the general galactic radiation. In this case, however, we have to take into account the ionizing effect of α Virginis itself. From Table 7 we see that a sphere or radius $13\,\mathfrak{N}_H^{2/3}$ parsecs around α Virginis will be an *H* II region. Now even for the highest permissible value of $\mathfrak{N}_H$, about 4 (cf. the Oort limit obtained from dynamical consideration), this is still about 10 per cent of the column between the observer and α Virginis. Consequently, the contribution of the *H* II part of the column to the strength of the *Na* I line will certainly be considerably larger than that of the *H* I part, as $\mathfrak{N}_e$ in the *H* II part will be larger than $\mathfrak{N}_e$ in the *H* I part by a factor much higher than 10. We can therefore neglect the contribution of the *H* I part.

[34] M. Schwarzschild, *Ap. J.*, **104**, 203, 1946; A. Unsöld, *Zs. f. Ap.*, **21**, 22, 1941; L. H. Aller, *Ap. J.*, **104**, 347, 1946; B. Strömgren, *Festschrift für Elis Strömgren* (Copenhagen: E. Munksgaard, 1940), p. 218; L. H. Aller and D. H. Menzel, *Ap. J.*, **102**, 239, 1945.

Thus we find that the density $\mathfrak{N}_1'$ of sodium atoms in the H II part of the column is equal to the number of absorbing sodium atoms N in the column, divided by the length of the H II part, or $13 \times 3.08 \times 10^{18}\, \mathfrak{N}_H^{-2/3}$ cm. Again using $N = 6 \times 10^{10}$ (upper limit), we find $\mathfrak{N}_1 = 1.5 \times 10^{-9}\, \mathfrak{N}_H^{2/3}$ (upper limit).

With the help of the ionization function given in Table 6, we get $\mathfrak{N}_H \mathfrak{N}_{Na} = 8 \times 10^{-8}\, \mathfrak{N}_H^{2/3}$, or $\mathfrak{N}_{Na} = 8 \times 10^{-8}\, \mathfrak{N}_H^{-1/3}$. We can again construct a table giving the relation of $\mathfrak{N}_H$, $\mathfrak{N}_{Na}$, and $\mathfrak{N}_H/\mathfrak{N}_{Na}$ (cf. Table 11). The values obtained are listed in Table 12. Two points should be noted in connection with this table. For values of $\mathfrak{N}_H$ less than 0.12 the whole column is converted into an H II region by α Virginis, and a length of path equal to 50 parsecs has to be used instead of $4 \times 10^{19}\, \mathfrak{N}_H^{-2/3}$; hence the values are the same as for the case covered by Table 11. For $\mathfrak{N}_H = 1$ the maximum extension of the H II part of the column from α Virginis is 13 parsecs. Owing to the closeness of α Virginis, the ionization of sodium will then be somewhat enhanced. The ionization function $\mathfrak{N}_1'\mathfrak{N}_e/\mathfrak{N}_1'$ was increased by a factor of 2 to take account of this effect.

With an assumed value of $\mathfrak{N}_H/\mathfrak{N}_{Na}$ equal to 3×10^5 we get an upper limit of $\mathfrak{N}_H$ equal to 0.08 as before. It may be noted that the values of $\mathfrak{N}_H/\mathfrak{N}_{Na}$ for relatively high values of $\mathfrak{N}_H$ are not so extreme on the hypothesis covered by Table 12 as on that corresponding to Table 11.

TABLE 12

$\mathfrak{N}_H$	$\mathfrak{N}_{Na}$(Upper Limit)	$\mathfrak{N}_H/\mathfrak{N}_{Na}$ (Lower Limit)
1	1.6×10^{-7}	6×10^{6}
0.1	2×10^{-7}	5×10^{5}
0.01	2×10^{-6}	5×10^{3}

The observations by Dunham regarding the interstellar K line of *Ca* II in α Virginis can be discussed in quite a similar manner. There is an additional uncertainty here, however, connected with the possibility of a deviation of the relevant abundance ratio of sodium and calcium from that in stellar atmospheres (cf. Sec. VII). Making two extreme hypotheses regarding the *Ca*/*Na* ratio, we obtain values for the upper limit of $\mathfrak{N}_H$ equal to 0.07 and 0.5, respectively.

Dunham's observations of extremely weak interstellar lines in the neighboring B star, η Ursae Majoris, can be utilized as those for α Virginis. Quite similar results are obtained.

Finally, we shall analyze the observations[35] of the interstellar D1 and D2 lines of *Na* I in ι Orionis by the same method, with a view to obtaining an upper limit to the density of interstellar hydrogen between the clouds. This particular O8 star has weak interstellar lines. Although it seems certain that there is at least one cloud between the observer and ι Orionis,[1] it still would appear possible to get a useful upper limit to the contribution of the medium between the clouds to the total line strength and hence a good upper limit to the product of the sodium and hydrogen densities between the clouds.

The observed equivalent widths of D2 and D1 for ι Orionis are 0.14 A and 0.07 A, respectively. The corresponding number of absorbing sodium atoms is found to be $N = 7 \times 10^{11}$. This is an upper limit to the number of absorbing atoms outside clouds in the column between the observer and the star. Proceeding as in the case of α Virginis, we get, on the hypothesis that the column is an H II region (length 300 parsecs), an upper limit $\mathfrak{N}_H = 0.11$ (corresponding to $\mathfrak{N}_H/\mathfrak{N}_{Na} = 3 \times 10^5$), while the

[35] P. W. Merrill, R. F. Sanford, O. C. Wilson, and Cora G. Burwell, *Ap. J.*, **86**, 274, 1937.

hypothesis that the only *H* II region in the column is that produced by ι Orionis itself leads to practically the same upper limit, $\mathfrak{N}_H = 0.12$. In the former case, $\mathfrak{N}_H = 1$ would correspond to $\mathfrak{N}_H/\mathfrak{N}_{Na} = 2.5 \times 10^7$ (lower limit), in the latter to $\mathfrak{N}_H/\mathfrak{N}_{Na} = 5 \times 10^6$ (lower limit).

The possibility that the *H* II part of the column between ι Orionis and the observer might be seriously reduced through the absorption of the ionizing radiation by a cloud across the column, relatively close to the star, can be ruled out through consideration of the sodium line absorption in the *H* II region of the cloud that would then be produced by the star (cf. Secs. V and esp. IX). In fact, if a cloud between the observer and the star were closer to the star than about 150 parsecs, the *Na* I absorption in the *H* II region produced in the cloud by the star would be stronger than the observed interstellar line absorption.

We conclude that a relatively reliable upper limit to the density of the interstellar gas between the clouds can be derived, namely, $\mathfrak{N}_H$ about 0.1. The possibility cannot be entirely ruled out, however, that the hydrogen density between the clouds is considerably higher, while the sodium density here is extremely low (sodium being much more strongly concentrated in clouds than hydrogen is). With a view to this possibility, it would appear desirable to attempt a determination of the hydrogen density between the clouds with the help of observations of the interstellar hydrogen emission lines (cf. Sec. V).

With regard to the sodium density between the clouds, the assumed value of the ratio $\mathfrak{N}_H/\mathfrak{N}_{Na} = 3 \times 10^5$ gives an upper limit equal to 1.5×10^{-7} (cf. Tables 11 and 12). (Even the improbably low value $\mathfrak{N}_H/\mathfrak{N}_{Na} = 5 \times 10^3$ only raises the upper limit of $\mathfrak{N}_{Na}$ to 2×10^{-6}.) In the following section we shall see that the most probable sodium density in the average clouds is about 4×10^{-5}. We may thus conclude that sodium is quite strongly concentrated in the clouds—in fact, so strongly that the total mass of sodium present in the clouds ($a = 0.05$) is probably considerably larger than the total mass of sodium between the clouds.

VII

The doublet ratio method of analysis of the total line strengths of interstellar D2 and D1, or K and H, lines is most suitable when the lines are weak or of intermediate strength, i.e., for distances of the stars in which the interstellar lines are observed up to, say, 500 parsecs. We shall make use of the available observation[35, 36] to investigate the properties of the average interstellar gas cloud within 500 parsecs. No attempt will be made in this section to analyze the properties of single clouds.

Wilson and Merrill,[8] using the doublet ratio method, derived a sodium density of 3×10^{-9} absorbing atoms per cubic centimeter, assuming the space density to be uniform. Their result applies to the case considered here of the region within 500 parsecs.

From seven stars nearer than 500 parsecs we find (cf. Table 2, p. 248), using the observations of Merrill, Sanford, Wilson, and Burwell[35] on the equivalent widths of the D2 and D1 lines and distances of the star according to Morgan, that the density of absorbing neutral sodium atoms is 2×10^{-9} per cubic centimeter, assuming uniform density. The accuracy of this value appears sufficient for the present purpose.

Assuming, now, that the clouds occupy, on the average, the fraction $a = 0.05$ of the space concerned (cf. Sec. I), we get a density of neutral sodium atoms in the clouds equal to 4×10^{-8}.

We now proceed as in Section VI. We treat as a separate hypothesis the cases that the average cloud is an *H* II region, and an *H* I region. In the case of *H* II regions we take the kinetic electron temperature to be $T_e = 10{,}000°$.

Spitzer[37] has shown that the temperature of *H* I regions, assumed to contain inter-

[36] R. F. Sanford and O. C. Wilson, *Ap. J.*, **90**, 235, 1939.

[37] *A.J.*, **52**, 130, 1947 (abstract).

stellar solid particles, is probably quite low because of the loss of gas energy by inelastic collisions between the hydrogen atoms and the solid particles.

Collisions between clouds may contribute to raising the average kinetic temperature of the clouds somewhat above the temperature of undisturbed clouds. The data necessary for predicting an average temperature are rather uncertain, however. We shall carry out our calculations for *H* I regions for values of T equal to 100° and 1000° and also for 10,000°, in order to be able to judge the effects of the low temperature.

Using the values of the ionization function $\mathfrak{N}_1''\mathfrak{N}_e/\mathfrak{N}_1'$ given in Table 6, we arrive at the values given in Table 13, which is analogous to Tables 11 and 12. In the case of *H* II regions $\mathfrak{N}_e = \mathfrak{N}_H$ as before. In *H* I regions the free electron density is probably very nearly equal to the sum of the densities of carbon, magnesium, silicon, and iron. The expected value of the ratio $\mathfrak{N}_e/\mathfrak{N}_{Na}$ according to the data on stellar atmos-

TABLE 13

HYPOTHESIS *H* II, $T_e = 10{,}000°$

$\mathfrak{N}_H$	$\mathfrak{N}_{Na}$	$\mathfrak{N}_H/\mathfrak{N}_{Na}$
10	2×10^{-7}	5×10^{7}
1	2×10^{-6}	5×10^{5}
0.1	2×10^{-5}	5×10^{3}

$\mathfrak{N}_H/\mathfrak{N}_{Na} = 3\times10^{5}$ gives $\mathfrak{N}_H = 0.8$
$\mathfrak{N}_{Na} = 3\times10^{-6}$

HYPOTHESIS *H* I, $T_e = 10{,}000°$

$\mathfrak{N}_H$	$\mathfrak{N}_e$	$\mathfrak{N}_{Na}$	$\mathfrak{N}_e/\mathfrak{N}_{Na}$
150	0.1	2×10^{-5}	5000
15	0.01	2×10^{-4}	50
1.5	0.001	2×10^{-3}	0.5

$\mathfrak{N}_e/\mathfrak{N}_{Na} = 200$ gives $\mathfrak{N}_H = 30$
$\mathfrak{N}_e = 0.02$, $\mathfrak{N}_{Na} = 1\times10^{-4}$

HYPOTHESIS *H* I, $T_e = 1000°$

$\mathfrak{N}_H$	$\mathfrak{N}_e$	$\mathfrak{N}_{Na}$	$\mathfrak{N}_e/\mathfrak{N}_{Na}$
150	0.1	3×10^{-6}	3×10^{4}
15	0.01	3×10^{-5}	300
1.5	0.001	3×10^{-4}	3

$\mathfrak{N}_e/\mathfrak{N}_{Na} = 200$ gives $\mathfrak{N}_H = 12$
$\mathfrak{N}_e = 0.008$, $\mathfrak{N}_{Na} = 4\times10^{-5}$

HYPOTHESIS *H* I, $T_e = 100°$

$\mathfrak{N}_H$	$\mathfrak{N}_e$	$\mathfrak{N}_{Na}$	$\mathfrak{N}_e/\mathfrak{N}_{Na}$
150	0.1	7×10^{-7}	1.5×10^{5}
15	0.01	7×10^{-6}	1500
1.5	0.001	7×10^{-5}	15

$\mathfrak{N}_e/\mathfrak{N}_{Na} = 200$ gives $\mathfrak{N}_H = 5$
$\mathfrak{N}_e = 0.004$, $\mathfrak{N}_{Na} = 2\times10^{-5}$

pheres and planetary nebulae (cf. p. 265) is about 200. In this case, also, the value of $\mathfrak{N}_H$ is given in accordance with the expected ratio $\mathfrak{N}_H/\mathfrak{N}_{Na} = 3 \times 10^5$, for the sake of comparison with other results, although for *H* I regions the hydrogen density is irrelevant to the present analysis.

It is apparent that hypothesis *H* II leads to a much lower cloud density than does hypothesis *H* I. That this must be so is immediately clear, in view of the much greater electron density for equal gas density in *H* II regions as compared to *H* I regions. This again means relatively less ionization of sodium. Consequently, a much lower density of the cloud will produce *Na* I lines of a given strength.

We now have to discuss the question of whether the *H* II hypothesis or the *H* I hypothesis leads to the most plausible result. The hydrogen density derived on the hypothesis that the clouds are *H* II region is quite low, $\mathfrak{N}_H = 0.8$. The corresponding large-scale average density $\rho = a\mathfrak{N}_H$ is only 0.04, and the geometric mean of $\mathfrak{N}_H$ and ρ is about 0.2. These values are about ten times lower than those derived from the extent and intensity of the hydrogen emission regions (cf. Sec. V).

On the other hand, the *H* I hypothesis, with T_e intermediate between 100° and 1000°, leads to a density $\mathfrak{N}_H$ about equal to 10, with $\rho = 0.5$, and $(\mathfrak{N}_H\rho)^{1/2} = 2$. This checks very well with the result derived from the hydrogen emission lines.

Thus it appears that the hypothesis that the average gas clouds within 500 parsecs are *H* I regions is to be preferred. In fact, speaking quite generally, it seems very difficult to reconcile the *H* II hypothesis with the existence of emission regions of diameter and intensity as observed.

Combining the densities found on the *H* I hypothesis with the known space densities of O and B stars, we find that most of the interstellar hydrogen near the galactic plane within, say, 500 or 1000 parsecs is un-ionized, so that the hypothesis is self-consistent.

It may be noticed that the result obtained depends essentially on the inclusion of the correction factor to the equation of ionization (cf. Sec. IV). In fact, omitting this factor, one would, according to the *H* I hypothesis, derive densities so high as to conflict seriously with the Oort limit, i.e., the *H* I hypothesis would appear ruled out.

Although the result that hydrogen in the average cloud is un-ionized appears to be relatively well established, it should be emphasized that the derivation involves various assumptions and uncertainties, which have been mentioned. Therefore, it would still seem very desirable to approach the problem of the density distribution and ionization of interstellar hydrogen with the help of more extensive and complete observations regarding the interstellar hydrogen emissions.

TABLE 14

HD	Name	l	b	Color Excess*	log $\mathfrak{N}_{Ca\,II}$	log $\mathfrak{N}_{Na\,I}$	log ($\mathfrak{N}_{Ca\,II}/\mathfrak{N}_{Na\,I}$)
37128....	ϵ Ori	173°	−16°	+0.02	12.1	12.2	−0.1
37490....	ω Ori	168	−13	+ .02	12.1	12.8	− .7
50896....		202	− 9	.....	12.2	12.6	− .4
57061....	τ CMa	206	− 4	− .02	12.1	12.1	.0
214167....	8 LacFt.	65	−17	− .04	12.1	12.3	− .2
214168....	8 LacBr.	65	−17	+ .05	12.2	12.4	− .2
214680....	10 Lac	65	−17	0.00	12.5	12.5	0.0

* J. Stebbins, C. M. Huffer, and A. E. Whitford, *Ap. J.*, **91**, 20, 1940.

We shall consider, next, the ratio of the abundances of calcium and sodium in the average cloud within about 500 parsecs. Merrill and Sanford[38] have derived a value of 3 for the ratio $\mathfrak{N}_{Ca\,II}/\mathfrak{N}_{Na\,I}$ while Wilson and Merrill estimated this ratio to be about 1.[39] For seven stars equivalent widths of the interstellar D2 and D1 lines,[35] as well as the interstellar K and H lines,[36] are available and suitable for analysis according to the doublet ratio method. Table 14 contains the stars and the values of N (the number of absorbing atoms) derived from the equivalent widths.

The average value of log ($\mathfrak{N}_{Ca\,II}/\mathfrak{N}_{Na\,I}$) is −0.23, corresponding to $\mathfrak{N}_{Ca\,II}/\mathfrak{N}_{Na\,I} = 0.6$. It should be noted that the value thus derived might be somewhat affected by selection effects. Very faint lines are not included in the observational material, and strong lines are excluded because they are saturated and therefore unsuitable for determinations of the number of absorbing atoms by the doublet ratio method. Still, the derived value is probably reasonably representative.

Again using the values of the ionization function given in Table 6, we find the corresponding ratio $\mathfrak{N}_{Ca}/\mathfrak{N}_{Na}$ to be 0.04, independent of the electron density $\mathfrak{N}_e$ and practically independent of the assumed electron temperature T_e.

The value $\mathfrak{N}_{Ca}/\mathfrak{N}_{Na}$ found for interstellar space is considerably smaller than the value, about 1.5, expected according to the abundance ratio of calcium and sodium found in stellar atmospheres. This discrepancy has long been realized. The introduction of the correction factors in the equation of ionization has reduced the discrepancy by a fac-

[38] *Ap. J.*, **87**, 118, 1938.

[39] O. C. Wilson, *Ap. J.*, **90**, 244, 1939.

tor of about 4, but it is still considerable. In this connection it should be noticed that some of the quantum-mechanical data upon which the determination of the correction factors was based are still somewhat uncertain. Furthermore, it is quite possible that considerable revision of the intensity of the ionizing radiation in the wave-length region 1000–2000 A is needed (cf. Sec. IV). This will affect the calculated degree of ionization of *Ca* II more than it will that of *Na* I. Finally, the adopted value of $\mathfrak{N}_{Ca\,II}/\mathfrak{N}_{Na\,I}$ might also be somewhat in error. Altogether, it is entirely possible that future work will reduce the discrepancy quite considerably. It appears very desirable to carry out this work in order to establish whether or not there is here a real discrepancy between stellar and (local) interstellar abundance ratios.

VIII

A number of interstellar absorption lines have been observed in the spectrum of χ^2 Orionis. Dunham[9] gives equivalent widths for the lines 5890, 5896, 3302, and 3303 of *Na* I, and for lines of *K* I, *Ca* I, *Ca* II, and *Ti* II. Equivalent widths for molecular lines, *CH* I, *CH* II, have also been observed by Dunham.[40]

From the observed equivalent widths of the four sodium lines, and the known oscillator strengths for these lines, Dunham constructed an empirical curve of growth for the interstellar lines in χ^2 Orionis.

We shall make use of the data for the sodium lines to determine the number of absorbing sodium atoms, N, and the Doppler constant, b, with the help of Table 2. The D2 and D1 lines are so strong here that the D2/D1 method fails, but the D1/3303 method can be used. The following result is obtained, namely, $N = 1.0 \times 10^{14}$ and $b = 4.8$ km/sec.

Comparing this with typical values corresponding to the distance of χ^2 Orionis (1200 parsecs), we see that the number of absorbing atoms is abnormally high (by a factor of about 10), while the Doppler constant is considerably lower (by a factor of about 2). This strongly suggests that the absorption in this case is by one cloud of abnormally high line-absorption power. Such an assumption is not contradicted by the observations made at high dispersion by Adams[1] and Dunham,[9] who observed single components of the interstellar lines in the spectrum of this star.

In analyzing the observational data for χ^2 Orionis, we shall, accordingly, assume a value of the length of the absorbing path smaller than that normally corresponding to the distance of the star ($a \times 1200$ parsecs = 60 parsecs). We shall put the length in question equal to 15 parsecs.

The analysis of the observed line strengths can now be carried out according to the methods already described. As in the case of the average clouds, we treat separately the hypotheses that the absorbing cloud is an *H* II region and that it is an *H* I region.

The lines of *K* I, *Ca* I, and *Ti* II are relatively faint and hence give the number of absorbing atoms without much uncertainty. Small corrections were applied with the aid of Table 2 to allow for the small effects of saturation still present. In determining these corrections, a Doppler constant equal to that found from the sodium lines was used. This means that the motions described by the Doppler constant are interpreted as large-scale internal motions within the cloud rather than as thermal motion.

The K line of *Ca* II is unfortunately so strong that it cannot be utilized for a reliable determination of the number of absorbing *Ca* II ions. A lower limit, only, to this number can be found.

The ionization functions given in Table 6 were used in the calculations. For the ionization of *K* II, which is of importance in hypothesis *H* II, the correction factor corresponding to recombinations to excited states is not yet known (cf. Sec. IV). It should

[40] *Pub. A.A.S.*, **10**, 123, 1941.

be noted that in the case of hypothesis *H* I there is no ionization of atoms or ions with ionization potentials greater than that of hydrogen, or 13.6 volts.

The results of the calculations are summarized in Table 15, which is analogous in its general arrangement to Table 13.

The case of the interstellar lines in the spectrum of χ^2 Orionis is characterized by the abnormal strength of *Na* I, as indicated by the nonsaturated lines 3303 and 3302 and the

TABLE 15

HYPOTHESIS *H* II, $T_e = 10{,}000°$

$\mathfrak{N}_H$	$\mathfrak{N}_{Na}$	$\mathfrak{N}_H/\mathfrak{N}_{Na}$	$\mathfrak{N}_{Ca}$	$\mathfrak{N}/\mathfrak{N}_{Ca}$	$\mathfrak{N}_K$	$\mathfrak{N}_{Ca}/\mathfrak{N}_{Na}$	$\mathfrak{N}_K/\mathfrak{N}_{Na}$
10....	1.1×10^{-5}	9×10^{5}	6×10^{-6}	2×10^{6}	4×10^{-6}/capt. corr. *K* II	0.5	0.4/capt. corr. *K* II
1....	1.1×10^{-4}	9×10^{3}	2×10^{-4}	4×10^{3}	4×10^{-4}/capt. corr. *K* II	2	4 /capt. corr. *K* II
0.1...	1.1×10^{-3}	90	2×10^{-2}	5	4×10^{-2}/capt. corr. *K* II	18	40/capt. corr. *K* II

HYPOTHESIS *H* I, $T_e = 10{,}000°$

$\mathfrak{N}_H$	$\mathfrak{N}_e$	$\mathfrak{N}_{Na}$	$\mathfrak{N}_e/\mathfrak{N}_{Na}$	$\mathfrak{N}_{Ca}$	$\mathfrak{N}_e/\mathfrak{N}_{Ca}$	$\mathfrak{N}_K$	$\mathfrak{N}_{Ti}$	$\mathfrak{N}_{Ca}/\mathfrak{N}_{Na}$	$\mathfrak{N}_K/\mathfrak{N}_{Na}$	$\mathfrak{N}_{Ti}/\mathfrak{N}_{Na}$
1500..	1	1.1×10^{-4}	9000	1.4×10^{-4}	7000	7×10^{-6}	5×10^{-6}	1.3	0.06	0.05
150..	0.1	1.1×10^{-3}	90	1.1×10^{-2}	9	7×10^{-5}	5×10^{-6}	10	.06	.005
15..	0.01	1.1×10^{-2}	9	1.0	0.01	7×10^{-4}	5×10^{-6}	100	0.06	0.0005

HYPOTHESIS *H* I, $T_e = 1000°$

$\mathfrak{N}_H$	$\mathfrak{N}_e$	$\mathfrak{N}_{Na}$	$\mathfrak{N}_e/\mathfrak{N}_{Na}$	$\mathfrak{N}_{Ca}$	$\mathfrak{N}_e/\mathfrak{N}_{Ca}$	$\mathfrak{N}_K$	$\mathfrak{N}_{Ti}$	$\mathfrak{N}_{Ca}/\mathfrak{N}_{Na}$	$\mathfrak{N}_K/\mathfrak{N}_{Na}$	$\mathfrak{N}_{Ti}/\mathfrak{N}_{Na}$
1500..	1	1.6×10^{-5}	6×10^{4}	8×10^{-6}	1.2×10^{5}	9×10^{-7}	5×10^{-6}	0.5	0.06	0.3
150..	0.1	1.6×10^{-4}	600	4×10^{-4}	300	9×10^{-6}	5×10^{-6}	2	.06	.03
15..	0.01	1.6×10^{-3}	6	3×10^{-2}	0.3	9×10^{-5}	5×10^{-6}	20	0.06	0.003

HYPOTHESIS *H* I, $T_e = 100°$

$\mathfrak{N}_H$	$\mathfrak{N}_e$	$\mathfrak{N}_{Na}$	$\mathfrak{N}_e/\mathfrak{N}_{Na}$	$\mathfrak{N}_{Ca}$	$\mathfrak{N}_e/\mathfrak{N}_{Ca}$	$\mathfrak{N}_K$	$\mathfrak{N}_{Ti}$	$\mathfrak{N}_{Ca}/\mathfrak{N}_{Na}$	$\mathfrak{N}_K/\mathfrak{N}_{Na}$	$\mathfrak{N}_{Ti}/\mathfrak{N}_{Na}$
1500..	1	3×10^{-6}	3×10^{5}	1×10^{-6}	1×10^{6}	2×10^{-7}	5×10^{-6}	0.3	0.05	1.6
150..	0.1	3×10^{-5}	3×10^{3}	2×10^{-5}	4×10^{3}	2×10^{-6}	5×10^{-6}	0.7	.05	.16
15..	0.01	3×10^{-4}	30	2×10^{-3}	7	2×10^{-5}	5×10^{-6}	5	0.05	0.016

appearance of the line 4226 of *Ca* I. In a general way we see from Table 15 (cf. the columns for *Na* I and *Ca* I) that this can be interpreted in either of two ways. It can be explained by assuming that the absorbing cloud is like the average clouds with respect to hydrogen ionization and hence relative electron density, i.e., is an *H* I region, but that it has an abnormally high density; or it can be explained on the assumption that the cloud differs from the average, being an *H* II region of, relatively, very high electron density, while the total density is about equal to that of a normal cloud.

The case of *Ti* II requires special comment. In deriving the number of absorbing ions from the equivalent widths of the lines 3383 and 3242 given by Dunham,[9] oscillator strengths $f = 0.0040$ and $f = 0.0029$, respectively, were used. These values of the

oscillator strengths were derived from Stekelenburg's[41] absolute measures of oscillator strengths of *Ti* II lines, and R. B. King's[42] relative measures.

The ionization potential of *Ti* I is 6.8 volts, so that *Ti* I is strongly ionized to *Ti* II in all cases considered. The ionization potential of *Ti* II is 13.6 volts, slightly larger than that of *H* I, which means that *Ti* II is not further ionized in *H* I regions, while in *H* II regions there is considerable reduction in the number of *Ti* II ions due to ionization to *Ti* III.

On hypothesis *H* II—i.e., if we explain the abnormal strength of the *Na* I and *Ca* I lines by high relative electron density with normal total density—we find that the contributions of the abnormal cloud considered to the strength of the *Ti* II lines is smaller than that of the average cloud. On this hypothesis, therefore, we have to attribute the *Ti* II absorption to the normal average clouds, which for a distance of 1200 parsecs would correspond to a path of $a \times 1200$ parsecs = 60 parsecs (cf. p. 270). This gives $\mathfrak{N}_{Ti} = 1.3 \times 10^{-6}$ for the average cloud, which is to be compared with $\mathfrak{N}_{Na} = 3 \times 10^{-5}$ for the average cloud (cf. Table 13), thus $\mathfrak{N}_{Ti}/\mathfrak{N}_{Na} = 0.04$ on hypothesis *H* II.

On hypothesis *H* I, the lines of *Ti* II, like others, are strengthened by the assumed high total density in the cloud. With regard to the calculation of the degree of ionization, this is the simplest case of all, the number of *Ti* II ions being practically equal to the total number of all titanium atoms and ions.

In the case of *Ca* I it may be noted that the value of the ratio $\mathfrak{N}_H/\mathfrak{N}_{Ca}$ varies as the third power of $\mathfrak{N}_H$ for small values of $\mathfrak{N}_H$. For higher values of $\mathfrak{N}_H$ the variation is somewhat less pronounced, because of the fact that the number of *Ca* II ions here is no longer small compared to the number of *Ca* III ions. The rapid variation of $\mathfrak{N}_H/\mathfrak{N}_{Ca}$ with $\mathfrak{N}_H$ renders the determination of $\mathfrak{N}_H$ relatively more certain.

Again it should be emphasized that the average density $\mathfrak{N}_H$ in the case of hypothesis *H* I is irrelevant to the cases considered, the quantity of importance being the density of the elements furnishing the free electrons. The hydrogen density corresponding to the assumed ratio $\mathfrak{N}_H/\mathfrak{N}_e = 1500$ (hypothesis *H* I) is given here also for the sake of comparison with other cases. The possibility of less pronounced concentration of hydrogen in clouds should be kept in mind.

As before, we derive the values of the quantities computed which correspond to certain assumed values of abundance ratios, namely, $\mathfrak{N}_H/\mathfrak{N}_{Na} = 3 \times 10^5$, $\mathfrak{N}_e/\mathfrak{N}_{Na} = 200$, $\mathfrak{N}_H/\mathfrak{N}_{Ca} = 2 \times 10^5$, $\mathfrak{N}_e/\mathfrak{N}_{Ca} = 150$. These values are given below in Table 16, separately for the hypotheses *H* II, $Te = 10{,}000°$, and *H* I, $T_e = 300°$.

From the data given in Table 16 it appears that the observed strengths of the interstellar lines in χ^2 Orionis can be explained about equally well on the hypothesis that the line absorption is in a cloud of about normal density—that is, an *H* II region—and on the hypothesis that the absorption takes place in an *H* I cloud of about six times the average density.

A definite choice between the two possibilities can hardly be made at the present time. The problem can, however, be approached in two different ways.

First, if the cloud is an *H* II region, we expect it to give rise to an emission region. The emission measure of the cloud itself is only about 400–500, but it is improbable that the hydrogen ionization, if at all present, is restricted to a single cloud (cf. Sec. V), no O star or O stars very close to the absorbing column in question being known. Therefore, a somewhat stronger emission would be expected if hypothesis *H* II is the correct one. Observations indicate that hydrogen emission around χ^2 Orionis, if present, is less than that corresponding to emission measure 1000.[43]

If χ^2 Orionis (spectral type B1) were imbedded in a cloud of somewhat above average density, it would produce an *H* II region of sufficient extent (cf. Table 7) to give rise to

[41] Dissertation, Utrecht, 1943.

[42] *Ap. J.*, **94**, 27, 1941.

[43] W. A. Hiltner and B. Strömgren (unpublished).

the observed interstellar absorption lines; but again observable hydrogen emission would be expected.

Quite generally, it is easily seen that any *H* II region with a number *N* of absorbing *Na* I atoms will give rise to a hydrogen emission region with an emission measure given by the equation,

$$\text{Ionization function} \times N = 3 \times 10^{18} \times \text{emission measure} \times \frac{\mathfrak{N}_{Na}}{\mathfrak{N}_H}$$

or (cf. Table 6)

$$\text{Emission measure} = 2 \times 10^{-17} \times \frac{\mathfrak{N}_H}{\mathfrak{N}_{Na}} \times N\,. \tag{58}$$

In our case $\mathfrak{N}_H/\mathfrak{N}_{Na} = 3 \times 10^5$ and $N = 1 \times 10^{14}$ give the emission measure 600.

TABLE 16

HYPOTHESIS *H* II, $T_e = 10{,}000°$

	$\mathfrak{N}_H$	$\mathfrak{N}_{Na}$	$\mathfrak{N}_{Ca}/\mathfrak{N}_{Na}$	$\mathfrak{N}_K/\mathfrak{N}_{Na}$
From *Na* I.	6	2×10^{-5}	0.6	0.7/capt. corr. *K* II
From *Ca* I.	4	3×10^{-5}	0.7	1 /capt. corr. *K* II

HYPOTHESIS *H* I, $T_e = 300°$

	$\mathfrak{N}_H$	$\mathfrak{N}_e$	$\mathfrak{N}_{Na}$	$\mathfrak{N}_{Ca}/\mathfrak{N}_{Na}$	$\mathfrak{N}_K/\mathfrak{N}_{Na}$	$\mathfrak{N}_{Ti}/\mathfrak{N}_{Na}$
From *Na* I.	60	0.04	2×10^{-4}	2	0.06	0.03
From *Ca* I.	70	0.05	2×10^{-4}	2	0.06	0.03

The possibility of future application of this equation for the determination of the ratio $\mathfrak{N}_H/\mathfrak{N}_{Na}$ from observations of the strength of sodium lines produced by line absorption in hydrogen emission regions may be noted in passing.

Second, information can be derived from the observed strength of the interstellar molecular absorption line 4300 of *CH*. The equivalent width of this line in χ^2 Orionis has been found by Dunham[31] to be equal to 0.014 A. The oscillator strength can be estimated from theoretical calculations to be about $f = 0.002$.[44] This gives $N = 4 \times 10^{13}$, and $\mathfrak{N}_{CH} = 1 \times 10^{-6}$. The complicated problem regarding the equilibrium of *C* II, *H*, *CH* I, and *CH* II in interstellar space has been considered by P. Swings,[45] and by H. A. Kramers and D. ter Haar.[46] The following equation, valid for an *H* I region with $T_e = 300°$, gives the relation between the densities of *C*, *H*, and *CH*, resulting from this discussion,[47] $\mathfrak{N}_{CH} = 2 \times 10^{-6}\,\mathfrak{N}_C\mathfrak{N}_H$.

The numerical factor in this equation is as yet rather uncertain. Assuming $\mathfrak{N}_H/\mathfrak{N}_C =$

[44] G. Herzberg, private communication. The author is much indebted to Dr. Herzberg for comments on the problems of interstellar molecules.

[45] *Ap. J.*, **95**, 270, 1942.

[46] *B.A.N.*, No. 371, 1946.

[47] The author is indebted to Dr. D. ter Haar for communicating, in advance of publication, his calculations on the molecular equilibrium at lower temperatures, made in connection with a discussion of the origin of the solar system.

3000, we find, with $\mathfrak{N}_{CH} = 1 \times 10^{-6}$, that $\mathfrak{N}_H = 40$. This result, although rather uncertain, tends to indicate the existence of an *H* I cloud of density considerably higher than the average in the path from the observer to χ^2 Orionis. This again points in the direction of the *H* I hypothesis as the most plausible.[48]

It should be emphasized that more accurate quantum-mechanical calculations of the oscillator strengths of the observed interstellar lines of *CH* I and *CH* II, and of the ionization and dissociation equilibrium of *CH* I and *CH* II in interstellar space are highly desirable. Ultimately, one may hope in this way to derive, in a direct way, interstellar densities of hydrogen, carbon, and free electrons.

IX

The discussion in the previous sections has led to a picture of interstellar clouds of an average density $\mathfrak{N}_H = 10$, the density in space between the clouds being much smaller, probably smaller than $\mathfrak{N}_H = 0.1$.

Normally, hydrogen in the clouds is un-ionized. Regions where hydrogen is ionized are known to exist. It is not yet known with certainty, however, whether or not hydrogen in these regions is largely concentrated in clouds of density equal to, say, $\mathfrak{N}_H = 10$. It is possible that the thermal velocities in such *H* II clouds make them dynamically unstable.[49] *H* II clouds of higher density, with $\mathfrak{N}_H$ from, say, 50 to 1000, are known to exist and are observable as diffuse emission-line nebulae.

The derived relative abundances in interstellar space are roughly similar to those found for the stars. Various causes of uncertainty concerning the abundances obtained have been pointed out in the discussion. It may be hoped that at least some of these will be removed in the near future. Profitable discussion of the question of systematic differences between the chemical constitution of the stars and the interstellar gas may then become possible.

The question of the relation between the interstellar gas and the interstellar particles was briefly touched in Section I. According to the investigations of D. ter Haar,[50] H. A. Kramers and D. ter Haar,[46] and J. H. Oort and H. van de Hulst,[2] it appears very probable that interstellar solid particles are formed from the interstellar gas and are destroyed through mutual collision, so that an equilibrium between gas and solid particles is reached.

If the picture of the properties of the interstellar gas arrived at here is generally correct, it would follow that interstellar solid particles are formed almost exclusively in the clouds. Before the particles are ultimately destroyed, they may, of course, spread to some extent over larger volumes. Still, a strong correlation between solid-particle absorption and interstellar line absorption is to be expected.

Although such a correlation exists, very striking exceptions are known.[51] Three

[48] We may note that, since the molecular line in χ^2 Orionis is very weak, a density somewhat less than the actual would make the line unobservable. Hence the appearance of an observable interstellar line 4300 of *CH* requires absorption in a cloud of density considerably above the average. This tends to explain that multiple 4300 lines, or 4300 lines strengthened through absorption in two or more clouds, are hardly ever observed. The occurrence of two exceptionally dense clouds in one line of sight will in itself be rare. Furthermore, the observed relation between molecular absorption and absorption by solid particles indicates that double or strengthened molecular lines would presumably be accompanied by an interstellar absorption of 2–3 mag., which would render high-dispersion observations of the stellar spectrum in question difficult.

[49] This point was emphasized by Dr. L. Spitzer in a private communication. The author is much indebted to Dr. Spitzer for comments on problems of interstellar matter.

[50] *B.A.N.*, No. 361, 1943; also *Ap. J.*, **100**, 288, 1944.

[51] J. L. Greenstein and O. Struve, *Ap. J.*, **90**, 625, 1939; W. W. Morgan, *Ap. J.*, **90**, 632, 1939.

factors may be mentioned that might possibly tend to reduce, and in certain cases destroy, the correlation. Under certain circumstances building-up of particles might go on undisturbed in a cloud until exhaustion occurred of that part of the gas from which the particles are formed. This would lead to cases of strong particle absorption combined with weak line absorption. On the other hand, hydrogen ionization might lead to strengthening of line absorption without corresponding strong particle absorption. Finally, strong local variations of the ionizing radiation, connected, say, with strong variations in the space density of B stars, may appreciably affect the strengths of interstellar absorption lines. The latter effect may affect different lines (e.g., *Ca* II and *Na* I lines, also *Ca* II and molecular lines) rather differently. Altogether, it would seem that the picture of interstellar matter considered has sufficient flexibility to be applicable in a more detailed discussion of the observations.

THE DISTRIBUTION OF INTERSTELLAR SODIUM*

LYMAN SPITZER, JR.
Princeton University Observatory
Received May 6, 1948

ABSTRACT

Equivalent widths of the interstellar D lines in stellar spectra and the corresponding color excesses are analyzed to investigate the distribution of *Na* gas in space. As part of the program, new measurements of the D lines were obtained for thirty-seven stars, based on Mount Wilson spectrograms.

Analysis of the available data indicates that the interstellar clouds, some 5–10 pc in radius, which are responsible for the observed selective absorption, also produce the strong D lines observed in reddened stars, with a photoelectric color excess, E_1, equal to 0.10 or greater. The change of equivalent width of the lines and of the doublet ratio, D_2/D_1, with changes of distance, color excess, and galactic longitude are all consistent with this belief. The root-mean-square radial velocity of the individual clouds is 9 km/sec, in rough agreement with the 7 km/sec found by Whipple for the strong components of K and H observed by Adams. The optical depth of a single cloud in the center of its line is about 2.3 for D_1 and about 4.6 for D_2. The density of neutral *Na* in such clouds is about 5×10^{-9} atoms/cm^3, if averaged over the space in and between the clouds, but inside each cloud it is probably about ten times this value. If seven such clouds per kiloparsec in the line of sight are assumed, the photoelectric color excess per cloud is 0.024 mag.; a single cloud produces D lines of width 0.15 A, and has 2×10^{12} atoms of neutral *Na* per square centimeter in the line of sight; the root-mean-square velocities of these atoms are 2.1 km/sec, corresponding to a kinetic temperature of 12,000° if the motions were thermal.

In stars with E_1 less than 0.10, the behavior of the D lines and their doublet ratio is quite different. These lines are apparently produced in less opaque clouds, whose optical depth in the center of each D line is much less than unity. The density of neutral *Na* in such relatively transparent clouds is about 2×10^{-9} atoms per cubic centimeter, when averaged over all space near the galactic plane; and thus the total number of atoms in such clouds is about one-third the number in the more opaque clouds. The data are inadequate to indicate whether the ratio of grains to atoms is as great in these transparent clouds as it is in the more opaque clouds. The root-mean-square velocity of these transparent *Na* clouds is at least 5 km/sec but may be less than the 9 km/sec found for the more opaque clouds.

The change of equivalent width with distance depends on the color excess and galactic longitude; this dependence affects the determination of individual stellar distances from interstellar line intensities. From an examination of stars which show strong D lines, a list is given of two stars that may be supergiants and two supergiants that may be extraordinarily luminous.

I. INTRODUCTION

The irregular distribution of interstellar matter is well known. The most cursory glance at Milky Way photographs indicates that the clouds of obscuring matter are scattered very unevenly about the sky and, moreover, that clouds of widely different thicknesses exist. Considerable evidence on the distribution both of small solid grains and of the interstellar atoms has accumulated in recent years. We shall first review and summarize this evidence, as a background to a more detailed analysis of the distribution of interstellar sodium atoms.

a) DISTRIBUTION OF SOLID PARTICLES

The general and selective extinction produced by the solid particles, or grains, in interstellar space has been investigated in many ways. Stebbins, Huffer, and Whitford have obtained[1] extensive photoelectric data on selective absorption and have shown[2] that the photoelectric color excess, E_1, based on the color difference between about λ 4260 and

* This investigation was made possible by a co-operative arrangement with the Mount Wilson Observatory.

[1] *Mt. W. Contr.*, No. 621; *Ap. J.*, **91**, 20, 1940.

[2] *Mt. W. Contr.*, No. 632; *Ap. J.*, **92**, 193, 1940.

λ 4770, increases by 0.17 mag., on the average, per kiloparsec. However, the distribution of the obscuring matter is so irregular that in some regions this average coefficient of selective absorption, which we may denote by E_{1c}, is as low as 0.09, while in others it rises to 0.22.

The total photographic extinction, A_p, has been determined in a number of ways, which have been summarized by van Rhijn[3] and Seares.[4] Most of these determinations suffer from the disadvantage that they give particular weight to transparent regions, where distant objects can be seen. This factor of observational selection is less important in color-excess investigations, which are concerned with closer stars. For this reason the most reliable method of determining an average coefficient of general photographic extinction, denoted by A_{pc}, is to multiply the coefficient of selective extinction by a factor of about 9, corresponding to a variation of the extinction with the inverse first power of the wave length. Direct spectrophotometric measurements by Stebbins and Whitford[5] and by Whitford[6] have shown that marked deviations from this law become appreciable only at wave lengths of 20,000 A or more. Additional direct evidence supporting this ratio of photographic to selective extinction is summarized by Oort[7] and van Rhijn.[8] Thus the photographic extinction increases about 1.5 mag. per kiloparsec, on the average.

This value of A_{pc} is about one-third greater than the value 1.1 mag. per kiloparsec adopted by van Rhijn,[3] who made a correction to Joy's results for the effect of observational selection referred to above. This correction is rather difficult to make, however, and a value as low as 1.1 for A_{pc} would be very difficult to reconcile with the observed values of E_{1c} and with present knowledge about A_p/E_1. Thus we shall here adopt 1.5 mag. per kiloparsec as the most probable value of the average photographic extinction.

The evidence indicates that the obscuring matter is uniform in composition almost everywhere. The law of reddening is apparently the same in most regions near the sun, except in the Trapezium cluster, where Baade and Minkowski[9] and, more recently, Stebbins and Whitford[5] have found a somewhat different change of extinction with wave length for θ^1 Orionis A (HD 37022) than for stars in other parts of the sky. The early color measures of elliptical galaxies by Stebbins and Whitford[10] seem to show a value of about 15 for the ratio A_p/E_1, which led Seares[4] to assume that the "stratum" responsible for high-latitude absorption was physically different from the obscuring clouds in the galactic plane. However, Oort[7] has shown, from a more extended analysis of stellar color indices, that A_p/E_1 in this region of the sky has apparently a normal value of about 9. Thus, despite this rather disturbing discrepancy, we may assume that the solid particles usually have a uniform composition and size distribution.

The density of the obscuring medium is unquestionably most irregular, and one must consider that separate clouds or condensations are present rather than a uniform medium. The few largest, most prominent clouds in the Milky Way have been investigated by Greenstein.[11] He finds that these have a mean diameter of 100 pc and that each produces an average photographic extinction of 1 mag. However, a straight line in the galactic plane intersects only one of these great clouds every 6000 pc, and thus these large clouds contribute only about one-ninth of the total extinction. The obscuring clouds responsible for most of the observed general and selective extinction must be assumed to be smaller.

[3] *Groningen Pub.*, No. 47, 1936.

[4] *Pub. A.S.P.*, **52**, 80, 1940.

[5] *Mt. W. Contr.*, No. 712; *Ap. J.*, **102**, 318, 1945.

[6] *Ap. J.*, **107**, 102, 1948.

[7] *B.A.N.*, Vol. **8**, No. 308, 1938.

[8] *Groningen Pub.*, No. 51, 1946.

[9] *Mt. W. Contr.*, Nos. 571, 572; *Ap. J.*, **86**, 119, 123, 1937.

[10] *Mt. W. Contr.*, No. 577; *Ap. J.*, **86**, 247, 1937.

[11] *Harvard Ann.*, **105**, 359, 1937.

To evaluate the numbers and sizes of the average clouds, statistical methods must be used. The distribution of the clouds is not wholly random, since there is apparently a tendency for clouds to cluster together in vast cloud complexes. Nevertheless, over sufficiently large regions the assumption of random distribution may be an adequate approximation, and we shall make this assumption throughout. We shall let n be the number of clouds per cubic parsec in the galactic plane, and r the average cloud radius in parsecs; since a typical cloud is presumably quite irregular in size, one may define r as the radius of the sphere which presents the same average cross-section as do the clouds. If k is the average number of clouds intersected by a line, 1 kpc long, in the galactic plane, then

$$k = 1000\pi r^2 n \ . \tag{1}$$

If A_{pc} again represents the average coefficient of photographic extinction, expressed in magnitudes per kiloparsec and if τ is the photographic extinction per cloud, then we may write

$$A_{pc} = k\tau \ . \tag{2}$$

Since A_{pc} is known, independent determinations of τ and n will yield both k and r.

The photographic extinction per cloud has been determined by Ambarzumian[12] from the fluctuation of Hubble's counts of external galaxies at galactic latitudes between 25° and 45°. His value of 0.27 mag. is increased somewhat by a consideration of the higher-order terms neglected in his analysis but is decreased by the intrinsic fluctuation of the number of galaxies, resulting primarily from the clustering tendency of galaxies. The smaller value of 0.18 has been found by Markarian[13] from the fluctuation of star counts in a number of regions. A simple average of these two determinations gives a value of 0.23 for τ, yielding a value of about 7 for k in equation (2). We shall see later that this value of k is in reasonable agreement with the apparent number of gas clouds per kiloparsec.

The density n of clouds per cubic parsec may best be determined from an analysis of Hubble's data on the reflection nebulae. Ambarzumian and Gordeladse[14] have shown that the relative numbers of reflection nebulae accompanying stars of different spectral types are about what one would expect from a random distribution of nebulae in space. Since computation shows that all the stars would be expected to illuminate only 1/2000 of space, the authors infer that the total density of dark clouds is about two thousand times that of the bright ones. This latter density is not well determined; but, with reasonable assumptions, Ambarzumian and Gordeladse find a value of 1.2×10^{-4} clouds per cubic parsec for n. With k set equal to 7, equation (1) then gives a value of 4.3 pc for r. This is a lower limit on r, since the basic assumptions overestimate n. Only a small part of a cloud need lie within the computed zone of illumination about the bright star to be seen as a bright nebula, i.e., the effective radius of the zone of illumination should be increased by the radius of the cloud.

Oort and van de Hulst,[15] on the other hand, point out that only 14 per cent of the stars with spectra between O and B2 are associated with bright nebulae; if one then concludes that the dark nebulae occupy 14 per cent of space near the galactic plane and if k is again set equal to 7, it follows that n is 1.0×10^{-5}pc^3 and r is 15 pc. This analysis gives a lower limit on n and an upper limit on r, since not all the region of illumination about a hot star must be filled with clouds to produce a bright nebula, and thus the fraction of space occupied by clouds must be less than 14 per cent. Obviously, if nr^3 is less, n must be increased and r decreased to preserve the same k in equation (2). Clearly, r has a consid-

[12] *Bull. Abastumani Ap. Obs.*, **4**, 17, 1939.

[13] *Contr. Burakan Obs., Academy of Sciences of the Armenian S.S.R.*, No. 1, 1946.

[14] *Bull. Abastumani Ap. Obs.*, **2**, 37, 1937. This paper contains several misprints, but a recalculation shows that the numerical results are essentially correct.

[15] *B.A.N.*, Vol. **10**, No. 376, 1946.

erable range of uncertainty, and a spread of cloud radii between 1 and 50 pc must be considered; however, an average value in the neighborhood of about 8 pc seems reasonable. This may be compared with the value of 5–10 pc assumed by Eddington[16] in his Bakerian Lecture.

The density of grains between the obscuring clouds is at present a completely open question. A uniform stratum, with about one-tenth as much matter as in the coluds, could apparently not be detected at the present time.

b) DISTRIBUTION OF INTERSTELLAR ATOMS

While most interstellar absorption lines are weak and have not been extensively measured, the K line of Ca^+ and the D lines of Na have been well investigated. The steady increase in the strength of these lines with increasing stellar distance has been analyzed most recently by van Rhijn,[17] who gives a mean curve relating equivalent width to distance. Merrill and Sanford[18] have shown that the radial velocities of these lines show the familiar galactic-rotation effect. Thus it seems well established that, viewed in the large, the interstellar atoms have at least a statistically uniform distribution and have no large systematic motion with respect to the stars.

A more detailed examination shows, however, that the density distribution of the interstellar gas is by no means uniform in detail and that appreciable random velocities characterize the gas in different regions. Irregular motions of elements within the interstellar gas were adduced by Beals[19] from his study of data on the intensities and velocities of interstellar K, D_1, and D_2. In particular, the complex profiles observed for the interstellar K lines in several stars were cited by Beals as confirmation of this suggestion. This result was much strengthened by Wilson and Merrill,[20] who made use of the extensive catalogue of interstellar line data published by Merrill, Sanford, Wilson, and Burwell.[21] These data showed, first, that the equivalent width of the D lines increases almost linearly with increasing distance out to 2000 pc, even for stars near the nulls of galactic rotation. Second, they showed that the doublet ratio D_2/D_1 drops gradually from a value of nearly 2.0 at close distances to an average value of about 1.2 at 700 pc but shows no further decrease at greater distances. These two observational results can apparently be explained only if an increase of distance from 700 out to 2000 pc penetrates regions where the radial velocity of the atoms is different from that in closer regions, thus permitting the atoms to scatter light in a region of the spectrum not otherwise weakened. The observed lack of strong dependence of equivalent widths on galactic longitude requires the assumption of large-scale random motions rather than galactic rotation.

More recently, Adams[22] has shown that complex profiles are the rule rather than the exception for interstellar K and H. Merrill and Wilson[23] have found that these complexities are apparently much less marked for the Na D lines than for K and H, but the spread in large-scale velocities required to explain the intensity data for the D lines is of the same order of magnitude as is the spread in velocity of the components of K and H. While the detailed distribution of velocities in the interstellar gas is still obscure, the presence of streams or other large-scale motions in this gas can scarcely be doubted. The moving elements of the gas may legitimately be called "clouds." The acceptance of this conclusion casts some doubt on the analyses of interstellar line intensities by Evans[24] and

[16] *Proc. R. Soc. London*, *A*, **111**, 424, 1926.

[17] *Groningen Pub.*, No. 50, 1946.

[18] *Mt. W. Contr.*, No. 585; *Ap. J.*, **87**, 409, 1935.

[19] *M.N.*, **96**, 661, 1936.

[20] *Mt. W. Contr.*, No. 570; *Ap. J.*, **86**, 44, 1937.

[21] *Mt. W. Contr.*, No. 576; *Ap. J.*, **86**, 274, 1937.

[22] *Mt. W. Contr.*, No. 673; *Ap. J.*, **97**, 105, 1943.

[23] *Pub. A.S.P.*, **59**, 132, 1947.

[24] *Ap. J.*, **93**, 275, 1941.

by Schilt,[25] both of whom consider that the interstellar gaseous medium is essentially homogeneous. The conclusions reached by these two authors are treated in more detail at the end of this paper.

Preliminary results on the distribution and velocity of the calcium clouds have been obtained by Whipple[26] in his analysis of Adams' data. He finds that the average number of components per kiloparsec is "six to eight." The close agreement between this estimate and the value of seven obscuring clouds per kiloparsec found in Section I-*a* is probably fortuitous. On the one hand, half the clouds in Whipple's analysis are relatively transparent in the K and H lines; and, if they resemble the transparent clouds of *Na* discussed later in this paper, they produce relatively little selective absorption. On the other hand, it is likely that there occurs some overlapping of the lines produced by the more slowly moving opaque clouds, with the result that the true number of such clouds may be greater than the observed number of such components. Whipple finds a root-mean-square velocity of about 7 km per second for the relatively opaque clouds, producing a strong K line, and about 23 km/sec for the more transparent ones, producing a weak line.

c) RELATIVE DISTRIBUTION OF GAS AND GRAINS

One is naturally tempted to assume that an obscuring cloud is also a gas cloud. The fact that diffuse nebulae always exhibit a gaseous spectrum when the exciting star is of type B0 or earlier is certainly a strong indication that atoms are concentrated in the clouds of solid grains; and the analysis of the distribution of these nebulae by Ambarzumian and Gordeladse[14] implies that the obscuring clouds must contain a relatively high abundance of atoms. It should be noted that Struve[27] has shown that in at least one case (σ Sco), where the nebula shows both a continuous and an emission spectrum combined, the regions of emission are asymmetrical compared to the regions of reflection. This may arise either from a difference in excitation conditions or from a variable ratio of atoms to grains within the cloud. Probably such differences in detail do not affect the general conclusion that atoms are concentrated in the obscuring clouds. However, a physical association of atoms and grains does not necessarily imply that the interstellar lines are produced primarily within the obscuring clouds. It is possible that in most clouds the atoms are in such a state that they do not scatter radiation; for example, the atoms might combine with other atoms to form molecules, dissociation of these molecules occurring only near early-type stars.

One must therefore appeal to the data on interstellar lines to determine whether these lines are actually produced in the obscuring clouds. There are two ways in which such data can be used for this purpose. First, if the obscuring clouds are identical with the clouds of gas, the radii of these two types of clouds should, of course, be equal. Second, the equivalent widths of the interstellar lines in the spectrum of a star should show some relationship with the observed color excess for that star. The information on the sizes of gas clouds is contradictory. Wilson and Merrill[20] have found a cloud radius of some 700 pc. They observed that, on the average, the D lines approach saturation gradually with increasing distance out to about 700 pc, with no systematic change at greater distances. Since their data require the assumption that each cloud is optically thick and produces a saturated line, it follows that the thickness of each cloud, or of each region with nearly uniform radial velocity, is about a hundred times the thickness of the obscuring clouds. On the other hand, the interstellar K and H profiles observed by Adams[22] show two separate components, presumably produced by two separate clouds, for a number of stars about 300 pc from the sun, and even for a few stars about 150 pc away. This evidence certainly requires that some of the gas clouds be less than 100 pc in thickness; and Merrill[28]

[25] *A.J.*, **52**, 209, 1947.

[26] *Harvard Observatory Centennial Volume* (Cambridge, Mass.: Harvard College Observatory, 1948).

[27] *Ap. J.*, **86**, 94, 1937.

[28] *Pub. A.S.P.*, **358**, 354, 1946.

has even suggested, as a preferable alternative to the customary uniform distribution, that the interstellar lines are formed in relatively thin curtains. Clearly, a reconciliation of these two lines of evidence is necessary.

The comparisons between color excess and interstellar line intensity have thus far pointed to a lack of any close correlation between atoms and grains. The correlation between the intensity of the K line and the color excess shows very large scatter, as pointed out by many workers, including Miss Westgate,[29] Williams,[30] and Sanford.[31] A similar result for the D lines was obtained by Merrill and Wilson.[32] Some very weak interstellar lines have been observed in strongly reddened spectra. Greenstein and Struve[33] have observed a very weak K line—less than 0.06 A—in the spectrum of HD 147889, which has the high photoelectric color excess of 0.50. The interstellar D lines in this star are also much weaker than the lines found in less reddened stars. Similarly, Morgan[34] observed that in two stars—HD 194279 and HD 194839—with photoelectric color excesses of 0.55 and 0.54, respectively, the K line was weaker than in adjacent, less reddened stars. While it has been suggested[15] that these variations result from the saturation of the lines, no analysis of such effects has yet been carried out.

An important argument against any association between grains and atoms has been made by Evans.[24] His analysis shows that, of the stars with a particular D-line intensity, those stars with a photoelectric color excess E_1 greater than 0.15 have an average distance which is closely equal to that of the less reddened stars. The same result was also obtained for the K line. The distances were deduced from the measured radial velocities of the D and K lines and use of the formula derived from galactic rotation; stars within 15° of the nulls of galactic rotation were not used. At first sight, this investigation would seem to exclude the possibility of any connection between the atoms responsible for the interstellar lines and the grains responsible for the selective extinction. Unless Evans' result can be accounted for in some other way, one cannot legitimately assume that the observed gas clouds are identical with the observed obscuring clouds.

d) SUMMARY AND OUTLINE OF PAPER

The salient features of our present knowledge in these respects may be briefly summarized. The interstellar grains responsible for the general and selective extinction of starlight are concentrated in clouds whose effective radius varies from 1 to 50 pc and probably averages about 8 pc. A straight line in the galactic plane will pass through a cloud of average size, with a photographic extinction of about 0.2 mag., about every 150 pc, while a cloud of the largest size, with an extinction of about 1 mag., will be intersected about every 6000 pc. Grains may also be present between the clouds. Sodium and calcium atoms also occur in clouds whose random radial velocities average about 10 km/sec. The thicknesses of some of these clouds are less than 100 pc, but for some purposes the effective cloud size seems to be 700 pc. While it seems reasonable to assume that the density of atoms in an obscuring cloud is greater than its average value outside the clouds, all investigations have indicated a relatively weak correlation between selective absorption and the intensity of the interstellar atomic lines. It is not known to what extent this lack of strong correlation is the result of saturation effects in the atomic lines.

The present paper is designed to analyze the available data on selective absorption and D-line intensities and to investigate how much connection between grains and atoms may be deduced. In particular, account is taken of the saturation effects to be expected. As will be seen below, the results are consistent with a rather close association between gas clouds and clouds of grains, but a variety of types of gas clouds must be assumed in

[29] *Ap. J.*, **78**, 65, 1933.

[30] *Mt. W. Contr.*, No. 487; *Ap. J.*, **79**, 280, 1934.

[31] *Mt. W. Contr.*, No. 573; *Ap. J.*, **86**, 136, 1937.

[32] *Mt. W. Contr.*, No. 582; *Ap. J.*, **87**, 9, 1938.

[33] *Ap. J.*, **90**, 625, 1939.

[34] *Ap. J.*, **90**, 632, 1939.

order to explain the observations. A preliminary account of these conclusions was given by the author[35] some years ago, but publication of the full results, based on more complete material, was delayed by the war. It should be emphasized that this investigation is somewhat preliminary and considers only the D lines. For a more complete picture the K and H lines must also be treated. Previous data on these lines are somewhat inadequate, since in most stars the blending of H with $H\epsilon$ prevents an accurate determination of the doublet ratio K/H. The beautiful high-dispersion spectra obtained by Adams[22] permit a complete resolution of H from $H\epsilon$ and also show many interesting complexities in the line profiles. These plates are now being reduced to obtain accurate measurements of equivalent widths of the separate components in each line. When this material becomes available, it is planned to extend the present analysis to the K and H lines. It would also be desirable to complete the picture by measurement of the complex profiles of the D lines in an adequate number of stars.

In Section II of this paper new observational material on D-line intensities is presented. In Section III the variation of the D-line intensities with color excess and galactic co-ordinates is considered. Section IV discusses the variation of the doublet ratio, while in Section V the determination of stellar distances from D-line intensities is treated.

II. OBSERVATIONAL DATA

The present paper investigates the dependence of the D-line intensities on the color excesses, the distances, and the galactic co-ordinates of the stars. Thus, for each star of known galactic co-ordinates, information must be obtained on the equivalent widths of the D lines, the color excess, and the stellar distance.

Quantitative measurements of equivalent widths for about 200 stars were available from the Mount Wilson catalogue[21] of interstellar line intensities and radial velocities, referred to subsequently here as "MWC 576." The footnotes to this catalogue indicate that the D-line measurements for nine of these stars are unreliable, owing to blends with stellar lines of *Na* or *C* II; the data for these nine stars were not used. For a number of stars visual estimates of line intensity are given in MWC 576. If the lines were estimated to be of Intensity I, "Line either not seen or a barely perceptible trace," the equivalent width was assumed to be, in fact, low—less than 0.04 A. If the lines were estimated to be of Intensity II, III, or IV, the data were not used in the present analysis.

To interpret the extensive observational material in MWC 576, information is needed on the color and distance modulus of each star. The values of the photoelectric color excess E_1 were taken from the catalogue of Stebbins, Huffer, and Whitford,[1] subsequently referred to as "MWC 621." Values of the distance modulus $m - 7E_1 - M$ were mostly taken from MWC 621; for several supergiant stars spectroscopic absolute magnitudes determined by Morgan[36] were available and were used instead. All these moduli rest, of course, on the assumption that the visual absorption is seven times E_1, corresponding to the previously assumed ratio of 9 for A_p/E_1. The validity of this assumption has been verified by van Rhijn,[8] who found $7.1E_1$ for the visual absorption. This same paper also shows that the mean absolute magnitudes for each spectral type are about those of MWC 621 for types O through B2 and for the c stars; for the stars of later spectral type, van Rhijn's absolute magnitudes are more strongly negative than are those of MWC 621, the correction amounting to -0.8 mag. at B5. In view of the large scatter in absolute magnitudes within each spectral type, it was not considered worth while to revise the absolute magnitudes used in computing the distance moduli.

a) NEW MEASUREMENTS

In addition, new measurements of interstellar D-line intensities in thirty-seven stars were made at the Mount Wilson Observatory. These are listed in Table 1. The first three

[35] *Pub. A.A.S.*, **10**, 235, 1941.

[36] Unpublished material, kindly communicated to the author by Dr. Morgan.

columns of this table give the number of the star in the *Henry Draper Catalogue* and the 1900 co-ordinates obtained from the same source. The magnitudes and spectral types in the fourth and fifth columns, the galactic co-ordinates in the sixth and seventh columns, and the photoelectric color excesses in the eighth column were all taken from MWC 621. In the ninth column are given values of the distance modulus $m - 7E_1 - M$, also taken from MWC 621, except for the values in italics, which were calculated from Morgan's absolute magnitudes. Since Morgan's determinations were all for supergiant stars, a prefix "c" is added to the spectral type of each such star in the fifth column.

TABLE 1

OBSERVED EQUIVALENT WIDTHS OF INTERSTELLAR D LINES

HD	R.A. (1900)	DEC. (1900)	m	SP.*	l	b	E_1	m_0-M	EQUIV. WIDTH (ANGSTROMS)	
									D_2	D_1
1337..	0^h12^m5	+50° 53′	6.12	O8n	85.6	−10.9	+0.03	10.4	0.65A	0.43A
13866..	2 10.0	+56 15	7.4	cB2	102.3	− 3.6	+ .14	11.9	0.79D	0.62D
14956..	2 19.6	+57 14	7.32	cB1s	103.2	− 2.2	+ .37	*11.9*	0.83D	0.50D
16243..	2 31.3	+57 23	8.4	cB2	104.6	− 1.5	+ .31	*11.2*	1.13D	1.10D
17088..	2 39.5	+57 19	7.54	B2	105.6	− 1.0	+ .45	7.4	1.09D	0.93D
21278..	3 20.9	+48 43	4.94	B5	115.3	− 5.3	+ .07	6.0	0.23B	0.22B
23193..	3 38.1	+36 09	5.57	cA3	125.6	−13.3	− .01	11.1	0.26C	0.17C
34578..	5 13.4	+33 52	5.16	cA5	140.5	− 0.5	+ .04	10.4	0.49B	0.43B
35619..	5 21.0	+34 41	8.5	*B0*	140.7	+ 1.3	+ .20	11.0	0.85B	0.64B
E248753..	5 47.3	+25 43	8.5	B0ne	151.3	+ 1.3	+ .16	11.3	0.57B	0.52B
43078..	6 09.2	+22 20	8.9	*B0*	156.7	+ 4.0	+ .25	11.0	0.68C	0.71C
158661..	17 25.4	−17 03	8.2	*B0*	336.1	+ 7.6	+ .16	11.0	0.64B	0.58B
159864..	17 31.8	−17 46	8.6	*B0*	336.3	+ 5.9	+ .20	11.1	0.96B	0.69B
163472..	17 51.2	+00 42	5.73	B2	354.9	+11.1	+ .12	7.9	0.34C	0.27C
164353..	17 55.6	+02 56	3.92	cB3	357.4	+11.2	+ .07	*8.9*	0.38B	0.32B
167263..	18 09.3	−20 25	6.02	c*B1*	338.4	− 3.1	+ .07	*11.2*	0.28C	0.29C
167264..	18 09.3	−20 46	5.42	cB0	338.1	− 3.2	+ .09	*11.3*	0.38B	0.32B
167838..	18 11.9	−15 28	6.64	cB0	343.1	− 1.2	+ .30	*11.5*	0.96C	0.76C
169034..	18 17.6	−13 39	8.6	cB0	345.3	− 1.6	+ .67	*10.4*	0.84D	0.73D
170938..	18 26.9	−15 46	8.1	c*B0*	344.5	− 4.5	+ .50	*11.8*	1.00B	0.88B
175876..	18 52.3	−20 33	6.73	*Oe5*	342.7	−12.2	+ .03	11.0	0.51C	0.37C
180587..	19 12.0	+10 49	8.6	*B5*	13.3	− 1.9	+ .02	10.1	0.69A	0.48B
184915..	19 31.5	−07 15	5.04	B0n	359.6	−14.7	+ .08	9.4	0.29B	0.22B
184927..	19 31.6	+31 04	7.4	*B2*	33.2	+ 4.2	.00	10.4	0.12	0.09
185780..	19 35.7	+40 24	7.47	B2	41.7	+ 8.2	+ .03	10.3	0.63C	0.41C
186618..	19 40.4	+47 01	7.6	B1n	47.9	+10.8	− .04	11.5	0.31C	0.12C
186994..	19 42.5	+44 43	7.3	*B0*	46.1	+ 9.3	.00	11.2	0.49B	0.38B
188209..	19 49.0	+46 47	5.51	cO8s	48.5	+ 9.4	+ .06	*11.6*	0.52B	0.44B
189550..	19 55.5	+19 37	7.5	*B2*	26.3	− 6.4	+ .04	10.2	0.46B	0.36B
E227415..	20 00.1	+35 16	9.9	B3	39.9	+ 1.4	+ .27	10.2	0.52D	0.47D
190919..	20 02.2	+35 24	7.30	cB1	40.2	+ 1.1	+ .21	11.3	0.77D	0.48D
192968..	20 12.7	+40 39	7.9	*B2*	45.7	+ 2.4	+ .03	10.7	0.63A	0.54A
193322..	20 14.6	+40 25	5.82	O8	45.8	+ 2.0	+ .16	9.2	0.55C	0.53C
199478..	20 52.4	+47 02	5.76	cB8ea	55.2	+ 0.9	+ .22	9.7	0.60C	0.54C
201345..	21 03.9	+33 00	7.76	*B0*	46.4	−10.3	.00	11.7	0.51C	0.51C
204172..	21 21.7	+36 14	5.84	cB0	51.3	−10.6	+ .03	*11.1*	0.43A	0.27A
E235565..	21 34.3	+51 03	8.8	B2ne	62.9	− 1.0	0.00	11.8	0.35D	0.43D

* Spectral types in italics are from the *Henry Draper Catalogue;* the others are from Victoria.

The measured equivalent widths of the two interstellar lines, D_2 and D_1, are given in the last two columns. The weight of each determination is also given, with A, B, C, and D representing weights 3, 2, 1, and $\frac{1}{2}$, respectively. The D determinations were mostly based on various old plates, with a low dispersion—about 35 A/mm—and of rather low quality. The others were obtained from plates taken with a grating spectrograph at the coudé focus of the 100-inch telescope. Two cameras were used; one, with a focal length of 72 inches, gave a dispersion of 8.9 A/mm, while the 32-inch camera, used for most of the plates, gave a dispersion of 20 A/mm. All but two of these coudé plates were taken for this particular program, five of them by O. C. Wilson and the others by the present author. The spectra were photographed in the first order, on 103*a*-D emulsion. The photometric calibration used has been described by Williams.[30, 37]

A weight was assigned to each line on every tracing, based on the graininess and density of the background and on possible ambiguities in defining the line profile. Intensities of class A are all based on a number of different tracings. In some cases, when the spectrum was wide but of variable density across its width, these different tracings were made of different strips of the spectrum. In the other cases the different tracings were obtained from different spectrograms. It is believed that the final system of weights is consistent with that used in MWC 576. Examination of the internal agreement of the measures indicates that, for a measurement of weight C, the probable error for either of the D lines is about 10 per cent of the equivalent width, while for weight A, the probable error is about 6 per cent.

There are four stars in this list for which equivalent widths of the D lines are given in MWC 576. The relative agreement is about what one would expect from the estimated errors, except in the case of one star, HD 167264. The equivalent widths listed in Table 1 for this star are 30 per cent greater than those in MWC 576. This difference may arise from the fact that the lines show two clearly separated components, the stronger components being only about 10 per cent greater than the values given in MWC 576. It is possible that the earlier measurements included only the main component, the weaker component being lost in the plate grain. However, for all four stars a weighted mean for each of the D lines was used in the subsequent work.

The D-line measurements by Beals[19] have not been used in this investigation. It has been pointed out[20] that the equivalent widths measured by Beals are systematically greater than the Mount Wilson values by a factor of 1.44, though the random errors are satisfactorily small. The data in Table 1 naturally agree with the Mount Wilson values in MWC 576, determined in the same fashion as the present set. The unexplained discrepancy between the Mount Wilson measurements and those of Beals is most disturbing and must be kept in mind when the data are interpreted.

III. VARIATION OF EQUIVALENT WIDTH WITH COLOR EXCESS

Before we look at the variation of D-line intensity with color excess, it may be helpful to consider what one would expect if all the absorbing atoms were concentrated in the clouds of grains discussed in Section I-*a*. To simplify this discussion, the clouds may all be assumed identical. This assumption is obviously unrealistic, but an examination of its consequences may help to indicate how much variation actually exists from one cloud to another. Throughout the present section the two D lines will be treated as a single line, whose equivalent width, denoted by D, is $0.5\ (D_1 + D_2)$, where D_1 and D_2 are the equivalent widths of the two actual lines.

If a line 1 kpc in length within the galactic plane intersects seven identical clouds, the photoelectric color excess produced by each one will be about 0.024, corresponding to an average color excess of 0.17 mag./kpc. A star with zero color excess will, on this basis, show no interstellar D lines. A star with a color excess of 0.024 will show the lines pro-

[37] *Mt. W. Contr.*, No. 541; *Ap. J.*, **83**, 279, 1936.

duced by a single cloud; and on this simplified model all stars with this color excess should show D lines with exactly the same intensity. Let D_0 be the value of the equivalent width D produced by one such cloud.

If the color excess increases to 0.05, the lines will be produced by two clouds, and the equivalent width will depend on whether the radial velocities of the two clouds are sufficiently different so that the lines produced by the two clouds do not overlap. It will be shown in Section IV-*b* that each cloud which produces an appreciable color excess must produce a nearly saturated line, and the overlapping effect must be very important. Thus for a color excess of 0.05 the D-line intensities will vary from slightly greater than D_0 (if the two clouds have identical radial velocities) to $2D_0$ (if the clouds have widely different radial velocities). Similarly, as the color excess E_1 and the number of clouds n in the line of sight increase, the D-line intensities will vary from slightly greater than D_0 to nD_0. As n continues to increase, the dispersion in cloud velocities will ultimately limit the number of nonoverlapping clouds that are possible.

a) CURVE OF GROWTH FOR SINGLE CLOUDS

To make possible a comparison with observation, it is necessary to put these considerations into a quantitative form. First, we consider the formation of a line by a single cloud. For a Maxwellian velocity distribution, the probability $P(\Delta\lambda)\, d(\Delta\lambda)$ that the Doppler shift for any star lies between $\Delta\lambda$ and $\Delta\lambda + d(\Delta\lambda)$ is given by

$$P(\Delta\lambda) = \frac{2}{\pi^{1/2} b}\, e^{-(\Delta\lambda/b)^2}, \tag{3}$$

where b is related to the mean square $\Delta\lambda$ and the mean square velocity in the line of sight by the equation

$$b = (2\overline{\Delta\lambda^2})^{1/2} = \frac{\lambda}{c}\,(2\overline{v^2})^{1/2}. \tag{4}$$

For random thermal motions of Na atoms within a cloud,

$$b = \frac{\lambda}{c}\,\frac{(2kT)^{1/2}}{m} = 5.4 \times 10^{-4} T^{1/2} \text{ angstroms}. \tag{5}$$

This quantity b is simply related to the equivalent width. For any interstellar line the emission may be neglected; and, if the velocity distribution is given by equation (3), the equivalent width W may, in general, be written[38]

$$W = 2bF(C), \tag{6}$$

where C is the optical depth in the center of the line. The function $F(C)$ has been tabulated by Ladenburg.[39] For C large or small relative to unity we have

$$F(C) = \begin{cases} \dfrac{\pi^{1/2}}{2} C, & C < 1, \\ (\log C)^{1/2}, & C > 1. \end{cases} \tag{7}$$

For a saturated line, $F(C)$ changes relatively slowly with C; for C equal to 1, 10, and 100, $F(C)$ equals 0.63, 1.6, and 2.5, respectively. It will be shown in the next section that the values of C relevant to the interstellar D lines produced by one or more clouds are about

[38] A. Unsöld, *Physik der Sternatmosphären* (Berlin: J. Springer, 1938), p. 166.

[39] *Zs. f. Phys.* **65**, 200, 1930; Ladenburg's $S(C)$ equals $2F(C)/\pi^{1/2}C$.

2.3 and 4.6 for D_1 and D_2, respectively. If these values are inserted into equation (6), we have

$$D_0 = 2b_i \left\{ \frac{F(2.3) + F(4.6)}{2} \right\} = 2.5\, b_i , \tag{8}$$

where b_i characterizes the spread of radial velocities within a cloud.

b) STATISTICAL CURVE OF GROWTH FOR MANY CLOUDS

Next we must consider the equivalent width produced by many clouds. If Maxwellian velocity profiles are used, this problem becomes very complicated. One may expect to reproduce most of the essential features of the problem by considering a rectangular profile for the velocity-distribution function. In accordance with equation (8) we shall assume that the line formed by a single cloud has a width $2Fb_i$ angstroms, where F is a constant, numerically equal to 1.25 for the interstellar D lines.

Similarly, Doppler velocities of the separate clouds will be assumed to vary the central wave length of the line over a range $2Fb_e$, where b_e represents the spread of external cloud velocities. We compute here the average value of D when an average is taken over all cloud velocities. For the sake of generality we shall let the constant intensity within the line produced by a single cloud equal r_0 instead of zero; as will be seen, the resultant average value of D depends on the equivalent width D_0 and not on r_0 and b_i separately.

If the line of sight penetrates n clouds, the intensity r in the resultant line will be the product of the intensities in the individual lines. Let $\lambda_1, \lambda_2, \lambda_3, \ldots, \lambda_n$ represent the wave lengths of the centers of the line produced by clouds 1 to n. For a single cloud, the intensity r_j is given by

$$r_j = \begin{cases} 1 \text{ if } |\lambda - \lambda_j| > Fb_i \\ r_0 \text{ if } |\lambda - \lambda_j| < Fb_i . \end{cases} \tag{9}$$

For the equivalent width D we have

$$D = \int d\lambda \{ 1 - r_1 r_2 r_3 \ldots r_n \} . \tag{10}$$

To obtain the average value of D, denoted here by $\bar{D}$, we must average equation (10) over all values of λ_j. Since, by assumption, all values of λ_j are equally likely from $\lambda_0 - Fb_e$ to $\lambda_0 + Fb_e$, where λ_0 is the mean central wave length of the line, we have

$$\bar{D} = \frac{1}{(2Fb_e)^n} \int\int_{\lambda_0 - Fb_e}^{\lambda_0 + Fb_e} \cdots \int d\lambda_1 d\lambda_2 \ldots d\lambda_n \int_0^\infty d\lambda \, (1 - r_1 r_2 \ldots r_n) , \tag{11}$$

which may be written as

$$\bar{D} = \int_0^\infty d\lambda \left[1 - \frac{1}{(2Fb_e)^n} \int_{\lambda_0 - Fb_e}^{\lambda_0 + Fb_e} r_1 d\lambda_1 \int_{\lambda_0 - Fb_e}^{\lambda_0 + Fb_e} r_2 d\lambda_2 \ldots \int_{\lambda_0 - Fb_e}^{\lambda_0 + Fb_e} r_n d\lambda_n \right] . \tag{12}$$

The separate integrals in equation (12) are all identical, and we may therefore write

$$\bar{D} = \int_0^\infty d\lambda \left\{ 1 - \left(\frac{A}{2Fb_e} \right)^n \right\} , \tag{13}$$

where

$$A = \int_{\lambda_0 - Fb_e}^{\lambda_0 + Fb_e} r_j d\lambda_j . \tag{14}$$

If we now write

$$A = 2F b_e (1 - B), \tag{15}$$

then

$$\left(\frac{A}{2F b_e}\right)^n = (1 - B)^n \approx e^{-nB}, \tag{16}$$

provided that n is large. When B is small, which is the case of interest, equation (16) is a valid approximation even when n is small.

To evaluate B and thus to permit integration of equation (13), we examine equation (14) for A. In this equation the integral extends over the Doppler velocities of a cloud. If the absolute value of $\lambda - \lambda_0$ is greater than the total possible Doppler shift $F(b_e + b_i)$, r_j is 1 for all λ; in the range of integration $A = 2Fb_e$, and thus B is zero, and the integrand of equation (13) is also zero. This result corresponds to the fact that such wave lengths can obviously make no contribution to the equivalent width. If $|\lambda - \lambda_0|$ is less than $F(b_e - b_i)$, then, during the integration, $\lambda - \lambda_j$ will sweep over the entire line width, $2Fb_i$, for a single cloud; thus, for a range $2Fb_i$ of λ_j, the relative intensity r_j equals r_0 instead of 1, and A equals $2F(b_e - b_i + b_i r_0)$. Thus we have

$$B = \begin{cases} \dfrac{(1 - r_0)\, b_i}{b_e}, & |\lambda - \lambda_0| \leq F(b_e - b_i) \\ 0, & F(b_e + b_i) \leq |\lambda - \lambda_0|. \end{cases} \tag{17}$$

For $\lambda - \lambda_0$ between $F(b_e - b_i)$ and $F(b_e + b_i)$, B varies linearly between the two values in equation (17) and is given by

$$B = (1 - r_0) \left\{ \frac{F(b_e + b_i) - |\lambda - \lambda_0|}{2F b_e} \right\}. \tag{18}$$

If these relations are used in equation (16), equation (13) may be integrated directly. The resulting expression for $\bar{D}$ may be put in the form

$$\bar{D} = 2F b_e (1 - e^{-x}) \left\{ 1 + \frac{b_i}{b_e} \psi(x) \right\}, \tag{19}$$

where

$$x = n(1 - r_0) \frac{b_i}{b_e} \tag{20}$$

and

$$\psi(x) = \frac{1 + e^{-x}}{1 - e^{-x}} - \frac{2}{x}. \tag{21}$$

The function $\psi(x)$ is always less than unity, and, for small x, varies as $x/6$. The case of greatest interest is when b_i is assumed small compared to b_e; we may then set $1 + b_i\psi/b_e$ equal to 1. Those situations in which ψ is important are also those in which the assumption of a rectangular profile gives different results from the true Maxwellian profile. As we shall see in the next section, the central intensity in the D lines produced by one cloud must be quite small compared to 1, and thus we have, finally, setting F equal to 1.25,

$$\bar{D} = 2.5 b_e (1 - e^{-qE_1/b_e}), \tag{22}$$

where we have introduced the constant q, given by

$$q = \frac{n b_i}{E_1}. \tag{23}$$

On the basis of this picture no correlation of $\bar{D}$ with distance is to be expected, other than that resulting from the weak correlation of E_1 with distance. If galactic rotation is taken into account, however, the situation changes. Obviously, the radial velocity produced by galactic rotation increases the spread of velocities within the clouds. If the total spread of velocities out to the distance r is now denoted by $2.5b_e$, while $2.5b_{e0}$ denotes the spread at close distances, then we have, from the usual formula,

$$2.5\,b_e = 2.5\,b_{e0} + \frac{A\,r\lambda}{c} \sin\, 2\,(l - l_0)\,, \tag{24}$$

where A is Oort's constant, r is the distance of the star, and l_0 is the longitude of the galactic center. Distant stars at galactic latitudes farther than 20° away from the galactic plane will not be considered, and thus the term in cos b has been omitted from equation (24). From equations (22) and (24) it is possible to predict the change of $\bar{D}$ with color excess E_1, distance r, and galactic longitude l.

c) COMPARISON BETWEEN THEORY AND OBSERVATION

We turn next to a survey of the observational data. The stars were divided into four distance-modulus groups, and for each group $0.5(D_1+D_2)$, denoted again by D, was plotted against E_1, yielding Figures 1–4. Circles represent stars within 15° of the nulls of galactic rotation, while triangles were used for other stars. Filled-in circles and triangles represent stars at low galactic latitudes, while open symbols are used for stars at higher galactic latitudes. On each figure two theoretical curves are drawn. The lower curve, the same for all figures, shows $\bar{D}$ taken from equation (22) for stars with no galactic rotation, i.e., at such close distances or so near the nulls that b_e may be set equal to a constant value. The upper curve in each figure shows $\bar{D}$ for stars in the direction of maximum radial velocity; these upper curves were drawn for distances corresponding to distance moduli of 8.0, 9.5, 10.5, and 11.5 for the four groups. In applying equation (24), Oort's constant has been set equal to 15 km/sec, in agreement with the result already obtained for interstellar lines by Merrill and Sanford.[18]

The lower curve shown on all four figures involves two adjustable parameters which have been chosen to provide the best fit. These parameters are: the intrinsic dispersion, b_{e0}, of cloud velocities and the constant q, which measures the equivalent width per unit of color excess. The former quantity has been taken equal to 0.26 A, corresponding to a root-mean-square cloud velocity of 9.3 km/sec. This value is somewhat greater than the 7 km/sec found by Whipple[26] for clouds producing a strong K line. The general order of magnitude seems to be in good agreement and indicates that the clouds producing strong D lines have about the same velocities as the clouds producing strong K and H lines. More detailed information on the equivalent widths of the K and H lines and on the components of the D lines would be required to verify this tentative conclusion.

The constant q, equal to nb_i/E_1, has been taken equal to 2.4 A/mag. This is the ratio of b_i to the color excess produced by a single cloud. If the separate clouds all had widely different velocities, a star with a color excess E_1 would show interstellar D lines with a width $2.5\,nb_i$, or $2.5\,E_1q$. The value adopted for q gives D equal to, at most, 0.60 A when E_1 equals 0.10. If, as assumed above, the color excess produced by a single cloud is 0.024, then b_i is 0.058 A. If this is attributed entirely to the effect of thermal motions within each cloud, the kinetic temperature found from equation (5) is 12,000° K; the corresponding root-mean-square velocity in the line of sight is 2.1 km/sec. Since these values depend entirely on the uncertain value of the color excess per cloud, their reliability is not high.

The upper curve in each figure is determined from equations (22) and (24), without the introduction of any additional parameters. The good agreement between these curves

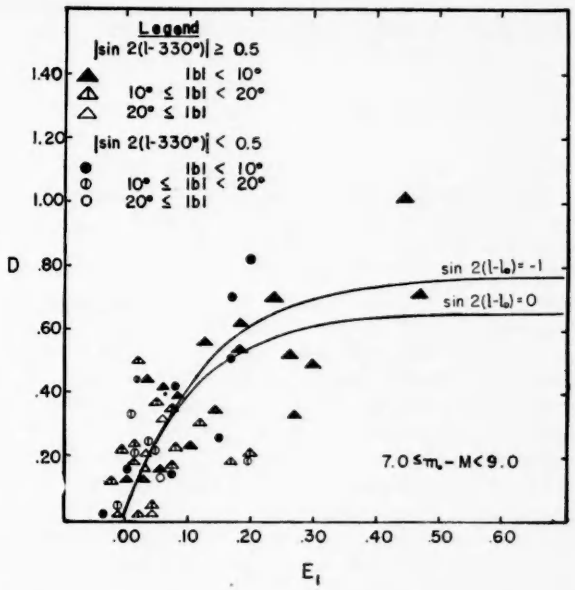

FIG. 1.—D-line intensities plotted against photoelectric color excess for stars with distance moduli between 7 and 9 mag.

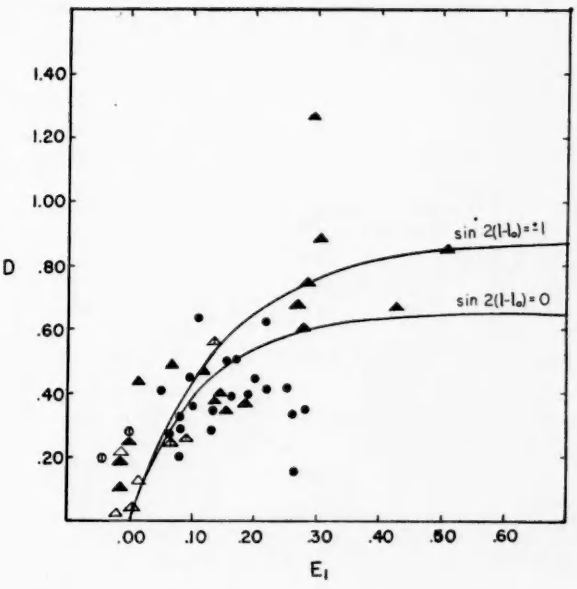

FIG. 2.—D-line intensities plotted against photoelectric color excess for stars with distance moduli between 9 and 10 mag. The symbols have the same meaning as in Fig. 1.

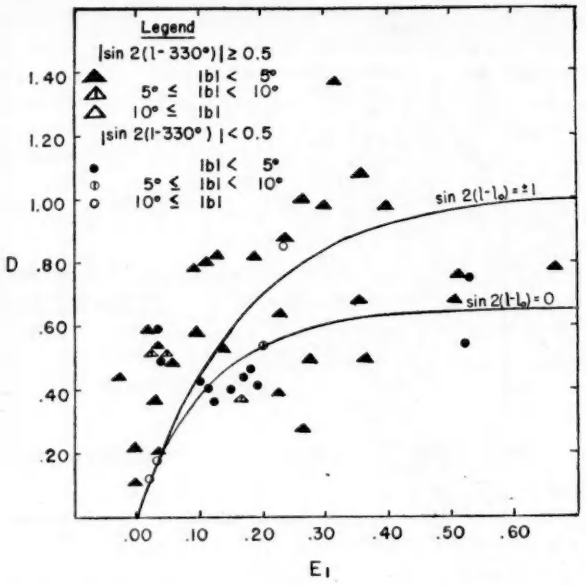

FIG. 3.—D-line intensities plotted against photoelectric color excess for stars with distance moduli between 10 and 11 mag.

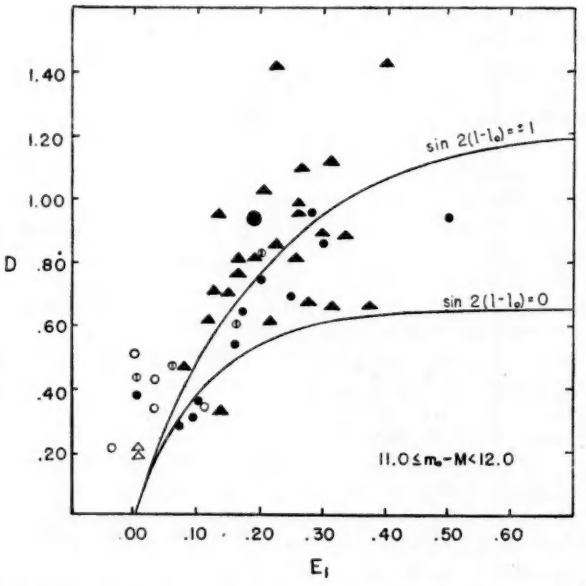

FIG. 4.—D-line intensities plotted against photoelectric color excess for stars with distance moduli between 11 and 12 mag. The symbols have the same meaning as in Fig. 3.

and the triangles in each of the four figures indicates that the simple model under discussion here does describe some of the major features of the observational data. Since the theoretical curve represents the mean value of D, averaged over all velocities for the individual clouds, some scatter is to be expected, especially in the region where the theoretical curve is just starting to flatten off.

It may be noted that the rough agreement found here between the cloud velocities observed by Adams and those required by the data shown in Figures 1–4 has also been found by Melnikov.[40] Further, Melnikov finds a root-mean-square velocity of 7 km/sec from a curve of growth for the interstellar Na and Ca^+ lines. However, Melnikov's approach is wholly different from that used here, and, in particular, the validity of his curve of growth is open to question, since he does not consider in detail the irregular distribution of the scattering atoms, indicated by the more extensive data analyzed here.

While the general agreement between observations and theory shown in Figures 1–4 is surprisingly good, considering the simplified model treated, one important discrepancy should be noted. The D lines seem to be much too strong in the stars with very low color excess, 0.04 or less. This is the region in which, according to the simple theory, no true scatter whatever should be present, since the number of clouds is 0 or 1, no overlapping of clouds is possible, and D should equal D_0 if one cloud is present and should equal zero otherwise. Yet the observations indicate that D may be considerable, even when E_1 vanishes. The random errors in E_1 (about 0.02) and in D (between 5 and 10 per cent) cannot explain this effect. If, as suggested by Oort[7] and van Rhijn,[8] the true zero point of the color excesses is between -0.025 and -0.049 on the scale of MWC 621, much of this discrepancy would disappear, but not all. A gaseous medium between the clouds of grains, or clouds of gas and grains which are more transparent than the average, would be consistent with these observations. This additional assumption receives strong confirmation in the next section.

There is one additional discrepancy apparent in the figures. Some of the points lie considerably above the asymptotic value approached by the theoretical curve for very high E_1. Since this limiting value represents the width attained when clouds are present with all possible velocities, these points require a wider velocity distribution for the clouds than that assumed. But a Maxwellian velocity distribution with a greater value of b_e would give for each E_1 an average D greater than the observations would permit. The most direct explanation of these anomalously strong lines is that the velocity distribution is non-Maxwellian. It is also possible that errors in distance and thus in the computed effect of galactic rotation might explain this result. This possibility is discussed again in Section V, where these exceptional stars are listed and their possible absolute magnitudes are discussed.

d) DEPENDENCE OF D ON GALACTIC LONGITUDE AND LATITUDE

One important test of the simple theory is the behavior of stars at the nulls of galactic rotation, which should show no systematic change with distance for a fixed E_1. That this test is very nearly fulfilled is evident from the four figures, which show only a relatively small increase of $\overline{D}$ with distance for the circles, as compared with a very marked increase for the triangles. This same effect is also shown by a comparison between Figures 10 and 11 in Section V-*a*. What little increase of D with distance appears for stars near the nulls may, in part, be accounted for by the fact that most of the stars are not exactly at the nulls.

To indicate how much the circles in Figure 4 are affected by galactic rotation, all points in this figure have been corrected for the effect of galactic rotation and replotted in Figure 5. It is not possible to compute this correction exactly for each star, since the detailed velocities of the many individual clouds producing the D lines in each stellar

[40] *A.J. Soviet Union*, **24**, 73, 1947.

spectrum are unknown. The average value of this correction for stars in a particular region of space and with a particular color excess is readily computed, however, by means of equations (22) and (24), which give the dependence of $\bar{D}$ on galactic longitude. By means of these equations one may compute how much $\bar{D}$ would be decreased for stars with particular values of l, b, r, and E_1, if sin 2 $(l-l_0)$ were reduced to zero, the other quantities remaining constant. A separate value of this change in $\bar{D}$ was computed for the co-ordinates and color excess of each star and was subtracted from the observed value of D for that star, to yield D_{corr}. While this correction is not exact for specific stars, it should give correct results on the average.

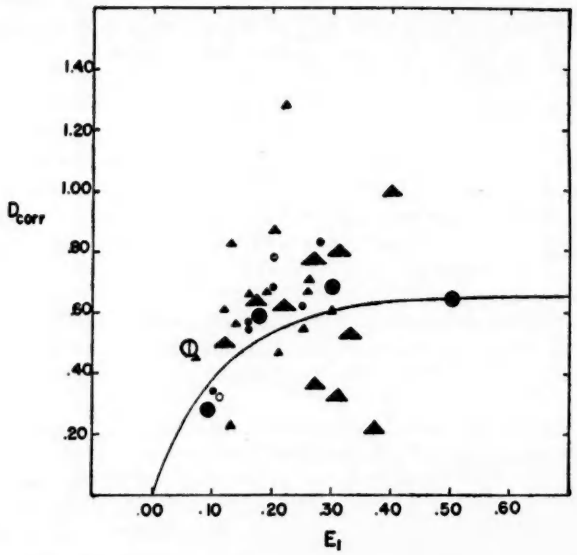

FIG. 5.—D-line intensities corrected for the effect of galactic rotation and plotted against photoelectric color excess. Only those stars with a distance modulus of 11 mag. or more and with E_1 greater than 0.05 mag. are included. The symbols have the same meaning as in Fig. 3, except that larger symbols have been used to denote stars of measured spectroscopic parallax.

In the final plot, given in Figure 5, the large symbols represent stars whose spectroscopic absolute magnitudes have been determined by Morgan. This figure shows that stars at all galactic longitudes follow relatively closely the expectations based on the simple theory. A comparison of Figures 1 and 5 shows in particular that the D lines in reddened stars near the nulls of galactic rotation vary only slightly with distance, when correction is made for the small amount of galactic rotation present. This result is also borne out by Figure 11 and the accompanying discussion, which indicates that the observed values of D at distances of only a few hundred parsecs are about 70 per cent of the values of D_{corr} at 2000 pc and beyond.

This result differs from that obtained by Wilson and Merrill,[20] who found no large systematic change of D with galactic longitude for stars at each distance. This difference in result is due in large part to the additional information now available on the D-line intensities for distant stars near the nulls. Since the data on the velocities shown by the interstellar lines indicate conclusively that the gaseous medium shares in the galactic rotation, it would be most surprising if this rotation did not also affect the line intensities in some way.

While the change of the average D-line intensity with distance is apparently small, when correction is made for the effect of galactic rotation, the data suggest that some increase is definitely present. There are at least two ways in which such an increase might be explained. Either a large scatter of E_1 between different clouds or an increase of the turbulent velocity, b_{e0}, with distance would produce this result. We shall consider each of these mechanisms separately.

If different clouds have widely different values of E_1, then the average number of clouds corresponding to a particular color excess will be different at different distances. At close distances a high value of E_1 is probably produced by a single cloud, while at greater distances many small clouds are more likely to contribute to a high observed color excess. If the equivalent width D_0 produced by each cloud were about the same for all clouds, one would then expect stars with a fixed E_1 near the nulls to show stronger D lines at greater distances. This effect may well explain some of the tendency shown by the points in Figures 1–4 to lie higher than one would expect on the basis of the simplified theory.

That the effective turbulent velocity of the clouds might increase with distance was suggested to the author by A. Unsöld, who kindly communicated an advance copy of his paper[41] on the interpretation of interstellar lines. The idea advanced in this work is that a cloud has a velocity greater than the random velocities of its components, that each group of clouds has a velocity greater than the random velocities of clouds within the group, that systems of groups are moving faster than the groups within each system, and so on. This suggestion is based on observations of turbulence in the earth's atmosphere and would yield a systematic increase of b_{e0} with distance. While the data presented here suggest that this effect is not large, a slight increase in b_{e0} with distance may be present. It may be noted that the differences which Unsöld stresses between a square-topped profile and a Maxwellian one must also be taken into account in a more refined theory.

One must always bear in mind the possibility that the trends shown in Figures 1–5 may, in fact, result from systematic changes of D-line intensity from one part of the sky to another. In view of the concentration of data in certain regions, this possibility is especially serious. A breakdown of the data by different galactic longitudes failed to show much difference between different regions except for the differences in galactic rotation already described. This is in accord with an earlier result by Merrill,[42] who concluded that "regional differences [in the density of sodium vapor], while probably present, are not extremely great."

It is of interest to note that the stars of higher galactic latitudes plotted in the accompanying figures show D lines of about the same strength as do the low-latitude stars at the same distance and with the same color excess. This indicates that the association between grains and gas persists even to considerable distances away from the galactic plane.

e) SUMMARY

One may conclude that to a surprisingly good first approximation the D lines may be regarded as formed by individual identical clouds, each cloud producing a photoelectric color excess, E_1, about one-sixth the equivalent width D_0 of the *Na* lines which it absorbs. The root-mean-square velocity of the individual clouds is 9 km/sec. If the color excess produced by a single cloud were 0.024, then the equivalent width D_0 produced by a single cloud would be about 0.15 A, corresponding to a root-mean-square velocity of 2.1 km/sec and, if the motions were random, to a kinetic temperature of about 12,000°. The dependence of D on E_1, on distance, and on galactic longitude is generally in agreement with expectations based on this simplified model. However, for values of E_1 close to zero, the D lines appear to be stronger than the theory predicts, indicating the presence of clouds

[41] *Zs. f. Ap.* (in press).

[42] *Mt. W. Contr.*, No. 569; *Ap. J.*, **86**, 28, 1937.

more tenuous than the average or possibly the presence of a uniform intercloud gas. It should be remembered that the measurements by Beals suggest that the Mount Wilson measurements of equivalent width should all be increased by a factor of 1.44. Such an increase would increase correspondingly the values found for the cloud velocities.

IV. VARIATION OF DOUBLET RATIO

The doublet ratio D_2/D_1, which will here be denoted by Q, provides a powerful tool for analysis of the distribution of the interstellar atoms. While the observational errors are much more serious here than in the study of D, the available information on the doublet ratio permits a number of important conclusions.

Let us consider, first of all, how this doublet ratio would be expected to change with D and E_1. In the case of a homogeneous medium, in which the atoms have only their random thermal motions, the doublet ratio may be found from the familiar curve of growth. The parameter b, introduced in the previous section to describe the distribution of atomic velocities, will be constant; if we now let C be the optical depth in the center of D_1, then $2C$ will be the optical depth in the center of D_2, and, in accordance with equation (6) above, we have

$$Q = \frac{D_2}{D_1} = \frac{F(2C)}{F(C)}, \tag{25}$$

while

$$D = b\,[F(C) + F(2C)]. \tag{26}$$

It is readily shown that N, the number of atoms in the line of sight per square centimeter, is related to b and C by the equation

$$N = \frac{m\,c^2}{\pi^{1/2}\,e^2\lambda^2}\,\frac{bC}{f} = 1.72 \times 10^{13}\,bC. \tag{27}$$

The numerical value is computed with b given in angstroms, and with f set equal to $\frac{1}{3}$, its appropriate value for D_1. From the values of $F(C)$ given by Ladenburg[39] the relationship between D_2/D_1 and D for a given b is readily found. Curves of this general nature have been plotted and their importance emphasized by Wilson and Merrill[20] and by Wilson.[43] When D is low, the lines are on the linear section of the curve of growth; as D increases, saturation sets in, the equivalent width increases more and more slowly with increasing C and N, and D_2/D_1 falls rapidly toward unity.

a) DOUBLET RATIO PRODUCED BY MANY CLOUDS

If the interstellar gas is concentrated in individual clouds, a separate analysis is necessary. This analysis depends both on the distribution of atomic velocities within each cloud and on the distribution of cloud velocities. We shall assume here that the cloud velocities are considerably greater than the relative velocities of the atoms within a cloud; this assumption appears to be realistic. We shall also assume that all velocities are distributed according to the Maxwellian law; this assumption is probably not correct in detail but should provide a useful first analysis. The assumption of a flat-top profile, made in Section II-*b*, was adequate for the computation of D but is unsatisfactory for the computation of Q, since for saturated lines this ratio depends primarily on the velocity-distribution function for velocities much greater than the average.

The nature of the absorption lines produced by many clouds depends also on the optical depth of a single cloud. We shall consider, first, the situation in which the optical depth through a cloud is small compared to unity. It is readily shown that in this case the relation between D_2/D_1 and D (called a "ratio-curve" by Wilson) is the same as in a homogeneous medium. Such relatively transparent clouds will not produce saturation

[43] *Mt. W. Contr.*, No. 614; *Ap. J.*, **90**, 244, 1939.

at any wave length unless the line of sight intersects a large number of clouds. But the velocity distribution of all the atoms in a large number of clouds will not deviate much from a Maxwellian distribution, with b set equal to $(b_e^2 + b_i^2)^{1/2}$, which is about equal to b_e. In other words, saturation does not appear until many clouds are present; and the profile of the line produced by many clouds will begin to approach the wide, smooth profile to be expected in a homogeneous medium. Obviously, if the number of clouds is steadily increased, with a corresponding decrease in the optical depth of a single cloud, the separate clouds may be treated essentially as separate absorbing particles, with a velocity distribution given by the Maxwellian law and a uniform density distribution; such a distribution of clouds would be observationally indistinguishable from a uniform gas.

When the optical depth of each individual cloud becomes large compared to unity, a quite different situation prevails. There is now a certain minimum value of D, denoted by D_0, found when the line of sight penetrates just one cloud, and a corresponding maximum value of the doublet ratio Q, denoted by Q_0. If two clouds are present and they do not overlap (i.e., if their radial velocities are sufficiently different so that the components of each line do not overlap), D will be twice D_0, and Q will be unchanged. If the clouds overlap exactly, the number of absorbing atoms is doubled, with no change in the velocity distribution; D will be slightly increased, and Q slightly decreased. Thus, with a fixed value of N, different values of Q and D are possible, depending on the degree of overlap of the clouds.

As the number of clouds is increased, D approaches $2b_e$, and overlapping of clouds (i.e., of the line components which they produce) becomes certain. Any further increase in the number of clouds must decrease Q without any large change in D. In the limiting case where the number of clouds becomes large, the velocity distribution of all the absorbing atoms approaches a Maxwellian distribution, characterized by the parameter b_e; Q may then be computed in terms of D, b_e, and C by the same formulae used for a homogeneous medium. To summarize, we see that, as the number of clouds increases, Q remains nearly constant, on the average, with increasing D until the different clouds overlap, after which Q follows the theoretical ratio-curve for a homogeneous medium with b set equal to b_e.

The above discussion refers to the average value of Q for each number of clouds. There will be considerable variation from this average value. If the clouds all overlap, Q and D will both be less than the average, while if none of the clouds overlap, both Q and D will exceed their average values for a fixed N. To consider how Q and D vary in this case, we shall discuss in more detail the relationship between these two quantities when N, the number of atoms in the line of sight per square centimeter, is held fixed.

The exact relationship between Q, D, and N is rather difficult to compute, since it depends on the detailed overlapping between clouds. For approximate results, we may assume that, for any value of N and D, the value of Q is the same as it would be for a homogeneous medium with the same N and D. On this assumption, Q is obtained from equation (25), with b and C determined by equations (26) and (27) and the given values of D and N. The values of b and C found in this way are simply parameters, without much physical significance, and may be denoted by b_{eff} and C_{eff}.

It may seem surprising that the relation between Q, D, and N found for a homogeneous medium should have any applicability to the situation in which a number of clouds, with different radial velocities, are present. It may be seen, however, that this relationship is clearly valid in the two limiting cases: (1) where the n clouds all overlap exactly and (2) where none of the clouds overlap at all. In the first case, D and Q are correctly given if C_{eff} is taken to be n times its value C_0 for a single cloud, without change of b; in the second case C_{eff} equals C_0, but b_{eff} is n times its value for a single cloud. In both cases the number N of absorbing atoms per square centimeter is obviously n times its value for a single cloud.

Before we use in all cases the relationsip between Q, D, and N found for a homo-

geneous medium, it is desirable to test the accuracy of this relationship in the case where the clouds overlap partially. This requires, first, that we evaluate Q and D numerically to find their true values. Next we must investigate whether or not these true values satisfy the relations for a homogeneous medium. To do this, we use equations (26) and (27) to find the values of C_{eff} and b_{eff} which yield the true values of D and N. Substitution of C_{eff} and b_{eff} in equation (25) then yields Q_h, the value which the doublet ratio would have in a homogeneous medium for a particular D and N; comparison between Q_h and the true value of Q indicates whether the relation between Q, D, and N for a homogeneous medium is, in fact, applicable in the case under consideration.

Such computations are rather complicated and have been carried out in only one case —that in which two clouds are present and the Doppler shift of one relative to the other is just equal to b_i, the parameter characterizing the random motions in each cloud. This situation is about intermediate between exact overlap of the two clouds and no overlap. The results of this computation are given in Table 2 for different values of the optical depth of a single cloud in the center of D_1. It is evident that the actual values of Q given in the fifth column do not deviate appreciably from the ones for a homogeneous medium

TABLE 2

ACCURACY OF EQUATIONS (25), (26), AND (27) FOR OVERLAPPING COMPONENTS

C	$\frac{D}{2b_i}$	$\frac{b_{\text{eff}}}{b_i}$	$\frac{C_{\text{eff}}}{C}$	Q	Q_h
0.5	0.883	1.25	1.60	1.59	1.59
1	1.296	1.23	1.63	1.39	1.39
2	1.674	1.22	1.64	1.22	1.21
4	1.966	1.21	1.65	1.14	1.16

found from equations (25), (26), and (27) and listed in the last column of Table 2. Thus in the general case we may assume that the relationship between Q, D, and N is usually given to a good approximation by equations (25), (26), and (27).

On the basis of the simplified picture in which all clouds are identical, the following general picture emerges as a result of this theoretical discussion. In the plot of Q against D, most of the weak lines, produced by a few clouds only, should show the same value of Q—that corresponding to a single cloud—which we denote by Q_0. The few weak lines in stars of high color excess will be those in which several clouds all overlap, and the value of Q for these lines will be substantially less than Q_0. With increasing D, some overlapping of clouds will become the rule rather than the exception, and the average value of Q will gradually decline. The decrease will not become marked until D is close to its saturation value at that distance; for greater D, Q will follow the ratio-curve given by equations (25) and (26) with b set equal to b_e. If we focus attention on stars all of the same color excess and thus with the same value of N, these will show the lowest value of Q when D is low; with increasing D the doublet ratio, Q, will increase gradually until it reaches its maximum value, Q_0, after which no further increase is possible.

b) OBSERVED DOUBLET RATIO IN REDDENED STARS

We turn next to an examination of the observational data on the doublet ratio for stars with color excess of 0.10 or more. Since the data are not sufficient to show the variation of Q with D for lines of each color excess and distance, all the observations were divided into two color-excess groups, with 0.10 as the dividing line. Each of these groups was subdivided into two distance subgroups, and plots were made of Q against D for each

subgroup. In constructing these plots, measurements of weight C or D have not been included; even for estimates of weight A or B, the probable error of each value of Q is about 0.10, which is larger than many of the expected variations.

Figures 6 and 7 present the data for the reddened stars. The symbols have the same meaning as before. The three dashed lines represent the variation of Q with D, predicted from equations (25), (26), and (27) for different fixed values of N, the number of atoms per square centimeter in the line of sight. As we have already seen, these curves may be used to indicate approximately the expected variation of Q with D when the clouds pres-

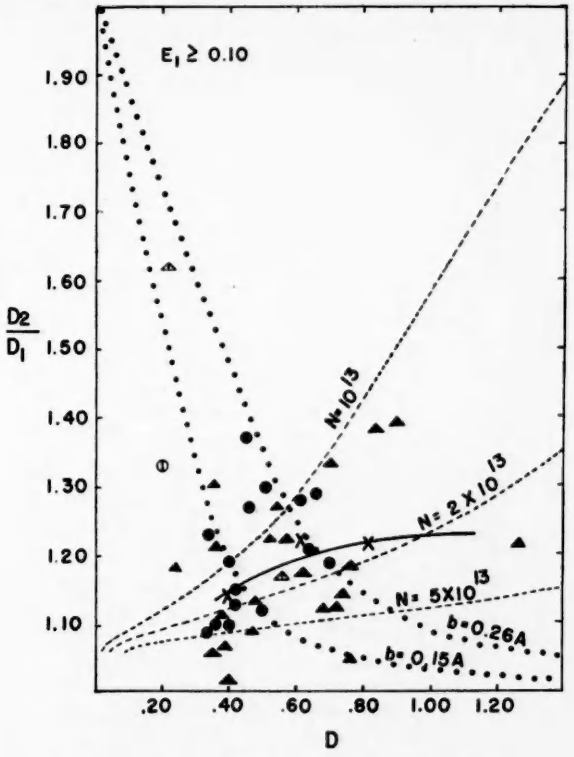

FIG. 6.—Values of the doublet ratio for reddened stars (E_1 equal to 0.10 or greater) within less than 1000 pc from the sun. The symbols have the same meaning as in Fig. 1.

ent overlap by all different amounts. The dotted curves are the ratio curves found for a homogeneous medium when b is fixed and equal to the values 0.15 A and 0.26 A; the former value is found from Figures 8 and 9, while the latter is the value of b_{e0} found in Section III-*c*. The crosses represent normal points, computed for all the points within each 0.20 interval of D. The solid line, the same on both figures, is drawn to provide the best empirical fit with the observed points.

It is evident from both figures that the values of Q tend to be smallest for the weakest lines. Since only the reddened stars are included, the weak lines may be regarded as produced by overlapping clouds, with the anticipated result that Q is less. While the effect is not large, it seems definitely to be present and indicates that the theory of many separate identical clouds, each containing atoms and grains, represents some of the major features of the observations. After its initial rise, Q levels off at about 1.20 and shows no further change with increasing D.

This dependence of Q on D proves immediately one important point—that the optical depth of a single cloud must be large. We have already seen that the line produced by many nearly transparent clouds, moving at random, is indistinguishable from that produced by a homogeneous medium. When such a medium produces a saturated line, a further increase in line width is possible only with an enormous increase in the number of absorbing atoms and a corresponding sharp decrease in Q—the latter effect is evident from the dotted curves in the figures. Galactic rotation could account for some of the observed points if the medium were homogeneous; but it is evident that stars at close dis-

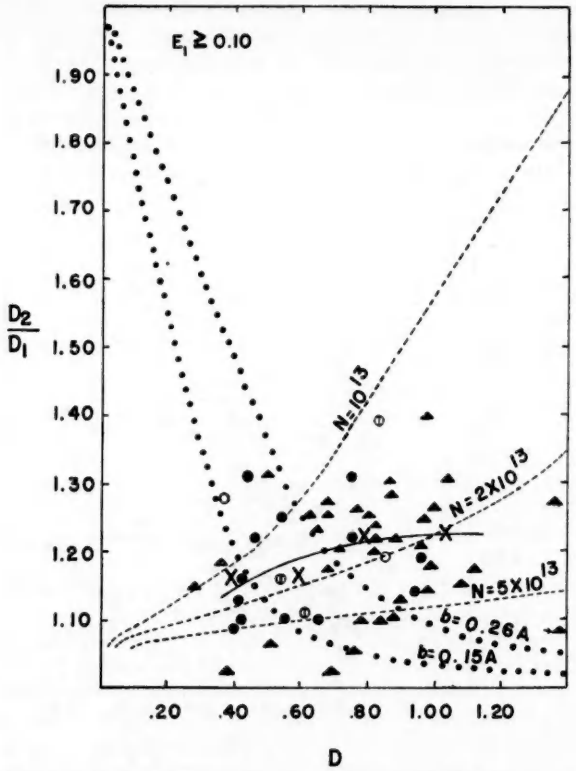

FIG. 7.—Values of the doublet ratio for reddened stars (E_1 equal to 0.10 or greater), 1000 pc or more from the sun. The symbols have the same meaning as in Fig. 3.

tances and near the nulls of galactic rotation do not behave very differently from the others. This evidence therefore justifies the assumption, made in Section III-*b*, that the optical depth of a single cloud for radiation at the center of either of the D lines is greater than unity.

The value of this optical depth through a single cloud may be determined from Q_0, the doublet ratio produced by a single cloud. While this latter quantity is difficult to evaluate precisely, Figures 6 and 7 indicate that it probably lies between 1.20 and 1.30. From equation (25) we find that C_0 equals 4.0 and 2.2 at these two limits. The most likely value is therefore about 3 for the optical depth in D_1, with 6 for the optical depth in D_2. The number of atoms, N_0, in a column 1 cm^2 in area extending through one cloud may be found directly from equation (27); if b_i is set equal to 0.058 A, we find that N_0 equals about 3×10^{12}/cm^{-2}. Thus the number of neutral *Na* atoms in a cylinder 1 cm^2 in cross-section and 1 kpc in length averages about 2×10^{13}.

Further examination of Figures 6 and 7 indicates general agreement with expectations. One would expect that, for close stars and for those near the nulls, the values of Q would not exceed those given by the equations for a homogeneous medium, with b replaced by the value 0.26 A found in Section III-c for b_{e0}, characterizing the distribution of cloud velocities. This expectation seems to be fulfilled, in general; most of the stars above and to the right of this dotted theoretical curve in Figure 7 are more than 15° from the nulls of galactic rotation, and the relevant value of b_e for these exceeds 0.26 A.

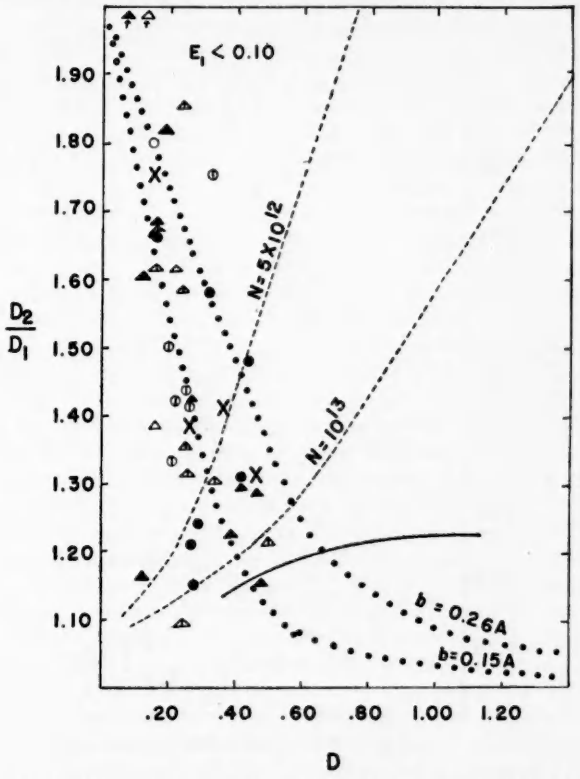

FIG. 8.—Values of the doublet ratio for unreddened stars (E_1 less than 0.10) within less than 1000 pc from the sun. The symbols have the same meaning as in Fig. 1.

The point in Figure 6 at D equal to 0.21 and Q equal to 1.63 seems way out of line with this entire picture. The probable error of Q perhaps increases somewhat with decreasing D; but, while observational error can perhaps explain why the barred circle at $Q = 1.32$ lies so high, it cannot explain away this much higher point. This anomalous point represents the D-line intensity in the spectrum of θ^1 Orionis A (HD 37022), the brightest star in the Trapezium cluster. The law of space reddening has also been shown to be anomalous for this star; and Baade and Minkowski[9] have determined that the grains of smaller size are apparently lacking. Figure 6 suggests that sodium atoms are also missing from this unusual nebula. That the one anomalous point in Figures 6 and 7 should also be anomalous in quite other ways is consistent with the belief that the present picture is essentially correct.

On the basis of this picture, one would expect to find for each value of D a correlation of Q with E_1 for the points in Figures 7 and 8. No such correlation seems to be present;

and, in fact, there is some evidence that for E_1 greater than 0.10 a further increase in E_1, with D held fixed, gives a less saturated line. If this effect is real, it may perhaps be explained by a difference in physical properties between different clouds. It is highly probable that a considerable dispersion exists in the color excesses produced by single clouds. If, in the clouds of higher color excess and probably of greater density, the atoms disappear rapidly, as, for example, by sticking to the grains, the very dense clouds might contain fewer sodium atoms than the somewhat less dense ones. The Trapezium cloud is apparently one in which the atoms have disappeared in this way. One might thus explain

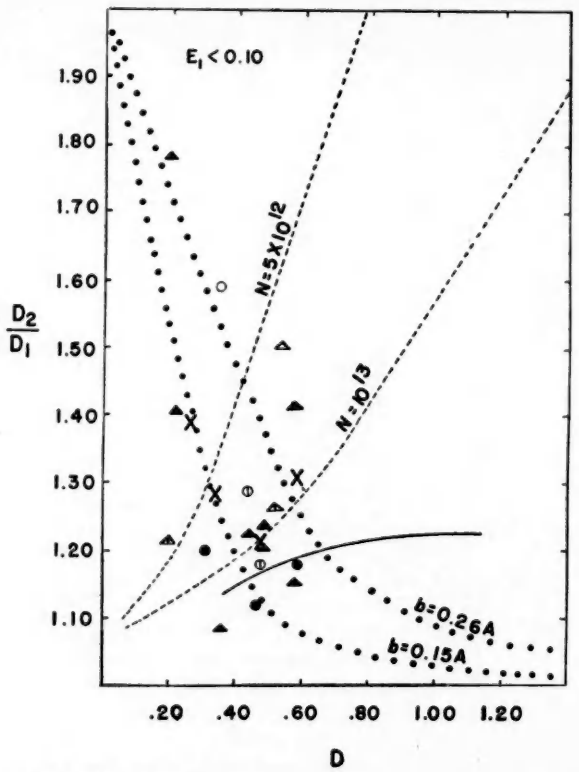

FIG. 9.—Values of the doublet ratio for unreddened stars (E_1 less than 0.10), 1000 pc or more from the sun.

an inverse correlation of Q with E_1, without impairing the observed increase of Q with D for low values of D. However, the data are quite inadequate to support in detail an interpretation of this sort. Discussion of the effects produced by such differences of density between the clouds must await more complete and accurate evidence.

c) OBSERVED DOUBLET RATIO IN UNREDDENED STARS

Next we look at the points for unreddened stars, shown in Figures 8 and 9. The symbols have the same meaning as before, and the dotted, dashed, and solid curves have the same meaning as in Figures 6 and 7. The crosses are normal points, now computed for all the stars within an interval of 0.10 in D.

It is evident at once that the simple picture of small, separate, identical clouds, each producing a saturated line, is wide of the truth for these unreddened stars. Instead of a

flat ratio-curve, giving a low and constant value of Q, we find that the normal points now follow quite closely the theoretical curve for a homogeneous medium, with b equal to 0.15 A. A comparison between Figures 6 and 8 shows how differently the reddened stars behave from the unreddened ones. The conclusion that the D lines in unreddened stars are produced in a somewhat different way from the lines in the more reddened stars has already been suggested by the high line widths noted in Figures 1–4 for E_1, close to zero. The present evidence is much stronger and makes the result quite definite. Incidentally, the difference between Figures 6 and 8 provides another strong proof that color excess is directly related to the process of interstellar line formation.

As pointed out by Wilson and Merrill,[20] this decrease in Q with increasing D can be reconciled with a more nearly constant Q for greater D if the cloud elements are large. On this picture, a cloud extends some 500 pc or more, and the gradual decrease of Q with increasing D is the result of gradual penetration of more and more cloud with increasing distance. It is a necessary part of this theory that the distribution of velocities remain the same throughout the cloud, and with a value of b_i certainly not in excess of 0.15 A. The number of components found by Adams in interstellar H and K for stars within 300 pc and the wide lines found in reddened stars at similar distances make it difficult to see how all the clouds can be so large. Thus there seems no escape from the conclusion that the weak lines in unreddened stars are formed by an essentially different type of cloud from that which is responsible for strong lines in unreddened stars.

In view of the importance of this result, let us review briefly the evidence on which it is based. On the one hand, as pointed out by Merrill and Wilson,[20] the constancy of D_2/D_1 for stars near the nulls, as D increases from 0.4 A to 1.0 A, requires that different elements of gas in the line of sight have different radial velocities and that the optical depth through each element of uniform velocity be large compared to 1. This seems to be the only way that an increase of D can be produced without a sharp decrease in the doublet ratio. On the other hand, the high doublet ratio in unreddened stars with D equal to 0.20 A indicates that the optical depth between these stars and us is less than unity. These two conclusions seem definite. If the distances to these unreddened stars were less than the dimensions of a moving element, there would be no problem; but, in fact, the reverse seems to be true. These unreddened stars, with unsaturated lines, are found at all distances between 100 and 1000 pc; and, unless the assumed average absolute magnitudes are off by more than 1 mag., a substantial number of these stars must be at distances of 300–500 pc. The dimensions of a moving element are apparently much less than this, at least in many cases. Adams' data on the Ca^+ lines indicate a number of components in stars 300–500 pc away, and a similar number for Na seems reasonable. Also, many stars between 500 and 1000 pc show wide D lines, which must be produced by many moving elements. Finally, the general association between grains and gas suggested by this paper indicates that the moving elements may, in fact, be the individual obscuring clouds responsible for the general and selective extinction; we have already seen that the radius of a typical such cloud is probably about 8 pc. Thus the weight of evidence definitely favors the belief that two essentially different media produce the Na absorption in reddened and in unreddened stars.

What can be said about the medium responsible for the D lines in unreddened stars? The two important facts which we must consider are that the ratio-curve agrees with that of a homogeneous medium and that the line intensities do not seem to be correlated very exactly either with distance or with color excess. The large scatter in the correlation of D with distance is evident from Figures 1–4 and may also be seen in Figure 12 in the next section. If the scatter in the distance relation is real rather than a result of the dispersion in absolute magnitudes about the assumed values, then one cannot assume a homogeneous medium. An attractive possibility is the assumption of many small clouds, each of which has small optical depth in the D lines. Since each such cloud will absorb only a minute fraction of the radiation in the D lines passing through it, we shall refer to it as a

"transparent cloud," in contrast to the "opaque clouds" responsible for high selective absorption and strong D lines. As we have seen, such an assembly of transparent clouds will produce the same ratio-curve as a homogeneous medium but will have sufficient irregularity to give quite different D-line intensities for stars at the same distance. To predominate for close stars, these clouds must be intrinsically more numerous or of greater size than are the more opaque clouds. It is not impossible that each transparent cloud might consist of a less dense atmosphere or aura surrounding a dense or opaque cloud. If accurate data were available on the line intensities in stars of accurately known distance, the sizes and space distribution of these nearly transparent clouds might be assessed; but at the present time such an attempt would be difficult.

The velocity of these transparent clouds and the average number of atoms which they contain per square centimeter can be evaluated only approximately. First, we consider the average velocity. Figures 8 and 9 give a ratio-curve with b equal to 0.15 A, yielding a root-mean-square velocity of 5.4 km/sec, about 60 per cent of the corresponding velocity found in the preceding section for the opaque clouds. However, this value is almost certainly too low. Since the color excess of a single opaque cloud is assumed to be 0.024, the light from many of the relatively unreddened stars will pass through at least one of these opaque clouds and possibly as many as two or three. In Figures 8 and 9, the location of the points shown for Q between 1.1 and 1.3 are about what one would expect for a line produced by one to three opaque clouds. Figures 8 and 9 indicate only that, when the contribution of the opaque clouds disappears, that of the transparent clouds becomes dominant. If the values of Q and D were much more accurate, the greatest values of Q for each D would presumably be those unaffected by the opaque clouds, and these would permit an independent determination of b_e for these transparent clouds. At present we can conclude only that the data presented here indicate a root-mean-square velocity greater than 5 km/sec and are not inconsistent with the velocity of 9 km/sec found for the denser clouds. Whipple's[26] analysis of Adams' data[22] on the K and H lines shows that the more transparent clouds of Ca^+ have relatively high velocities, in the neighborhood of 25 km/sec. On the other hand, the data presented in the next section point very tentatively to a value more nearly 5 km/sec for the relatively transparent clouds of Na. While the failure of Merrill and Wilson[23] to find noticeable components for the D lines supports the hypothesis that the relatively transparent clouds of Ca^+ are moving much more rapidly than those of Na, more data are required before definite conclusions may be drawn.

One would expect that the lines absorbed by these relatively transparent clouds would show the effects of galactic rotation and that distant stars far from the nulls would show stronger, less saturated lines than would distant stars, close to the nulls. The observations do not support this expectation, since the triangles and circles in Figure 9 show no outstanding differences. However, the observational evidence is not strong, especially since there is only one star with a distance modulus greater than 11.0 and more than 15° away from the nulls. Moreover, stars of zero color index, known to be at great distance, are difficult to find. A search through the catalogues for faint unreddened stars of early spectral type should be an excellent method for locating stars below the main sequence. Thus an investigation of the galactic-rotation effects for these relatively transparent clouds would not be simple.

Next we consider the average number of neutral Na atoms in these transparent clouds. Here, again, care must be taken to disentangle the effects produced by the more opaque clouds. The unsaturated lines, with Q about equal to 1.60 A and D equal to 0.20 A, can obviously not be much affected by the opaque clouds, a single one of which produces a saturated line with D equal to about 0.15 A. The number of atoms producing an unsaturated line with D equal to 0.20 A is about $2 \times 10^{12}/\text{cm}^2$. The distance of the stars in question averages about 400 pc, as may be seen from Figure 12 in the next section. Thus we find 5×10^{12} Na atoms in transparent clouds per square centimeter per kiloparsec.

This is about one-fourth the value found in the preceding section for the average number in opaque clouds per kiloparsec.

However, a correction to the computed properties of the opaque clouds must also be made, since the relatively transparent clouds must contribute to the interstellar D lines in reddened stars also. Evidently, the saturation value of D for large E_1 will not be much affected by additional absorbing atoms, and thus the value of b_{e0} found for the opaque clouds remains unchanged. The constant q might be somewhat altered; but, since this constant is determined to give the best fit for the close stars, shown in Figure 1, the change will not be large. In any case, the selective absorption produced by a single opaque cloud is so uncertain that a precise estimate of q is not of much physical interest. The chief effect of the relatively transparent clouds will be to increase somewhat the saturation of the strong D lines produced by the opaque clouds and thus to increase the computed value of N_0, the number of atoms per square centimeter in a single opaque cloud, over its true value. One would expect the importance of this effect to increase with distance; a comparison of Figures 6 and 7 does not show any indication of this effect; but, in view of the large observational scatter, this is not too unexpected. We may therefore proceed to correct N_0 by subtracting out the number of atoms found above in the relatively transparent clouds. The value of N for the opaque clouds was previously determined as 2×10^{13} atoms/cm^2/kpc. If the corresponding estimate for the transparent clouds, 5×10^{12} atoms/cm^2/kpc, is subtracted, we find 1.5×10^{13} atoms/cm^2/kpc as the final number of atoms in the opaque clouds. The ratio of the number of atoms in opaque and transparent clouds is therefore 3:1, and the corrected value of C_0, the optical depth of a single cloud in the center of its D_1 line, must be reduced to three-fourths of the value found above, or about 2.3. If it is again assumed that a straight line in the galactic plane intersects seven opaque clouds per kiloparsec, the corrected value of N_0 becomes 2×10^{12}.

These results make it possible to evaluate the density of neutral *Na* in interstellar space, a quantity of considerable physical interest. If the atoms in both types of clouds near the galactic plane are averaged over the space in and between the clouds, the total particle density is 2×10^{13}/cm^2/kpc, which gives about 7×10^{-8} atoms/cm^3. The corresponding averages for the opaque clouds and transparent clouds separately are 5.3×10^{-8} and 1.7×10^{-8}, respectively. The earlier estimate of 3×10^{-8} atoms/cm^3, obtained by Wilson and Merrill,[20] is about midway between the present values for the two types of clouds. The actual density of atoms inside the transparent clouds cannot be estimated, since there is no information on the sizes of these clouds. However, the density within an opaque cloud can be estimated, if, in accordance with the discussion in Section I-*a*, the radius of a typical opaque cloud is taken to be 8 pc and the number of clouds per kiloparsec is set equal to 7. A line through seven clouds then passes through 112 pc of cloud, and the average density of *Na* atoms found above may be multiplied by 1000/112 to obtain a true space density of about 5×10^{-8} neutral *Na* atoms per cubic centimeter inside an opaque cloud.

Finally, we may consider the ratio of grains to atoms in these two types of clouds. We have already seen that the opaque clouds are apparently also clouds of grains. If the relative number of grains in the transparent clouds is the same as the relative number of neutral *Na* atoms, these clouds should produce an average selective extinction of about 0.05 mag. per kiloparsec. With the present data such a small extinction could not be disentangled from the extinction produced by a few opaque clouds. Thus no conclusions on the density of solid particles in the transparent *Na* clouds can be drawn at the present time.

d) SUMMARY

We have seen in this section that the doublet ratio behaves consistently with the assumption that in reddened stars the interstellar D lines are formed by small clouds, each

with an optical depth at the line center equal to about 2.3 and 4.6 for D_1 and D_2, respectively, and with 2×10^{12} atoms/cm^2 of neutral *Na* in each cloud. For these reddened stars, any effects produced by differences between different clouds cannot be detected with certainty from the present observational material. In the spectra of unreddened stars the doublet ratio behaves in a quite different way with D, providing another indication of the connection between color excess and the formation of interstellar lines. In these unreddened stars the D lines are apparently produced by clouds of small optical depth and with a root-mean-square cloud velocity probably greater than 5 km/sec. The total number of neutral *Na* atoms in the line of sight, including the contribution of both types of clouds, is about 2×10^{13} atoms in a cylinder 1 cm^2 in cross-section and 1000 pc in length. This corresponds to an average particle density of about 7×10^{-9} neutral atoms per cubic centimeter. Roughly three-fourths of these atoms are in relatively opaque clouds, with the remaining fourth in relatively transparent clouds. With reasonable assumptions for the number of opaque clouds per kiloparsec and the average radius of each such cloud, the density of neutral *Na* in these opaque clouds is found to be 5×10^{-8} atoms/cm.[3]

V. VARIATION OF EQUIVALENT WIDTH WITH DISTANCE

In the past the intensities of the interstellar lines have frequently been used to determine the distances of individual early-type stars. Among the most recent such investigations is the thorough study by van Rhijn,[44] who found a mean error of about 40 per cent for a distance determined in this way. In view of the importance of these distance determinations, it is of interest to re-examine how the intensity of the interstellar D lines changes with distance. While such a study gives no new information on the distribution of *Na* atoms, other than that obtained in previous sections, it indicates certain limitations on the use of the D lines to determine individual distances of B and O stars and suggests possible improvements in this method of distance determination.

The theoretical picture developed in the preceding section makes certain definite predictions on the variation of D with distance r. Since we have already seen that different types of clouds must be assumed for the behavior of the D lines in reddened and unreddened stars, we shall consider these two groups of stars separately.

a) VARIATION WITH DISTANCE IN REDDENED STARS

We have seen that to an adequate first approximation the clouds forming D lines in reddened stars may all be assumed identical, with the number of such clouds in the line of sight proportional to E_1. Let us consider how D changes with r when E_1 and n, the number of clouds in the line of sight, are held constant. If E_1 is so small that the clouds do not overlap, D will equal nD_0, and there will be no change with r. When E_1 and n are large enough to guarantee considerable overlap of the clouds, the picture changes. Then at close distances D will again be independent of r but will show considerable scatter about its average value, depending on the varying overlapping between different clouds. At intermediate distances the effect of galactic rotation will be important in averting overlap between clouds, and a progressive increase of D with distance is to be expected. At very great distances, none of the clouds will overlap, D will equal nD_0 and will show no change with increasing distance.

Figures 1–4 have indicated that, if E_1 exceeds 0.10, the clouds are sufficiently numerous to overlap somewhat at close distances, and for E_1 greater than 0.20 the overlap becomes quite impressive. Thus, for stars of these color excesses, considerable variation of D with r is to be expected for a certain range of r. If all stars with a color excess equal to or greater than 0.10 are grouped together, this variation with r will be enhanced by the tendency of E_1 to increase with distance. For stars near the nulls the variation of D with r should

[44] *Groningen Pub.*, No. 50, 1946.

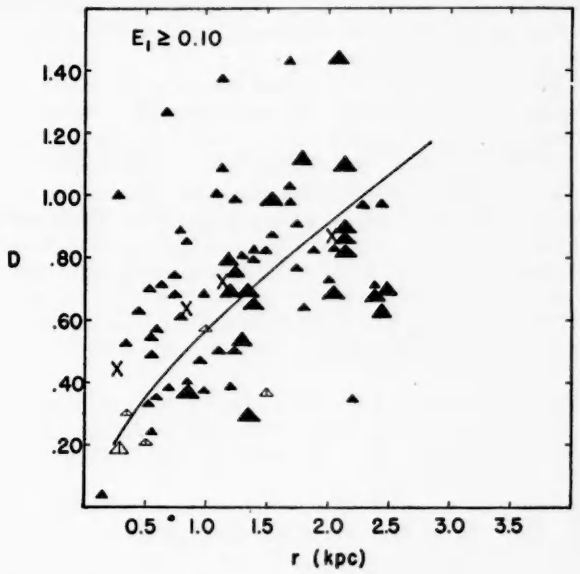

FIG. 10.—Change of D-line intensity with distance from the sun for reddened stars (E_1 equal to 0.10 or greater) at least 15° from the nulls of galactic rotation. Large symbols denote stars of measured spectroscopic parallax.

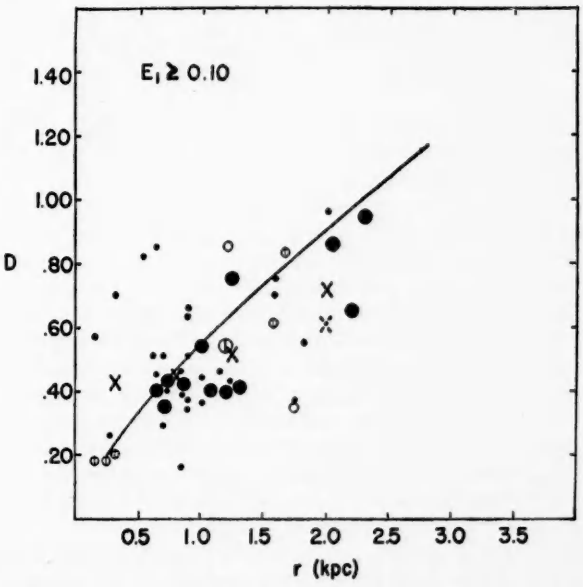

FIG. 11.—Change of D-line intensity with distance from the sun for reddened stars (E_1 equal to 0.10 or greater) within 15° of the nulls of galactic rotation. Large symbols denote stars of measured spectroscopic parallax.

be less marked; for stars exactly at the nulls there should, of course, be no variation of D with r on this picture, except for that resulting from the weak correlation of E_1 with distance.

Figures 10 and 11 indicate how the observed values of D actually vary with the distance r for reddened stars. The distances are determined as before from values of the spectroscopic distance modulus. Stars for which the absolute magnitude was determined spectroscopically by Morgan are represented by large symbols. These points were given twice the weight of other points in the computation of the normal points. The various symbols used have the same meaning as before.[45] The solid line represents the average curve adopted by van Rhijn;[44] his small term $f(l)$, giving a dependence of D on galactic longitude, has not been included. The dashed-line normal point for the most distant stars in Figure 11 indicates the average value of D_{corr} for these stars; the computation of D_{corr} has been discussed in Section III-*d*. This normal point indicates that when account is taken of the effects due to galactic rotation, the variation of D with r for stars near the nulls is materially reduced.

It is evident from these figures that the variation of D with r for reddened stars is about what one would expect on the basis of the considerations described immediately above. Stars near the nulls show only a small increase with distance, while for stars far

TABLE 3

STARS OF POSSIBLY HIGH LUMINOSITY

HD	Type	m	RA (1900)	Dec. (1900)	M_{SHW}	M_{theor}
17088	B6	7.54	2^h39^m5	+57° 19′	−1.4	−4
227836	B2e	9.6	20 4.3	+35 50	−3.0	−6
223385	cA2ea	5.61	23 44.0	+61 40	−5.5	−8
223960	cA0ea	6.98	23 48.9	+60 18	−5.5	−7

from the nulls a considerable increase occurs. Out to 1500 pc this increase is approximately linear but intersects the vertical axis not at zero but at about the nearly constant value for stars near the nulls, again in accord with expectations. For stars beyond 1500 pc no further increase of D with r is to be expected if E_1 is less than 0.20. For redder stars, an additional increase is to be expected, but for such highly reddened stars at such great distances additional data are not easily obtained.

There are no high latitude stars in Figures 10 and 11. The few stars at intermediate latitude seem to behave about the same as the low-latitude stars.

In Figure 10 there are four stars in which the D lines are much stronger than one would expect from the computed distance and for which no detailed spectroscopic absolute magnitudes are available. These stars, some of which have already been noted in Section III, may actually be brighter and hence more distant than assumed. A list of these stars is given in Table 3, with their HD number, spectral type, and visual magnitude, all taken from MWC 621. In the last two columns are given the average absolute magnitudes adopted by Stebbins, Huffer, and Whitford for each spectral type and the absolute magnitudes that would be required to make these stars agree more nearly with the other stars shown in Figures 10 and 11. Merrill[46] has characterized HD 223385 as "an outstanding c star, probably brighter than the average c." If the distance moduli given

[45] The open and barred circles and triangles have the same meaning as in Figs. 1 and 3. Thus an open point at a distance less than 1 kpc denotes a star whose galactic latitude exceeds 20°, while at a greater distance the same point indicates that the galactic latitude exceeds 10°. Similarly, a barred point indicates a galactic latitude between 10° and 20° if r is less than 1 kpc, but between 5° and 10° for greater r.

[46] Informal communication.

for these stars in MWC 621 are essentially correct, the distribution of cloud velocities must be non-Maxwellian. Thus a spectroscopic study of the absolute magnitudes of these stars should be of importance in the study of interstellar matter. The corresponding stars which show D lines too weak for their distances are less interesting, since this effect may be explained by overlapping of the components produced by separate clouds.

b) VARIATION WITH DISTANCE IN UNREDDENED STARS

Next we consider the unreddened stars, with E_1 less than 0.10 mag. If all clouds were identical, we should expect somewhat the same results as for the redder stars, except that now the number of clouds would be so small that the separate components would not be likely to overlap at any range. As a result, D would be independent of r at all distances

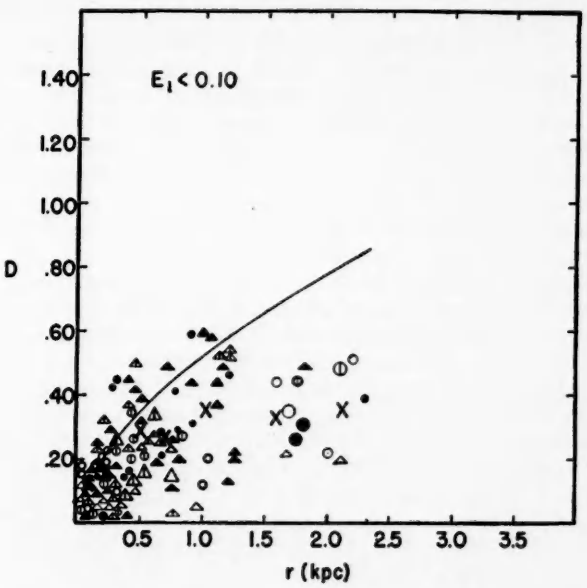

FIG. 12.—Change of D-line intensity with distance from the sun for unreddened stars (E_1 less than 0.10). Large symbols denote stars of measured spectroscopic parallax.

and would be directly proportional to E_1. If all stars with low E_1 are grouped together, the systematic increase of E_1 with distance would lead to a systematic increase of D with r, but with large scatter. However, we have already seen that the formation of the D lines in these unreddened stars must be explained on the basis of relatively transparent clouds, scattered more uniformly in space than are the relatively opaque clouds. Such clouds will give a more nearly linear increase of D with r, until the lines become saturated. For stars at distances beyond the saturation limit, the effect of galactic rotation should become significant, producing wider lines for stars far from the nulls.

Figure 12 presents the observational data for these unreddened stars. The symbols have the same meaning as before. The expected increase of D with r at close range is clearly evident. Beyond 1000 pc no further variation of D with r is found, the average value of D remaining constant at about 0.35 A. This saturation value is what we would expect if the root-mean-square velocity of the more transparent clouds were about 5 km/sec, corresponding to b equal to 0.14 A. This result suggests that the transparent clouds may, in fact, have lower velocities than do the more opaque clouds. However, eight of the twelve stars beyond 1500 pc lie more than 150 pc away from the galactic plane, with six

of these more than 300 pc away. Moreover, the color indices of these twelve stars are low, with only four values of E_1 exceeding 0.03. Possibly it is this observational selection at great distances rather than a low value of b_c which accounts for the failure of D to increase with increasing r. In view of the possibility, also, both of regional variations in the properties of the interstellar vapor and of considerable errors in the stellar distances used, no definite conclusions can be drawn in this connection at the present time.

c) CONCLUSIONS AND COMPARISONS WITH OTHER INVESTIGATIONS

While there are a number of theoretical problems in connection with these three figures, and especially with Figure 12, it is evident that the computed normal points for each group differ significantly from van Rhijn's[44] curve. Moreover, for reddened stars near the nulls of galactic rotation the change of the average D with distance becomes so small that for these stars the D lines become a poor criterion of individual distances. For unreddened stars D seems to show no change at all with distance beyond 1000 pc, and, if D has a value greater than 0.25 A, the distance is very poorly determined. One might argue that the average distance for stars whose D lines have a particular intensity would be more useful for distance determination than would the average line intensity for stars at a particular distance. As a result of various statistical effects, this former average is much less dependent on E_1 and on galactic longitude than is the latter. However, as van Rhijn points out, this former type of average has the disadvantage that it will be different for stars of each different spectral subclass.

One can draw two conclusions from this study of the change of D with r. In the first place, the correlation of D with E_1 and l must be kept in mind when the D lines are used for determining individual stellar distances. In the second place, the data are generally consistent with the results obtained from the previous sections and indicate that, in part, the D lines are formed by opaque clouds, identical with the clouds of grains responsible for selective extinction. In part, the lines are formed also by more numerous clouds, each one nearly transparent in the D lines and not necessarily associated with the solid grains. The behavior of unreddened stars beyond 1500 pc requires further study to indicate the velocity and space distribution of these relatively transparent clouds.

The conclusion that the *Na* atoms are concentrated in clouds is in contradiction to the work of Evans[24] and Schilt,[25] who found that the *Na* atoms were uniformly distributed in space and showed no physical connection with the clouds of solid grains. Evans' result is primarily based on the fact that the average distance found for stars with a particular D-line intensity showed no correlation with color excess. While Evans used the radial velocities of the interstellar lines to determine distances, the same result is obtained if the spectroscopic distance moduli are used, as may be seen by a comparison of Figures 10 and 11, on the one hand, with Figure 12, on the other. The overlap between the figures is significant only for D between 0.30 and 0.50 A. Within this region the distances of the reddened stars cluster about 1000 pc, with relatively low dispersion. The unreddened stars with D lines in this intensity range show about the same average distance as do the reddened ones. This results from a cancellation of two effects. On the one hand, the D lines in the most distant unreddened stars (r greater than 1500 pc) have intensities in this range. On the other hand, a quite small fraction of the unreddened close stars (r less than 500 pc) have D lines of this intensity; the number of these very close unreddened stars is so high, relatively speaking, that there are about as many close stars with D-line intensities between 0.30 and 0.50 A as there are distant ones. Thus the result obtained by Evans finds a qualitative explanation on the basis of the picture adopted here.

On the other hand, to explain the differences between Figures 10, 11, and 12 on the basis of a uniform and homogeneous distribution of *Na* atoms is quite difficult. Such an explanation would require not only that the distances be unreliable but also that the differences shown result from a high correlation between E_1 and r. Such a uniform distribu-

tion of obscuring matter is contrary to all recent evidence and is, in fact, ruled out by Evans in his paper. The assumption that the distribution of atoms and grains is independent faces, in any case, a great difficulty in the differences shown between Figures 6 and 7, on the one hand, and Figures 8 and 9, on the other. The difference between reddened and unreddened stars in the change of D_2/D_1 with D is independent of stellar distances and seems to require some connection between atoms and grains.

Evans also argues that the dispersion in D for stars at a given distance is relatively small—about 20 per cent. This result is obtained from the fact that the dispersion in the plot of r against D—about 0.84 kpc—is almost equal to that computed from the spread in velocities for stars near the nulls of galactic rotation. When account is taken of the possible correlation between equivalent width and radial velocity for stars at a constant distance, this argument loses much of its force, and van Rhijn's estimated 40 per cent for the mean error of an individual distance found in this way seems more realistic.

Schilt[25] bases his conclusions about the coextensiveness of *Na* atoms and clouds of grains on a study of the scatter in D, K, and E_1. The procedure followed is, first, to sort two of these items—D and K, for example—into groups, according to the values of the third item—in this example E_1. Then in each group the mean values of D and K are computed, together with the dispersion of D and K from their means in each group. The ratio of the dispersions found for D and K is then used as the "relation between D and K, sorted by the neutral item E_1." The same process gives relations between D and E_1, E_1 and K, etc. Since the observational errors of these three quantities are widely different, it seems doubtful whether the results obtained by computing the dispersions from group means would agree with those obtained in other ways. One may conclude that the arguments advanced by Evans and Schilt are not sufficiently compelling to cast serious doubt on the validity of the conclusions reached in the present paper.

It is a pleasure to record here my indebtedness to the Mount Wilson Observatory, and to its director, Dr. Ira S. Bowen, for use of the 100-inch telescope in the course of this investigation. I am particularly indebted to Dr. Bengt Strömgren and Dr. A. Unsöld for a number of useful comments and to Dr. Paul W. Merrill and Dr. Olin C. Wilson for patient guidance in observational matters, as well as for a number of helpful discussions on problems of interpretation. Mr. I. Epstein has aided materially by reducing the bulk of the tracings and carrying out many of the necessary computations.

ON THE CHEMICAL COMPOSITION OF THE SUN FROM ITS INTERNAL CONSTITUTION

MARJORIE HALL HARRISON
Yerkes Observatory
Received June 22, 1948

ABSTRACT

The variation in the guillotine factor having been taken into consideration, the chemical composition of the sun has been determined on the assumption that it consists of hydrogen, helium, and some combination of oxygen and Russell mixture. The abundances of hydrogen and helium as functions of the "oxygen" abundance have been determined.

I. THE GUILLOTINE FACTORS

1. *Introduction.*—By using both the mass-luminosity relation and the energy-generation equation, M. Schwarzschild[1] was able to determine the hydrogen and the helium content of the sun on the assumption that the rest of the composition consists of Russell mixture. Making the additional assumption that the chemical composition of the sun is uniform, Schwarzschild found a hydrogen-metal ratio which appears incompatible with the analysis of stellar atmospheres.

By the introduction of a third parameter this discrepancy between theory and observations might be partially removed. The additional parameter which may be used for this purpose is the abundance of elements of the oxygen group (*C*, *N*, *O*, *Fe*, *Ne*). The importance of such elements arises from the fact that at a temperature of $20 \times 10^{6\circ}$ K these atoms are beginning to be stripped to their bare nucleii, and their contribution to the opacity will decrease very rapidly for increasing temperatures. Also, the analysis of stellar atmospheres would appear to indicate that the abundances of these elements are underestimated in the Russell mixture.

In order to carry out an investigation of such stellar models, it was necessary, first of all, to compute opacity tables for various combinations, by weight, of Russell mixture and oxygen.

2. *The method.*—The calculations of opacity were carried out according to the theory and notation given by B. Strömgren.[2] We then have

$$\chi_n^{(z)} = \frac{2\pi^2 e^4 m_e Z^2}{n^2 h^2}, \tag{1}$$

$$D_n = D_{\text{f.e.}} \frac{2}{n} \frac{\chi_n}{kT} \frac{e^{\chi_n/kT}}{1 + \exp\left(\frac{\chi_n}{kT} - \frac{\psi}{kT}\right)}, \tag{2}$$

$$D(x) = D(x_i, x_{i+1}), \tag{3}$$

$$\tau(x_i, x_{i+1}) = \frac{\phi(x_i) - \phi(x_{i+1})}{D(x_i, x_{i+1})}, \tag{4}$$

and

$$\tau = \Sigma \tau(x_i, x_{i+1}). \tag{5}$$

The results of these calculations are given in Table 1 for various combinations of oxygen and Russell mixture. Some of these tables are incomplete, since only the values which were actually needed were computed.

[1] *Ap. J.*, **104**, 203, 1946.

[2] *Zs. f. Ap.*, **4**, 118, 1932.

In order to determine the guillotine factors for any combination of oxygen and Russell mixture, it was necessary to compute tables for oxygen and Russell mixture separately (Tables 2 and 3); then, by a suitable combination of these two tables, the guillotine factor for any combination could be computed. As an example, we have reproduced here sample tables for a combination of 60 per cent oxygen and 40 per cent Russell mixture for a temperature of $20 \times 10^{6^\circ}$ K. Table 4 was calculated by this method. It was found that an accuracy in the third decimal place in the D_n's could be reached; this is sufficient for our purposes.

It is evident from Table 5 that the absorption edges for this particular combination of oxygen and Russell mixture are given by multiplying all the D_n's for Russell mixture by 0.5 and adding 0.5 times the D_n's for pure oxygen.

II. THE STELLAR MODELS

3. *Introduction.*—We can derive some knowledge regarding the relative abundances of *H*, *He*, *O*, and Russell mixture if we assume that, according to the conditions found in the sun's atmosphere, the Russell mixture is replaced by some combination of oxygen and Russell mixture. The assumptions made for these models are as follows:

1. The composition (and consequently the molecular weight, μ) is constant throughout the star.
2. The radiation pressure is negligible.
3. The star consists of a convective core and an envelope in radiative equilibrium.
4. The entire energy generation from nuclear sources occurs within the convective core.

Since all the models are computed in exactly the same manner, we shall give the complete theory for only one model, namely, that for which the heavy elements are represented by a combination of 60 per cent oxygen and 40 per cent Russell mixture.

4. *Equations of the model for the outside.*—We have the usual envelope equations

$$\frac{dP}{dr} = -\frac{GM(r)}{r^2}\rho , \tag{6}$$

$$\frac{dM(r)}{dr} = 4\pi\rho r^2 , \tag{7}$$

$$\frac{d}{dr}\left(\tfrac{1}{3}aT^4\right) = -\frac{L}{4\pi c r^2}\frac{\kappa_0\rho^2 T^{-3.5}}{\tau} , \tag{8}$$

where the various symbols have their usual meaning and τ is the guillotine factor, which varies throughout the star. In order to be able to proceed with the problem, we must determine τ as a function of the density and temperature; but, since we have no knowledge of this distribution until the model has been computed, we must make a guess. In so far as there is not a great deal of difference in the guillotine factors as we pass along the sequence of tables that have been computed, it was decided to use the density-temperature distribution as it had been computed for another model. For the 60 per cent oxygen and 40 per cent Russell mixture model we used the temperature-density distribution as computed by M. Schwarzschild.[3] This method proved successful. We then have ρ, T throughout the star, and also the hydrogen content X, so that we can compute $\log_e G(T)/N_e$. Interpolation in the tables then yields τ.

A graphical method was used to determine the variation in τ. The best two lines (see Fig. 1) were drawn through a plot of $\log \tau$ against $\log \rho$, thus giving two forms for the guillotine factor, one for the outside and one for the inside. For the model under consideration we have, outside,

$$\tau = 1.7266\rho^{-0.0126} , \qquad \log\rho \leqslant +0.0261 , \tag{9}$$

inside,

$$\tau = 1.6757\rho^{+0.4849} , \qquad \log\rho \geqslant +0.0261 . \tag{10}$$

[3] *Op. cit.*, p. 205.

TABLE 1

Guillotine Factor $\text{Log}_{10}\,\tau$

	100% Oxygen						99% Oxygen 1% Russell Mixture						97.5 % Oxygen 2.5% Russell Mixture					
	$\log_e [G(T)/N_e]$																	
$Tx10^{-6}$	2	3	4	5	6	∞	2	3	4	5	6	∞	2	3	4	5	6	∞
0.625					0.344	0.320					0.336	0.274					0.326	0.255
0.714					0.408	0.386					0.389	0.301					0.367	0.267
0.833					0.533	0.516					0.491	0.417					0.449	0.326
1.0					0.695	0.684					0.666	0.593					0.605	0.505
1.25					0.802	0.794					0.733	0.699					0.658	0.604
1.67					0.773	0.769					0.740	0.729					0.694	0.548
2.0				0.679	0.668	0.661				0.657	0.643	0.639				0.627	0.611	0.598
2.5				0.512	0.499	0.482				0.481	0.470	0.438				0.470	0.449	0.403
3.0			0.480	0.429	0.407	0.394			0.473	0.415	0.387	0.328			0.461	0.398	0.360	0.297
4.0		0.732	0.630	0.585	0.567	0.556		0.721	0.611	0.549	0.509	0.425		0.708	0.586	0.508	0.449	0.340
5.0		0.930	0.856	0.825	0.813	0.806		0.915	0.828	0.777	0.740	0.695		0.894	0.791	0.718	0.661	0.588
6.0		1.099	1.044	1.021	1.012	1.007		1.074	1.008	0.964	0.928	0.840		1.052	0.962	0.896	0.845	0.774
6.25		1.136	1.084	1.062	1.055	1.050		1.115	1.047	1.003	0.967	0.874		1.086	0.999	0.933	0.881	0.806
7.0	1.331	1.234	1.189	1.172	1.165	1.161		1.210	1.147	1.103	1.059	0.944		1.175	1.092	1.024	0.964	0.876
8.0	1.423	1.341	1.305	1.290	1.285	1.281		1.289	1.257	1.202	1.147	1.023		1.269	1.186	1.108	1.036	0.933
9.0	1.500	1.428	1.406	1.384	1.380	1.377		1.408	1.330	1.271	1.210	1.100		1.340	1.251	1.163	1.082	0.985
10.0	1.565	1.501	1.473	1.462	1.459	1.456		1.456	1.392	1.326	1.263	1.174		1.399	1.303	1.207	1.124	1.027
11.0	1.618	1.560	1.538	1.528	1.522	1.520		1.508	1.437	1.364	1.298	1.220		1.441	1.337	1.235	1.155	1.072
12.0	1.667	1.614	1.592	1.584	1.581	1.579	1.634	1.549	1.470	1.387	1.317	1.253	1.590	1.477	1.366	1.262	1.185	1.113
12.5	1.689	1.638	1.617	1.609	1.606	1.604	1.654	1.571	1.491	1.408	1.337	1.260	1.607	1.492	1.376	1.270	1.195	1.126
13.0	1.708	1.659	1.640	1.632	1.628	1.627	1.672	1.589	1.507	1.418	1.344	1.264	1.623	1.505	1.387	1.278	1.203	1.135
14.0	1.744	1.700	1.680	1.673	1.671	1.669	1.706	1.621	1.534	1.438	1.357	1.271	1.651	1.531	1.405	1.292	1.215	1.149
15.0	1.776	1.734	1.724	1.710	1.707	1.706	1.734	1.649	1.563	1.455	1.368	1.276	1.682	1.561	1.421	1.302	1.222	1.153
16.0	1.800	1.762	1.745	1.739	1.737	1.735	1.756	1.673	1.579	1.473	1.383	1.289	1.700	1.574	1.437	1.312	1.229	1.158
16.7	1.822	1.785	1.769	1.763	1.761	1.759	1.777	1.693	1.598	1.490	1.401	1.309	1.716	1.588	1.449	1.321	1.236	1.164
17.0	1.830	1.793	1.777	1.771	1.769	1.768	1.784	1.700	1.605	1.497	1.409	1.319	1.722	1.595	1.454	1.326	1.240	1.168
18.0	1.852	1.818	1.803	1.798	1.795	1.795	1.806	1.723	1.628	1.523	1.439	1.358	1.742	1.614	1.471	1.343	1.258	1.187
19.0	1.869	1.835	1.821	1.816	1.814	1.813	1.822	1.741	1.649	1.551	1.476	1.404	1.764	1.636	1.515	1.367	1.285	1.217
20.0	1.892	1.861	1.848	1.842	1.841	1.839	1.845	1.766	1.677	1.585	1.519	1.461	1.780	1.655	1.517	1.395	1.317	1.230
21.0	1.909	1.879	1.866	1.862	1.860	1.859	1.862	1.786	1.701	1.619	1.562	1.514	1.798	1.675	1.542	1.427	1.357	1.302
22.0	1.925	1.896	1.884	1.880	1.878	1.877	1.878	1.804	1.726	1.653	1.605	1.566	1.815	1.696	1.568	1.463	1.400	1.365
23.0	1.940	1.912	1.900	1.896	1.894	1.893	1.894	1.823	1.755	1.686	1.646	1.615	1.831	1.716	1.589	1.482	1.445	1.404
24.0	1.953	1.926	1.915	1.911	1.910	1.909	1.908	1.840	1.773	1.717	1.684	1.659	1.846	1.736	1.624	1.538	1.490	1.455
25.0	1.966	1.940	1.929	1.925	1.924	1.923	1.921	1.857	1.795	1.747	1.720	1.700	1.860	1.755	1.651	1.575	1.534	1.504
26.0	1.977	1.952	1.942	1.938	1.937	1.936	1.934	1.873	1.817	1.775	1.752	1.736	1.873	1.774	1.678	1.610	1.575	1.550
28.0	1.998	1.975	1.966	1.962	1.960	1.960	1.957	1.902	1.856	1.825	1.809	1.798	1.901	1.810	1.730	1.677	1.651	1.617
30.0	2.016	1.994	1.986	1.982	1.981	1.980	1.978	1.928	1.890	1.867	1.856	1.848	1.925	1.843	1.776	1.736	1.716	1.703

TABLE 1-Continued

	95% Oxygen 5% Russell Mixture						90% Oxygen 10% Russell Mixture						80% Oxygen 20% Russell Mixture					
$Tx10^{-6}$	2	3	4	5	6	∞	2	3	4	5	6	∞	2	3	4	5	6	∞
0.625					0.314	0.240					0.294	0.225					0.276	0.212
0.714					0.342	0.243					0.310	0.217					0.279	0.199
0.833					0.401	0.265					0.346	0.238					0.294	0.204
1.0					0.536	0.425					0.452	0.342					0.364	0.270
1.25					0.573	0.508					0.468	0.398					0.360	0.292
1.67					0.631	0.611					0.501	0.474					0.425	0.393
2.0				0.585	0.565	0.548				0.521	0.494	0.474				0.425	0.391	0.364
2.5				0.441	0.417	0.384				0.400	0.369	0.334				0.326	0.255	0.253
3.0			0.442	0.371	0.326	0.260			0.413	0.332	0.281	0.217			0.314	0.274	0.217	0.161
4.0		0.687	0.550	0.452	0.375	0.255		0.658	0.501	0.380	0.292	0.176		0.606	0.423	0.286	0.193	0.097
5.0		0.862	0.737	0.641	0.522	0.483		0.814	0.663	0.543	0.456	0.362		0.732	0.546	0.405	0.308	0.210
6.0		1.011	0.899	0.814	0.752	0.683		0.950	0.812	0.705	0.633	0.563		0.850	0.678	0.549	0.467	0.389
6.25		1.043	0.934	0.851	0.790	0.757		0.980	0.844	0.740	0.671	0.636		0.877	0.708	0.583	0.504	0.430
7.0		1.128	1.024	0.939	0.874	0.799		1.058	0.928	0.827	0.759	0.694		0.945	0.790	0.671	0.591	0.528
8.0		1.216	1.115	1.019	0.944	0.860		1.139	1.009	0.904	0.912	0.764		1.024	0.872	0.756	0.680	0.610
9.0		1.279	1.169	1.067	0.984	0.894		1.192	1.066	0.947	0.969	0.797		1.075	0.924	0.804	0.727	0.659
10.0		1.331	1.214	1.103	1.017	0.930		1.239	1.098	0.977	0.895	0.822		1.120	0.963	0.838	0.758	0.690
11.0		1.364	1.239	1.124	1.041	0.964		1.265	1.123	0.992	0.911	0.843		1.142	0.981	0.855	0.777	0.713
12.0	1.533	1.393	1.261	1.146	1.068	1.000	1.454	1.287	1.134	1.009	0.932	0.869	1.349	1.155	0.997	0.872	0.797	0.739
12.5	1.546	1.404	1.267	1.153	1.078	1.014	1.464	1.294	1.137	1.014	0.939	0.878	1.356	1.166	0.999	0.876	0.803	0.748
13.0	1.559	1.413	1.274	1.159	1.086	1.025	1.475	1.301	1.142	1.019	0.945	0.888	1.363	1.170	1.003	0.880	0.810	0.757
14.0	1.582	1.431	1.285	1.169	1.098	1.041	1.491	1.312	1.150	1.028	0.958	0.905	1.374	1.176	1.007	0.888	0.822	0.774
15.0	1.604	1.445	1.293	1.173	1.102	1.047	1.506	1.320	1.154	1.032	0.964	0.915	1.383	1.179	1.009	0.890	0.828	0.783
16.0	1.622	1.460	1.301	1.178	1.105	1.050	1.521	1.330	1.158	1.035	0.968	0.918	1.391	1.182	1.007	0.891	0.830	0.787
16.7	1.634	1.470	1.308	1.181	1.108	1.052	1.531	1.337	1.162	1.037	0.970	0.921	1.399	1.185	1.008	0.892	0.832	0.790
17.0	1.640	1.475	1.311	1.183	1.108	1.052	1.536	1.340	1.163	1.038	0.970	0.921	1.402	1.187	1.008	0.891	0.831	0.790
18.0	1.658	1.490	1.322	1.191	1.116	1.058	1.550	1.350	1.170	1.043	0.974	0.925	1.412	1.192	1.010	0.892	0.832	0.791
19.0	1.677	1.507	1.338	1.206	1.130	1.073	1.567	1.365	1.181	1.053	0.984	0.934	1.423	1.202	1.014	0.894	0.835	0.792
20.0	1.693	1.524	1.355	1.224	1.150	1.095	1.581	1.378	1.194	1.065	0.997	0.951	1.436	1.209	1.021	0.901	0.841	0.800
21.0	1.710	1.543	1.376	1.250	1.180	1.127	1.597	1.395	1.211	1.084	1.017	0.970	1.449	1.221	1.033	0.912	0.853	0.812
22.0	1.726	1.562	1.401	1.280	1.214	1.166	1.613	1.413	1.232	1.109	1.045	1.000	1.464	1.236	1.048	0.929	0.870	0.830
23.0	1.743	1.583	1.428	1.315	1.254	1.211	1.630	1.433	1.257	1.139	1.079	1.037	1.479	1.252	1.080	0.951	0.895	0.857
24.0	1.759	1.604	1.456	1.352	1.297	1.259	1.646	1.453	1.284	1.173	1.117	1.078	1.495	1.271	1.090	0.978	0.924	0.888
25.0	1.774	1.625	1.486	1.390	1.342	1.308	1.663	1.475	1.313	1.175	1.158	1.124	1.511	1.291	1.116	1.009	0.958	0.925
26.0	1.790	1.646	1.516	1.429	1.386	1.357	1.679	1.497	1.344	1.248	1.201	1.170	1.528	1.313	1.144	1.044	0.996	0.966
28.0	1.819	1.688	1.575	1.505	1.471	1.449	1.711	1.543	1.407	1.326	1.288	1.263	1.562	1.359	1.206	1.118	1.078	1.052
30.0	1.847	1.728	1.632	1.576	1.549	1.532	1.742	1.588	1.470	1.403	1.372	1.352	1.596	1.407	1.270	1.195	1.162	1.140

TABLE 1-Continued

	70% Oxygen 30% Russell Mixture						60% Oxygen 40% Russell Mixture						50% Oxygen 50% Russell Mixture					
$Tx10^{-6}$	2	3	4	5	6	∞	2	3	4	5	6	∞	2	3	4	5	6	∞
0.625					0.272	0.209					0.272	0.212					0.275	0.216
0.714					0.266	0.194					0.262	0.193					0.263	0.198
0.833					0.272	0.192					0.262	0.190					0.258	0.200
1.0				0.412	0.322	0.236					0.297	0.220					0.282	0.210
1.25				0.448	0.306	0.237					0.274	0.204					0.252	0.188
1.67				0.403	0.353	0.318					0.288	0.267					0.270	0.230
2.0				0.364	0.325	0.293				0.320	0.279	0.243				0.289	0.244	0.205
2.5			0.369	0.282	0.242					0.250	0.207	0.164				0.227	0.180	0.138
3.0		0.506	0.338	0.235	0.177				0.316	0.210	0.149	0.100				0.190	0.131	
4.0	0.823	0.570	0.374	0.248	0.143			0.543	0.340	0.201	0.114	0.033			0.343	0.175	0.113	
5.0	0.895	0.676	0.474	0.325				0.632	0.423	0.274	0.179	0.093			0.386	0.236		
6.0	1.013	0.780	0.593	0.456				0.728	0.531	0.391	0.308	0.236			0.484	0.343		
6.25								0.751	0.558	0.422	0.340	0.270		0.708	0.509			
7.0	1.091	0.872						0.814	0.631	0.504	0.428	0.364		0.767	0.580			
8.0	1.153	0.944						0.882	0.710	0.591	0.513	0.450		0.818	0.657			
9.0	1.198							0.927	0.759	0.636	0.562	0.502		0.876	0.704			
10.0	1.233							0.969	0.797	0.670	0.594	0.535		0.915	0.742			
11.0	1.254							0.988	0.814	0.686	0.613	0.556	1.152	0.936	0.757			
12.0	1.273						1.215	1.003	0.827	0.702	0.630	0.577	1.168	0.950				
12.5							1.219	1.006	0.828	0.704	0.635	0.584	1.172	0.953				
13.0							1.223	1.009	0.831	0.708	0.642	0.592	1.175	0.955				
14.0							1.229	1.012	0.833	0.713	0.651	0.605	1.180	0.957				
15.0							1.234	1.011	0.833	0.716	0.656	0.614	1.183	0.956				
16.0							1.238	1.011	0.831	0.716	0.659	0.618	1.186	0.955				
16.7							1.242	1.012	0.830	0.717	0.660	0.621						
17.0							1.243	1.012	0.830	0.716	0.660	0.621						
18.0							1.249	1.013	0.829	0.716	0.660	0.622						
19.0							1.257	1.022	0.831	0.717	0.663	0.624						
20.0							1.266	1.023	0.835	0.720	0.666	0.627						
21.0							1.277	1.032	0.843	0.728	0.673	0.636						
22.0							1.289	1.043	0.854	0.740	0.686	0.650						
23.0							1.300	1.057	0.881	0.757	0.704	0.669						
24.0							1.317	1.073	0.888	0.780	0.728	0.695						
25.0							1.332	1.092	0.911	0.806	0.757	0.725						
26.0							1.349	1.112	0.937	0.836	0.790	0.753						
28.0							1.383	1.157	0.995	0.905	0.864	0.839						
30.0							1.419	1.205	1.058	0.979	0.945	0.923						

TABLE 1-Continued

	25% Oxygen 75% Russell Mixture						100% Russell Mixture					
$Tx10^{-6}$	2	3	4	5	6	∞	2	3	4	5	6	∞
0.625					0.293	0.236					0.320	0.263
0.714					0.274	0.216					0.296	0.239
0.833					0.264	0.204					0.279	0.226
1.0					0.270	0.208					0.273	0.217
1.25					0.213	0.165					0.246	0.162
1.67					0.214	0.173					0.188	0.144
2.0				0.223	0.189	0.143				0.218	0.162	0.109
2.5				0.194	0.140					0.184	0.123	0.074
3.0			0.284	0.166	0.104				0.283	0.160	0.097	0.000
4.0			0.282	0.146	0.072			0.476	0.269	0.138	0.069	0.013
5.0		0.542	0.326	0.180				0.508	0.293	0.154	0.115	0.014
6.0		0.613	0.404	0.289				0.564	0.316	0.219	0.142	0.080
6.25		0.631	0.426					0.580	0.374	0.239	0.163	0.102
7.0	0.939	0.684	0.490					0.628	0.431	0.302	0.229	0.170
8.0	0.989	0.745	0.562					0.685	0.498	0.373	0.302	0.245
9.0	1.026	0.784						0.722	0.542	0.419	0.349	0.295
10.0	1.054	0.825						0.761	0.578	0.452	0.381	0.328
11.0	1.069	0.841						0.777	0.593	0.467	0.399	0.348
12.0	1.083	0.855					1.023	0.790	0.605	0.481	0.415	0.368
12.5	1.086	0.857					1.026	0.791	0.606	0.483	0.419	0.373
13.0	1.088						1.027	0.792	0.608	0.486	0.424	0.379
14.0							1.029	0.793	0.609	0.491	0.431	0.390
15.0							1.029	0.790	0.606	0.492	0.435	0.396
16.0							1.030	0.788	0.604	0.492	0.438	0.400
16.7							1.030	0.786	0.603	0.492	0.438	0.402
17.0							1.031	0.786	0.602	0.491	0.437	0.401
18.0							1.032	0.785	0.599	0.490	0.437	0.402
19.0							1.038	0.794	0.600	0.491	0.440	0.404
20.0							1.042	0.789	0.601	0.492	0.441	0.406
21.0							1.050	0.794	0.606	0.497	0.446	0.412
22.0							1.060	0.803	0.615	0.506	0.455	0.422
23.0							1.071	0.814	0.638	0.520	0.470	0.438
24.0							1.084	0.828	0.642	0.537	0.489	0.458
25.0							1.098	0.844	0.662	0.560	0.513	0.483
26.0							1.114	0.862	0.685	0.586	0.542	0.513
28.0							1.147	0.905	0.738	0.648	0.608	0.583
30.0							1.182	0.952	0.798	0.718	0.684	0.662

TABLE 2

100% Oxygen

	D_n							
x \ Ψ	2kT	3kT	4kT	5kT	6kT	∞ kT	$\phi(x)$	Δ
0.0315	0.0142	0.0154	0.0159	0.0161	0.0162	0.0162	.....	.....
0.0553	0.0341	0.0374	0.0383	0.0387	0.0389	0.0390	.....	.....
0.1253	0.1219	0.1331	0.1377	0.1395	0.1402	0.1406	.....	.....
0.4998	1.3473	1.5228	1.5997	1.6298	1.6411	1.6477	.....	196.5
∞							196.5	
D(x)	2.5185	2.7087	2.7916	2.8241	2.8365	2.8435		
τ	78.05	72.56	70.39	69.58	69.28	69.10		

TABLE 3

Russell Mixture

x \ Ψ	D_n 2kT	3kT	4kT	5kT	6kT	∞kT	φ(x)	Δ	D(x) Ψ=2kT	τ(x_i,x_{i+1})
0.0315	0.0047	0.0051	0.0053	0.0054	0.0054	0.0054				
0.0553	0.0114	0.0123	0.0127	0.0129	0.0130	0.0130				
0.0623	0.0072	0.0079	0.0082	0.0082	0.0083	0.0082				
0.0938	0.0037	0.0041	0.0042	0.0042	0.0043	0.0042				
0.1113	0.0180	0.0196	0.0203	0.0206	0.0206	0.0207				
0.1253	0.0410	0.0448	0.0464	0.0470	0.0472	0.0473				
0.1666	0.0094	0.0103	0.0107	0.0108	0.0109	0.0109				
0.2001	0.0087	0.0096	0.0100	0.0101	0.0102	0.0101				
0.2499	0.0683	0.0754	0.0784	0.0795	0.0800	0.0802				
0.3122	0.0450	0.0499	0.0520	0.0528	0.0532	0.0533				
0.3332	0.0218	0.0242	0.0252	0.0256	0.0258	0.0259				
0.3753	0.0380	0.0424	0.0443	0.0450	0.0453	0.0455	0.0002	0.0001	1.277	....
0.4998	0.4490	0.5076	0.5329	0.5433	0.5469	0.5492	0.0003	0.0012	1.726	0.001
0.5558	0.1306	0.1486	0.1565	0.1596	0.1608	0.1614	0.0015	0.0037	1.857	0.002
0.7498	0.1029	0.1198	0.1274	0.1305	0.1317	0.1324	0.0052	0.0055	1.960	0.003
1.000	0.9935	1.197	1.295	1.335	1.350	1.359	0.0107	0.0394	2.953	0.013
1.250	0.7408	0.9292	1.025	1.066	1.082	1.091	0.0501	0.0394	3.694	0.011
1.500	0.6971	0.9155	1.034	1.087	1.108	1.120	0.0895	2.958	4.391	0.674
3.000	2.703	5.026	7.348	8.857	9.541	10.05	3.048	24.82	7.094	3.499
5.000	17.60	44.22	99.80	185.5	271.2	371.0	27.87	168.6	24.69	6.829
∞							196.5			
τ										11.032

TABLE 3-Continued

x	D(x) Ψ=3kT	τ_i	Ψ=4kT	τ_i	Ψ=5kT	τ_i	Ψ=6kT	τ_i	Ψ=∞kT	τ_i
0.3753	1.306	....	1.318	....	1.322	....	1.324	....	1.325	....
0.4998	1.813	0.001	1.851	0.001	1.865	0.001	1.871	0.001	1.874	0.001
0.5558	1.962	0.002	2.007	0.002	2.025	0.002	2.032	0.002	2.035	0.002
0.7498	2.082	0.003	2.134	0.002	2.156	0.002	2.164	0.002	2.168	0.002
1.000	3.279	0.012	3.430	0.011	3.490	0.011	3.514	0.011	3.527	0.011
1.250	4.208	0.009	4.454	0.009	4.556	0.009	4.596	0.008	4.618	0.008
1.500	5.123	0.577	5.488	0.539	5.644	0.524	5.704	0.518	5.738	0.516
3.000	10.15	2.445	12.84	1.933	14.50	1.712	15.24	1.629	15.79	1.572
5.000	54.37	3.101	112.6	1.497	200.0	0.843	286.4	0.589	386.8	0.436
τ		6.150		3.894		3.104		2.760		2.548

TABLE 4

60% Oxygen 40% Russell Mixture

x	D(x) Ψ=2kT	τ_i	Ψ=3kT	τ_i	Ψ=4kT	τ_i	Ψ=5kT	τ_i	Ψ=6kT	τ_i	Ψ=∞kT	τ_i
0.4998	2.122	....	2.260	....	2.322	....	2.344	....	2.353	....	2.359	....
0.5558	2.197	0.002	2.335	0.002	2.400	0.002	2.424	0.002	2.434	0.002	2.440	0.002
0.7498	2.239	0.002	2.395	0.002	2.463	0.002	2.490	0.002	2.500	0.002	2.506	0.002
1.000	2.736	0.014	2.994	0.013	3.110	0.013	3.158	0.012	3.175	0.012	3.185	0.012
1.250	3.106	0.013	3.458	0.011	3.623	0.011	3.690	0.011	3.716	0.011	3.731	0.010
1.500	3.454	0.856	3.916	0.755	4.140	0.714	4.234	0.699	4.270	0.693	4.291	0.689
3.000	4.806	5.164	6.429	3.861	7.914	3.176	8.662	2.865	9.040	2.746	9.316	2.664
5.000	13.60	12.40	28.54	5.907	57.71	2.922	101.4	1.663	144.6	1.166	194.8	0.866
τ		18.448		10.551		6.840		5.254		4.632		4.245

The formulae for the other models are given in Table 6.

The envelope equations can now be reduced to a nondimensional form by the transformations

$$r = R\xi\,, \qquad \rho = \rho_0\sigma\,, \qquad T = T_0\Theta\,, \qquad M(r) = M\psi\,, \tag{11}$$

where

$$\rho_0 = \frac{M}{4\pi R^3}, \qquad T_0 = \frac{\mu H}{k}\frac{GM}{r}. \tag{12}$$

Then we have

$$\frac{d(\sigma\Theta)}{d\xi} = -\frac{\psi\sigma}{\xi}; \qquad \frac{d\psi}{d\xi} = \sigma\xi^2, \tag{13}$$

$$\frac{d\Theta}{d\xi} = -\frac{Q\sigma^{2.0126}}{\Theta^{6.5}\xi^2}, \tag{14}$$

where

$$Q = \frac{3\kappa_0 L}{16\pi a c}\,\frac{\rho_0^{2.0126}}{1.7266 T_0^{7.5} R}. \tag{15}$$

TABLE 5

60 PER CENT OXYGEN AND 40 PER CENT RUSSELL MIXTURE

Element	Relative Weight	Relative Contribution to Opacity $\propto \frac{Z^2}{A}$ × Relative Weight
O	24/40	0.5000
O	8/40	.1667
Na, Mg	4/40	.1250
Si	1/40	.0416
K, Ca	1/40	.0417
Fe	2/40	0.1250

5. *Construction of the model.*—Near $\xi = 1$ equations (13) and (14) can be approximately integrated; for, in the immediate neighborhood of the boundary of the star, $M(r)$ remains constant to a high degree of accuracy. Accordingly, letting ψ have its boundary value, which we shall denote by ψ_1, equations (13) can be re-written in the form

$$\frac{d(\sigma\Theta)}{d(\Theta^4)} = \frac{\psi_1\Theta^{3.5}}{4Q\sigma^{1.0126}}; \qquad \frac{d(\Theta^4)}{d\xi} = -\frac{4Q\sigma^{2.0126}}{\xi^2\Theta^{3.5}}. \tag{16}$$

Now let

$$\sigma = \frac{\psi_1^{60/4.0252}}{4^{1/2.0126}Q^{32/4.0252}}\,s; \qquad \Theta = \frac{\psi_1^4}{Q^2}\,t, \tag{17}$$

and

$$K = \frac{\psi_1^3}{Q^2}. \tag{18}$$

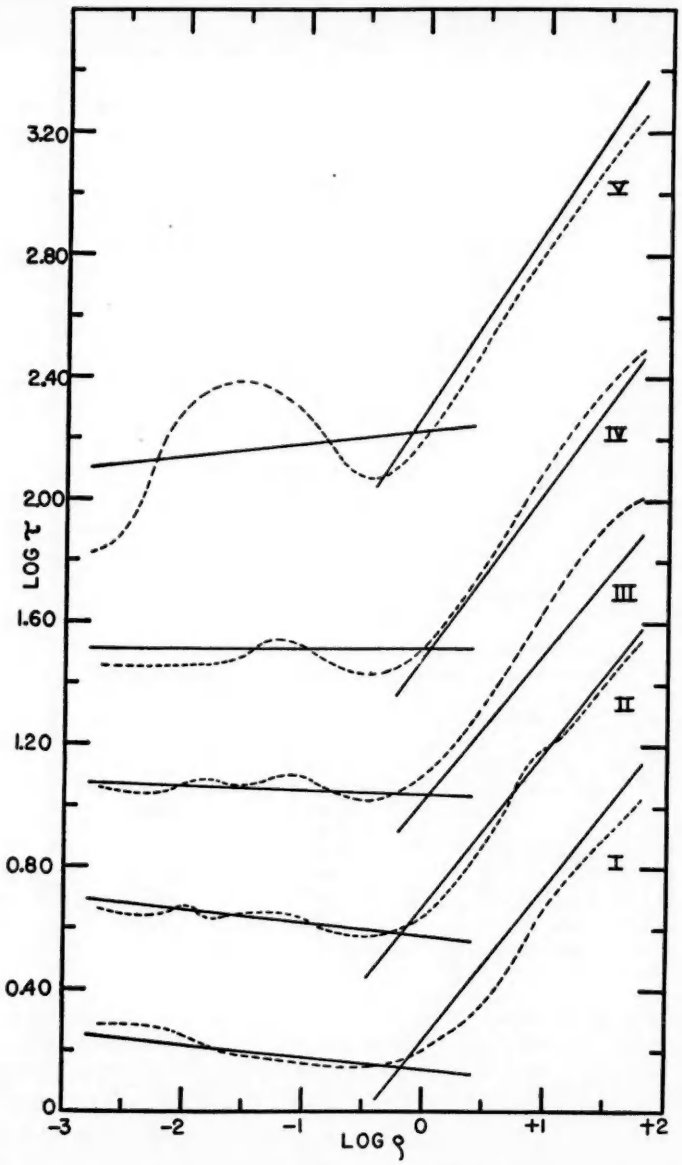

FIG. 1.—The curves illustrate the variation in the guillotine factor as a function of the density. The full lines are the assumed distribution, and the dotted curves are computed from the integrations. The curves are *I*, 100 per cent Russell mixture; *II*, 50 per cent oxygen and 50 per cent Russell mixture; *III*, 60 per cent oxygen and 40 per cent Russell mixture; *IV*, 70 per cent oxygen and 30 per cent Russell mixture; *V*, 100 per cent oxygen. The ordinates are the values for *I;* for each of the other curves subtract the following amounts, *II*, 0.40; *III*, 0.80; *IV*, 1.20; *V*, 1.60.

Introducing these substitutions into equations (16) and making the further substitutions

$$t = \frac{u^2}{K^2}; \qquad s^{1.0063} = \frac{zu^6}{K^7}, \tag{19}$$

we have

$$0.124803\,u\,z\,\frac{dz}{du} = 1.004718u - z^2 \tag{20}$$

and

$$\frac{du}{d\xi} = -\frac{K}{8}\,\frac{z^2}{\xi^2 u^2}. \tag{21}$$

The solutions of equations (20) and (21), satisfying the boundary condition that z and u tend to zero simultaneously, are

$$z^2 = 0.945704u; \qquad \frac{1}{\xi} = 1 + \frac{4.229653u^2}{K}. \tag{22}$$

TABLE 6

Model	Outside	Inside
100% Russell mixture	$1.3753\rho^{-0.0404}$	$1.7274\rho^{+0.5045}$
50% oxygen 50% Russell mixture	$1.4962\rho^{-0.0404}$	$1.9063\rho^{+0.5045}$
70% oxygen 30% Russell mixture	$2.0854\rho^{+0.0007}$	$1.9588\rho^{+0.5444}$
100% oxygen	$4.2658\rho^{+0.0348}$	$5.1286\rho^{+0.5580}$

The corresponding solutions for σ and Θ are

$$\sigma = \frac{0.488436u^{6.459307}Q^{5.962436}}{\psi_1^{5.962436}}, \qquad \Theta = \frac{u^2Q^2}{\psi_1^2}. \tag{23}$$

The solutions thus started will have to be continued by numerical methods. For this purpose it is convenient to introduce the variable

$$a = \frac{1}{\xi} \tag{24}$$

and to re-write equations (13) and (14) in the forms

$$\frac{d(\sigma\Theta)}{da} = \psi\sigma, \qquad \frac{d\psi}{da} = -\frac{\sigma}{a^4}, \tag{25}$$

and

$$\frac{d\Theta}{da} = \frac{Q\sigma^{2.0126}}{\Theta^{6.5}}. \tag{26}$$

6. *Equations of the model for the inside.*—When the point is reached at which $\log \rho = 0.0261$, it is necessary to use a new set of equations and to make a fit at the interface. We have, as before, equations (6), (7), and (8), except that r now has the form (10). By using the transformations

$$\rho = \rho_0 a^{-3} f = \rho_0 \sigma; \qquad r = Ral = R\xi,$$
$$T = T_0 a^{-1} t = T_0 \Theta; \qquad M(r) = 4\pi r^3 \rho_0 \psi = M\psi, \tag{27}$$

equations (6), (7), and (8) become

$$\frac{d(ft)}{dl} = -\frac{\psi f}{l^2}, \qquad \frac{d\psi}{dl} = l^2 f, \tag{28}$$

$$\frac{dt}{dl} = -\frac{Q_0 f^{1.5151}}{t^{6.5} l^2}, \tag{29}$$

where

$$Q_0 = \frac{3\kappa_0 L}{16\pi a c} \frac{\rho_0^{1.5151} a^{1.9547}}{1.6757 T_0^{7.5} R}. \tag{30}$$

7. *Construction of the model from the interface.*—It was found that it was possible to use an analytical development to continue the integration across the interface, provided that very small intervals for the radius factor are used.

Equations (28) can be re-written in the form

$$\frac{d(ft)}{d(t^4)} = \frac{\psi t^{3.5}}{4Q f^{0.5151}}, \tag{31}$$

and

$$\frac{d(t^4)}{dl} = -\frac{4Q_0 f^{1.5151}}{t^{3.5} l^2}. \tag{32}$$

Now let

$$f = \frac{\psi^{60/3.0302}}{4^{1/1.5151} Q_0^{32/3.0302}} x, \qquad t = \frac{\psi^4}{Q_0^2} y, \tag{33}$$

and

$$M = \frac{\psi^3}{Q_0^2}. \tag{34}$$

Introducing these substitutions into equations (31) and (32) and making the further substitutions

$$y = \frac{g^2}{M^2}; \qquad x^{0.757550} = \frac{X g^6}{M^7}, \tag{35}$$

we have

$$0.133065 g X \frac{dX}{dg} = 0.806430 g - X^2 \tag{36}$$

and

$$\frac{dg}{dl} = -\frac{M}{8} \frac{X^2}{g^2 l^2}. \tag{37}$$

Hence the solutions of equations (36) and (37) are

$$X^2 = 0.756124 a; \qquad \frac{1}{l} = 1 + \frac{0.529011 g^2}{M}. \tag{38}$$

The corresponding solutions for f and t are

$$f = \frac{0.333043 g^{8.580291} Q^{7.920269}}{\psi^{7.920269}}, \qquad t = \frac{g^2 Q^2}{\psi^2}. \tag{39}$$

It is convenient to introduce the variable

$$b = \frac{1}{l} \tag{40}$$

and to re-write equations (28) and (29) in logarithmic form.

8. *Fitting at the interface.*—Now the conditions at the interface are that the values of the temperature, pressure, and mass should be identical. The constants α and Q_0 can be determined from equations (27) and (39). The integrations can then be continued inward by means of equations (28) and (29). It is thus seen that for any specified Q the equations can be integrated, starting from the boundary and going inward. However, as we go along such a solution, a point is generally reached at which the radiative gradient breaks down. This point, ξ_i, where the convective gradient sets in, is defined by the place where the effective polytropic index,

$$n = \frac{\psi t^{6.5}}{Q_0 f^{1.5151}} - 1 , \tag{41}$$

becomes $\frac{3}{2}$. The solution interior to ξ_i must be described by a Lane-Emden function $\theta_{3/2}$. For an initially arbitrary choice Q, the solution obtained by the integration cannot be fitted to $\theta_{3/2}$. The condition that the fit be made determines Q and hence Q_0. Now the conditions at the interface are that the values of the temperature, pressure, and mass of the core should be identical at the interface, along with the condition that the effective polytropic index n attain the value 1.5 at the interface.

TABLE 7

Model	log Q	log Q_0	u_e	v_e	ξ_e	ψ_e	Θ	σ_i
100% Russell mixture	−4.9968	−4.7081	2.6748	0.3762	0.1011	0.0970	0.8305	262.5
50% oxygen	−4.9968	−4.7081	2.6748	.3762	.1011	.0970	.8305	262.5
60% oxygen	−5.1310	−4.7017	2.6680	.3844	.0996	.0943	.8272	251.9
70% oxygen	−4.9888	−4.4075	2.6812	.3685	.0908	.0893	.8367	317.5
100% oxygen	−4.7526	−4.3496	2.6468	0.4099	0.0846	0.0984	0.8439	418.0

Introducing the homology invariant quantities u and v, defined as in Chandrasekhar's *Stellar Structure* (pp. 146 ff.), we have for the conditions at the interface

$$u_i = \frac{4\pi p_e(r_i)\, r_i^3}{M_e(r_i)} = u_e = \left(\frac{v}{\psi}\frac{1}{b^3}\right)_{r=r_i} \tag{42}$$

and

$$v_i = \frac{2}{5}\frac{GM_e(r_i)}{r_i T_e(r_i)}\frac{\mu H}{k} = v_e = \left(\frac{2}{5}\frac{\psi b}{t}\right)_{r=r_i} , \tag{43}$$

where e refers to the envelope and i to the core.

All calculations were carried out logarithmically to six decimal places. When the point was reached at which the radiative gradient broke down, u and v were calculated. For the regions of the star inside $r = r_i$ the *British Association Mathematical Tables* (Vol. II) were used.

9. *Results.*—From the integrations we find the values given in Table 7. We must have

$$\sigma_i = \sigma_c \theta_i^{3/2} . \tag{44}$$

From equation (44) we obtain

$$\sigma_c = 334.9 . \tag{45}$$

Also, since

$$\bar{\rho} = \frac{M}{\frac{4}{3}\pi R^3} = 3\rho_0 \tag{46}$$

and

$$\rho_c = \rho_0 \sigma_c , \tag{47}$$

we find

$$\rho_c = 111.6\bar{\rho} . \tag{48}$$

Moreover,

$$\sigma_i\Theta_i = K\theta_c^{5/2}\theta_i^{5/2} \tag{49}$$

or

$$K = 0.0251 \tag{50}$$

and

$$\sigma_c\Theta = K\sigma_c^{5/3}\,, \tag{51}$$

or

$$\Theta_c = 1.210\,. \tag{52}$$

Finally, we have

$$\rho_c = 111.6\bar{\rho}\,, \tag{53}$$

$$T_c = T_0\Theta_c = 27.98\times 10^6\,\frac{\mu M}{R}\,, \tag{54}$$

$$\rho_c = 157.5\,\frac{M}{R^3}\,, \tag{55}$$

where M and R are expressed in solar units.

10. *Mass-luminosity equation.*—If the eigenvalue Q found by the integration is introduced into equation (15), we obtain the mass-luminosity relation. The expression for the mean molecular weight μ is

$$\frac{1}{\mu} = 2X + \tfrac{3}{4}Y + \tfrac{1}{2}(1 - X - Y)\,, \tag{56}$$

where X is the hydrogen content and Y the helium content. We also have

$$\kappa_0 = 3.90\times 10^{25}(1+X)(1-X-Y)\,. \tag{57}$$

Expressing L, M, and R in solar units and introducing the above expressions for μ and κ_0, we have for the mass-luminosity equation

$$[2X + \tfrac{3}{4}Y + \tfrac{1}{2}(1-X-Y)]^{7.5}(1+X)(1-X-Y) = 1.76\,\frac{M^{5.4874}}{LR^{0.4622}}\,. \tag{58}$$

11. *Energy-output equation.*—The second equation necessary for the determination of X and Y is derived by integrating the energy production over the entire core. The rate of energy generation by the carbon cycle is given by

$$\epsilon = \frac{Eh}{m_{14}t}(1-X-Y)\,\frac{X}{0.35}\,\frac{\rho}{80}\left(\frac{T}{2\times 10^7}\right)^{17} = \epsilon_0\rho T^{17}\,, \tag{59}$$

where

$E = 4\times 10^{-5}$ ergs = total energy released per cycle ;

$m_{14} = 2\times 10^{-23}$ gm = mass of one N^{14} nucleus ;

$t = 4\times 10^6$ years = time for a complete reaction if $\rho = 80$, $T = 2\times 10^{7\circ}K$, and $X = 0.35$;

$h = 0.02$ = carbon plus nitrogen content of the Russell mixture .

The integration over the core gives

$$\frac{L}{M} = \frac{\epsilon_0\rho\, T_c^{17}}{52}\,. \tag{60}$$

The energy-output equation can then be written in the form

$$\frac{[2X+\frac{3}{4}Y+\frac{1}{2}(1-X-Y)]^{17}}{(1-X-Y)X}=\frac{5419M^{19}}{LR^{20}}. \tag{61}$$

III. DISCUSSION OF THE MODELS

12. *Summary of the results.*—The main features of the models are summarized in Tables 8 and 9.

TABLE 8

Model	ρ_c	$T_c\times10^{-6}$	$\xi_{interface}$	$\psi_{interface}$	μ	Weight			
						H	*He*	*O*	Metals
100% Russell mixture	163.1	19.83	0.5024	0.9652	0.715	0.54	0.36	0.050	0.050
50% oxygen	163.1	19.74	.5024	.9652	.712	.54	.35	.082	.028
60% oxygen	157.5	20.12	.4710	.9478	.719	.53	.37	.080	.020
70% oxygen	196.2	19.85	.4534	.9484	.687	.59	.30	.094	0.016
100% oxygen	253.6	18.92	0.4666	0.9672	0.594	0.77	0.12	0.110	.....

TABLE 9

Model	Numbers		
	H/He	*H/O*	*H*/Metals
100% Russell mixture	6.0	173	373
50% oxygen	6.17	108	677
60% oxygen	5.73	106	914
70% oxygen	7.87	105	1234
100% oxygen	25.7	112	.....

In so far as there is an uncertainty in the half-life of N^{14} used in the energy-generation equation, we have used two values, namely, 4×10^6 and 1×10^6 years. This results in another set of abundances, which are shown in Table 10.

TABLE 10

Model	μ	Weight				Numbers		
		H	*He*	*O*	Metals	*H/He*	*H/O*	*H*/Metals
100% Russell mixture	0.675	0.598	0.338	0.032	0.032	7.08	299	645
50% oxygen	.671	.605	.328	.050	.017	7.38	194	1228
60% oxygen	.675	.597	.343	.048	.012	6.96	199	1716
70% oxygen	.645	.653	.279	.058	0.010	9.36	180	2253
100% oxygen	0.559	0.845	0.085	0.070	.....	39.8	193	.....

The temperature-density distribution throughout each model is shown in Table 11.

It is readily seen from Figure 1 that the variation in the guillotine factor as computed from the temperature-density distribution determined from the integrations agrees very well with the formulae for τ.

TABLE 11

ξ	Temperature degrees K					Density grams/cc*			
	100%	70%	60%	50%	0%	100%	70%	60%	50%
0.9949	16.19 (+3)	18.98 (+3)	19.96 (+3)	19.97 (+3)	20.00 (+3)	12.09 (-9)	22.47 (-9)	30.12 (-9)	33.71 (-9)
.9082	32.19 (+4)	37.74 (+4)	39.68 (44)	39.72 (+4)	39.77 (+4)	23.86 (-5)	37.44 (-5)	47.08 (-5)	46.20 (-5)
.8900	39.38 (+4)	46.15 (+4)	48.54 (+4)	48.58 (+4)	48.65 (+4)	46.44 (-5)	72.08 (-5)	90.20 (-5)	87.74 (-5)
.8634	50.42 (+4)	59.10 (+4)	62.16 (+4)	62.22 (+4)	62.30 (+4)	10.53 (-4)	16.11 (-4)	20.05 (-4)	19.29 (-4)
.7962	81.58 (+4)	95.63 (+4)	10.05 (+5)	10.06 (+5)	10.07 (+5)	51.68 (-4)	76.95 (-4)	94.51 (-4)	89.04 (-4)
.7802	89.76 (+4)	10.52 (+5)	11.06 (+5)	11.07 (+5)	11.08 (+5)	70.92 (-4)	10.50 (-3)	12.88 (-3)	12.09 (-3)
.7416	11.09 (+5)	13.01 (+5)	13.68 (+5)	13.69 (+5)	13.71 (+5)	14.27 (-3)	20.93 (-3)	25.60 (-3)	23.80 (-3)
.6702	15.67 (+5)	18.36 (+5)	19.32 (+5)	19.32 (+5)	19.34 (+5)	44.62 (-3)	64.18 (-3)	77.89 (-3)	71.14 (-3)
.6436	17.63 (+5)	20.66 (+5)	21.73 (+5)	21.73 (+5)	21.76 (+5)	65.92 (-3)	94.06 (-3)	11.38 (-2)	10.35 (-2)
.6056	20.73 (+5)	24.28 (+5)	25.50 (+5)	25.55 (+5)	25.58 (+5)	11.23 (-2)	15.87 (-2)	19.07 (-2)	17.31 (-2)
.5816	22.89 (+5)	26.81 (+5)	28.16 (+5)	28.21 (+5)	28.25 (+5)	15.58 (-2)	21.87 (-2)	26.22 (-2)	23.69 (-2)
.5585	25.14 (+5)	29.44 (+5)	30.92 (+5)	30.97 (+5)	31.01 (+5)	21.22 (-2)	29.58 (-2)	35.38 (-2)	31.84 (-2)
.5363	27.47 (+5)	32.16 (+5)	33.78 (+5)	33.33 (+5)	33.88 (+5)	28.42 (-2)	39.38 (-2)	46.96 (-2)	42.12 (-2)
.5024	31.42 (+5)	36.69 (+5)	38.66 (+5)	38.66 (+5)	38.72 (+5)	44.25 (-2)	60.24 (-2)	72.04 (-2)	64.14 (-2)
.4710	35.56 (+5)	40.39 (+5)	43.63 (+5)	.....	.....	66.47 (-2)	82.09 (-2)	10.62 (-1)	.....
.4666	36.18 (+5)	40.94 (+5)	.....	.....	.....	70.34 (-2)	85.72 (-2)	.....	.....
.4534	.....	44.53 (+5)	.....	.....	.....	.....	11.22 (-1)	.....	.....
.4480	38.22 (+5)	45.22 (+5)	46.73 (+5)	45.71 (+5)	45.77 (+5)	89.87 (-2)	12.00 (-1)	16.05 (-1)	13.17 (-1)
.4302	40.43 (+5)	47.66 (+5)	49.46 (+5)	48.40 (+5)	48.47 (+5)	11.57 (-1)	15.11 (-1)	18.07 (-1)	16.82 (-1)
.4131	42.73 (+5)	50.29 (+5)	52.25 (+5)	51.19 (+5)	51.26 (+5)	14.79 (-1)	19.14 (-1)	22.75 (-1)	21.34 (-1)
.3815	47.48 (+5)	55.72 (+5)	58.05 (+5)	56.92 (+5)	57.00 (+5)	23.58 (-1)	29.91 (-1)	35.20 (-1)	33.31 (-1)
.3590	51.32 (+5)	60.06 (+5)	62.69 (+5)	61.55 (+5)	61.63 (+5)	33.14 (-1)	41.30 (-1)	48.24 (-1)	46.08 (-1)
.3310	56.70 (+5)	66.14 (+5)	69.15 (+5)	67.94 (+5)	68.03 (+5)	51.16 (-1)	62.33 (-1)	71.70 (-1)	69.22 (-1)
.3053	62.40 (+5)	72.56 (+5)	75.86 (+5)	74.59 (+5)	74.70 (+5)	77.11 (-1)	91.73 (-1)	10.35	10.10
.2815	68.36 (+5)	79.21 (+5)	84.06 (+5)	81.54 (+5)	81.66 (+5)	11.35	13.16	14.54	14.33
.2596	74.54 (+5)	86.08 (+5)	89.87 (+5)	88.61 (+5)	88.74 (+5)	16.25	18.38	19.84	19.74
.2394	80.96 (+5)	93.11 (+5)	97.05 (+5)	95.76 (+5)	95.90 (+5)	22.74	24.99	26.31	26.45
.2208	87.84 (+5)	10.02 (+6)	10.28 (+6)	10.30 (+6)	10.31 (+6)	30.90	33.06	33.92	34.44
.2036	94.23 (+5)	10.74 (+6)	11.14 (+6)	11.02 (+6)	11.03 (+6)	41.17	42.54	42.51	43.33
.1977	10.10 (+6)	11.45 (+6)	11.86 (+6)	11.73 (+6)	11.75 (+6)	53.21	53.26	52.94	53.36
.1731	10.77 (+6)	12.15 (+6)	12.55 (+6)	12.43 (+6)	12.44 (+6)	72.81	64.61	62.36	68.28
.1472	12.09 (+6)	13.51 (+6)	13.87 (+6)	13.76 (+6)	13.78 (+6)	98.33	89.70	81.24	85.02
.1357	12.73 (+6)	14.16 (+6)	14.97 (+6)	14.38 (+6)	14.40 (+6)	11.49 (+1)	10.19 (+1)	90.66	94.86
.1252	13.34 (+6)	14.78 (+6)	15.09 (+6)	14.98 (+6)	15.00 (+6)	13.13 (+1)	11.36 (+1)	99.15	10.41 (+1)
.1154	13.94 (+6)	15.37 (+6)	15.66 (+6)	15.55 (+6)	15.57 (+6)	14.72 (+1)	12.43 (+1)	10.69 (+1)	11.22 (+1)
.1064	14.51 (+6)	15.94 (+6)	16.21 (+6)	16.10 (+6)	16.12 (+6)	16.21 (+1)	13.39 (+1)	11.19 (+1)	11.95 (+1)
.1011	14.86 (+6)	16.29 (+6)	16.54 (+6)	16.40 (+6)	16.45 (+6)	17.09 (+1)	13.90 (+1)	11.75 (+1)	12.35 (+1)
.0996	14.96 (+6)	16.39 (+6)	16.64 (+6)	16.49 (+6)	16.54 (+6)	17.34 (+1)	14.05 (+1)	11.86 (+1)	12.45 (+1)
.0982	15.06 (+6)	16.48 (+6)	16.73 (+6)	16.58 (+6)	16.63 (+6)	17.57 (+1)	14.18 (+1)	11.95 (+1)	12.55 (+1)
.0908	15.57 (+6)	16.61 (+6)	17.17 (+6)	16.99 (+6)	17.05 (+6)	18.71 (+1)	14.94 (+1)	12.43 (+1)	13.03 (+1)
.0846	15.99 (+6)	16.95 (+6)	17.52 (+6)	17.33 (+6)	17.40 (+6)	19.66 (+1)	15.48 (+1)	12.82 (+1)	13.42 (+1)
.0800	15.99 (+6)	17.22 (+6)	17.78 (+6)	17.58 (+6)	17.65 (+6)	19.69 (+1)	15.27 (+1)	13.11 (+1)	13.72 (+1)
.0600	16.69 (+6)	18.32 (+6)	18.77 (+6)	18.48 (+6)	18.55 (+6)	21.80 (+1)	17.40 (+1)	14.21 (+1)	14.79 (+1)
.0400	18.07 (+6)	19.14 (+6)	19.50 (+6)	19.17 (+6)	19.25 (+6)	23.68 (+1)	18.58 (+1)	15.04 (+1)	15.62 (+1)
.0200	18.69 (+6)	19.66 (+6)	19.95 (+6)	19.60 (+6)	19.68 (+6)	24.91 (+1)	19.35 (+1)	15.57 (+1)	16.13 (+1)
0.	18.92 (+6)	19.85 (+6)	20.12 (+6)	19.74 (+6)	19.83 (+6)	25.36 (+1)	19.62 (+1)	15.75 (+1)	16.31 (+1)

*The density distribution in the model for 0% Oxygen is the same as in the model for 50% Oxygen. The numbers in parentheses give the powers of ten by which the corresponding entries should be multiplied.

With regard to Figure 2, the undetermined portions of each curve were established by determining the hydrogen and helium content for other combinations of oxygen and Russell mixture. It was found that one of the integrations for another mixture could be used for this purpose if the constants in the formulae for τ were suitably changed. It should be noted, however, that this method cannot be applied if it is necessary to change the exponent of ρ or to move the lines in a horizontal direction.

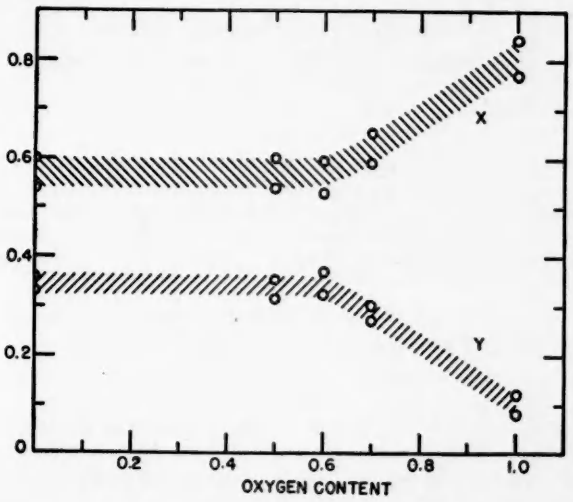

FIG. 2.—The curves illustrate the variation in the hydrogen and the helium content for various combinations of oxygen and Russell mixture as shown in Tables 8 and 10. The ordinates represent the percentage of hydrogen or helium, and the abscissae represent the percentage of oxygen in the mixture of oxygen and Russell mixture.

TABLE 12

Element	Weight (Per Cent)	Numbers
Hydrogen	70	1600
Helium	28	160
Oxygen group	1.4	2
Metals	0.4	0.315

13. *Conclusions.*—Table 12 was compiled by Dr. J. L. Greenstein from spectroscopic results. Comparing these values with the values determined from the integrations, we find a fairly good agreement for the H/He and $H/$metals ratios for a mixture of about 70 per cent oxygen and 30 per cent Russell mixture; however, our oxygen abundance is perhaps a little too high. This high value of the oxygen abundance follows even if we assume that the metals are composed of 100 per cent Russell mixture. An important conclusion we may draw now is that there is no divergence in the absolute abundance of hydrogen and the important H/He ratio as determined from stellar atmospheres and the theory of the internal constitution.

It is again a pleasure to record my indebtedness to Dr. S. Chandrasekhar for his helpful advice.

LINE STRENGTHS IN THE IRON SPECTRUM IN INTERMEDIATE COUPLING WITH APPLICATION TO THE SOLAR CURVE OF GROWTH*

WINSTON M. GOTTSCHALK
Raytheon Manufacturing Company, Waltham, Massachusetts
Received March 3, 1948

ABSTRACT

Line strengths for the $3d^7(^4P)4s-3d^7(^4P)4p$ and $3d^7(^4F)4s-3d^7(^4F)4p$ transitions in *Fe* I are computed in intermediate coupling by means of quantum mechanics. Spin-orbit interaction is taken into account, but configuration interaction is neglected. It is further assumed that the L and S of the core are "good quantum numbers." Where experimental intensities are available, the agreement of the computed line strengths with the experimental values is reasonable. Lande g-factors, calculated with the transformation matrices derived in the intensity calculations, are in accord with the latest published values.

The line strengths thus computed are used to derive a curve of growth for the sun. A temperature for the solar reversing layer is determined from this curve as $4800° \pm 200°$ K.

INTRODUCTION

Theoretical values of line strengths are known for atomic spectra in the two extreme coupling cases, Russell-Saunders and jj-coupling.[1] In electric-dipole radiation the line strength is proportional to the electric dipole moment between the two states involved in the transition. The term "line strength" was introduced by Condon and Shortley and has, for theoretical purposes, definite advantages over the use of intensity, transition probability, and f-value.[2]

Most of the atoms whose spectra are of astrophysical interest are cases of intermediate coupling, and hence line strengths based on either of the two extreme cases are, at best, rough approximations. Thus many lines of considerable intensity have a theoretical strength of zero in Russell-Saunders coupling. In the problem of the curve of growth, in which the stellar equivalent width is plotted against the line strength, accurate values of line strengths are of great importance. Experimental values in absorption are difficult to measure, and extensive tables of measured intensities do not exist. This work was undertaken to provide a beginning for tables of theoretical line strengths which would at least be more accurate than the values based on incorrect coupling.

THEORY OF LINE STRENGTH IN INTERMEDIATE COUPLING

In the masterly monograph, *Theory of Atomic Spectra*, by Condon and Shortley, the theory of line strengths in any coupling is given in some detail. It is shown there that if $S^{1/2}(\alpha J, \beta J')$ represents the matrix whose elements are the square roots of the line strengths between states characterized by the quantum numbers αJ and $\beta J'$, then, in a system of representation where the quantum numbers are aJ and bJ', the corresponding matrix is

$$S^{1/2}(aJ, bJ') = \sum_{\alpha\beta} (aJ/\alpha J)\, S^{1/2}(\alpha J, \beta J')\, (\beta J'/bJ') \ldots . \tag{1}$$

* This paper is part of a thesis submitted to the Faculty of Harvard University in partial fulfilment of the requirements for the degree of Doctor of Philosophy, June, 1946.

[1] Condon and Shortley, *Theory of Atomic Spectra* (Cambridge: At the University Press, 1935).

[2] *Ibid.*, p. 98.

Here (aJ/aJ) is the transformation matrix which diagonalizes the energy matrix for one state and $(\beta J'/bJ')$ is the inverse of the transformation matrix which diagonalizes the other state. One must keep the phases consistent throughout these matrices, in order to see that the matrix components on the right of this equation are taken between states having the same phases as those for which the transformation coefficients are taken. In this respect one feels a debt of gratitude to Condon and Shortley for the pains with which they have kept phase choice consistent and explicit throughout their book. In this work a further check was made when the formulae of H. M. Johnson, Jr.,[3] were used for the spin-orbit energies in the $LSJM_J$ representation. An expansion of the precessing l, s, and j vectors was made in a multiple Fourier series in the manner of the old quantum theory. The signs of the terms in the expansion correspond to the phases of the matrix components. It was found that the phases in Johnson's paper agree with the choice in Condon and Shortley.

In terms of equation (1) the problem of computing line strengths in intermediate coupling resolves itself into finding the transformation matrices. This involves writing down the energy matrix as accurately as possible, solving the secular equation, and, from the solution, determining the transformation matrix. Quantum mechanics provides the mechanism of perturbation theory to carry out this procedure.

CHOICE OF TRANSITION ARRAY

The transition array chosen for application of this method was the $3d^74s-3d^74p$ transition in *Fe* I. This array has many lines of astrophysical interest, and the measurements of A. S. King and R. B. King[4] provide some experimental check on the results of the calculation. The first work was done with the ^4F core; and here the results were quite good, since this core is not far from obeying Russell-Saunders coupling. In the method of setting up the energy equation, it was assumed that the L and the S of the core are good quantum numbers. Calculations were also carried out on the transition involving the ^4P core. Here the L and the S of the core are not good quantum numbers, but the results are felt to have some significance. Attempts on the ^2H and ^2G cores were not successful.

The same matrices with different constants should also be of value in the cases of *Ti* I $3d^34s-3d^34p$ and *Fe* I $3d^74p-3d^75s$. In the case of the ^4F core the calculation for *Ti* I gave results so close to the Russell-Saunders values that further computation was felt to be meaningless. For the higher iron transition no equivalent width values could be found in Allen's extensive tables.[5] Since the first object of the work was to derive a curve of growth based on theoretical line strengths, the iron computation was not done at this time.

THE ENERGY MATRIX

In setting up the energy matrix, the four-vector method was utilized, wherein the L and S of the core played the part of the first electron. This method then depends on the fact that the parent-ion obeys Russell-Saunders coupling, as exemplified by the Landé interval rule.

The Coulomb and exchange terms, which occur on the diagonal of the energy matrix written in the $LSJM_J$ representation, were put in as constants for the centers of gravity of the multiplets involved. The spin-orbit terms are the elements of the matrix of $a_1l_1s_1+a_2l_2s_2$. These were written down from the formulae given by Johnson.[3] For reference by others working on these configurations, the matrices for $3d^7(^4F)4s$, $3d^7(^4F)4p$, $3d^7(^4P)4s$, and $3d^7(^4P)4p$ are given in Table 1.

[3] *Phys. Rev.*, **38**, 1628, 1931.

[4] *Ap. J.*, **87**, 24, 1938.

[5] *Mem. Commonwealth Solar Obs.*, Nos. 5 and 6.

TABLE 1

ENERGY MATRIX $3d^7(^4F)4s$

	$^5F_5$
$^5F_5$	$\frac{9}{2}a_1 - W$

	$^5F_4$	$^3F_4$
$^5F_4$	$\frac{3}{4}a_1 - W$	$-\frac{3}{4}a_1\sqrt{5}$
$^3F_4$	$-\frac{3}{4}a_1\sqrt{5}$	$\frac{15}{4}a_1 + \beta - W$

	$^5F_3$	$^3F_3$
$^5F_3$	$-\frac{9}{4}a_1 - W$	$-\frac{3}{4}a_1\sqrt{5}$
$^3F_3$	$-\frac{3}{4}a_1\sqrt{5}$	$-\frac{5}{4}a_1 + \beta - W$

	$^5F_2$	$^3F_2$
$^5F_2$	$-\frac{9}{2}a_1 - W$	$-\frac{a_1}{2}\sqrt{6}$
$^3F_2$	$-\frac{a_1}{2}\sqrt{6}$	$-5a_1 + \beta - W$

	$^5F_1$
$^5F_1$	$-6a_1 - W$

TABLE 1—*Continued*

ENERGY MATRIX $3d^7(^4F)\ 4p$

	$^5G6$
$^5G6$	$\frac{1}{2}(9a_1+a_2)$ $+\alpha-W$

$\alpha = {}^5G-{}^5D$
$\beta = {}^3G-{}^5D$
$\delta = {}^3F-{}^5D$
$\gamma = {}^5F-{}^5D$
$\varepsilon = {}^3D-{}^5D$

	$^5G5$	$^3G5$	$^5F5$
$^5G5$	$\frac{9}{8}a_1+\frac{1}{8}a_1$ $+\alpha-W$	$-\frac{3\sqrt{2}}{8}(3a_1-a_2)$	$\frac{3}{8}(3a_1-a_2)$
$^3G5$	$-\frac{3\sqrt{2}}{8}(3a_1-a_2)$	$\frac{15}{4}a_1-\frac{1}{4}a_2$ $+\beta-W$	$\frac{3\sqrt{2}}{8}(a_1+a_2)$
$^5F5$	$\frac{3}{8}(3a_1-a_2)$	$\frac{3\sqrt{2}}{8}(a_1+a_2)$	$\frac{1}{8}(33a_1+a_2)$ $+\gamma-W$

	$^5G4$	$^3G4$	$^5F4$	$^3F4$	$^5D4$
$^5G4$	$-\frac{3}{16}(9a_1+a_2)$ $+\alpha-W$	$-\frac{\sqrt{77}}{16}(3a_1-a_2)$	$\frac{3\sqrt{77}}{112}(3a_1-a_2)$	$-\frac{\sqrt{1155}}{336}(a_1+a_2)$	0
$^3G4$	$-\frac{\sqrt{77}}{16}(3a_1-a_2)$	$-\frac{1}{16}(15a_1-a_2)$ $+\beta-W$	$\frac{3\sqrt{3}}{16}(a_1+a_2)$	$\frac{\sqrt{15}}{16}(5a_1+a_2)$	0
$^5F4$	$\frac{3\sqrt{77}}{112}(3a_1-a_2)$	$\frac{3\sqrt{3}}{16}(a_1+a_2)$	$\frac{11}{16}a_1+\frac{1}{48}a_2$ $+\gamma-W$	$-\frac{3\sqrt{5}}{80}(11a_1-a_2)$	$\frac{5}{\sqrt{14}}(a_1-\frac{1}{3}a_2)$
$^3F4$	$-\frac{\sqrt{1155}}{336}(a_1+a_2)$	$\frac{\sqrt{15}}{16}(5a_1+a_2)$	$-\frac{3\sqrt{5}}{80}(11a_1-a_2)$	$\frac{1}{16}(55a_1-a_2)$ $+\delta-W$	$\frac{\sqrt{70}}{14}(a_1+a_2)$
$^5D4$	0	0	$\frac{5}{\sqrt{14}}(a_1-\frac{1}{3}a_2)$	$\frac{\sqrt{70}}{14}(a_1+a_2)$	$\frac{1}{3}(12a_1-a_2)$ $-W$

TABLE 1—*Continued*

ENERGY MATRIX $3d^7(^4F)4p$ (*Continued*)

	$^5G_3$	$^3G_3$	$^5F_3$	$^3F_3$	$^5D_3$	$^3D_3$
$^5G_3$	$-\frac{7}{16}(9a_1+a_2)+\alpha-W$	$-\frac{3\sqrt{5}}{16}(3a_1-a_2)$	$\frac{15\sqrt{7}}{112}(3a_1-a_2)$	$-\frac{9\sqrt{35}}{112}(a_1+a_2)$	0	0
$^3G_3$	$-\frac{3\sqrt{5}}{16}(3a_1-a_2)$	$-\frac{5}{16}(15a_1-a_2)+\beta-W$	$\frac{3\sqrt{35}}{112}(a_1+a_2)$	$\frac{9\sqrt{7}}{112}(5a_1+a_2)$	0	0
$^5F_3$	$\frac{15\sqrt{7}}{112}(3a_1-a_2)$	$\frac{3\sqrt{35}}{112}(a_1+a_2)$	$-\frac{1}{16}(33a_1+a_2)+\gamma-W$	$-\frac{\sqrt{5}}{16}(11a_1-a_2)$	$\frac{\sqrt{42}}{14}(3a_1-a_2)$	$-\frac{1}{\sqrt{7}}(a_1+a_2)$
$^3F_3$	$-\frac{9\sqrt{35}}{112}(a_1+a_2)$	$\frac{9\sqrt{7}}{112}(5a_1+a_2)$	$-\frac{5}{16}(11a_1-a_2)$	$-\frac{1}{48}(55a_1-a_2)+\delta-W$	$\frac{\sqrt{210}}{42}(a_1+a_2)$	$\frac{\sqrt{35}}{21}(5a_1+a_2)$
$^5D_3$	0	0	$\frac{\sqrt{42}}{14}(3a_1-a_2)$	$\frac{\sqrt{210}}{42}(a_1+a_2)$	$0-W$	$-\frac{2\sqrt{6}}{3}a_1-\frac{a_2}{\sqrt{6}}$
$^3D_3$	0	0	$-\frac{1}{\sqrt{7}}(a_1+a_2)$	$\frac{\sqrt{35}}{21}(5a_1+a_2)$	$-\frac{2\sqrt{6}}{3}a_1-\frac{a_2}{\sqrt{6}}$	$\frac{1}{6}(20a_1+a_2)+\varepsilon-W$

	$^5G_2$	$^5F_2$	$^3F_2$	$^5D_2$	$^3D_2$
$^5G_2$	$-\frac{5}{8}(9a_1+a_2)+\alpha-W$	$\frac{3\sqrt{21}}{56}(3a_1-a_2)$	$-\frac{9\sqrt{14}}{56}(a_1+a_2)$	0	0
$^5F_2$	$\frac{3\sqrt{21}}{56}(3a_1-a_2)$	$-\frac{1}{8}(33a_1+a_2)+\beta-W$	$\frac{-\sqrt{6}}{24}(11a_1-a_2)$	$\frac{1}{\sqrt{7}}(3a_1-a_2)$	$-\frac{1}{\sqrt{3}}(a_1+a_2)$
$^3F_2$	$-\frac{9\sqrt{14}}{56}(a_1+a_2)$	$\frac{-\sqrt{6}}{24}(11a_1-a_2)$	$-\frac{1}{12}(55a_1-a_2)+\delta-W$	$\frac{1}{\sqrt{42}}(a_1-a_2)$	$\frac{\sqrt{2}}{6}(5a_1+a_2)$
$^5D_2$	0	$\frac{1}{\sqrt{7}}(3a_1-a_2)$	$\frac{1}{\sqrt{42}}(a_1-a_2)$	$-3a_1+\frac{1}{4}a_2-W$	$-\frac{\sqrt{21}}{3}(a_1+\frac{1}{4}a_2)$
$^3D_2$	0	$-\frac{1}{\sqrt{3}}(a_1+a_2)$	$\frac{\sqrt{2}}{6}(5a_1+a_2)$	$-\frac{\sqrt{21}}{3}(a_1+\frac{1}{4}a_2)$	$-\frac{1}{12}(20a_1+a_2)+\varepsilon-W$

	$^5F_1$	$^5D_1$	$^3D_1$
$^5F_1$	$-\frac{11}{2}a_1-\frac{1}{6}a_2+\gamma-W$	$\frac{1}{\sqrt{2}}(a_1-\frac{a_2}{3})$	$-\frac{1}{\sqrt{2}}(a_1+a_2)$
$^5D_1$	$\frac{1}{\sqrt{2}}(a_1-\frac{a_2}{3})$	$-5a_1+\frac{5}{12}a_2-W$	$-a_1-\frac{a_2}{4}$
$^3D_1$	$-\frac{1}{\sqrt{2}}(a_1+a_2)$	$-a_1-\frac{a_2}{4}$	$-\frac{1}{4}(20a_1+a_2)+\varepsilon-W$

	$^5D_0$
$^5D_0$	$-6a_1+\frac{a_2}{2}-W$

TABLE 1—*Continued*

ENERGY MATRIX $3d^7(^4P)4p$ SECULAR EQUATION

	$^5D_4$
$^5D_4$	$\frac{3}{2}a_1 + \frac{a_2}{2}$

	$^5D_3$	$^3D_3$	$^5P_3$
$^5D_3$	0	$-\frac{\sqrt{6}}{4}(a_1 - a_2)$	$\frac{1}{\sqrt{8}}(3a_1 - a_2)$
$^3D_3$	$-\frac{\sqrt{6}}{4}(a_1 - a_2)$	$\frac{5}{4}a_1 - \frac{1}{4}a_2$	$\frac{a_1}{4}\sqrt{3} + \frac{a_2}{4}\sqrt{3}$
$^5P_3$	$\frac{1}{\sqrt{8}}(3a_1 - a_2)$	$\frac{a_1}{4}\sqrt{3} + \frac{a_2}{4}\sqrt{3}$	$\frac{3}{4}a_1 + \frac{1}{4}a_2$

	$^5D_2$	$^3D_2$	$^5P_2$	$^3P_2$	$^5S_2$
$^5D_2$	$-\frac{9}{8}a_1 - \frac{3}{8}a_2$	$-\frac{\sqrt{21}}{8}(a_1 - a_2)$	$\frac{1}{4}\sqrt{\frac{7}{5}}(3a_1 - a_2)$	$-\frac{\sqrt{7}}{8}(a_1 + a_2)$	0
$^3D_2$	$-\frac{\sqrt{21}}{8}(a_1 - a_2)$	$-\frac{5a_1}{8} + \frac{a_2}{8}$	$\frac{\sqrt{3}}{8}(a_1 + a_2)$	$\frac{\sqrt{3}}{8}(5a_1 - a_2)$	0
$^5P_2$	$\frac{1}{4}\sqrt{\frac{7}{3}}(3a_1 - a_2)$	$\frac{\sqrt{3}}{8}(a_1 + a_2)$	$-\frac{3a_1}{8} - \frac{a_2}{8}$	$-\frac{3}{8}(a_1 - a_2)$	$\frac{3}{2}a_1 - \frac{a_2}{2}$
$^3P_2$	$-\frac{\sqrt{7}}{8}(a_1 + a_2)$	$\frac{\sqrt{3}}{8}(5a_1 - a_2)$	$-\frac{3}{8}(a_1 - a_2)$	$\frac{5}{8}a_1 - \frac{a_2}{8}$	$\frac{1}{2}(a_1 + a_2)$
$^5S_2$	0	0	$\frac{3a_1}{2} - \frac{a_2}{2}$	$\frac{1}{2}(a_1 + a_2)$	0

	$^5D_1$	$^3D_1$	$^5P_1$	$^3P_1$	$^3S_1$
$^5D_1$	$-\frac{15}{8}a_1 - \frac{5}{8}a_2$	$-\frac{3}{8}(a_1 - a_2)$	$\frac{3\sqrt{3}}{8}a_1 - \frac{\sqrt{3}}{8}a_2$	$-\frac{\sqrt{15}}{8}(a_1 + a_2)$	0
$^3D_1$	$-\frac{3}{8}(a_1 - a_2)$	$-\frac{15}{8}a_1 + \frac{3}{8}a_2$	$\frac{\sqrt{3}}{24}(a_1 + a_2)$	$\frac{\sqrt{15}}{24}(5a_1 + a_2)$	0
$^5P_1$	$\frac{3\sqrt{3}}{8}a_1\ \frac{\sqrt{3}}{8}a_2$	$\frac{\sqrt{3}}{24}(a_1 + a_2)$	$-\frac{9}{8}a_1 - \frac{3}{8}a_2$	$-\frac{\sqrt{5}}{8}(a_1 - a_2)$	$-\frac{\sqrt{5}}{2}(a_1 + a_2)$
$^3P_1$	$-\frac{\sqrt{15}}{8}(a_1 + a_2)$	$\frac{\sqrt{15}}{24}(5a_1 + a_2)$	$-\frac{\sqrt{5}}{8}(a_1 - a_2)$	$-\frac{5}{8}a_1 + \frac{1}{8}a_2$	$\frac{\sqrt{3}}{6}(5a_1 + a_2)$
$^3S_1$	0	0	$-\frac{\sqrt{5}}{2}(a_1 + a_2)$	$\frac{\sqrt{3}}{6}(5a_1 + a_2)$	0

	$^5D_0$	$^3P_0$
$^5D_0$	$-\frac{9}{4}a_1 - \frac{3}{4}a_2$	$-\frac{\sqrt{5}}{4}(a_1 + a_2)$
$^3P_0$	$-\frac{\sqrt{5}}{4}(a_1 + a_2)$	$-\frac{5}{4}a_1 + \frac{1}{4}a_2$

TABLE 1—*Continued*

ENERGY MATRIX $3d^7(^4P)4s$ SECULAR EQUATION

	$^5P_3$
$^5P_3$	$\frac{3}{2}a_1$

	$^5P_2$	$^3P_2$
$^5P_2$	$-\frac{3}{4}a_1$	$-\frac{3}{4}a_1$
$^3P_2$	$-\frac{3}{4}a_1$	$\frac{5}{4}a_1$

	$^5P_1$	$^3P_1$
$^5P_1$	$-\frac{9}{4}a_1$	$-\frac{\sqrt{5}}{4}a_1$
$^3P_1$	$-\frac{\sqrt{5}}{4}a_1$	$-\frac{5}{4}a_1$

	$^3P_0$
$^3P_0$	$-\frac{5}{2}a_1$

CHOICE OF CONSTANTS

The Coulomb and exchange constants were related by the fact that for each J value the diagonal sum should agree with the sum of the energy values. This requirement does not fix all these electrostatic constants, but it does reduce the number of free constants to fit levels. The a_1 coupling parameter for the core was taken from the separation of the levels of the *Fe* II parent. It is a coincidence that this constant should theoretically be the same for both the ^4F and the ^4P core. The value used was $a_1 = -116$, which may be compared with the value $a_1 = -117$ used by Goudsmit and Humphries[6] and $a_1 = -118$ used by R. A. Merrill.[7]

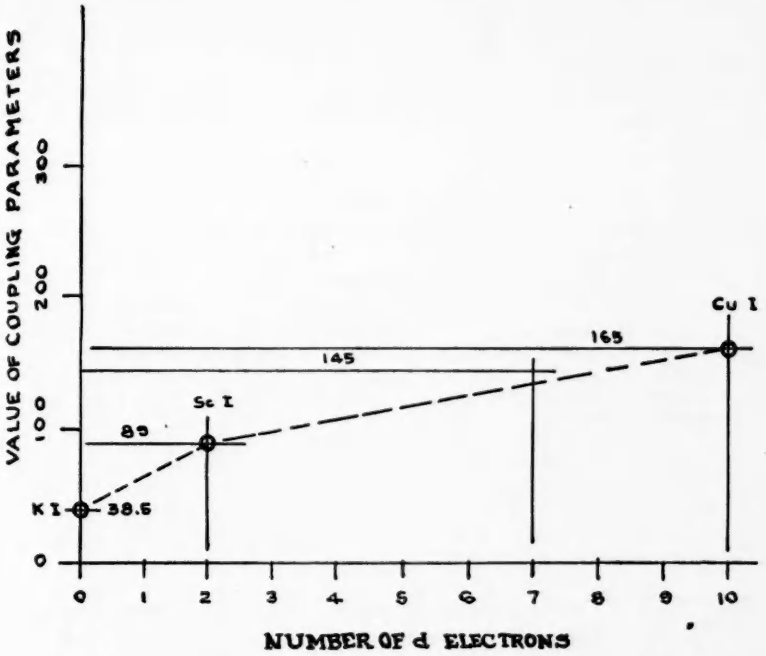

FIG. 1.—Coupling parameter variation with number of d electrons

The value of the a_2, the coupling parameter for the 4p electron, was a bit more difficult to set. It was not felt that it should be a free constant to be chosen to give the best fit with the energy levels. The coupling value for a 4p electron outside a partially filled d-shell can perhaps be reasonably chosen to fit the trend of known values of 4p electrons outside partially filled d-shells through the transition group. Only two neutral atoms with a 4p electron outside an S core were found in Bacher and Goudsmit's "Atomic Energy States." If one plots the values of the separation constant for the 4p electron in *K* I ^2P, *Sc* I $3d^2(^1S)4p$, and *Cu* I $3d^{10}4p$ against the number of d electrons as in Figure 1, a value of $a_2 = 145$ is found to be a reasonable choice.

METHOD OF CALCULATION

With the constants set at the above values, the numerical secular equations can be written down. These secular equations cannot be solved exactly, and approximate meth-

[6] *Phys. Rev.*, **46**, 960, 1928.

[7] *Phys. Rev.*, **46**, 487, 1934.

ods must be employed. For the cases of the $3d^7(^4F)4s$, $3d^7(^4P)4s$, and the $3d^7(^4P)4p$ configurations, the standard formulae of first-order perturbation theory were used to obtain the transformation coefficients.

The $3d^7(^4F)4p$ secular equation has large off-diagonal terms connecting the levels $^5G_5-{}^3G_5$, $^5G_4-{}^3G_4$, $^5F_4-{}^5D_4$, $^5G_3-{}^3G_3$, and $^3F_3-{}^3D_3$. To take these strong interactions into account, the quadratics involving the two levels concerned were solved accurately. Hence a linear combination of the two states is found. Consequently, a rearrangement of the S matrix is necessary to allow for the mixing of the two states.

In the energy matrix the nondiagonal terms outside the quadratic are affected by the fact that neither of the states is "pure." The change is made by multiplication of the sections involved by the transformation matrix which diagonalizes the quadratic. In sections which are affected by several of the partial diagonalizations, the readjustment is done step by step.

From this point on, both energy levels and transformation coefficients were found by first-order perturbation theory. The energy levels for the $3d^7(^4F)4p$ configuration

TABLE 2

ENERGY LEVELS $3d^7(^4F)4p$

Level	Calculated	Experimental	Level	Calculated	Experimental	Level	Calculated	Experimental
$^5G_6$	34844	34844	$^5F_5$	33695*	33695	$^5D_4$	32942	33096
$^5G_5$	34767	34782	$^5F_4$	34122	34039	$^5D_3$	33452	33507
$^5G_4$	35246	35257	$^5F_3$	34440	34328	$^5D_2$	33891	33801
$^5G_3$	35622	35611	$^5F_2$	34615	34547	$^5D_1$	34147	34017
$^5G_2$	35856*	35866	$^5F_1$	34769	34692	$^5D^0$	34276	34121
$^3G_5$	35345	35379	$^3F_4$	36686	36686	$^3D_3$	38150	38175
$^3G_4$	35782	35767	$^3F_3$	37214	37162	$^3D_2$	38678	38678
$^3G_3$	36106	36079	$^3F_2$	37638	37521	$^3D_1$	39041	38996

* These levels adjusted to fit experimental values.

are listed in Table 2. The agreement between calculated and observed levels is seen to be satisfactory. One particularly pleasing result is that the partial inversion of the ^5G multiplet is obtained in the calculated levels.

As a check on the transformation matrices used, the Landé g-factors for the strongly mixed pairs were computed from the g-factors for the Russell-Saunders coupling and the transformation matrices derived in this work. The computed values, with the latest experimental values,[8] are listed in Table 3. The agreement here is excellent and gives one confidence in the transformation coefficients.

The $S^{1/2}$ matrix was then obtained by matrix multiplication according to equation (1), and the line strengths were computed. For comparison, the experimental gf-values, given by A. S. King and R. B. King,[4] were translated into line strengths. Since the total strengths must be conserved, the two sets of line strengths were set to have approximately the same sun. Here again the agreement of the calculated values with the experimental values is seen to be reasonable. Table 4 gives the calculated values for the line strengths in the $3d^7(^4F)4s-3d^7(^4F)4p$ transitions with the experimental values for comparison. Table 5 gives the line strengths computed for the $3d^7(^4P)4s-3d^7(^4P)4p$ transition.

[8] Russell, Moore, and Weeks, "The Arc Spectrum of Iron," *Trans. Amer. Phil. Soc.*, N.S., Vol. XXXIV, Part II.

TABLE 3*

g-VALUES

Level	*LS*	Experimental	Calculated
$^5G_5$	1.267	1.218	1.221
$^3G_5$	1.200	1.248	1.245
$^5G_4$	1.150	1.103	1.100
$^3G_4$	1.050	1.100	1.094
$^5F_4$	1.350	1.344	1.354
$^5D_4$	1.500	1.496	1.499
$^5G_3$	0.917	0.887	0.886
$^3G_3$	0.750	0.791	0.791
$^5F_3$	1.250	1.265	1.264
$^5D_3$	1.500	1.492	1.482
$^3F_3$	1.083	1.086	1.084
$^3D_3$	1.333	1.324	1.323

* R.M.S. deviation from experimental values:

LS-values	0.032
Calculated	0.0048

TABLE 4*

LINE STRENGTHS FOR $3d^7(^4F)4s-3d^7(^4F)4p$

Line	Wave Length in A.U.	Experimental	*LS*	Calculated	Line	Wave Length in A.U.	Experimental	*LS*	Calculated
$a^5F_1-y^5D_0$	3849.97	6.0	7.7	7.7	$a^5F_5-z^5G_4$	.....	.....	0.3	0.4
$a^5F_1-y^5D_1$	3865.53	4.9	7.7	4.1	$a^5F_5-z^5G_5$	3589.11	0.55	8.5	5.7
$a^5F_1-y^5D_2$	3898.01	0.64	1.09	0.12	$a^5F_5-z^5G_6$	.....	†	100.	100.
$a^5F_2-y^5D_1$	3840.44	10.4	15.7	11.8	$a^3F_2-y^3D_1$	3841.05	42.0	23.1	23.2
$a^5F_2-y^5D_2$	3872.50	4.84	11.0	5.0	$a^3F_2-y^3D_2$	3888.52	14.2	4.4	10.7
$a^5F_2-y^5D_3$	3917.19	0.5	1.09	2.1	$a^3F_2-y^3D_3$	.....	.....	0.1	0.0025
$a^5F_3-y^5D_2$	3834.23	17.5	26.7	17.0	$a^3F_3-y^3D_2$	3827.83	55.0	34.2	29.5
$a^5F_3-y^5D_3$	3878.02	4.95	11.6	4.1	$a^3F_3-y^3D_3$	3902.95	21.4	4.4	15.9
$a^5F_3-y^5D_4$	3940.88	0.18	0.5	2.8	$a^3F_4-y^3D_3$	3815.84	60.5	49.5	55.0
$a^5F_4-y^5D_3$	3825.88	25.5	41.3	29.4	$a^3F_2-y^3F_2$	4071.75	47.1	34.2	29.5
$a^5F_4-y^5D_4$	3887.05	3.2	8.3	2.25	$a^3F_2-y^3F_3$	4132.06	13.8	4.3	7.2
$a^5F_5-y^5D_4$	3820.95	36.0	60.5	50.0	$a^3F_3-y^3F_2$	4005.25	14.7	4.3	10.6
$a^5F_1-y^5F_1$	3767.19	15.0	15.3	19.3	$a^3F_3-y^3F_3$	4063.60	53.0	45.3	50.0
$a^5F_1-y^5F_2$	3787.88	5.8	7.1	5.0	$a^3F_3-y^3F_4$	4143.87	17.6	4.4	4.5
$a^5F_2-y^5F_1$	3743.34	6.4	7.7	4.2	$a^3F_4-y^3F_3$	3969.26	18.2	4.4	9.5
$a^5F_2-y^5F_2$	3763.79	20.7	19.2	24.7	$a^3F_4-y^3F_4$	4045.82	74.0	65.0	68.0
$a^5F_2-y^5F_3$	3795.00	6.85	11.6	6.2	$a^3F_2-z^3G_3$	4325.77	50.7	49.5	41.2
$a^5F_2-y^5F_2$	3727.62	8.65	11.6	4.2	$a^3F_3-z^3G_3$	4250.79	11.5	4.3	5.3
$a^5F^3-y^5F_3$	3758.24	32.1	30.4	35.1	$a^3F_3-z^3G_4$	4307.91	43.0	65.0	30.5
$a^5F_3-y^5F_4$	3799.55	5.8	12.1	7.0	$a^3F_4-z^3G_3$	.....	.....	0.8	0.03
$a^5F_4-y^5F_3$	3709.25	7.9	12.1	6.94	$a^3F_4-z^3G_4$	4202.03	11.5	4.3	4.4
$a^5F_4-y^5F_4$	3749.49	42.4	48.7	45.1	$a^3F_4-z^3G_5$	4271.76	32.0	85.0	20.0
$a^5F_4-y^5F_5$	3798.51	3.05	8.4	7.0	$a^5F_5-z^3G_5$	3513.82	3.05	00.0	2.9
$a^5F_5-y^5F_4$	3687.46	4.74	8.4	2.3	$a^5F_4-z^3G_4$	3521.26	3.7	00.0	7.7
$a^5F_5-y^5F_5$	3734.87	53.5	76.4	70.0	$a^5F_3-z^3G_3$	3526.17	2.1	00.0	3.9
$a^5F_1-z^5G_2$	3608.86	22.0	29.7	29.4	$a^5F_2-z^3G_3$	3558.52	7.8	00.0	11.8
$a^5F_2-z^5G_2$	3586.99	6.0	8.2	9.0	$a^5F_3-z^3G_4$	3565.38	21.2	00.0	28.5
$a^5F_2-z^5G_3$	3618.39	32.0	41.2	33.6	$a^5F_4-z^3G_5$	3570.10	30.5	00.0	52.0
$a^5F_3-z^5G_2$	.....	.....	0.5	1.1	$a^3F_4-z^5G_4$	4294.13	4.4	00.0	2.4
$a^5F_3-z^5G_3$	3585.32	5.25	12.0	11.6	$a^3F_4-z^5G_3$	4337.05	1.5	00.0	0.02
$a^5F_3-z^5G_4$	3641.46	22.2	56.7	23.0	$a^3F_4-z^5G_5$	4383.55	68.0	00.0	65.0
$a^5F_4-z^5G_3$	.....	.....	0.6	0.8	$a^3F_3-z^5G_4$	4404.75	35.0	00.0	34.0
$a^5F_4-z^5G_4$	3585.71	2.84	12.2	8.8	$a^3F_2-z^5G_3$	4415.13	11.7	00.0	13.0
$a^5F_4-z^5G_5$	3647.85	17.8	70.2	15.3	$a^3F_4-y^5F_5$	4602.95	1.4	00.0	1.8

* These values have been normalized to approximately the same sum, leaving out the strongest line $a^5F_5-Z_5G_6$. There are numerous other lines which have a calculated line strength, small but finite.

† This line, the strongest of the array, was too strong to be measured by A. S. King and R. B. King.

TABLE 5*

LINE STRENGTHS IN THE $3d^7(^4P)4s-3d^7(^4P)4p$ TRANSITIONS

Line	Wave Length in A.U.	*LS*	Calculated	Line	Wave Length in A.U.	*LS*	Calculated
$^5P^3-{}^5D^4$	3427.121	68.0	68	$^3P_1-{}^3P_0$	4213.650	7.6	7.8
$^5P^3-{}^5D^3$	3424.284	18.0	10.8	$^3P_0-{}^3P_1$	4191.685	7.6	2.25
$^5P^3-{}^5D^2$	†	2.5	5.9	$^3P_0-{}^3P_0$	†	0	0
$^5P^2-{}^5D^3$	3445.151	35.4	28.4	$^3P_2-{}^3S_1$	4044.614	12.2	16.6
$^5P^2-{}^5D^2$	3428.192	22.0	20.8	$^3P_1-{}^3S_1$	4062.451	7.3	10.3
$^5P^2-{}^5D^1$	3394.583	5.7	7.8	$^3P_0-{}^3S_1$	4079.848	2.4	3.18
$^5P^1-{}^5D^2$	3451.915	13.2	17.0	$^3P_1-{}^5S_2$	4635.846	0	0.0025
$^5P^1-{}^5D^1$	3417.842	17.0	19.0	$^3P_2-{}^5D_3$	4181.758	0	4.8
$^5P^1-{}^5D^0$	3418.507	7.5	7.3	$^3P_1-{}^5D_2$	4175.640	0	0.073
$^5P^3-{}^5D^3$	3286.755	34.0	41.0	$^3P_2-{}^5D_2$	4156.803	0	0.91
$^5P^3-{}^5D^2$	†	17.0	15.0	$^3P_1-{}^5D_0$	4126.88	0	0.014
$^5P^2-{}^5D^3$	3305.971	17.0	25.0	$^3P_1-{}^5D_1$	4125.884	0	0.73
$^5P^2-{}^5D^2$	3284.588	3.1	6.8	$^3P_2-{}^5D_1$	4107.492	0	0.45
$^5P^2-{}^5D^1$	3271.002	16.4	15.0	$^3P_1-{}^5P_2$	3964.522	0	0.041
$^5P^1-{}^5D^2$	3306.356	16.4	13.8	$^3P_1-{}^5P_1$	3944.748	0	0.0009
$^5P^1-{}^5D^1$	3292.590	5.7	4.0	$^5P_3-{}^3D_3$	3392.652	0	1.50
$^5P^3-{}^5D^2$	†	17.7	15.2	$^5P_2-{}^3D_3$	3413.135	0	2.75
$^5P^2-{}^5D^2$	†	12.6	12.1	$^5P_2-{}^3D_2$	3399.336	0	0.41
$^5P^1-{}^5D^2$	†	7.5	5.7	$^5P_2-{}^3P_2$	3447.278	0	0.13
$^3P^2-{}^3D^3$	4134.681	51.8	52.0	$^5P_2-{}^3S_1$	3351.529	0	0.03
$^3P^2-{}^3D^2$	4119.449	9.3	0.96	$^5P_1-{}^3S_1$	3374.221	0	0.03
$^3P_2-{}^3D_1$	4091.561	0.6	0.03	$^5P_3-{}^3D_2$	3379.017	0	0.04
$^3P_1-{}^3D_2$	.....	28.0	22.0	$^5P_2-{}^3D_1$	3383.692	0	0.09
$^3P_1-{}^3D_1$	4109.808	9.3	10.4	$^5P_1-{}^3D_1$	3406.803	0	0.25
$^3P^0-{}^3D_1$	4127.612	12.3	11.4	$^5P_1-{}^3D_2$	3422.656	0	0.17
$^3P_2-{}^3P_2$	4184.895	38.6	53.0	$^5P_3-{}^3P_2$	3426.383	0	0.25
$^3P_2-{}^3P_1$	4154.502	9.5	6.0	$^5P_2-{}^3P_1$	3426.637	0	0.60
$^3P_1-{}^3P_2$	4203.987	9.5	9.6	$^5P_1-{}^3P_1$	3450.328	0	0.89
$^3P_1-{}^3P_1$	4173.322	5.7	3.9	$^5P_1-{}^3P_2$	3471.27	0	0.40

* These strengths have been arranged to be on the same scale as those for $3d^7(^4F)4s-3d^7(^4F)4p$.
Lines with a dagger (†) were not found in table of Russell, Moore, and Weeks.

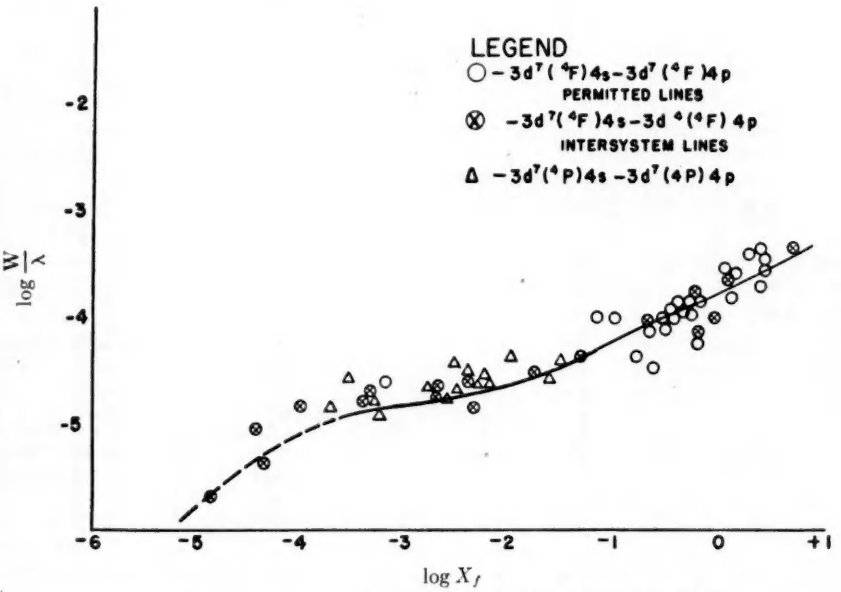

FIG. 2.—Curve of growth from calculated line strengths

CURVE OF GROWTH

The theory of the curve of growth, as given by Menzel,[9] relates the stellar equivalent widths to the line strengths, excitation potentials, and temperature. One check on a table of line strengths is the amount of scatter obtained when the table is used to derive a curve of growth. If one had more accurate equivalent widths, a table of line strengths could be derived from the curve of growth.

The line strengths calculated in this paper were used to draw a curve of growth for the sun. The method of drawing this curve is identical with that of Wright,[10] who used the empirical values of A. S. King and R. B. King.[4] The derived curve is shown in Figure 2.

The temperature of the solar reversing layer calculated from this curve is 4800° ± 200° K.

In conclusion I wish to express my gratitude to Professor J. H. Van Vleck, who guided the quantum-mechanical side of this work and who was a constant help throughout the investigation. Professor Menzel gave freely of his time and experience in clarifying the astrophysical aspects of the problem. Dr. Wright, of the Dominion Observatory, kindly made available equivalent width values not found in Allen's tables.

[9] *Ap. J.*, **84**, 462, 1936.

[10] *Ap. J.*, **99**, 249, 1944.

THE PRIMARY AND SECONDARY SCATTERING OF SUNLIGHT IN A PLANE-STRATIFIED ATMOSPHERE OF UNIFORM COMPOSITION

A. HAMMAD
Department of Mathematics, Faculty of Science, Cairo

Received March 2, 1948

ABSTRACT

The scattering of a parallel beam of unpolarized radiation by a plane-stratified atmosphere of finite optical thickness is considered, taking into account the polarization of radiation by scattering. Expressions are given for the component light-intensities and the degree of polarization of the scattered radiation, as far as primary and secondary scattering are concerned.

INTRODUCTION

1. In a previous paper,[1] here referred to as "Paper I," with the same title as this, exact formulae are given for the primary and secondary scattered sunlight, of any wave length, λ, emitted and received in any direction, at any point in a plane-stratified atmosphere of uniform composition, extending to infinity in all horizontal directions. No account was taken of the diffraction of radiation or its polarization by scattering. The object of this paper is to express the effect of polarization on these formulae and to give an estimate of the degree of polarization of the scattered radiation, taking into account the optical anisotropy of the molecules of air. The results given here can be applied to the light scattered by planetary atmospheres.

The problem of the scattering of light in a plane-stratified atmosphere, considering the resulting polarization, was treated long ago by Tichanowsky[2] and more recently by Chandrasekhar,[3] on different bases. In Tichanowsky's work the laws of scattering of light by anisotropic gas molecules are formulated and then applied to the earth's atmosphere, on the supposition that it is stratified in parallel planes. An expression is also given for the degree of polarization of sky radiation, as far as primary and secondary scattering are concerned. In Tichanowsky's work, no account was taken of the attenuation of radiation by absorption and scattering. His results may thus be assumed to apply to radiations which are weakly attenuated.

Chandrasekhar, on the other hand, considers, first, atmospheres of infinite optical thickness. Atmospheres of finite optical thickness are next dealt with, and the results obtained are now in a form suitable for numerical evaluation. These results show, however, that an exact solution of the problem is rather tedious and elaborate. We therefore give here an approximate solution, following a method developed in an earlier paper,[1] the approximation being such that the terms neglected can be identified physically. Extensive tables for the functions involved are now available,[4] so that the results given here might be put to the test of observation.

SCATTERING OF LIGHT BY ANISOTROPIC GAS MOLECULES

2. We shall now state, in brief terms, the results of the theory of scattering of light by a number of anisotropic gas molecules, all intrinsically alike and oriented at random.

Consider an element of volume, dv, of such a gas, and let a parallel beam of plane-

[1] *Phil. Mag.*, Ser. 7, **28**, 99, 1939.

[2] *Phys. Zs.*, **28**, 252, and 680, 1927.

[3] *Ap. J.*, **104**, 110, 1946; also **105**, 441, 1947, and **106**, 152, 1947.

[4] *Phil. Mag.*, Ser. 7, **38**, 515, 1947; also *Phil. Mag.*, in press.

polarized monochromatic radiation be incident on it, the dimensions of dv being taken large compared to the wave length of the incident light. Owing to the random motions of the molecules in dv, their contribution to the intensity of the light scattered by that element is simply additive. It can be shown that the light-intensity, at a distance r from dv, of the vibration scattered at an angle ψ with the incident vibration is

$$r^{-2} I'(r, \psi)\, dv\,,$$

where

$$I'(0, \psi) = \frac{3}{16\pi(1 + \frac{1}{2}d)}\, \sigma\rho\{d + 2(1 - d)\cos^2\psi\}\, I\,, \tag{1}$$

I being the intensity of the incident light; σ the mass coefficient of scattering of the gas for the particular radiation; d the depolarization factor (sometimes called the "coefficient of molecular anisotropy"); and ρ the density of the gas in dv.

The relation between $I'(r, \psi)$ and $I'(0, \psi)$ is

$$I'(r, \psi) = I'(0, \psi) \exp\left\{-(\sigma + \alpha)\int_0^r \rho\, dr\right\}, \tag{2}$$

where α is the mass coefficient of absorption.

When the light falling on dv is unpolarized, the light scattered in the direction of the unit vector $\boldsymbol{k}$, making an angle β with the incident light, may be regarded as due to two plane-polarized components of the incident light, with their electric intensities in the directions of the unit vectors $\boldsymbol{n}$ and $\boldsymbol{e}$, which, together with the unit vector $\boldsymbol{s}$ (in the direction of the incident light), form a right-handed orthogonal triad $\boldsymbol{n}$, $\boldsymbol{e}$, and $\boldsymbol{s}$, such that $\boldsymbol{e}$ is in the plane $\boldsymbol{sk}$. The scattered light is then obtained as the combination of two plane-polarized components with their electric intensities along the unit vectors $\boldsymbol{n}$ and $\boldsymbol{t}$, where $\boldsymbol{t} = \boldsymbol{k} \times \boldsymbol{n}$. Now, in natural light, the corresponding electric intensities along $\boldsymbol{n}$ and $\boldsymbol{e}$ have the same mean amplitude, but their phase angles vary irregularly; hence their phase difference takes all values at random in any interval of time, which, though short, is long, compared with the periodic time of the light. On this account the contributions of these two components to the electric intensities (along $\boldsymbol{n}$ or $\boldsymbol{t}$) of the scattered light have no systematic phase relation to one another; hence their contributions to the light-intensities of the scattered light are simply additive. At a distance r from dv, the two component light-intensities of the scattered light, with their electric intensities along $\boldsymbol{n}$ and $\boldsymbol{t}$, will be denoted by

$$r^{-2} I_n(r)\, dv\,, \qquad r^{-2} I_t(r)\, dv\,,$$

respectively, where, by means of equation (1),

$$I_n(0) = \frac{3}{16\pi(1 + \frac{1}{2}d)}\, \sigma\rho I\,, \tag{3}$$

$$I_t(0) = \frac{3}{16\pi(1 + \frac{1}{2}d)}\, \sigma\rho\{d + (1 - d)\cos^2\beta\}\, I\,, \tag{4}$$

I being the intensity of the incident natural light.

The relation between $I_q(r)$ and $I_q(0)$, where q stands for n or t, is similar to equation (2).

The total intensity is, therefore,

$$r^{-2}\{I_n(r) + I_t(r)\}\, dv \qquad \text{or} \qquad r^{-2} I_{nt}(r)\, dv\,,$$

where

$$I_{nt}(0) = \frac{3}{16\pi(1 + \frac{1}{2}d)}\, \sigma\rho\{1 + \cos^2\beta + d\sin^2\beta\}\, I\,. \tag{5}$$

It is worth noting that the two electric intensities of the scattered light have no systematic phase relation to each other, since each arises from a single component of the incident natural vibration.

APPLICATION TO THE EARTH'S ATMOSPHERE

3. We shall now apply the laws of scattering, given in the previous article, to the earth's atmosphere, taken as uniformly mixed and resting on a plane earth.

NOTATIONS

4. As in Paper I, the height of any point in the atmosphere will be specified in terms of the fraction $\bar{m}$ (or m), of the total mass of the atmosphere that lies above (or below) that point. Clearly, $\bar{m} + m = 1$; $\bar{m} = 1, m = 0$, at the ground; also $\bar{m} = 0, m = 1$, at the top of the atmosphere.

The absorption and scattering coefficients of the air, per unit mass, for light of wave length λ, will be denoted by $\alpha(\lambda)$ and $\sigma(\lambda)$, respectively, or, more briefly, by α and σ. We shall also write

$$a = \alpha M , \qquad s = \sigma M , \qquad c = a + s ,$$

where M is the total mass of air in a vertical column of unit cross-sectional area (1 sq. cm.) extending from the ground to the top of the atmosphere.

As in Paper I, the zenith angle of the sun will be denoted by z. Relative to the vertical and the vertical half-plane through the sun, any other direction may be specified by its polar angles (θ, φ). Light traveling in the direction of the unit vector $\boldsymbol{k}$ and that traveling in the opposite direction, $-\boldsymbol{k}$, will be denoted by the same polar angles (θ, φ), so that $\sec\theta \geqslant 1$. When it is necessary to distinguish between upgoing and downgoing light, a letter u or d will be attached to our symbols.

The symbols $c \sec z$, $c \sec \theta$, and $c \sec \theta'$ occur often in our formulae, and it is convenient to write

$$Z = c \sec z , \qquad \Theta = c \sec \theta , \qquad \Theta' = c \sec \theta' .$$

THE EMISSION AND RECEPTION OF PRIMARY SCATTERED SUNLIGHT

5.1. As in Paper I, we shall denote by $E_1(z, m, \boldsymbol{k})$ the intensity of the primary scattered light emitted per unit mass of air at level m, per unit solid angle in the direction $\boldsymbol{k}$. By equation (5) of this paper, we have

$$E_1(z, \bar{m}, \boldsymbol{k}) = \frac{3}{16\pi(1 + \frac{1}{2}d)} \sigma \{1 + \cos^2\psi + d \sin^2\psi\} I(z, \bar{m}) ,$$

where ψ is the angle between $\boldsymbol{k}$ and the direction of the incident solar beam, and $I(z, \bar{m})$ is the intensity of the solar beam at level m. As shown in Paper I, § 10,

$$I(z, \bar{m}) = I_\infty e^{-Z\bar{m}} ,$$

where I_∞ is the intensity of the direct sunlight (of wave length λ) outside the atmosphere.

Thus

$$E_1(z, \bar{m}, \boldsymbol{k}) = \frac{3}{16\pi(1 + \frac{1}{2}d)} \sigma I_\infty \{1 + \cos^2\psi + d \sin^2\psi\} e^{-Z\bar{m}} .$$

The directional distribution of E_1 is represented by the primary emission surface, $r = E_1$, where r is the radius in the direction (θ, φ); this is a surface of revolution about the direction of the incident sunlight, and its polar equation relative to that direction is

$$r = K(1 + \cos^2\Psi + d \sin^2\psi)$$

$$= K\{1 + d(1 - d)\cos^2\psi\} .$$

The mean value of r is $K\{1 + d + (1 - d)/3\}$, and the percentage root-mean-square departure of r from its mean is

$$22.4\,\frac{1-d}{1+\frac{1}{2}d}$$

per cent of the mean. This decreases as d increases, being 22.4 per cent of the mean when $d = 0$ and zero for $d = 1$. Thus the emission of primary scattered light is much more isotropic in the case of anisotropic molecules and less isotropic in the case of spherically symmetrical molecules. This is very interesting to note and may be utilized in the measurement of the anisotropy of the gas molecules.

5.2. The primary scattered light emitted from any point at level m, in any direction $\boldsymbol{k}$ making an angle ψ with the direction $\boldsymbol{s}$ of the incident solar beam, is partially polarized and has two plane-polarized components with their electric vibrations along $\boldsymbol{n}$ and $\boldsymbol{t}$, such that $\boldsymbol{n}$ is perpendicular to $\boldsymbol{k}$ and $\boldsymbol{s}$, and $\boldsymbol{t} = \boldsymbol{k} \times \boldsymbol{n}$ (cf. § 2). Denoting the light-intensities of these two components by E_{1n} and E_{1t}, respectively, we have, by equations (3) and (4),

$$E_{1n}(z, \bar{m}, \boldsymbol{k}) = \frac{3}{16\pi(1+\frac{1}{2}d)}\,\sigma I_\infty e^{-Z\bar{m}} \tag{6}$$

and

$$E_{1t}(z, \bar{m}, \boldsymbol{k}) = \frac{3}{16\pi(1+\frac{1}{2}d)}\,\sigma I_\infty \{d + (1-d)\cos^2\psi\}\, e^{-Z\bar{m}}. \tag{7}$$

This light arrives at any level m as primary received light, with two electric components along the vectors $\boldsymbol{n}$ and $\boldsymbol{t}$. For upgoing light, the two component light-intensities will be denoted by Ru_{1n} and Ru_{1t}, where

$$Ru_{1n}(m, z, \boldsymbol{k}) = \frac{3s}{16\pi c(1+\frac{1}{2}d)}\, I_\infty \Theta F u\,,$$

$$Ru_{1t}(m, z, \boldsymbol{k}) = \frac{3s}{16\pi c(1+\frac{1}{2}d)}\, I_\infty \Theta \{d + (1-d)\cos^2\psi\} F u\,,$$

and

$$Fu = \frac{e^{Zm} - e^{-\Theta m}}{Z+\Theta}\, e^{-Z} \qquad \text{(cf. Paper I, § 6)}.$$

Similarly, the two component light-intensities in the downgoing light are

$$Rd_{1n}(\bar{m}, z, \boldsymbol{k}) = \frac{3s}{16\pi c(1+\frac{1}{2}d)}\, I_\infty \Theta F d\,,$$

$$Rd_{1t}(\bar{m}, z, \boldsymbol{k}) = \frac{3s}{16\pi c(1+\frac{1}{2}d)}\, I_\infty \Theta \{d + (1-d)\cos^2\psi\} F d\,,$$

where, from § 6 of Paper I, we obtain

$$Fd = \frac{e^{-\Theta\bar{m}} - e^{-Z\bar{m}}}{Z-\Theta}.$$

THE EMISSION AND RECEPTION OF SECONDARY SCATTERED SUNLIGHT

6.1. The air at any level receives primary scattered light from all directions, and all such light is scattered in all directions, giving rise to secondary emission. The light emitted by secondary scattering, per unit mass of air at level m, in directions lying within the cone $\boldsymbol{k}$, $d\boldsymbol{k}$, will be denoted, as in Paper I, by $E_2(m, z, \boldsymbol{k})\, d\boldsymbol{k}$; its components, with electric vibrations along the vectors $\boldsymbol{n}$ and $\boldsymbol{t}$ of § 5.2, will be denoted by $E_{2n}d\boldsymbol{k}$ and $E_{2t}d\boldsymbol{k}$,

respectively. We shall now calculate the contributions made to E_{2n} and E_{2t} by the primary scattered light coming from directions lying within the cone $\boldsymbol{k}'$, $d\boldsymbol{k}'$. As indicated in § 5.2, the primary scattered light received at any level from the direction $\boldsymbol{k}'$ has two plane-polarized components (denoted there by $R_{1n'}$, $R_{1t'}$, with a u or d added), with their vibrations along the vectors $\boldsymbol{n}'$ and $\boldsymbol{t}'$, respectively, such that $\boldsymbol{n}'$ is perpendicular to $\boldsymbol{k}'$ and $\boldsymbol{s}$, and $\boldsymbol{t}' = \boldsymbol{k}' \times \boldsymbol{n}'$. For the reasons expressed in § 2, the contributions of $R_{1n'}$ and $R_{1t'}$ to E_{2n} or E_{2t} are simply additive.

The contribution made to E_{2n} by $R_{1n'}d\boldsymbol{k}'$ is obtained by means of equation (1): if $\chi_{nn'}$ is the angle between the two vectors $\boldsymbol{n}$ and $\boldsymbol{n}'$, the required contribution is equal to

$$\frac{3\sigma}{16\pi(1+\frac{1}{2}d)}[d+2(1-d)\cos^2\chi_{nn'}]R_{1n'}d\boldsymbol{k}'.$$

Similarly, the contribution made to E_{2n} by $R_{1t'}d\mathbf{k}'$ is equal to

$$\frac{3\sigma}{16\pi(1+\frac{1}{2}d)}[d+2(1-d)\cos^2\chi_{nt'}]R_{1t'}d\boldsymbol{k}',$$

where, as before, $\chi_{nt'}$ is the angle between the two vectors $\boldsymbol{n}$ and $\boldsymbol{t}'$. Thus the contribution made to E_{2n} by the primary scattered light received from all directions within the cone $\boldsymbol{k}'$, $d\boldsymbol{k}'$ is equal to

$$\frac{3\sigma}{16\pi(1+\frac{1}{2}d)}\{[d+2(1-d)\cos^2\chi_{nn'}]R_{1n'}+[d+2(1-d)\cos^2\chi_{nt'}]R_{1t'}\}d\boldsymbol{k}'.$$

Integrating over all directions $\boldsymbol{k}'$, we get

$$\begin{aligned}E_{2n}(c,z,m,\boldsymbol{k}) &= \frac{3\sigma}{16\pi(1+\frac{1}{2}d)}\int_0\{[d+2(1-d)\cos^2\chi_{nn'}]R_{1n'}(c,z,m,\boldsymbol{k}')\\ &\qquad +[d+2(1-d)\cos^2\chi_{nt'}]R_{1t'}(c,z,m,\boldsymbol{k}')\}d\boldsymbol{k}'\\ &= \frac{3\sigma}{16\pi(1+\frac{1}{2}d)}\int_\smile\{[d+2(1-d)\cos^2\chi_{nn'}][Ru_{1n'}(\boldsymbol{k}')+Rd_{1n'}(\boldsymbol{k}')]\\ &\qquad +[d+2(1-d)\cos^2\chi_{nt'}][Ru_{1t'}(\boldsymbol{k}')Rd_{1t'}+(\boldsymbol{k}')]\}d\boldsymbol{k}',\end{aligned}$$

where the integration in the last line extends over a hemisphere and in the preceding line over a sphere, except at the ground and the top of the atmosphere, where the integration extends over a hemisphere.

Similarly,

$$\begin{aligned}E_{2t}(c,z,m,\boldsymbol{k}) &= \frac{3\sigma}{16\pi(1+\frac{1}{2}d)}\int_\smile\{[d+2(1-d)\cos^2\chi_{tn'}][Ru_{1n'}(\boldsymbol{k}')+Rd_{1n'}(\boldsymbol{k}')]\\ &\qquad +[d+2(1-d)\cos^2\chi_{tt'}][Ru_{1t'}(\boldsymbol{k}')+Rd_{1t'}(\boldsymbol{k}')]\}d\boldsymbol{k}',\end{aligned}$$

where $\chi_{tn'}$ and $\chi_{tt'}$ are the angles between $\boldsymbol{t}$ and $\boldsymbol{n}'$ and $\boldsymbol{t}$ and $\boldsymbol{t}'$, respectively, and the integration extends over a hemisphere.

Substituting for $Ru_{1n'}$, $Rd_{1n'}$, $Ru_{1t'}$, and $Rd_{1t'}$ from § 5.2 and remembering that

$$Fd=\int_0^m e^{-z\bar{m}'}e^{-\Theta(\bar{m}-\bar{m}')}d\bar{m}', \qquad Fu=\int_{\bar{m}}^1 e^{-z\bar{m}'}e^{-\Theta(\bar{m}'-\bar{m})}d\bar{m}',$$

so that

$$Fd+Fu=\int_0^1 e^{-z\bar{m}'}e^{-\Theta(\bar{m}'-\bar{m})}d\bar{m}',$$

we get

$$E_{2n}(c, z, m, k) = \frac{9s\sigma}{(16\pi)^2(1+\frac{1}{2}d)^2} I_\infty \int_0^{2\pi}\int_0^{\pi/2}\int_0^1 \{d + 2(1-d)\cos^2\chi_{nn'} + [d + 2(1-d)\cos^2\chi_{nt'}][d + (1-d)\cos^2\psi']\} e^{-z\bar{m}' - \Theta(\bar{m}-\bar{m}')} \times \sec\theta' \sin\theta' d\bar{m}' d\theta' d\varphi' \quad (8)$$

and

$$E_{2t}(c, z, m, k) = \frac{9s\sigma}{(16\pi)^2(1+\frac{1}{2}d)^2} I_\infty \int_0^{2\pi}\int_0^{\pi/2}\int_0^1 \{d + 2(1-d)\cos^2\chi_{tn'} + [d + 2(1-d)\cos^2\chi_{tt'}][d + (1-d)\cos^2\psi']\} e^{-z\bar{m}' - \Theta(\bar{m}-\bar{m}')} \times \sec\theta' \sin\theta' d\bar{m}' d\theta' d\varphi' . \quad (9)$$

To evaluate the integrals in equations (8) and (9), we have to express the angles ψ', $\chi_{nn'}$, $\chi_{nt'}$, $\chi_{tn'}$, $\chi_{tt'}$ in terms of θ' and φ'. For this purpose we introduce a local system of rectangular axes XHY, such that the X-axis is in the direction of the sun and the XH-plane is parallel to the vertical plane through the sun's rays. Relative to the X-axis and the XH-plane, the vector k has polar angles (ψ, ξ), which are connected to the polar angles (θ, φ) by the relations

$$\cos\psi = \cos z\cos\theta + \sin z\sin\theta\cos\varphi ,$$
$$\sin\psi\cos\xi = \sin z\cos\theta - \cos z\sin\theta\cos\varphi ,$$
$$\sin\psi\sin\xi = \sin\theta\sin\varphi .$$

The angles $\chi_{nn'}$, $\chi_{nt'}$, $\chi_{tn'}$, and $\chi_{tt'}$ are then given by

$$\cos\chi_{nn'} = \cos(\xi - \xi') ,$$
$$\cos\chi_{nt'} = \cos\psi' \sin(\xi - \xi') ,$$
$$\cos\chi_{tn'} = \cos\psi \sin(\xi' - \xi) ,$$
$$\text{coc}\,\chi_{tt'} = \sin\psi \sin\psi' + \cos\psi\cos\psi'\cos(\xi' - \xi) .$$

In this way the angles $\chi_{nn'}$, $\chi_{nt'}$, $\chi_{tn'}$, and $\chi_{tt'}$ can be expressed in terms of θ' and φ'.

Neglecting the terms in d^2 in equations (8) and (9) and integrating with respect to φ', we get

$$E_{2n}(c, z, m, k) = \frac{9s\sigma}{256\pi^2(1+\frac{1}{2}d)^2} I_\infty \int_0^{\pi/2}\int_0^1 \{B_1 + B_2\cos^2\theta' + B_3\cos^4\theta' + d(B_4 + B_5\cos^2\theta' + B_6\cos^4\theta')\} e^{-z\bar{m}' - \Theta(\bar{m}-\bar{m}')} \sec\theta' \sin\theta' d\bar{m}' d\theta' ,$$

$$E_{2t}(c, z, m, k) = \frac{9s\sigma}{256\pi^2(1+\frac{1}{2}d)^2} I_\infty \int_0^{\pi/2}\int_0^1 \{C_1 + C_2\cos^2\theta' + C_3\cos^4\theta' + d(C_4 + C_5\cos^2\theta' + C_6\cos^4\theta')\} e^{-z\bar{m}' - \Theta(\bar{m}-\bar{m}')} \sec\theta' \sin\theta' d\bar{m}' d\theta'$$

where

$$B_1 = 4 - \tfrac{1}{2}\cos^2\xi\,(5 - Q^2) - \tfrac{1}{2}\sin^2\xi\,(7 - 3Q^2)\,Q^2\,,$$

$$B_2 = 3S^2\cos^2\xi - 3\,(2 - 7Q^2 + 5Q^4)\sin^2\xi\,,$$

$$B_3 = \tfrac{1}{2}\,(5Q^2 - 1)\cos^2\xi + \tfrac{1}{2}\,(4 - 35Q^2S^2)\sin^2\xi\,,$$

$$B_4 = -S^2 + (3 - Q^2)\cos^2\xi + (5Q^2 - 3Q^4)\sin^2\xi\,,$$

$$B_5 = 3Q^2 - 1 + (6Q^2 - 4)\cos^2\xi + (8 - 36Q^2 + 30Q^4)\sin^2\xi\,,$$

$$B_6 = -2B_3\,;$$

$$C_1 = \{\,(4 - 3\tfrac{1}{2}Q^2 + 1\tfrac{1}{2}Q^4)\cos^2\xi + \tfrac{1}{2}\,(3 + Q^2)\sin^2\xi\,\}\cos^2\psi + (\tfrac{1}{2} + Q^2 - 1\tfrac{1}{2}Q^4)\sin^2\psi - 3QS^3\cos\psi\sin\psi\cos\xi\,,$$

$$C_2 = \{\,(-6 + 21Q^2 - 15Q^4)\cos^2\xi + 3S^2\sin^2\xi\,\}\cos^2\psi + (1 - 12Q^2 + 15Q^4)\sin^2\psi + 2SQ\,(9 - 15Q^2)\cos\psi\sin\psi\cos\xi\,,$$

$$C_3 = \{\,(2 - 17\tfrac{1}{2}Q^2S^2)\cos^2\xi - \tfrac{1}{2}\,(1 - 5Q^2)\sin^2\xi\,\}\cos^2\psi + \tfrac{1}{2}\,(-3 + 30Q^2 - 35Q^4)\sin^2\psi - 5SQ\,(3 - 7Q^2)\cos\psi\sin\psi\cos\xi\,,$$

$$C_4 = \{\,(-4 + 5Q^2 - 3Q^4)\cos^2\xi - (1 + Q^2)\sin^2\xi\,\}\cos^2\psi + 3 - Q^2 + (1 + 3Q^2)\sin^2\psi + SQ\,(2 - 6Q^2)\cos\psi\sin\psi\cos\xi\,,$$

$$C_5 = \{\,(8 - 36Q^2 + 30Q^4)\cos^2\xi + (6Q^2 - 4)\sin^2\xi\,\}\cos^2\psi + 3Q^2 - 1 + 6\,(3Q^2 - 5Q^4)\sin^2\psi + 12SQ\,(-2 + 5Q^2)\cos\psi\sin\psi\cos\xi\,,$$

$$C_6 = -2C_3\,;$$

and

$$Q = \cos z\,, \qquad S = \sin z\,.$$

The above value of E_{2n} agrees with that given by Tichanowsky,[5] while E_{2t} disagrees.[6]

The further integration with respect to θ' and $\bar{m}'$ leads to the following result:

$$E_{2n}(c, z, \bar{m}, \boldsymbol{k}) = \frac{9s\sigma}{256\pi\,(1 + \frac{1}{2}d)^2}\,I_\infty\{B_1L_1(c, z, \bar{m}) + B_2L_3(c, z, \bar{m}) + B_3L_5(c, z, \bar{m}) + d\,[B_4L_1(c, z, \bar{m}) + B_5L_3(c, z, \bar{m}) + B_6L_5(c, z, \bar{m})]\}\,,$$

$$E_{2t}(c, z, \bar{m}, \boldsymbol{k}) = \frac{9s\sigma}{256\pi\,(1 + \frac{1}{2}d)^2}\,I_\infty\{C_1L_1(c, z, \bar{m}) + C_2L_3(c, z, \bar{m}) + C_3L_5(c, z, \bar{m}) + d\,[C_4L_1(c, z, \bar{m}) + C_5L_3(c, z, \bar{m}) + C_6L_5(c, z, \bar{m})]\}\,,$$

where

$$L_n(c, z, \bar{m}) = \int_0^1 e^{-z\bar{m}'}Ej_n(c\,\bar{m} \sim c\,\bar{m}')\,d\bar{m}'$$

and

$$Ej_n(t) = \int_1^\infty e^{-tx}x^{-n}\,dx\,.$$

[5] Tichanowsky, in his paper (*Phys. Zs.*, **28**, 684, 1927), considers the special case corresponding to $\xi = 0$.

[6] A. Hammad, *Phys. Zs.*, **39**, 168, 1938.

The functions L_n are evaluated and discussed in § 17 of Paper I; they are tabulated[7] and replaced[8] by simple approximate expressions in later papers.

6.2. The secondary scattered light emitted from any point at level m' and traveling in the direction $\boldsymbol{k}$ arrives at any point at level m, after loss by absorption and scattering, as secondary received light. The two component light-intensities of this light, with electric vibrations along the vectors $\boldsymbol{n}$ and $\boldsymbol{t}$ of § 5, will be denoted by Ru_{2n} and Ru_{2t} or Rd_{2n} and Rd_{2t}, corresponding to upgoing or downgoing light. It can be easily seen that

$$Ru_{2n}(c, z, m, \boldsymbol{k}) = \frac{9s^2 I_\infty}{256\pi(1+\frac{1}{2}d)^2}\sec\theta\{B_1 Lu_1(c, z, m, \theta) + B_2 Lu_3(c, z, m, \theta) + B_3 Lu_5(c, z, m, \theta) + d(B_4 Lu_1 + B_5 Lu_3 + B_6 Lu_5)\},$$

$$Ru_{2t}(c, z, m, \boldsymbol{k}) = \frac{9s^2 I_\infty}{256\pi(1+\frac{1}{2}d)^2}\sec\theta\{C_1 Lu_1 + C_2 Lu_3 + C_3 Lu_5 + d(C_4 Lu_1 + C_5 Lu_3 + C_6 Lu_5)\},$$

and

$$Rd_{2n}(c, z, \bar{m}, \boldsymbol{k}) = \frac{9s^2 I_\infty}{256\pi(1+\frac{1}{2}d)^2}\sec\theta\{B_1 Ld_1(c, z, \bar{m}, \theta) + B_2 Ld_3(c, z, \bar{m}, \theta) + B_3 Ld_5(c, z, \bar{m}, \theta) + d(B_4 Ld_1 + B_5 Ld_3 + B_6 Ld_5)\},$$

$$Rd_{2t}(c, z, \bar{m}, \boldsymbol{k}) = \frac{9s^2 I_\infty}{256\pi(1+\frac{1}{2}d)^2}\sec\theta\{C_1 Ld_1 + C_2 Ld_3 + C_3 Ld_5 \times d(C_4 Ld_1 + C_5 Ld_3 + C_6 Ld_5)\},$$

where

$$Lu_n(c, z, m, \theta) = e^{-\Theta m}\int_0^m e^{\Theta m'} L_n(c, z, m')\, dm',$$

$$Ld_n(c, z, \bar{m}, \theta) = e^{-\Theta \bar{m}}\int_0^{\bar{m}} e^{\Theta \bar{m}'} L_n(c, z, \bar{m}')\, d\bar{m}'.$$

These integrals are evaluated in terms of known functions in § 18 of Paper I; they are replaced by simple approximate expressions in Paper IV.

THE DEGREE OF POLARIZATION OF THE SCATTERED SOLAR RADIATION

7. We shall now give an expression for the degree of polarization of the scattered radiation received at any level $\boldsymbol{m}$ from any direction $\boldsymbol{k}$, taking account of the optical anisotropy of the molecules of air. If $R_n(c, z, m, \boldsymbol{k})$ and $R_t(c, z, m, \boldsymbol{k})$ are the two component light-intensities, with vibrations along the unit vectors $\boldsymbol{n}$ and $\boldsymbol{t}$, respectively, of the scattered light received from the direction $\boldsymbol{k}$ ($\boldsymbol{n}$, $\boldsymbol{t}$, and $\boldsymbol{k}$ form a right-handed orthogonal triad, such that $\boldsymbol{n}$ is perpendicular to the sun's rays), the degree of polarization $P(c, z, m, \boldsymbol{k})$ of such light is given by

$$P(c, z, m, \boldsymbol{k}) = \frac{R_n - R_t}{R_n + R_t};$$

the letter u or d may be added to the symbols to denote the upgoing or the downgoing light, respectively. When $P = 1$, polarization is complete, while $P = 0$ gives the neutral points.

[7] *Phil. Mag.*, Ser. 7, **38**, 515, 1947; this paper will be referred to as "Paper III."

[8] *Phil. Mag.* (in press); this paper will be referred to as "Paper IV."

Clearly, each of the components R_n and R_t is composed of parts due to the different orders of scattering. Thus

$$P(c, z, m, k) = \frac{(R_{1n} - R_{1t}) + (R_{2n} - R_{2t}) + \dots}{(R_{1n} + R_{1t}) + (R_2 + R_{2t}) + \dots}.$$

We shall denote by $P_1, P_2, \dots$, the values of P corresponding to the first bracket, the first two brackets, and $\dots$, of the above expression of P. These correspond to a series of approximations to P in which further orders of scattering, primary, secondary, $\dots$, are taken into account. Thus

$$P_1(c, z, m, k) = \frac{R_{1n} - R_{1t}}{R_{1n} + R_{1t}}$$

$$= \frac{(1-d)\sin^2\psi}{1+\cos^2\psi + d\sin^2\psi}, \qquad \text{from §5 .}$$

This is independent of the wave length and the constitution of the atmosphere. It is clear that, according to this formula, the direction of maximum polarization is perpendicular to the solar beam and the neutral points lie along that direction. This is contrary to the results of observation. We therefore have to take secondary and higher orders of scattering into account. Thus, if secondary scattering is taken into consideration, we get

$$P_2(c, z, m, k) = \frac{(R_{1n} - R_{1t}) + (R_{2n} - R_{2t})}{(R_{1n} + R_{1t}) + (R_{2n} + R_{2t})}.$$

Substituting for R_{1n}, R_{1t}, R_{2n}, and R_{2t} from §§ 5 and 6, we can specify the dependence of P on the wave length and the constitution of the atmosphere.

CONCLUSION

8. The preceding analysis completes the formal solution of the problem of the scattering of light in a plane-stratified atmosphere of uniform composition, as far as primary and secondary scattering are concerned, taking account of the polarization of radiation by scattering and allowing for the optical anisotropy of the molecules. In order that the solution may be of use in connection with actual observations of the scattered radiation, it must be supplemented with numerical results, and the nature of these results must be stated in general terms. In a forthcoming paper we shall give numerical results showing the dependence of the degree of polarization of sky radiation, as viewed from the ground, on wave length, on the sun's zenith distance, on the direction of observation, and on the constitution of the atmosphere. Numerical results concerning the directional distribution of the light returned to free space and its degree of polarization will also be given in a later paper.